Moscow State University

A Kinematically Complete Measurement of the Proton Structure Function F_2 in the Resonance Region and Evaluation of Its Moments

A Dissertation
by
MIKHAIL OSIPENKO

Submitted to the Physics Department of
Moscow State University
in partial fulfillment of the requirements
for the degree of

DOCTOR OF PHILOSOPHY

October 2002

Abstract

The inclusive inelastic electron scattering off the proton was measured at five different beam energies 1.5, 2.5 4.0, 4.2 and 4.4 GeV. The data were taken, during February-March 1999, on a liquid hydrogen target with the CLAS detector installed in Hall-B of the Thomas Jefferson National Accelerator Facility (TJNAF). The obtained high statistics and high precision data appear to be in good agreement with previously measured world data and permit to integrate experimental values of F_2 over x at fixed Q^2, allowing for the first time the evaluation of its experimental moments at low and moderate values of Q^2.

In a combined analysis of CLAS and world data, the Q^2-evolution of the experimental moments was explored in the range from 0.3 up to 100 GeV^2. This offered a unique possibility to trace changes of the proton structure function from hard DIS down to the non-perturbative regime through the transition region, which is of particular interest for the TJNAF physics program. The obtained experimental moments allowed to perform a separation between the leading twist, calculable in the framework of the perturbative QCD (pQCD), and higher twists, treated effectively. A comparison with theoretical predictions based either on lattice QCD simulations or obtained within models of the nucleon structure may represent an important test of our understanding of the nucleon structure as observed at large wavelengths.

Contents

List of Figures

List of Tables

Chapter 1

Introduction

1.1 Kinematics and observables

Two different sets of kinematic variables will be used below: one of them is dedicated to the raw data analysis, and it deals with natural quantities directly measured in the detector; the second set is used for the following physics analysis of the obtained cross sections.

The variables of the first set are defined in the laboratory frame, these are:

1. Beam energy (energy of the incident electron) - E;
2. Electron scattering angle - θ;
3. Energy (momentum) of the scattered electron - $E' \simeq P$ (since we operate in the region where $E, E', P >> m_e$).

The second set contains invariant variables, independent from a particular choice of the reference system:

1. four-momentum transfer:

   $$Q^2 = -q^2 = -(k - k')^2 \tag{1.1}$$

   usually the lepton mass is negligible and in the laboratory frame the four-momentum transfer can be written:

   $$Q^2 = 4EE' \sin^2 \frac{\theta}{2} \tag{1.2}$$

2. lepton energy loss:

   $$\nu = \frac{pq}{M} = \frac{W^2 + Q^2 - M^2}{2M} \tag{1.3}$$

   in the laboratory frame $\nu = E - E'$.

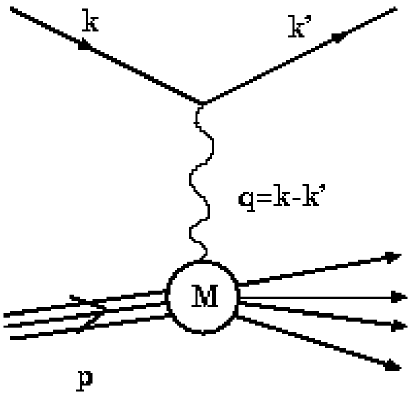

Figure 1.1: The lepton inelastic scattering diagram in the one photon exchange approximation: k, k' are the four-momentum of the initial and scattered lepton, p is the four-momentum of the target particle and q is the four-momentum of the virtual photon.

3. missing mass, equal to the total energy of the recoiling system in final state:

$$W = \sqrt{(q+p)^2} = \sqrt{M^2 + 2M\nu - Q^2} \tag{1.4}$$

4. Bjorken scaling variable:

$$x = \frac{-(k-k')^2}{2p(k-k')} = \frac{Q^2}{W^2 + Q^2 - M^2} = \frac{Q^2}{2M\nu} \tag{1.5}$$

5. improved scaling variable (Nachtmann [1]):

$$\xi = \frac{2x}{1 + \sqrt{1 + 4\frac{M^2x^2}{Q^2}}} \tag{1.6}$$

In lowest order of QED (one photon approximation) the differential cross section can be presented in the general form:

$$\frac{d^2\sigma}{d\Omega dE'} = A l_{\mu\nu}(k,q) W^{\mu\nu}(p,q) \tag{1.7}$$

where $l_{\mu\nu}$ and $W^{\mu\nu}$ are the leptonic and hadronic tensors, respectively, and A is an interaction dependent constant.

Particularly, in case of electromagnetic interactions the leptonic tensor averaged over polarization degrees of freedom can be calculated in QED, while the hadronic tensor can be written as:

$$W^{\mu\nu}(p,q) = W_1\left(-g^{\mu\nu} + \frac{q_\mu q_\nu}{q^2}\right) + \frac{W_2}{M^2}\left(-p^\mu - \frac{qp}{q^2}q^\mu\right)\left(-p^\nu - \frac{qp}{q^2}q^\nu\right) \tag{1.8}$$

where W_1 and W_2 are the nucleon structure functions. One can show [2] that the inclusive cross section is given by:

$$\frac{d^2\sigma}{d\Omega dE'} = \sigma_{Mott}\left[W_2(\nu,Q^2) + 2W_1(\nu,Q^2)\tan^2\frac{\theta}{2}\right] \tag{1.9}$$

where

$$\sigma_{Mott} = \frac{\alpha^2\cos^2\frac{\theta}{2}}{4E^2\sin^4\frac{\theta}{2}} \tag{1.10}$$

is the so called Mott cross section describing the scattering off a point-like nucleon.

Eq. 1.9 could be also expressed in terms of the absorption cross section of longitudinally or transversely polarized virtual photon: σ_L and σ_T:

$$\frac{d^2\sigma}{d\Omega dE'} = \Gamma(\sigma_T + \epsilon\sigma_L) = \Gamma\sigma_T(1+\epsilon R) \tag{1.11}$$

where $R \equiv \sigma_L/\sigma_T$ and the polarization parameter ϵ is defined as follows:

$$\epsilon \equiv \left(1 + 2\frac{\nu^2+Q^2}{Q^2}tan^2\frac{\theta}{2}\right)^{-1} \tag{1.12}$$

while the virtual photon flux is given by:

$$\Gamma = \frac{\alpha K}{2\pi^2 Q^2}\frac{E'}{E}\frac{1}{1-\epsilon} \tag{1.13}$$

where $K = (W^2 - M^2)/2M$.

Formally, one can define the scaling structure functions also in the low Q^2 region:

$$\begin{aligned} F_1(x,Q^2) &= MW_1(x,Q^2) \\ F_2(x,Q^2) &= \nu W_2(x,Q^2) \end{aligned} \tag{1.14}$$

In the parton model in Bjorken limit ($Q^2 \to \infty$ and x is fixed) the scale dependence has to disappear:

$$\begin{aligned} F_1(x,Q^2) &\to_{Q^2\to\infty} \mathfrak{F}_1(x) = \frac{1}{2x}\mathfrak{F}_2(x) \\ F_2(x,Q^2) &\to_{Q^2\to\infty} \mathfrak{F}_2(x) \end{aligned} \tag{1.15}$$

Through this thesis we will use GeV as the energy units, degrees for measuring angles and cross sections are given in mbn/ster/GeV, if not differently specified.

1.2 Two pictures of the proton structure

Despite the fact that the proton structure has been studied since the 50ths, nowadays one can observe two separate frameworks suited for different kinematic regimes. Although similar names for the proton constituents are used, those objects in fact have quite different properties in each approach; moreover, involved calculation techniques developed to handle different physical quantities do not allow a simple transition from one approach to the other. Most promising tentatives to describe both regions within one fundamental model based on computer simulations of basic processes are still far from the shape required for a complete understanding of the undergoing dynamics.

1.2.1 First scenario, a soup of current quarks

The first approach based on the Standard Model is the fundamental one; it operates with basic particles, the "current" quarks, pointlike, structureless and almost massless (their masses are so much less than proton mass that 98% of the latter has dynamic origin in this approach).

Bjorken Limit

The scaling behavior of the nucleon structure functions had been predicted by Bjorken in 1969 starting from current algebra. The idea of this effect is that, in the limit of $\nu, Q^2 \to \infty$ and $x = Q^2/2M\nu$ fixed (Bjorken limit), the structure functions do not depend on Q^2 (Bjorken scaling):

$$\begin{aligned} MW_1(x, Q^2) &\to \mathfrak{F}_1(x) \\ \nu W_2(x, Q^2) &\to \mathfrak{F}_2(x) \end{aligned} \tag{1.16}$$

In a series of experiments performed at SLAC the Bjorken scaling was confirmed (see Fig. 1.2).

Within the impulse approximation, the Quark Parton Model (QPM) describes DIS by the incoherent elastic scattering of the virtual photon off the quark as shown in Fig. 1.3.

One of the crucial assumptions here, the impulse approximation, implies that the target nucleon is essentially "frozen" during the short time in which the hard scattering took place; the quarks behaved as if they were free particles, i.e. no mutual interaction occurring between them during this time. Therefore, since this fast scattering does not disturb the nucleon structure, all the information about the internal nucleon interaction can be directly extracted from the quark impulse distribution.

Further, the experimental fact that quarks have spin $\frac{1}{2}$ led Callan and Gross to relate the two scaling structure functions:

$$\mathfrak{F}_2(x) = 2x\mathfrak{F}_1(x) \tag{1.17}$$

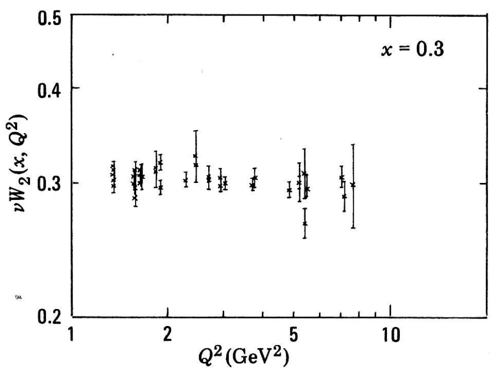

Figure 1.2: Structure function $\nu W_2(x, Q^2)$ at fixed x ($x \simeq 0.3$) measured at SLAC .

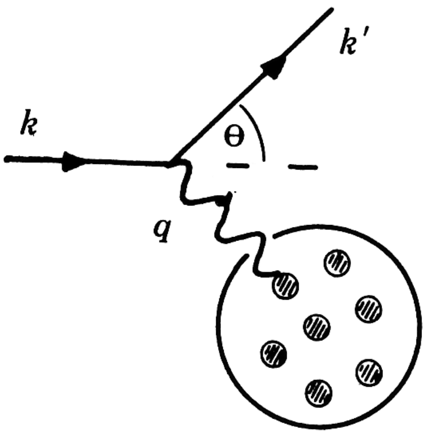

Figure 1.3: QPM picture of DIS.

Thus, since two scaling structure functions are linked by Eq. 1.17 it is conventional to study only one of them, namely $\mathfrak{F}_2(x)$.

Following the intuitive QPM picture of DIS one can express the proton structure function in a form:

$$\mathfrak{F}_2(x) = \sum_i e_i^2 x q_i(x) \tag{1.18}$$

where $q_i(x)$ is the probability of finding a quark of flavor i with fraction x of the proton momentum, e_i is the charge of the quark of flavor i and the sum runs over all valence and sea quark flavors. For instance in a four-quark model (u, d, s, c) in Leading Order (LO) one gets [3]:

$$\mathfrak{F}_2(x) = \frac{5}{18}x\Sigma(x) + \frac{1}{6}x\Delta(x) \tag{1.19}$$

where

$$\begin{aligned} \Sigma(x) &\equiv u(x) + \bar{u}(x) + d(x) + \bar{d}(x) + s(x) + \bar{s}(x) + c(x) + \bar{c}(x) \\ \Delta(x) &\equiv u(x) - d(x) + \bar{u}(x) - \bar{d}(x) + c(x) - s(x) + \bar{c}(x) - \bar{s}(x) \end{aligned} \tag{1.20}$$

and u and d distributions include both valence and sea quark contributions, $u(x) = u_v(x) + u_s(x)$ and $d(x) = d_v(x) + d_s(x)$, respectively.

Thus, Eq. 1.19 gives a possibility to directly connect the structure function $\mathfrak{F}_2$, measurable in DIS, with quark momentum distributions $q_i(x)$ (a combined analysis of lepton and neutrino DIS allows to separate flavor contributions).

But this simplified, intuitive, picture of DIS agrees with the experiment in a very limited kinematic domain only. The domain of Bjorken scaling is limited from both sides on Q^2:

1. *Small* Q^2 region ($Q^2 < 2$ GeV^2) does not satisfy the impulse approximation, and one has to take into account interactions between quarks inside the nucleon even during the time of the virtual photon scattering. Masses of hadrons become comparable with the value of Q^2 and the target mass corrections are necessary. Furthermore, the rising of nucleon resonance bumps results in extremely fast changes of the structure function in a small x-range around these states.

2. At *large* Q^2 ($Q^2 > 10$ GeV^2) the probability of gluon emission increases rapidly, leading to suppression of the "hard" ($x \sim 1$) quark component and consequently growth of the "soft" ($x \sim 0$) quark contribution (see Fig. 1.5 and Fig. 1.6).

In the following, we will describe these limitations in more detail, and concentrate on the small Q^2 region as a main topic of our interest.

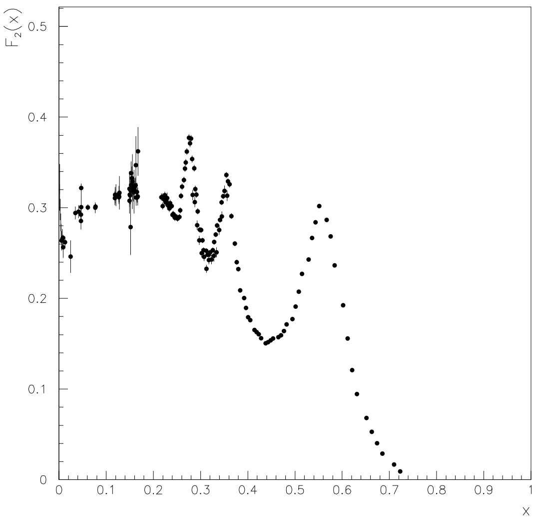

Figure 1.4: Structure function $F_2(x, Q^2)$ measured at fixed $Q^2 = 0.76$ GeV^2. The peaks situated in the high x region represent resonance contribution.

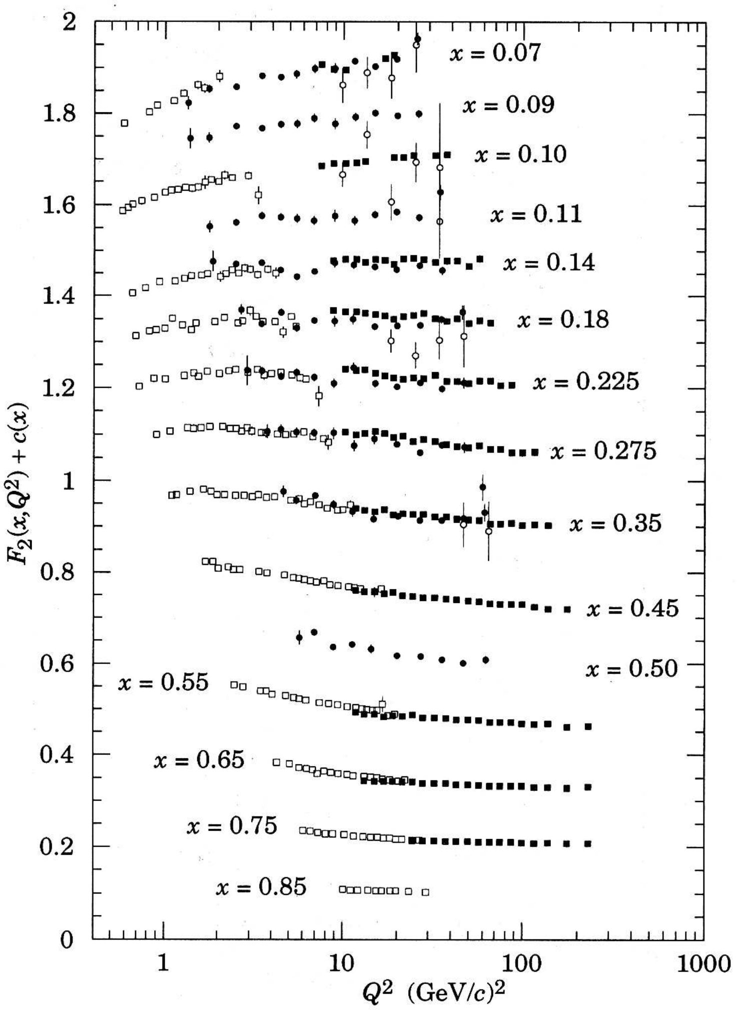

Figure 1.5: Structure function $F_2(x, Q^2)$ in DIS.

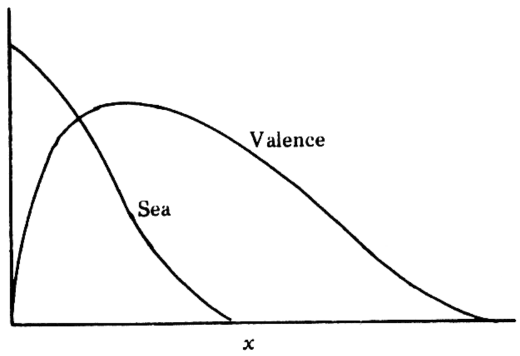

Figure 1.6: Separation between sea and valence quarks in QCD.

Large Q^2, logarithmic scaling violation

In the intuitive approach to asymptotic freedom one imagines that by increasing Q^2 of the virtual photon or equivalently by probing the inner structure of the proton at smaller distances one can resolve the quark into a quark and a gluon, the gluon into a quark-antiquark pair or into two gluons. These three basic processes are shown in Fig. 1.7. In a more quantitative level the evolution of the quark-gluon density obeys to the famous Altarelli-Parisi (AP) equation, which at LO of pQCD for the flavor non-singlet quark density, related to the valence quark contribution, has a form:

$$\frac{dq^{NS}(x,Q^2)}{d\ln Q^2} = \frac{\alpha_s(Q^2)}{2\pi}\int_x^1 \frac{yd}{y} q^{NS}(y,Q^2) P_{qc}(\frac{x}{y}) \tag{1.21}$$

where the splitting functions P_{qc} determine the probability for a quark to radiate a gluon such that the quark's momentum is reduced by a fraction z. For the singlet densities, related to the sea quark and gluon contributions, the AP equation is more sophisticated since mixing can occur between the gluon and singlet quark operators:

$$\frac{d}{d\ln Q^2}\begin{pmatrix} q^S(x,Q^2) \\ G(x,Q^2)\end{pmatrix} = \frac{\alpha_s(Q^2)}{2\pi}\int_x^1 \frac{dz}{z}\begin{pmatrix} P_{qq}(z) & N_f P_{qG}(z) \\ P_{Gq}(z) & P_{GG}(z)\end{pmatrix}\begin{pmatrix} q^S(\frac{x}{z},Q^2) \\ G(\frac{x}{z},Q^2)\end{pmatrix} \tag{1.22}$$

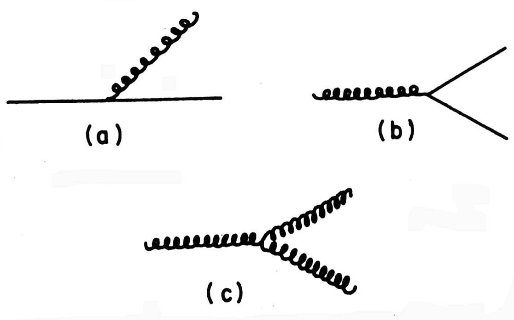

Figure 1.7: Basic processes of QCD.

The splitting functions are simply inverse Mellin transforms of the anomalous dimensions $\gamma_0^{n,ij}$:

$$\int_0^1 dz z^{n-1} P_{ij}(z) = -\frac{1}{4}\gamma_0^{n,ij} \tag{1.23}$$

where indexes i and j could be a quark flavor q or a gluon G. Eq. 1.21 leads to the following expression for the non-singlet structure function:

$$\frac{d\mathfrak{F}^{NS}(x,Q^2)}{d\ln Q^2} = \frac{\alpha_s(Q^2)}{2\pi}C_2(F)\left\{\left[\frac{3}{2}+2\ln(1-x)\right]\mathfrak{F}^{NS}(x,Q^2)+\right. \tag{1.24}$$
$$\left.\int_x^1 \frac{dz}{(1-z)}\left[(1+z^2)\mathfrak{F}^{NS}(\frac{x}{z},Q^2)-2\mathfrak{F}^{NS}(x,Q^2)\right]\right\}$$

The second term in Eq. 1.25 is negative for all x while the first term is positive for $x > 0.53$. For a typical non-singlet distribution the two terms cancel for $x \simeq 0.2$ and so scaling occurs (see Fig. 1.2).

1.2.2 Second scenario, three constituent quarks

The second approach is more phenomenological and describes the proton as built up from three "constituent" quarks. The latter ones could be imagined as fundamental current quarks which had absorbed some part of the interaction dynamics to form objects that appear massive, obviously structured and weakly interacting. In fact, most part of the interaction created their masses and the remaining weak fraction could be easily parametrized by a confining potential plus some direct interaction among them. This phenomenological approach can describe quite well physical quantities not accessible in PQCD due to calculation difficulties; even lattice simulations are presently not so successful in this region to be competitive with constituent quark models. This gives an indication that the transition from DIS regime to small Q^2 and large x could really create these massive weakly interacting objects absorbing most of QCD dynamics in their internal structure, whose investigation becomes therefore an important issue.

Nucleon resonances

Non-relativistic and relativistic three-quark models [4, 5] of baryons to describe the spectrum of excited baryon states and their couplings giving an intuitive picture of the baryon structure at non-perturbative scale. These models are designed to explain dynamics of constituent quarks, which have quite different properties with respect to "current" quarks explored in DIS. The constituent quark could be imagined as a complex object containing a "current" quark dressed by a cloud of virtual gluons and $q\bar{q}$-pairs. The cloud here is involved to absorb all non-perturbative effects of soft gluon emission, correlation with the sea etc., while remaining interaction mechanisms are parametrized in the frame of simple confining potential plus an "hyperfine" interaction between constituent quarks responsible for direct interaction of current quarks.

The baryon in such a model is described by an Hamiltonian of the following form:

$$H = \sum_{i=1}^{3} m_i + H_0 + H_{hyp} \tag{1.25}$$

where H_0 is the Hamiltonian of three uncorrelated constituent quarks in a flavor independent confining potential V_{conf}:

$$H_0 = \sum_{i=1}^{3} \frac{p_i^2}{2m_i} + V_{conf} \tag{1.26}$$

m_i are the constituent quark masses, which in fact are parameters of the model. The potential is a function of the relative quark separation:

$$V_{conf} = \sum_{i<j} V_{conf}^{ij}(r_{ij}) \tag{1.27}$$

which depending on model could be chosen either harmonic or of other forms giving reasonable description of the observed energy separation between different SU(6) multiplets. For instance, in model [5] the potential can be written in the form:

$$V_{conf}^{ij}(r_{ij}) = \frac{1}{2} k r_{ij}^2 + U(r_{ij}) \tag{1.28}$$

where in addition to the harmonic oscillator component $1/2kr_{ij}^2$ the anharmonicity U_{ij}, which is treated as a perturbation, has been introduced.

The most important term in Eq. 1.25 is the color hyperfine interaction H_{hyp} involved to explain spectrum and properties of excited baryon states; the choice of this term is rather ambiguous, but in principle can be justified aposteriori by a comparison of the obtained spectrum against the measured one The approach proposed first by N. Isgur [5] describes the hyperfine interaction term in the following form:

$$H_{hyp} = \sum_{i<j} \frac{2\alpha_s}{3m_i m_j} \left[\frac{8\pi}{3} (\vec{S}_i \cdot \vec{S}_j) \delta^3(\vec{r_{ij}}) + \frac{1}{r_{ij}^3} \left(\frac{3(\vec{S}_i \cdot \vec{r_{ij}})(\vec{S}_j \cdot \vec{r_{ij}})}{r_{ij}^2} - (\vec{S}_i \cdot \vec{S}_j) \right) \right] \tag{1.29}$$

the first term here is called Fermi contact term and operates only when the quark pair (ij) has zero angular momentum, while the second term often called the tensor term is operative only in states with nonzero orbital momentum between quarks i and j.

Eq. 1.29 in fact represents the familiar Breit Hamiltonian describing in QED the interaction of two magnetic dipoles $\vec{\mu_1}$ and $\vec{\mu_2}$ separated by a distance $\vec{r}$:

$$H_{QED} = -\frac{8\pi}{3} (\vec{\mu_1} \cdot \vec{\mu_2}) \delta(\vec{r}) + \frac{1}{r^3} \left[(\vec{\mu_1} \cdot \vec{\mu_2}) - \frac{3(\vec{r} \cdot \vec{\mu_1})(\vec{r} \cdot \vec{\mu_2})}{r^2} \right] \tag{1.30}$$

The spin-orbit coupling which in principle also has to contribute to the Hamiltonian was neglected; this lack of significant spin-orbit forces, mostly derived from the comparison of the calculations with experimental data [5], could be explained either by an highly anomalous origin of the quark-gluon color magnetic moment or by their cancellation with the Thomas precession term which has opposite sign.

The masses of the excited baryons have been calculated by solving Schrodinger equation $H\Psi = E\Psi$ and evaluating eigenvalues of this Hamiltonian. There are of course parameters like the unperturbated energy E_0 and the overall strength δ of the hyperfine interaction which cannot be calculated. These were fixed using experimental ground states masses, while the constituent quark masses were chosen to be $m_u = m_d = 0.33$ GeV and $m_s = 0.55$ GeV in order to give proper nucleon mass and reasonable values for baryon magnetic moments.

In zeroth order in the anharmonic perturbation U and hyperfine perturbation H_{hyp}, the introduction of the Jacobi coordinates:

$$\begin{aligned} \vec{\rho} &\equiv (\vec{r_1} - \vec{r_2})/\sqrt{2} \\ \vec{\lambda} &\equiv (\vec{r_1} + \vec{r_2} - 2\vec{r_3})/\sqrt{6} \end{aligned} \tag{1.31}$$

separates the Hamiltonian into two independent three-dimensional oscillators with well known spectrum and set of eigenfunctions:

$$\psi_{00} = \frac{\alpha_\rho^{3/2}\alpha_\lambda^{3/2}}{\pi^{3/2}} \exp\left[-\frac{1}{2}(\alpha_\rho^2\rho^2 + \alpha_\lambda^2\lambda^2)\right] \tag{1.32}$$

The solutions of the complete Hamiltonian 1.25 can be factorized in a product of the zeroth order eigenfunctions ψ_{00} and functions related to the hyperfine and anharmonic perturbation $\tilde{\psi}^{xy}$:

$$\psi_{lm}^{xy} = \tilde{\psi}_{lm}^{xy}\psi_{00} \tag{1.33}$$

The calculations taking into account the mixing between different states are in a good agreement with the experimental baryon mass spectrum (see Fig. 1.8). The main problem in this description is that many states predicted by the model were not observed; this could be explained either by strong suppression of such states by some dynamical reasons or due to additional limitations on the number of degree of freedom like constraints of the diquark model [6].

These models are suitable to describe not only mass spectrum, but also resonance decay amplitudes; the calculations of electro-magnetic decay amplitudes were most successful due to the fact that meson wave functions are not so well known as the photon one.

The Hamiltonian of the electromagnetic interaction of the system of three nonrelativistic quarks with the photon can be written in the following form:

$$H^{em} = \sum_i H_i^{em} = -\sum_i \left\{ \frac{e_i}{2m_i}[\vec{p_i} \cdot \vec{A}(\vec{r_i}) + \vec{A}(\vec{r_i}) \cdot \vec{p_i}] + \vec{\mu_i} \cdot [\vec{\nabla} \times \vec{A}(\vec{r_i})] \right\} \tag{1.34}$$

where $\vec{\mu_i} = e_i\vec{\sigma_i}/2m_i$ is the magnetic moment of the i-th quark, e_i, m_i, $\vec{\sigma_i}/2$, $\vec{p_i}$ are its charge, (constituent) mass, spin and momentum, and $\vec{A}$ is the photon field. For the sake of simplicity one can reduce H_{em}, exploiting the overall symmetry of the wave functions (without color component), to interaction with the third quark only $H^{em} \rightarrow 3H_3^{em}$.

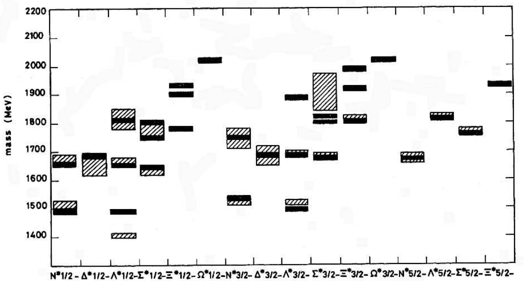

Figure 1.8: Comparison of the predicted and observed spectrum of negative-parity baryons. The shaded regions correspond to the likely mass of resonances; the solid bars are the predictions of Isgur and Karl model [5].

Therefore, in this approximation the T-matrix element of the process $B \to B'\gamma$ can be calculated using known baryon wave functions as follows:

$$< B'(p's')\gamma(K\lambda)|T|B(ps) >= -\frac{3ie}{(2\pi)^{3/2}}\left\langle B'(p's')\gamma(K\lambda)\right|\frac{e_3}{e}\left[\frac{\vec{\sigma_3}\cdot(\vec{K}\times\vec{\epsilon^\star})}{2m}+i\frac{\vec{p'_3}\cdot\vec{\epsilon^\star}}{m}\right]e^{-i\vec{K}\cdot\vec{r_3}}\left|B(ps)\right\rangle \tag{1.35}$$

where $\vec{\epsilon}(K\lambda)$ is the photon polarization vector, e_3, $\vec{\sigma_3}/2$ and $\vec{r_3}$ are charge, spin and position of the third quark and $\vec{p'_3}$ is the momentum of the third quark in B'.

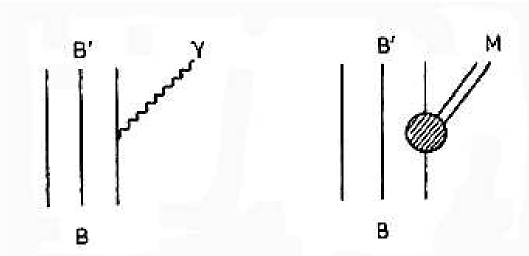

Figure 1.9: A baryon photon and meson emission diagrams.

Summarizing one can notice that many different constituent quark models are capable of reproducing the mass spectrum of the baryons reasonably well, while electromagnetic and strong coupling predictions are quite diverse. These differences could be used for a separation between models based on experimental data: this is essentially true for electromagnetic couplings which imply less model dependent comparison to experiment since the photon wave function is well known. Unfortunately, the experimental evaluation of the electromagnetic coupling amplitudes is extremely difficult and model dependent in case of high lying excited states due to the complexity of the dominant decay channels.

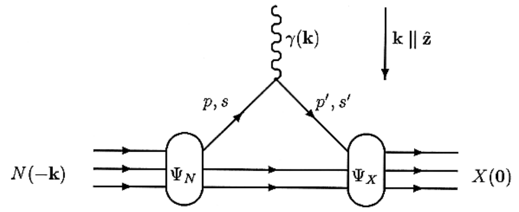

Figure 1.10: The impulse approximation for the electromagnetic interaction implied by all constituent quark models. The idea is that quarks are free and distributed according to the bound-state wave functions while interacting with photon.

Precocious scaling: small Q^2 and hadron-parton duality

The scaling behavior of the inclusive cross section turns out to be approximately satisfied even at values of Q^2 and ν in the 1 GeV range [8] (*precocious scaling*).

Since in this kinematic region the mass of the nucleon is not negligible $Q^2 \sim M^2$ the contamination of this purely kinematic effect should be separated and removed from the analyzed moments and structure functions. Fortunately, it was found possible to extend the explicit predictions of QCD down to low Q^2 if the right variable is used [1]: this variable can be written as:

$$\xi = \frac{2x}{1 + \sqrt{1 + 4x^2M^2/Q^2}} \tag{1.36}$$

Another interesting feature of data, observed by Bloom and Gilman, called electroproduction duality, relates the Q^2 dependence of the nucleon pole and prominent nucleon resonances to the asymptotic (scaling) structure function $\mathfrak{F}_2(\xi)$. Of course, the resonances themselves do not scale since the conventionally defined transition form-factors necessarily involve a certain mass scale M^2, but the average $\int F_2(\xi, Q^2)d\xi$ still follows the asymptotic structure function $\int \mathfrak{F}_2(\xi)d\xi$ down to $Q^2 \sim 0.5$ GeV^2 (see Fig. 1.11). Furthermore, duality appears to be local, in the sense that even average of separated resonance bumps obey the scaling behavior (see Fig. 1.12 and Fig. 1.13).

In both interpretations (comparison of $\mathfrak{F}_2^{exp}$ with its asymptotic behavior or with theoretical $\mathfrak{F}_2(\xi)$ extrapolated to low Q^2) duality seems to relate the structure function in the non-perturbative region to its perturbative value and therefore to current quarks. This conclusions appears in contradiction with the resonance analysis where the structure function behavior seems to be mostly determined by constituent quarks and their interactions. A physical description of duality consistent with the constituent quark picture (as attempted in Ref. [11]) its presently needed for a better understanding of the electromagnetic interactions in hadrons at low Q^2.

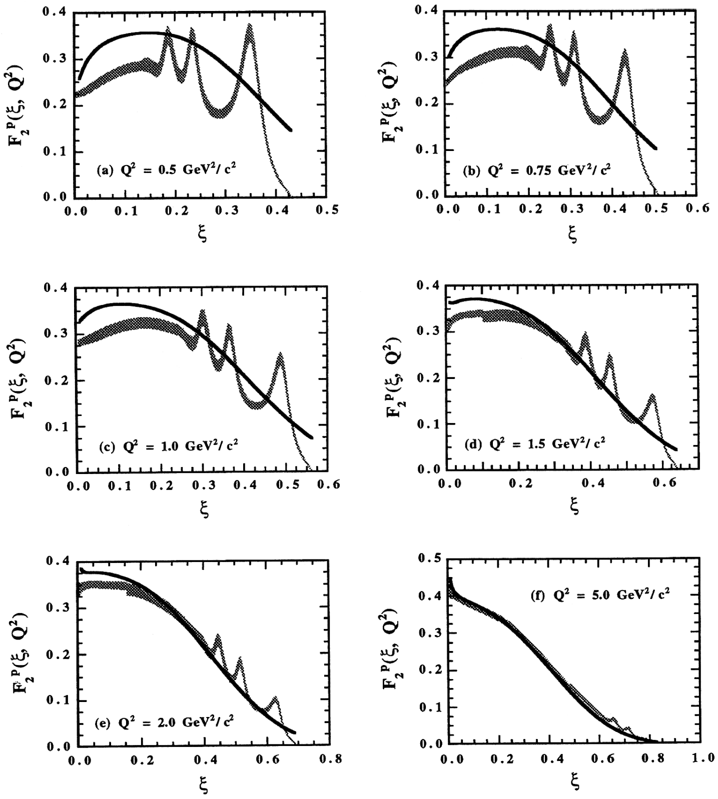

Figure 1.11: A comparison of quasi-data obtained from fit [7] with pQCD predictions fitted to data in DIS and extrapolated by using AP equation (see Eq. 1.21) to low Q^2 region.

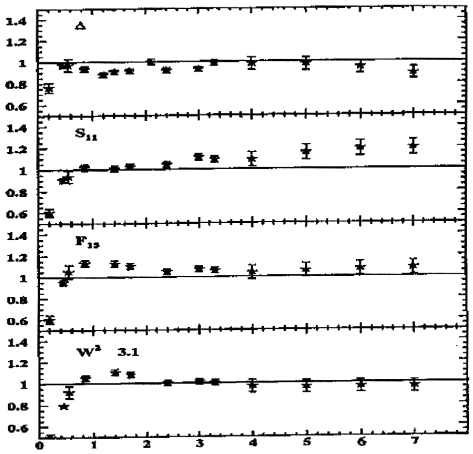

Figure 1.12: The ratio of the strength around the prominent resonance peaks in a limited range of ξ to the strength obtained from the experimental scaling structure functions taken at $Q^2 = 10$ GeV^2 in the same ξ interval [9].

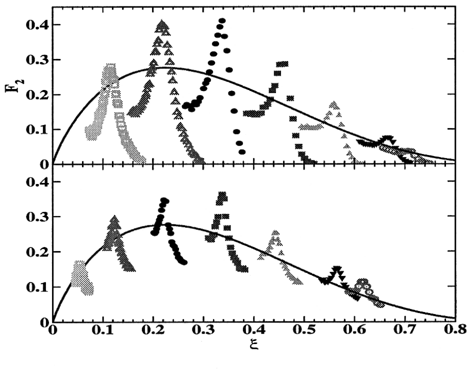

Figure 1.13: F_2 data in the regions $1.2 < W^2 < 1.9$ GeV^2 (top) and $1.9 < W^2 < 2.5$ GeV^2 (bottom); the solid line represents the scaling curve, determined by averaging all nucleon resonance data [10].

1.3 OPE approach

In the moment space the Operator Product Expansion (OPE), described hereby, gives an interpretation of the data in terms of current quarks and their interactions (higher twists), which is somewhat intermediate between the two approaches reported in section 1.2.

1.3.1 Twist Expansion and Multiparton Correlations

In general, the matrix element for DIS to a final state f can be written as (see Fig. 1.14):

$$iM_{ep\to ef} = (-ie)u(k')\gamma_\mu u(k)\frac{-i}{q^2}(ie)\int d^4x e^{iqx} < f|J^\mu(x)|P > \qquad (1.37)$$

where $J^\mu(x)$ is the quark electromagnetic current.

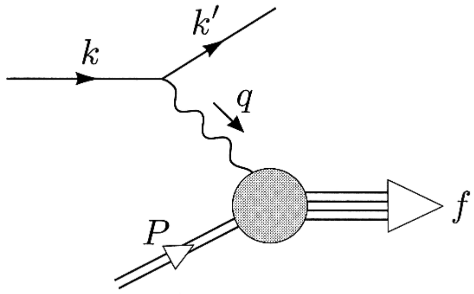

Figure 1.14: Picture of DIS.

This matrix element should be squared and summed over all possible final states. The leptonic part in Eq. 1.37 could be easily calculated in QED, while the remaining virtual photon-hadron scattering amplitude is given by:

$$M_{\gamma p\to f} = (ie)\epsilon_\mu(q)\int d^4x e^{iqx} < f|J^\mu(x)|P > \qquad (1.38)$$

The optical theorem as shown in Fig. 1.15 gives:

$$2\text{Im } M_{\gamma p\to\gamma p} = \sum_f \int d\prod_f |M_{\gamma p\to f}|^2 \qquad (1.39)$$

Substituting $M_{\gamma p\to f}$ by the r.h.s. of Eq. 1.38 one can transcript Eq. 1.39 in the following way:

$$2\text{Im } M_{\gamma p\to\gamma p} = (ie)^2\epsilon^*_\mu(q)\epsilon_\nu(q)\sum_f \int d\prod_f < P|J^\mu(x)|f >< f|J^\nu(0)|P > \qquad (1.40)$$

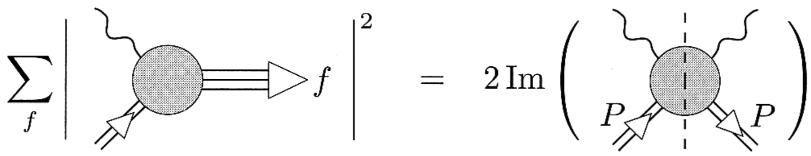

Figure 1.15: Application of the optical theorem.

or in other words:

$$2\text{Im } M_{\gamma p\to\gamma p} = (ie)^2\epsilon^*_\mu(q)\epsilon_\nu(q)i\int d^4xe^{iqx} < P|T\{J^\mu(x)J^\nu(0)\}|P > \tag{1.41}$$

The Operator Product Expansion (OPE) [13] gives a possibility to compute a product of two non-local operators separated by a small distance $x \to 0$ as a decomposition over a basis of local operators:

$$O_1(x)O_2(0) \overset{x\to 0}{\longrightarrow} \sum_n C^n_{12}(x)O_n(0) \tag{1.42}$$

where coefficients $C^n_{12}(x)$ are c-number functions.

Applying OPE to the virtual photon-nucleon scattering amplitude one can obtain the expansion of the time ordered products of hadronic currents having small light-cone separation:

$$iT\{J(x)J(0)\} \overset{x\to 0}{\longrightarrow} \sum_{\tau=2k}^{\infty}\sum_{n=0}^{\infty} C_{\tau,n}(x^2,\mu^2)x^{\mu_1}\cdots x^{\mu_n}O^\tau_{\mu_1\cdots\mu_n}(\mu^2) \tag{1.43}$$

The relation between amplitude and product of currents was derived in the unphysical kinematic region; in order to relate the amplitude obtained in Eq. 1.40 to DIS observables one can employ a dispersion integral in the following form (dropping indexes μ and ν for simplicity):

$$M_{\gamma p\to\gamma p}(q^2,\nu) = 4\int_{-q^2/2M}^{\infty}\frac{d\nu'\nu'}{\nu'^2-\nu^2}W(q^2,\nu') \tag{1.44}$$

or changing variables:

$$M_{\gamma p\to\gamma p}(q^2,x) = \sum_{n=2k}^{\infty}\left(\frac{1}{x}\right)^n\int_{-1}^{1} dx'x'^{n-1}W(q^2,x') \tag{1.45}$$

Combining Eq. 1.42 and Eq. 1.44 one gets:

$$\int_{-1}^{1} dx x^{n-1} W(q^2, x) = \frac{1}{4} \sum_{n=2k}^{\infty} C_{\tau,n}(Q^2, \mu^2) O^{\tau}_{\mu_1 \cdots \mu_n}(\mu^2) \left(\frac{1}{Q^2}\right)^{\frac{\tau}{2}-1} \tag{1.46}$$

This allows the description of the complete Q^2 evolution for the moments of the nucleon structure functions as [12]:

$$M_n^{CN}(Q^2) = \int_0^1 dx x^{(n-2)} \mathfrak{F}_2(x, Q^2) = \sum_{\tau=2k}^{\infty} E_{n\tau}(\mu, Q^2) O_{n\tau}(\mu) \left(\frac{\mu^2}{Q^2}\right)^{\frac{1}{2}(\tau-2)} \tag{1.47}$$

where $k = 1, 2, \ldots$, $M_n^{CN}(Q^2)$ is the n-th Cornwall-Norton [14] moment of the (asymptotic) structure function for a massless nucleon $\mathfrak{F}_2(x, Q^2)$; μ is the renormalization scale (about 1 GeV), $O_{n\tau}(\mu)$ is the reduced matrix element of operators with definite spin n and twist τ (dimension-spin), related to the non-perturbative structure of the target; $E_{n\tau}(\mu, Q^2)$ is a dimensionless coefficient function describing small distance behavior, which can be perturbatively expressed as a power expansion of the running coupling constant $\alpha_s(Q^2)$. The advantage of this expansion is that a measurement of the Q^2-evolution of the moments allows a direct separation of the "hard" parton dynamics (Wilson coefficients $E_{n\tau}(\mu, Q^2)$), which could be studied in the frame of pQCD, from all non-perturbative processes (local operators $O_{n\tau}(\mu)$), which are up to now far beyond any theoretical predictions.

At Q^2 values comparable with M_p, the moments still contain non-negligible mass dependent terms that produce in Eq. 1.46 further M_p^2/Q^2 power corrections (kinematic twists). To avoid these terms, the moments $M_n^{CN}(Q^2)$ of the massless $\mathfrak{F}_2$ have to be replaced in Eq. 1.46 by the corresponding Nachtmann [1] moment $M_n^N(Q^2)$ of the measured structure function $F_2^{exp}(x, Q^2)$ since:

$$\begin{aligned} M_n^{CN}(F_2(x, Q^2)) &\equiv \int_0^1 dx x^n \mathfrak{F}_2(x, Q^2) = M_n^N(F_2^{exp}(x, Q^2)) \equiv \\ &\int_0^1 dx \frac{\xi^{n+1}}{x^3} F_2(x, Q^2) \frac{3 + 3(n+1)r + n(n+2)r^2}{(n+2)(n+3)} \end{aligned} \tag{1.48}$$

where

$$\begin{aligned} r &\equiv \sqrt{1 + 4\frac{M^2 x^2}{Q^2}} \\ \xi &\equiv \frac{2x}{1+r} \end{aligned} \tag{1.49}$$

Further, the total moment can be expressed as:

$$M_n(Q^2) = \mu_n(Q^2) + \text{higher twists} \tag{1.50}$$

where the leading twist ($\tau = 2$) contribution $\mu_n(Q^2)$ consists of singlet and non-singlet parts:

$$\mu_n(Q^2) = \mu_n^S(Q^2) + \mu_n^{NS}(Q^2) \tag{1.51}$$

The latter can be computed in NLO with the well known perturbative logarithmic Q^2 evolution of singlet and non-singlet moments:

$$\begin{aligned}
\mu_n^{NS}(Q^2) &= a_n^{NS}\left[\frac{\alpha_s(Q^2)}{\alpha_s(\mu^2)}\right]^{\gamma_n^{NS}} \frac{1+\alpha_s(Q^2)R_n^{NS}/4\pi}{1+\alpha_s(\mu^2)R_n^{NS}/4\pi} \\
\mu_n^{S}(Q^2) &= a_n^{-}\left[\frac{\alpha_s(Q^2)}{\alpha_s(\mu^2)}\right]^{\gamma_n^{-}} \frac{1+\alpha_s(Q^2)R_n^{-}/4\pi}{1+\alpha_s(\mu^2)R_n^{-}/4\pi} + a_n^{+}\left[\frac{\alpha_s(Q^2)}{\alpha_s(\mu^2)}\right]^{\gamma_n^{+}} \frac{1+\alpha_s(Q^2)R_n^{+}/4\pi}{1+\alpha_s(\mu^2)R_n^{+}/4\pi}
\end{aligned} \tag{1.52}$$

where the functions R_n can be found in Ref. [15]; and the running coupling constant $\alpha_s(Q^2)$ at NLO is given by

$$\alpha_s(Q^2) = \frac{4\pi}{\beta_0 \ln(Q^2/\Lambda^2_{\overline{MS}})}\left\{1 - \frac{\beta_1}{\beta_0^2}\frac{\ln\ln(Q^2/\Lambda^2_{\overline{MS}})}{\ln(Q^2/\Lambda^2_{\overline{MS}})}\right\} \tag{1.53}$$

and $\Lambda^2_{\overline{MS}}$ is the QCD scale in the $\overline{MS}$ scheme, $\beta_0 = 11 - 2N_f/3$, N_f being the number of active flavors and $\beta_1 = 102 - 38N_f/3$. The singlet moment coefficients $a_n^{\pm}$ can be also written as follows:

$$\begin{aligned}
a_n^{+} &= (1-b_n)\mu_n^S(\mu^2) + c_n\mu_n^G(\mu^2) \\
a_n^{-} &= b_n\mu_n^S(\mu^2) - c_n\mu_n^G(\mu^2)
\end{aligned} \tag{1.54}$$

where $\mu_n^G = \int_0^1 dx x^{n-2} G(x, Q^2)$ is the Cornwall-Norton moment of the gluon distribution function $G(x, Q^2)$. At large x limit, since quark and gluons are decoupled, one has $b_n \sim 1$ and $c_n \sim 0$ already for $n \geq 4$. Moreover in that limit $\gamma_n^- \simeq \gamma_n^{NS}$ and $R_n^- \simeq R_n^{NS}$ [15] and therefore the evolution of the leading twist singlet moments $\mu_n^S(Q^2)$ of order $n \geq 4$ almost coincide with that of the non-singlet ones $\mu_n^{NS}(Q^2)$. Therefore, in the case of the second moment one has three unknown leading twist parameters a_2^{NS} and $a_2^{\pm}$, while for $n \geq 4$ the number of parameters can be reduced to one $a_n^{(2)} \equiv \mu_n^{NS}(Q^2) + \mu_n^S(Q^2)$. These parameters have to be determined by a comparison to experimental data at large Q^2, where higher order corrections and dynamical higher twists can be considered negligible.

If, however, one wants to go down in Q^2 as much as 0.5 GeV^2, where $\alpha_s(Q^2)$ becomes large, one should estimate the effect of higher order terms within the perturbative expansion of the coefficient function $E_{n\tau}(\mu, Q^2)$ in Eq. 1.47. To this end, two existing phenomenological approaches can be employed: one of these deals with infrared (IR) renormalons [16], another one uses soft gluon resummation technique [17].

In the first method the perturbative series is affected by the so-called IR-renormalon ambiguities. More precisely, the only way to interpret consistently the large order behaviour of the perturbation theory leads unavoidably to ambiguities *which have the general form of power-suppressed terms.* This happens because certain classes of high-order radiative corrections to the twist 2 (the so-called fermion bubble chains) are sensitive to large distances (i.e. to the non-perturbative domain). Nevertheless it should be stressed that the IR-renormalon contribution to the twist-2 has to cancel against the ultraviolet quadratic divergencies of twist-4 operators. This means that each twist in the expansion Eq. 1.47 is not defined unambiguously, while the entire sum (i.e. complete calculation) is free from ambiguities. Therefore, while the data cannot be affected by IR-renormalon uncertainties, the fitting procedure, based on the separation among various twists and on the theoretical perturbative treatment of the leading twist only, can suffer from IR-renormalon ambiguities.

Within the naive non-abelianization approximation the contribution of the renormalon chains (i.e. the sum of vacuum polarization insertions (fermion loops) on the gluon line at one-loop level as shown in Fig. 1.16).

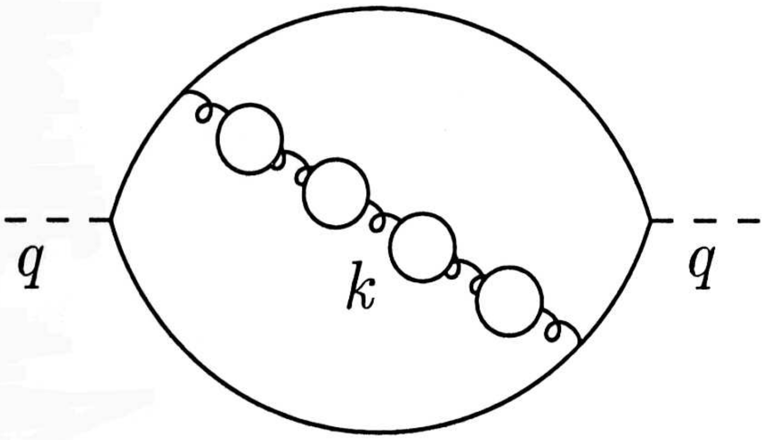

Figure 1.16: Example of the "bubble" diagram related to the renormalon which consist of all diagrams with any number of fermion loops inserted into a single gluon line.

The IR-renormalon contribution to the non-singlet moments is explicitly given by

$$\mu_n^{IR(NS)}(Q^2) = \mu_n^{NS}(Q^2)\left\{\frac{A_2^{IR}}{Q^2}\tilde{C}_2(n) + \frac{A_4^{IR}}{Q^4}\tilde{C}_4(n)\right\} \tag{1.55}$$

and coefficients are [18]:

$$\begin{aligned}
\tilde{C}_2(n) &= -n - 8 + \frac{4}{n} + \frac{2}{n+1} + \frac{12}{n+2} + 4S_n \\
\tilde{C}_4(n) &= \frac{1}{2}n^2 - \frac{3}{2}n + 16 - \frac{4}{n} - \frac{4}{n+1} - \frac{36}{n+3} - 4S_n
\end{aligned} \tag{1.56}$$

where $S_n = \sum_{i=1}^{n-1}(1/i)$. The signs of parameters A_2^{IR} and A_4^{IR} are not known, because they depend upon the prescription used to circumvent the renormalon singularities of the Borel integrals, while their absolute values are given by [16]:

$$\begin{aligned} A_2^{IR} &= \frac{6C_F\Lambda^2_{\overline{MS}}}{33-2N_f}e^{5/3} \\ A_4^{IR} &= \frac{3C_F\Lambda^4_{\overline{MS}}}{33-2N_f}e^{10/3} \end{aligned} \tag{1.57}$$

$C_F = 4/3$ gives $|A_2^{IR}| \simeq 0.13 \div 0.10$ GeV^2 and $|A_4^{IR}| \simeq 0.30 \div 0.15$ GeV^4 for the number of flavors $N_f = 3, 4$, respectively.

Eq. 1.55 describes the contribution of IR renormalons to the non-singlet structure functions, while the more involved case of the singlet parts of the DIS structure functions has been recently investigated in Ref. [19]. There is has been shown that the difference between the IR-renormalon contributions to the singlet and non-singlet moments is not relevant for $n \geq 4$ thanks to the quark-gluon decoupling at large x. Therefore, for $n \geq 4$ it suffices to consider only non-singlet contribution to the leading twist in Eq. 1.51.

As for the second moment one can simplify the analysis by taking only the non-singlet IR-renormalon contribution, i.e. by totally neglecting its singlet part. This approximation was found to be quite good in Ref. [18].

The IR-renormalon terms have to be added to the definition of the leading twist:

$$\tilde{\mu}_n^{S,NS}(Q^2) = \mu_n^{S,NS}(Q^2) + \mu_n^{IR(S,NS)}(Q^2) \tag{1.58}$$

IR-renormalon corrections cannot contribute in any form to the higher twist contribution which contains a genuine multiple field correlation, and which depends therefore on the exact internal hadron wave function. To show that one can assume that the same structure functions $F(x, Q^2)$ are measured for different hadrons and that the lowest-order leading twist $M_n^{twist-2}$ and $1/Q^2$ parts $M_n^{twist-4}$ can be separated experimentally; then the renormalon contribution cancels for the difference of ratio of moments:

$$\left.\frac{M_n^{twist-4}}{M_n^{twist-2}}\right|_{hadron1} - \left.\frac{M_n^{twist-4}}{M_n^{twist-2}}\right|_{hadron2} \tag{1.59}$$

while it is still sensitive to the genuine higher-twist contribution, which depends on the exact specific internal hadron wave function.

The second method is based on all-order summation of soft gluon emission contribution to pQCD calculations, performed at some finite order of running coupling constant $\alpha_s(Q^2)$ (i.e. LO, NLO and so on). The method employs a computation of multi-gluon emission amplitude, which in the soft limit fulfill generalized factorization formulas given in terms of process independent single-gluon emission probability (see Fig. 1.17). Thus, soft gluon radiation obtained at LO and NLO can be exponenziate in moment space for the large N-moments (corresponding to $x \to 1$) to all orders in perturbation theory.

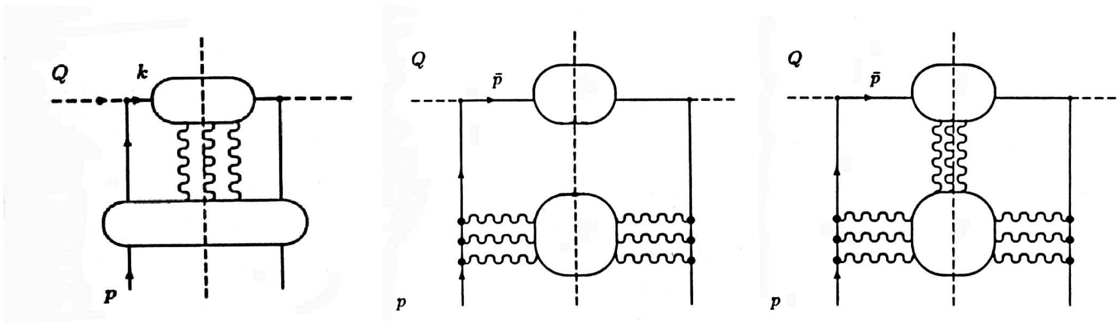

Figure 1.17: Picture of simplest soft gluon emission by an interacting quark in DIS: in general kinematic configuration (a), in the semi-inclusive limit (b) and the case of only collinear divergences (c) (three gluon lines are due to flavor conservation).

Practically instead of the pure NLO leading twist contribution one has:

$$\mu_n^{(SGR)}(Q^2) = \mu_n^{(NLO)}(Q^2) * r_n(Q^2) \tag{1.60}$$

where the ratio of the quark coefficient function calculated within SGR and NLO is given by

$$r_n(Q^2) = \frac{(1 + \frac{\alpha_s(Q^2)}{2\pi} C_{DIS}^{(NLO)}) e^{G_n(Q^2)} + \frac{\alpha_s(Q^2)}{2\pi}(C_n^{(NLO)} - C_{DIS}^{(NLO)} - C_{n,LOG}^{(NLO)})}{1 + \frac{\alpha_s(Q^2)}{2\pi} C_n^{(NLO)}} \tag{1.61}$$

here the most important quantity of the soft gluon resummation is described by the function:

$$G_n(Q^2) = \int_0^1 dz \frac{z^{n-1} - 1}{1 - z} \left\{ \frac{1}{2} B[\alpha_s(Q^2(1-z))] + \int_{Q^2}^{Q^2(1-z)} \frac{dq^2}{q^2} A[\alpha_s(q^2)] \right\} \tag{1.62}$$

and $A[\alpha_s] = C_F \alpha_s/\pi + C_F K (\alpha_s/\pi)^2/2$, $B[\alpha_s] = -3C_F\alpha_s/2\pi$ with $K = C_A(67/18 - \pi^2/6) - 10T_R N_f/9$, $C_A = N_c \to 3$, $T_R = 1/2$ and

$$\begin{aligned} C_n^{(NLO)} &= C_{DIS}^{(NLO)} + C_{n,LOG}^{(NLO)} + O(1/n) \\ C_{DIS}^{(NLO)} &= C_F[\gamma_E^2 + \frac{3}{2}\gamma_E - \frac{9}{2} - \frac{\pi^2}{6}] \\ C_{n,LOG}^{(NLO)} &= C_F \ln n [\ln n + 2\gamma_E + \frac{3}{2}] \end{aligned} \tag{1.63}$$

and γ_E is Euler-Mascheroni constant. One can write the function $G_n(Q^2)$ in a more convenient form

$$G_n(Q^2) = G_1(\lambda_n) \ln n + G_2(\lambda_n) + O[\alpha_s^k \ln^{k-1}(n)] \tag{1.64}$$

with $\lambda_n \equiv \beta_0 \alpha_s(Q^2) \log n/4\pi$ and

$$G_1(\lambda) = C_F \frac{4}{\beta_0 \lambda}[\lambda + (1-\lambda)\ln(1-\lambda)] \tag{1.65}$$

$$G_2(\lambda) = -C_F \frac{4\gamma_E + 3}{\beta_0} \ln(1-\lambda) - C_F \frac{8K}{\beta_0^2}[\lambda + \ln(1-\lambda)] + C_F \frac{4\beta_1}{\beta_0^3}[\lambda + \ln(1-\lambda) + \frac{1}{2}\ln^2(1-\lambda)]$$

Both approaches show the importance of higher order corrections for high moments at small Q^2.

For higher twist, $\tau > 2$, power terms $O_{n\tau}(\mu)$ are related to quark-quark and quark-gluon correlations, as illustrated by Fig. 1.18, and should become important at large x and small Q^2. In a phenomenological analysis they can be written [20, 18] in the simplified form, limited to twist 4 and 6:

$$M_n(Q^2) = \mu_n(Q^2) + a_n^{(4)} \left[\frac{\alpha_s(Q^2)}{\alpha_s(\mu^2)}\right]^{\gamma_n^{(4)}} \frac{\mu^2}{Q^2} + a_n^{(6)} \left[\frac{\alpha_s(Q^2)}{\alpha_s(\mu^2)}\right]^{\gamma_n^{(6)}} \frac{\mu^4}{Q^4} \tag{1.66}$$

where $\mu_n(Q^2)$ is the leading twist including renormalon or soft gluon resumation, and the parameters $a_n^{(4)}$, $a_n^{(6)}$ and $\gamma_n^{(4)}$, $\gamma_n^{(6)}$ represented the strength and the anomalous dimensions of the higher twist terms, related to multiparton correlation effects, can be directly extracted from our data analysis.

Therefore, a systematic analysis of Q^2 dependence of the experimental Nachtmann moments $M_n^N(F(x,Q^2))$ in the intermediate Q^2 range ($0.5 < Q^2 < 10\ GeV^2$) should therefore allow separation of twist two and higher twist terms in the nucleon structure function.

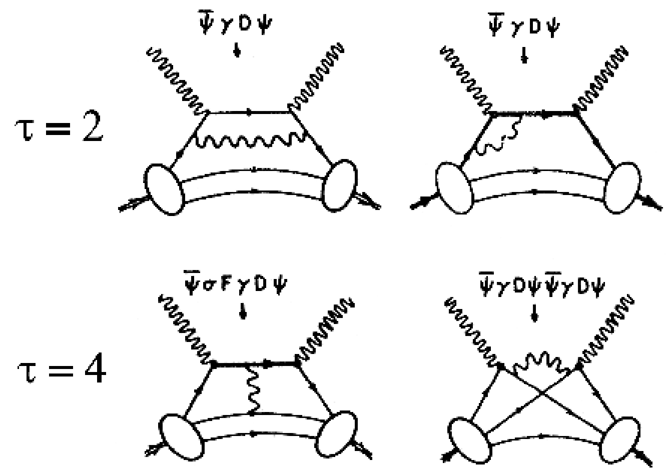

Figure 1.18: Twist diagrams.

Chapter 2

Experimental Apparatus

The main purpose of the Jefferson Laboratory facility is the basic research in intermediate energy and nuclear physics using electromagnetic probes. Presently most of the available knowledge is essentially limited to the electromagnetic structure of the nucleon as explored in inclusive experiments and to the lowest excited states of the baryonic spectrum. Moreover, kinematic range accessible in those experiments is not sufficient for evaluation of an integrated values such as moments of the structure function.

The reasons of this limitation can be found in the technical characteristics of previous accelerator facilities and detector equipments. The low duty cycle of several existing electron accelerators makes coincidence experiments difficult. In fact the measurements are limited to the narrow kinematic regions were a sufficient ratio of real-accidental coincidences can be obtained. In addition the standard equipment used at electron accelerator is based on magnetic spectrometers that, in spite of a high resolution ($dp/p \sim 10^{-4}$), cover small solid angles (10^{-3} of 4π) and small momentum range ($\Delta p/p \sim 10\%$). These characteristics allow precise measurements in a limited kinematic range but prevents from detecting many particles final states that would require a large acceptance. Finally experiments in which the luminosity is limited by external factor as beam intensity or target density are practically ruled out.

The solution to these problems is represented by large acceptance spectrometers that used in conjunction with high duty cycle electron beams allow the study of exclusive reactions, characterized by multi-particle final states, as well as inclusive and semi-inclusive ones in wide kinematic region simultaneously taken in one experiment.

2.1 Accelerator

The Continuous Electron Beam Accelerator Facility is based on superconducting (RF) cavities operated in continuous wave (CW) mode. A plan of the machine is shown in Fig. 2.1. Electrons, emitted by the injector with energy about 40 MeV, are accelerated by two linacs, connected on both ends by a set of five recirculating arcs. The accelerating power in each linac is supplied by 40 niobium cavities separated into 8 cryomodules, cooled with liquid helium. The cavities operate at a minimum gradient of 5 MeV per meter and at a frequency of 1.497 GHz. For each turn an electron receives a boost of approximately 1 GeV, allowing a maximum energy of 6 GeV after 5 passes.

The beam can be delivered simultaneously into three experimental Halls (Hall A, Hall B and Hall C). Because of the RF frequency of the niobium cavities the beam is structured in microbunches, separated by approximately 0.67 ns. They are delivered sequentially to the experimental Halls. The microbunches can be accelerated to different energies by recirculating them through a different number of passes so that the beam in the Halls can be at different multiples of the one pass energy. In addition the bunches can be loaded with different electron densities to provide independent beam currents in each Hall. The three beams are finally separated at the switchyard and delivered to the experimental areas with a separation between the closest bunches of 2.04 ns. Due to the reduced synchrotron radiation, the energy spread in the beam is approximately $\Delta E/E \sim 10^{-4}$. The accelerator can deliver beam currents ranging from 100 pA to 100 μA.

At present the performances of the machine are significantly above the original specification and a maximum energy of 5.7 GeV has already been reached and maintained in normal operation. The end stations are equipped with spectrometers for complementary experimental programs:

1. Hall A is equipped with two High Resolution Spectrometers (HRS) with $\Delta p/p \leq 10^{-4}$ and maximum momentum of 4 GeV, instrumented for electron and hadron detection.

2. Hall C contains two magnetic spectrometers of medium resolution with $\Delta p/p \leq 10^{-3}$ but different maximum momenta: the High Momentum Spectrometer (HMS) and the Short Orbit Spectrometer (SOS) have respectively maximum momenta of 7 GeV/c and 1.8 GeV/c.

3. Hall B houses the CEBAF Large Acceptance Spectrometer dedicated to exclusive multi-particle final state measurements.

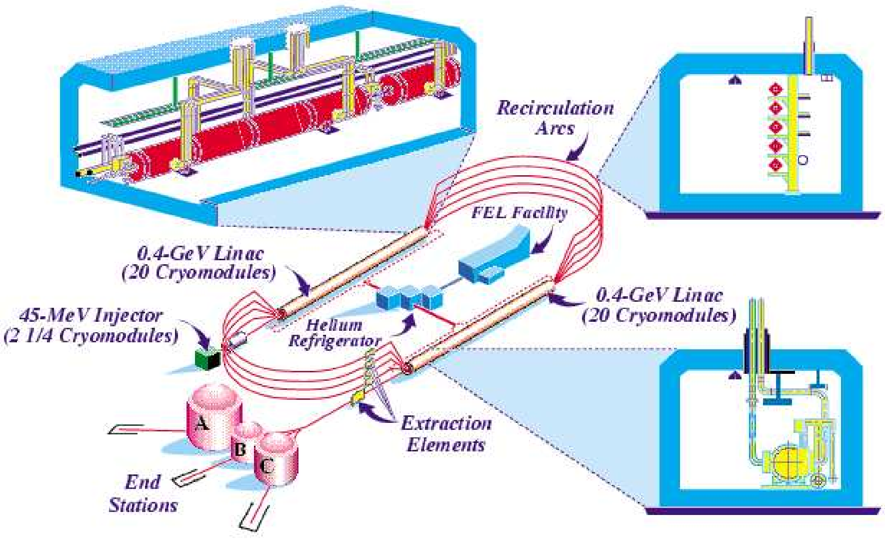

Figure 2.1: The CEBAF accelerator site.

2.2 Detector

The CLAS (**C**EBAF **L**arge Acceptance **S**pectrometer) spectrometer in Hall B has in fact been designed for experiments in which the final hadronic states are characterized by several uncorrelated particles and the luminosity is limited by beam, target or accidental background.

CLAS is a magnetic toroidal multigap spectrometer in which the magnetic field is generated by six superconducting coils (see Fig. 2.2). The particle detection system is based on drift chambers (DC) for the track reconstruction of charged particles, Cerenkov counters (CC) for electron identification, scintillation counters (TOF) for the trigger and for time of flight measurements, and electromagnetic shower calorimeters (EC) to identify electrons and to detect photons and neutrons. The six segments are instrumented individually to form six independent spectrometers and cover symmetrically 2/3 of the azimuthal angle ϕ around the beam line.

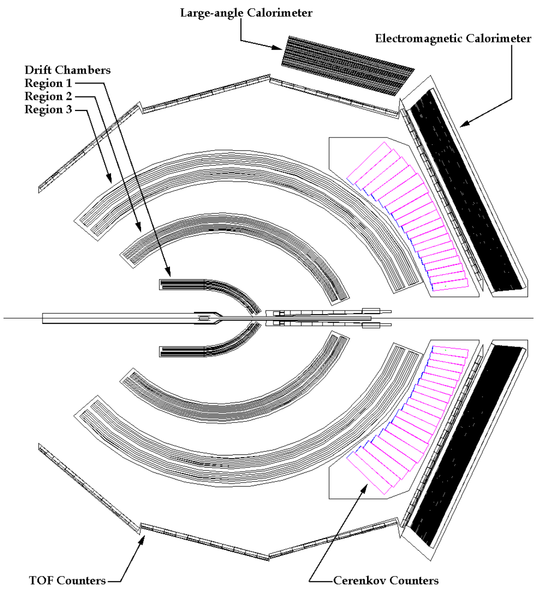

Figure 2.2: Schematic drawing of the CLAS detector showing a section along the beamline.

2.2.1 Torus System

CLAS is a magnetic spectrometer based on six super-conducting coils arranged around the beam line to produce a field primarily in the ϕ-direction [21]. The choice of this configuration has been driven by the necessity of satisfying precise requirements determined by the physics program:

1. Homogeneous coverage of a large angular and momentum range for charged and neutral particles.

2. Good momentum and angular resolution; due to the Lorentz boost, the average momentum increases with decreasing emission angle and the relative $\Delta p/p$ has to improve in the forward direction to maintain the absolute resolution constant.

3. Good particle identification.

4. High luminosity and counting rate capability: typical luminosity is $\sim 10^{34}$ cm^{-2}s^{-1}.

5. Low background from electromagnetic processes (Moller electron, e+e- pairs etc).

6. Azimuthal symmetry.

7. Compatibility with the operation of a polarized target.

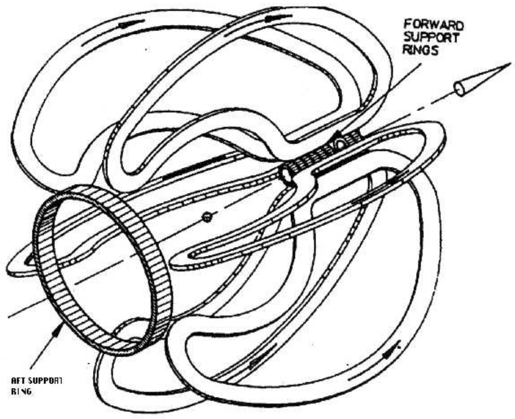

Figure 2.3: Configuration of the torus coils.

The toroidal setup in comparison with the more common solenoid and dipole configuration offers a field free region around the target and a magnetic field that is always transverse to the particle trajectory. The first characteristic allows the installation of a polarized target with no interference between the target and detector magnetic fields. In addition, since the ϕ-pattern of the event is preserved, the determination of ϕ is decoupled from the measurement of the polar angle θ and momentum p. A drawing of the torus system is shown in Fig. 2.3.

The six coils operate with a maximum current of 3860 A and have been shaped to give the desired magnetic field and therefore the requested resolution as a function of polar angle θ. The coil-operating temperature of 4.5 K is maintained by a forced flow of supercritical liquid helium supplied by the Central Helium Liquefier (CHL). The absence of strong field close the beam axis helps in limiting the electromagnetic background since forward-going charge particles (e+e- pairs) are not deflected, while low momentum particles emitted at large angle (Moller electron) can be easily screened by an additional magnetic field.

2.2.2 Drift Chambers

The measurement of the charged particle momentum and trajectory is accomplished by a DC system [22, 23]. The principle of operation of a drift chamber is the collection of the electrons produced through ionization of a gas by a charged particle that crosses it. The gas is maintained in an electric field so that the electron and ion created by ionization drift in opposite directions and are collected by the anode and cathode, respectively. While drifting, the electron can produce secondary ionization resulting in a multiplication and therefore amplification process. The detection of the corresponding electric signal gives information on the hit position of the original charged particle.

The CLAS tracking system consists of eighteen multi-wire drift chambers subdivided in three regions in each of the six sectors. Region 1 is a low magnetic field region located in the free space left inside the toroidal magnet, region 2 is a high magnetic field region placed within the large toroid while region 3 is located beyond the outer coil of the magnet. The wires are strung in the azimuthal direction and therefore perpendicular to the bend plane of the particle trajectories. The track position along these wires is measured by the "stereo" wires that are canted by $6.5°$ in respect to the previous ones called "normal" wires. Each chamber is wedge-shaped and is subdivided in two separate superlayers, one normal and one stereo. Each superlayer consist of six layers of sense wires surrounded by normal wires in an hexagonal arrangement as shown in Fig. 2.4. Guard wires are located at the borders of each superlayer and their potential is adjusted to simulate the electric field configuration of an infinite grid of hexagonal cells.

This configuration has been chosen because it offers a good independence from the entrance angle and is therefore well suited for this application since tracks are entering from widely varying angles. This design leads to maximum drift distances of 0.7 cm, 1 cm, 2 cm respectively in the three regions.

The gas used in DC is $90\% \div 10\%$ mixture of Argon and CO_2. The Argon provides a gain of $\sim 10^4$ while CO_2 is necessary to avoid the occurrence of uncontrolled ionization avalanches. The intrinsic resolution provided by this gas is ~ 100 μm. The final space resolution achieved in operating condition is ~ 500 μm, mostly limited by the knowledge of the geometry and time dependence of the calibration parameter. The resulting momentum resolution is $\sim 0.5\%$ for low momentum and 1.5% for high momentum tracks.

The use of small wire diameters and low wire tension makes possible the design of thin end plates that maximizes the solid angle coverage. The use of thin foil entrance windows minimizes multiple scattering. The total amount of material ranges between 0.1 and 0.4 radiation lengths. Circuit boards that provide pulse shaping and discrimination are mounted on the endplates, while the electronics that perform timing and readout for the data acquisition is lodged in external crates.

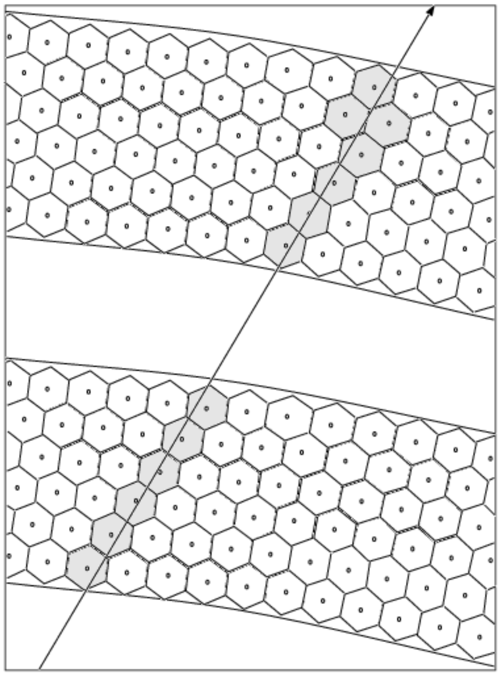

Figure 2.4: Scheme of a DC section, showing the two superlayers each consisting of 6 hexagonal-cells layers. The cells are electrostatic boundaries determined by field wires located at each corner of the hexagon. The guards wires (not shown) surround each superlayer. A charged particle is shown crossing the drift chambers, with the shaded area indicating the hit cells.

2.2.3 Cerenkov Counters

In electron scattering experiments the main source of background is represented by negative pions. For this reason CLAS is equipped with threshold Cerenkov counters that have the function of discriminating between electrons and pions [24]. Charged particles crossing a medium with velocity that is higher than the local phase velocity of light emit radiation known as Cerenkov light. The threshold at which this process occurs is given by $\beta = 1/n$ where n is the refraction index of the medium.

The gas adopted for the CLAS Cerenkov system is perfluorbutane C_4F_{10} that has a refraction index of 1.00153. This leads to a threshold for the particle energy of $E > \gamma m$, where $\gamma = 18.09$ and m is the mass of the particle. This results in a threshold for electrons of approximately 9 MeV, in comparison to the pion threshold of ~ 2.5 GeV. Above this particle energy the electromagnetic calorimeters become the fundamental tool for electron identification.

The Cerenkov light is collected by a system of mirrors and focused toward the photomultiplier tubes. Due to the symmetry of the CLAS toroidal magnet, the azimuthal angle of the scattered particles remains almost unchanged through the magnetic field. This allows the design of a mirror system that focuses the light from particles with different azimuthal angles and fixed polar angle to a point near the coil. The focal area is equipped with an array of photomultipliers, placed in the shadow of the torus coils, with a sensitivity to single photoelectrons.

Monte Carlo simulations were used to study and identify the best geometrical configuration for the mirrors and the results is shown in Fig. 2.5. Simulations and measurements indicate that the average number of photoelectrons collected is about seven giving a theoretical maximum inefficiency of 1×10^{-3}.

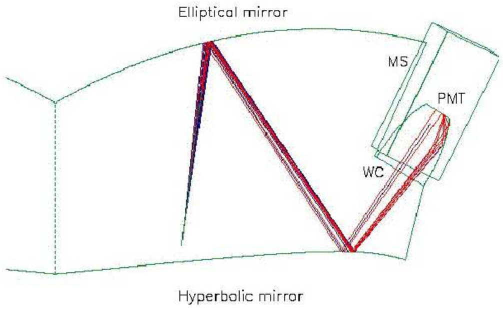

Figure 2.5: Optical arrangement of one of the 219 modules of the CLAS Cerenkov detector showing the optical and light collection components. The PMTs lie in the ϕ region hidden by the torus coils.

2.2.4 Electromagnetic Calorimeter

CLAS is equipped with 8 modules of electromagnetic shower calorimeter that serve three main functions:

1. Detection and trigger of electrons at energies above 0.5 GeV.
2. Detection of photons at energies above 0.2 GeV, allowing π^0 and η reconstruction from the measurements of their 2γ decays.
3. Detection of neutrons, with discrimination between photon and neutrons using the time-of-flight technique.

Six of the eight modules are located in each sector in the forward region, covering the polar angles from 10 to 45 degrees (Forward Angle Calorimeter), while the remaining two modules are placed in sector 1 and 2 covering from 50 to 75 degrees (Large Angle Calorimeter).

Forward Angle Calorimeter

The forward detector consists of six sampling calorimeters made of alternating layers of scintillator strips and lead sheets with a total thickness of 16 radiation lengths [25]. A lead÷scintillator thickness ratio of 0.2 was used, requiring 40 cm of scintillators and 8 cm of lead per module. With this configuration, approximately 1/3 of the energy of a shower is deposited in the scintillator.

The choice of readout granularity was a compromise between size constraints and resolution requirements, leading to a cell size of 10 cm. In order to match the hexagonal geometry of CLAS, the lead-scintillator sandwich has the shape of an equilateral triangle. The sandwich is made of 39 layers, each consisting of a 10 mm BC-412 scintillator followed by a 2.2 mm thick lead sheet. To minimize shower leakage and dispersion in arrival times, a "projective" geometry, in which the area of each successive layer increases, was used.

Each scintillator layer is made of 36 strips parallel to one side of the triangle, with the orientation of the strips rotated of 120 degrees in each successive layer. Thus there are three orientations or views each containing 13 layers which provide stereo information on the location of the energy deposition. Each view is further subdivided in an inner (5 layers) and outer (8 layers) stack, to provide longitudinal sampling of the shower for improved hadron identification.

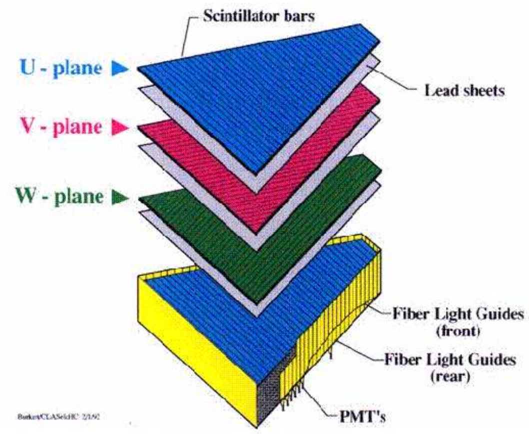

Figure 2.6: Exploded view of one of the six CLAS electromagnetic calorimeter modules.

A fiber-optic light readout system transmits the scintillator light to the PMTs. Their signal is sent to ADC and TDC boards that are then read by two FastBus crates. The forward calorimeter provides the main mean of discrimination between electrons and pions for momenta above 2 GeV. For this reason this detector is included in the electron trigger. The detector performances in running condition have shown that the position resolution estimated is approximately $\sigma \sim 2.3$ cm. This was estimated comparing the position reconstructed from the analysis of the EC signal and the projection of the associated track on the calorimeter plane. The energy resolution for electrons shown by the data is $\sigma/E = 0.003 + 0.093/\sqrt{E}$ (the energy is expressed in GeV) with a sampling fraction, i.e. the fraction of the shower energy collected by the active part of the detector, of ~ 0.27.

Neutrals hits in the EC are identified by the absence of a matched DC track. Neutral pions are identified requiring two neutral hits whose reconstructed energies combine to give the mass of a π^0. The data have shown a resolution of $\delta m/m \sim 0.11-0.14$. Neutrons can be discriminated from photons thanks to the time resolution of the calorimeter. This has been evaluated to be 500-600 ps. The neutron detection efficiency has been estimated using the $p(e, e', \pi^+)n$ reaction in which the neutron can be reconstructed by missing mass. The data showed an efficiency that rises from zero at 0.4 GeV/c to a plateau of approximately 60% above 1.6 GeV/c, in agreement with the expectation based on nuclear interaction lengths and Monte Carlo simulations.

A more detailed description of the design, calibration and performances of this detector can be found in Ref. [25].

Large Angle Calorimeter

The two large angle EC modules (LAC) of CLAS are similar to the forward detectors [26]. In this case the modules are made of the lead-scintillator sandwich with a rectangular shape. They consist of 33 layers, each composed by a 0.20 cm thick lead foil and NE110A plastic scintillator bars with average width of 10 cm and constant thickness of 1.5 cm. The module thickness corresponds to 12.9 radiation lengths and 1.0 absorption lengths. Teflon sheets with 0.2 mm thickness separate scintillators from lead while 0.2 mm thick Teflon strips between each pair of contiguous scintillators bars avoid optical crosstalk. Each layer is rotated by 90° to form a 40·24 matrix of 10·10 cm^2 cells. The bar width increases going from the inner side towards the outer to guarantee the tapering required by the CLAS geometry. The surface exposed to particle fluxes is 217·400 cm^2. The module is vertically divided into an inner and an outer part to improve electron/pion discrimination. Scintillators lying (for the inner and outer part separately) one on top of the other with the same orientation form 128 different stacks.

The electromagnetic showers originate in the lead sheets and propagate through the layers: the energy absorbed in the active material produces a light pulse that is collected at both scintillator ends with a Lucite light guide coupled to scintillators with an air gap on a 7.0·0.4 cm^2 area. The collected light is summed for each stack separately before a EMI 9945A photomultiplier. Therefore the light pulses emitted from 8 different scintillators are summed up on a single photomultiplier that is placed on the top surface of the LAC module several centimeters away from the scintillators (see Fig. 2.7).

To reduce photocathode-non-homogeneity effects, the light guides are glued together before coupling to photomultiplier. Scintillators placed in the inner and the outer parts are coupled to different photomultipliers. Monte Carlo simulations showed that the LAC performances are strongly affected by the efficiency of light transmission and collection.

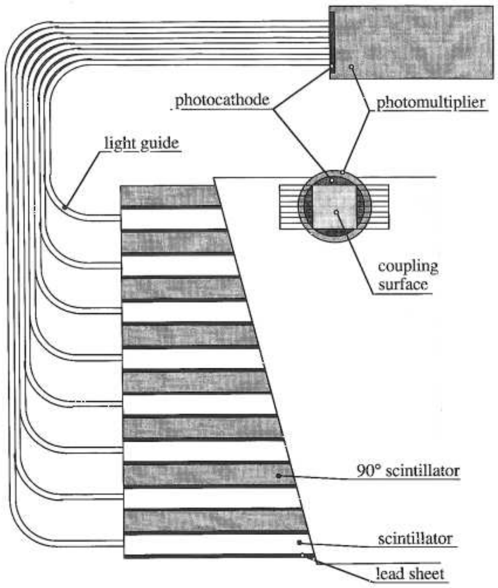

Figure 2.7: Light collection system for the CLAS Large Angle Calorimeter. The light pulse is collected at both scintillator ends with a Lucite light guide coupled to the scintillators. The collected light is summed for each stack separately before being transmitted to the PMTs.

For this reason, special attention was devoted to the production of high quality scintillators and light guides. In particular, scintillators with a light attenuation length longer than 300 cm and light guides that provide about 5 photoelectrons/MeV when coupled to a EMI 9945A PMT were selected.

2.2.5 Time of Flight System

CLAS is equipped with a system of scintillation counters whose purpose is to determine the time of flight for the charged particles and, in conjunction with the tracking system, the particle identification [27]. This detector was designed to ensure a good time resolution ($\sigma \sim 150$ ps) in particular at low polar angles since a large percentage of the scattered particles are emitted in the forward direction. This resolution is necessary to be able to discriminate pion and kaons with momenta up to 2 GeV/c. In addition the system was studied in order to match the typical rates expected for CLAS that with a luminosity of 10^{34} cm^{-2}s^{-1} can go up to 100kHz in the forward direction.

The time of flight system consists of scintillator strips (BC-408) that are located perpendicularly to the beam direction with an angular coverage of 2° each. The scintillators are located between the Cerenkov counters and the electromagnetic calorimeters. Each sector contains 48 strips with a uniform thickness of 5.08 cm. The width of the scintillators varies from 15 cm for the very forward angles to 22 for the large angles, while the lengths are between 30 and 450 cm.

With this design a coverage in the six sectors from 8 to 142 degrees was achieved, corresponding to a total area of the scintillator system of 206 m^2. Each scintillator strip is read by two photomultipliers that are located in the shadow of the torus coils. The light is transmitted to the PMTs by light guides.

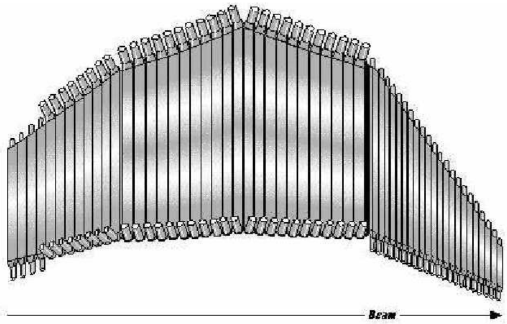

Figure 2.8: Scintillator strips of the Time of Flight system of the CLAS detector.

For each photomultiplier both the time and pulse height are measured. This allows the evaluation of the time-walk correction. In addition the measure of the pulse height allows the reconstruction of the energy released by the crossing particle, providing additional information for the particle identification. In relation to this feature, it is important to notice that for particle momenta below 500 MeV/c the energy resolution that characterizes the time of flight system is better than the resolution of the tracking system that for these low momenta is limited by multiple scattering.

Calibration with cosmic rays showed an intrinsic time resolution that varies from 80 ps for the forward angle up to 160 ps for the large angle strips. Real data were also used to study the time resolution of this system and, by comparing the interaction time reconstructed from the electron time of flight traced back to the vertex with the accelerator RF time, a resolution of $\sim$ 160 ps was found. This resolution is sufficient to separate, as requested, pion from kaons up to 2 GeV/c.

The time of flight signal can also be used to define the trigger: this possibility is exploited in photon runs to define hadron triggers.

2.2.6 Data Acquisition System and Event Trigger

The signals seen by the different detectors are recorded by the data acquisition when the event satisfies the chosen trigger condition. In electron scattering experiments with CLAS, the trigger is given by the detection of an electron in the final state. This condition is defined by a simultaneous hit in the Cerenkov counter and in the Electromagnetic calorimeter above a selected threshold. The thresholds used in the present case are reported in table 2.1. This loose condition allows the simultaneous measure of both inclusive and exclusive channels in a large W and Q^2 range.

Table 2.1: EC and CC trigger thresholds.

Detector	Threshold	
EC	150 mV	600 MeV
CC	38 mV	$<$ *1 photoelectron*

The CC threshold was below the single photoelectron peak in the PMTs to avoid the introduction of a bias. The EC threshold was chosen to maximize the accessible W range while maintaining a good electron versus pion selectivity. With this configuration approximately 60% of the recorded events contains an electron. The remaining 40% consists of events in which the trigger is due to noise in the Cerenkov Counters or to hadrons that, interacting with the detector structure, produce showers. These events are easily rejected in the event reconstruction process. A scheme of the Data Acquisition system is given in Fig. 2.9. The system was developed by the CODA group at Jefferson Lab and by the DAQ group of CLAS.

After passing the pre-trigger discriminators, the signals from the different detectors are sent to the Level-1 trigger that contains the final configuration of the Event Trigger. When these requirements are satisfied the data are sent to the Trigger Supervisor, which communicates with 17 FastBus crates. The data are therefore read out, converted to digital information and transferred through the ROC memory and the network to the Event Builder. The Event Recorder finally receives the information from Event Builder through the main Data Distribution shared memory. The data are written to a local disk to be later transferred to a tape silo for massive storage.

An online monitoring system is used to have continuous control on the status of the detector components and of the acquisition system. For this purpose events from the main Data Distribution system are transferred to a satellite computer where monitoring programs run during the data taking.

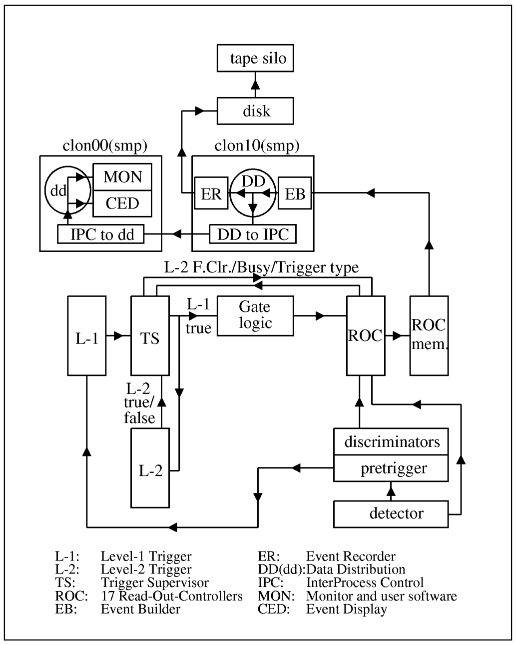

Figure 2.9: Schematic diagram of the DAQ Acquisition system.

2.3 Event Reconstruction

The CLAS event reconstruction code consists of several packages whose function is to analyze the information of the single detectors and combine them to obtain the complete determination of each physics event. Because of the complexity of the detector, the reconstruction process is subdivided into several steps. Initially the detector raw information (ADC and TDC values) is converted into the corresponding physical quantities (energy, time, etc.). All these information are then matched together to obtain the particles related variables (trajectory, time of flight, etc.). These quantities are finally analyzed to give the particle identification.

Both the input and output information of the reconstruction code are stored in BOS format. BOS is a Fortran-77 based dynamic memory management system [28]. The information in the BOS files is subdivided into "banks". A bank is a collection of data words formed by a "header" and a "body". The header provides the information on the number of columns and rows of the banks, the bank identifier and the location of the following bank. The body contains the real information. In the raw data files, each bank contains the information of a single detector or of a part of a detector.

These banks are elaborated during the reconstruction process to give the physical quantities. For example, the raw time of flight bank, that contains the ADC and TDC values for each PMT, is transformed into the reconstructed bank that contains the energy and timing information for each signal. The final output of the reconstruction is represented by few high level data banks that contain the four-vectors for each particle in the physics events and all the relevant information used in the physical analysis (live time, accumulated charge, etc.).

2.3.1 Data Processing

Detector Calibration

The first part of the data processing is represented by the detector calibration. In this preliminary phase, a selected sample of data ($\sim 10\%$ of the total) is processed to check the detector response. The data sample is chosen uniformly during the entire run period to verify the time stability. Both the energy and time calibration of each detector component are checked and the corresponding calibration constants are adjusted to give the correct behavior. This procedure is applied for each different run period to take into account the different running conditions, the hardware modification that may have occurred and the drift of the detectors response over time. The obtained results are checked monitoring the significant variables. When the reconstruction has reached to the desired level of accuracy the calibration constants are 'frozen' and the final data processing is performed.

Final Reconstruction Process

After the completion of the detector calibration, the full data processing is performed. The time required for the reconstruction of a single event is approximately 50-100 ms on a 600Mhz CPU, leading to a total time for the full processing that is $\sim$100 times larger than the corresponding data taking. This is a direct consequence of the complexity of the CLAS detector. Because of the large amount of data and the complexity of the reconstruction code, a particular care is dedicated to monitoring this process in order to identify any failure of the code or problem that may affect the data quality. This part of the process is also used to identify bad data files that are affected by hardware faults of the detector not seen at the time of the data taking. The outputs of the monitoring programs (trk_mon, pid_mon, sc_mon, rf_mon, scaler_mon, pdu_mon), for example number of tracks per sector, mean energy released by electrons in the calorimeters, etc., are saved together with the reconstructed data. An examples of monitoring histograms is shown in Fig. 2.10.

The result of the monitoring process are summarized in a database that is automatically updated during the data processing and can be browsed to perform an accurate selection of the "Gold" runs [29].

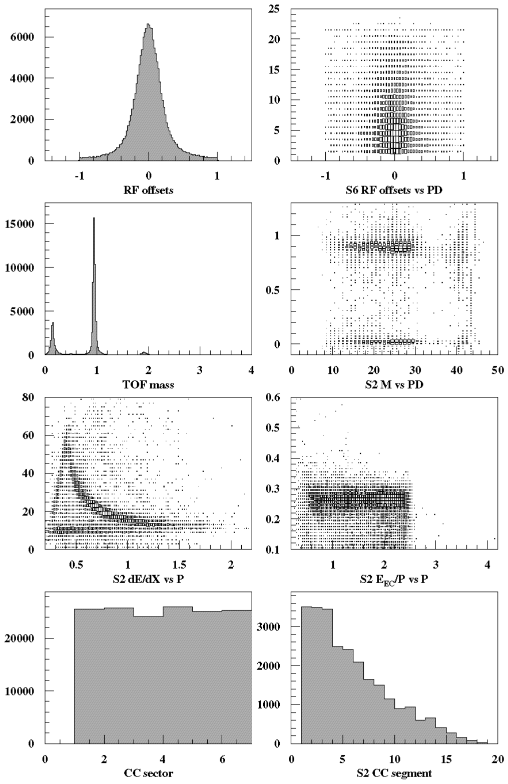

Figure 2.10: Sample of the monitoring histograms used to check the data quality. The top left plot shows the distribution of the RF correction. The same quantity is shown in the top right plot as a function of the TOF paddle in sector 6. The third and fourth plots are typical examples of the reconstructed hadron mass. The fifth plot shows the dE/dX versus momentum distribution reconstructed from EC, while the sixth plot represents the ratio between released energy and momentum for the primary electron. The bottom plots shows the number of hits in CC as a function of the CLAS sector and of the CC segment.

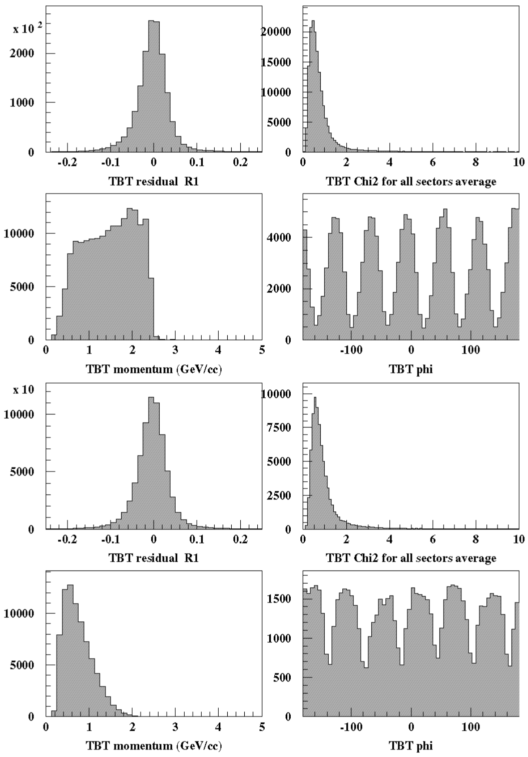

Figure 2.11: Sample of the monitoring histograms that are used to verify the quality of the tracking reconstruction. The top plots show the time base tracking residual (the distance between the measured and fitted hit position) and χ^2 for the primary electron, while the plots in the second row are a typical example of the momentum and ϕ distribution of the reconstructed electron candidates. The other plots represent the same quantities bu in the case of a proton candidate.

2.3.2 Tracking Reconstruction

The reconstruction of charged particle tracks is the most complex part of the reconstruction code. The tracking process is performed in two stages. In the first stage, individual tracks are fit only to the hit-wire position in a procedure known as "hit-base" tracking (HBT). In this part, tracking data are combined into track segments within the individual superlayers and these segments are then linked to form tracks across the three Regions within one sector. The segments finding procedure utilizes a dictionary of known segments that is generated from simulation. The same procedure is also used to link the segments to form a track: in this case a dictionary of tracks is used and the segments combination is considered a track candidate when a match for at least five superlayers is found. The candidate track is then fit using the cell centers as hit position to obtain the associated particle momentum. Due to the comparatively small size of the drift cells and the large number of wire layers, the track momenta can already be reconstructed with a resolution of 3% to 5%. Additional information on these tracks from the Cerenkov, time of flight and electromagnetic calorimeters, allows the determination of the identities and speeds of the charged particles.

In the second stage of the analysis, the drift time information is used to improve the tracking resolution. The particle time of flight from the target to the outer scintillators is used to correct the measured TDC times. A pre-determined table is then used to convert the corrected drift times to drift distances. These corrected track positions in each drift cells are fit in a procedure known as 'time based' tracking in order to determine the final track parameters.

The drift time is given by the following expressions:

$$t_{drift} = t_{start} + t_0 - t_{TDC} - t_{flight} - t_{prop} - t_{walk} \tag{2.1}$$

where t_{start} is the event start time, t_0 is the fixed time delay for the wire, t_{TDC} is the raw time measured by the TDC, t_{flight} is the flight time of the particle from the reaction vertex to the wire, t_{prop} is the signal propagation time along the wire, and t_{walk} is a time-walk correction made for short drift times due to different ionizations for slow and fast particles. The t_{TDC} is subtracted in the previous equation because the TDCs are operated in common stop mode[1]. All these parameters are fixed during the calibration of the drift chamber system. Through the use of an appropriate function, the drift time determines the distance of closest approach (DOCA) of the charge-particle track to the sense wire. However there remains an ambiguity regarding which side of the sense wire the track passed by. This "left-right ambiguity" is resolved within the individual superlayers by comparing the χ^2 values for the fit for all different combinations of the drift-distance sign. After the selection of the full set of drift-distance signs, a final fit results in improved track parameters.

[1] The start signal to the TDCs is provided from the individual wire hits, while the stop is provided by a delayed version of the CLAS trigger

2.3.3 Start Time Reconstruction

During electron scattering experiments in CLAS there is no direct measurement of the start time, i.e. the time when the interaction between the projectile and the target occurred. This information is derived indirectly by identifying the primary scattered electron in the event and reconstructing the event start time from its measured time of flight. The electron identification can in fact be performed independently from TOF information by analyzing the signal detected in the EC and CC, requiring the match with a negative track. As explained in section 2.2.6 these two detectors form in fact the electron trigger. When the electron is identified, its signal in TOF can be used as reference time and the path information provided by the tracking can be used to trace back the time of the interaction. The start time is given by the following expression:

$$t_{start} = t_{tof} - \frac{l}{\beta c} \tag{2.2}$$

where t_{tof} is the time corresponding to the electron signal in TOF, l is the path length of the electron track from the interaction vertex to the scintillators, and since the electrons are ultrarelativistic β is equal to 1. The resolution resulting from this method is affected by the intrinsic resolution of the TOF system. It varies from 80 ps to 160 ps moving from the forward angle to large angle strips, as reported in section 2.2.5.

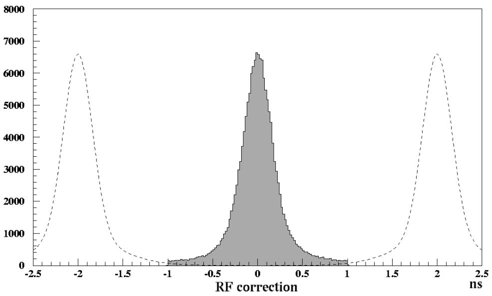

Figure 2.12: Time difference between the reconstructed start time from the TOF information and the accelerator RF signal. The TOF resolution is approximately 160 ps, resulting in the shown distribution. The use of the RF information allows the improvement of the start time definition. However, as indicated by the plot, there is a finite probability of assigning the electron to the wrong bunch since there is an overlap between the distributions of the close bunches. This overlap is anyhow less than 1%.

The determination of the start time can be improved exploiting the information of the RF structure of the electron beam. A signal synchronous with the arrival of the electron bunches is in fact recorded in the data stream. This signal has a period of ~2 ns corresponding to the time delay between to subsequent bunches. For an infinite TOF resolution, the start times reconstructed using Eq. 2.2 should correspond exactly to the arrival time of one of the electron bunches. Since the resolution is finite, the reconstructed start times gather around the RF signal with a width given by the TOF resolution (see Fig. 2.12). The time difference between the event-reconstructed start time and the arrival time of the closest bunch gives the RF correction. The corrected start time is therefore given by

$$t_{start} = t_{tof} - \frac{l}{\beta c} + t_{RF}. \tag{2.3}$$

As shown in Fig. 2.12, the start time distributions for events belonging to different electron bunches overlap, giving a non zero probability of associating an event to the wrong bunch. The resulting effects is represented in Fig. 2.13, that shows the β versus p distribution for positive hadrons obtained with RF correction. In addition to the expected pion, kaon, proton and deuteron lines, spurious lines appear when the start time is shifted by 2ns. This affects only a very small portion of the events giving instead a significant improvement in resolution necessary for the kaon detection.

For pion and proton detection the RF correction is not strictly necessary since while pion and proton produce an overwhelming contamination on the kaon sample, the kaon rate is intrinsically too low to produce a significant effect on the other hadrons.

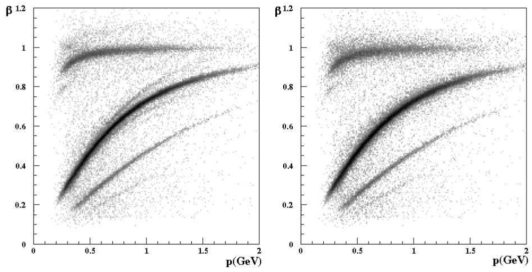

Figure 2.13: β versus p distribution for positive-charged hadrons with (left plot and without (right plot) RF correction.

2.3.4 Matching with the Outer Detectors

After the completion of the tracking reconstruction, the identified track paths are prolonged to hit the outer detectors. A hit in the outer detectors within a limited distance from the projected hit is associated with the track. The matching cut is chosen differently for each detector. For the Cerenkov Counter the required condition is a maximum polar angle of 12° between the projected track intersection with the CC plane and position of the detected hit. Since the Cerenkov Counter does not provide information on the azimuthal angle of the hit no further selection is applied. The cut correspond to approximately 3 CC segments and is therefore a very loose cut.

The matching of the track with the TOF hit is fixed requiring a maximum distance between the hits projection on the z-axis of 30 cm. The z-axis projection of the time of flight is completely determined by the geometry and simply depends on the scintillator strip that detected the signal. Again no information on the azimuthal position of the hit is used. The hit position in EC is reconstructed from the location of the scintillator strips that detected the signals. As reported in section 2.2.4 in each stack of the forward calorimeter the scintillators are positioned in three "views" rotated by 60° relative to each other and give a direct information on the hit position. The matching requirement consist on a radial cut of 30 cm from the detected hit.

An example of match between a charged particle track and its hit in the outer detectors is given in Fig. 2.14.

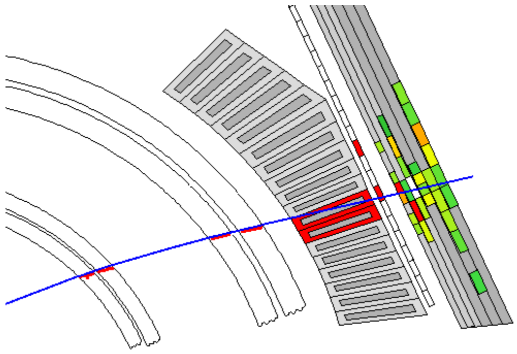

Figure 2.14: Matching between an electron track in EC and the CC signals.

2.3.5 Particle Identification

Electron Identification

Since the E1 trigger was a coincidence of EC and CC, each event has an electron candidate. At the level of the reconstruction process events in which the presence of an electron is not confirmed are rejected since no start time reconstruction is possible. The percentage of electron candidates that remains after the reconstruction depends on the beam energy, on the toroidal field and on the trigger thresholds.

At this stage an electron is represented by a negatively charged particle with track hits in the EC, CC, and TOF detectors. Since the matching requirements are given by loose cuts, the electron sample after the reconstruction can be still affected by contamination from other negative particles. The electron selection is improved at the level of the physics analysis by using additional cuts.

Charged Hadron Identification

Hadrons are identified by the combined information of the drift chambers and time of flight. The two detectors provided in fact the path and time of flight information necessary for the calculation of the β of the particle. This is obtained as

$$\beta = \frac{l}{tc} \tag{2.4}$$

where the l is the path length from the vertex to the time of flight plane and t the correspondent time obtained, as explained in section 2.3.3, as $t_{TOF} - t_{start}$. The mass of the hadrons can then be calculated as

$$m = \sqrt{\frac{p^2}{\beta^2} - p} \tag{2.5}$$

The resulting mass distribution for positive hadrons is shown in Fig. 2.15. Since the mass resolution depends on the time resolution that decreases for very fast particles, the final hadron identification is performed with cuts in the β versus p distribution that are chosen according to that resolution.

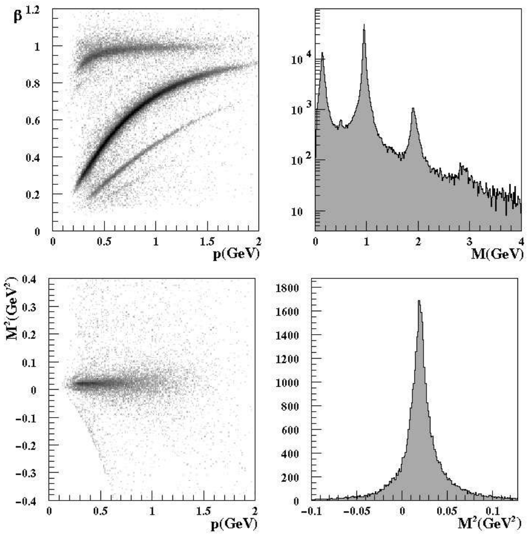

Figure 2.15: Identification of charged hadrons. The top-left plot shows the β versus p distribution for positive-charge hadrons while the top right plot shows the reconstructed mass. The bottom left-plot shows the mass squared versus momentum distribution for identified pions while the bottom right plots shows the projected squared mass.

Neutral Particle Identification

The detection of neutral particles in CLAS is performed by the electromagnetic calorimeters. The presence of a hit without a matching track represents in fact a neutral candidate. Such signal is then analyzed by the reconstruction code to reconstruct the β of the particle. The trajectories of the neutral particles are obviously not affected by the magnetic field and therefore the path length can be simply calculated as the distance between the vertex and the detected hit position. The β is therefore obtained as in Eq. 2.4. The resolution of the electromagnetic calorimeters is sufficient to obtain good photon-neutron discrimination up to a particle momentum of 1.5 GeV. At higher momenta, neutrons can be better identified by excluding the hits in the inner part of the calorimeter. Although this reduces the neutron detection efficiency, it efficiently removes photons since they rarely passes through six radiation lengths without depositing detectable energy.

Chapter 3

Data analysis

3.1 Analyzed data

Data taken on a hydrogen target were collected with the CLAS detector during the so called "E1b" and "E1c" electron beam running periods, completed in February 1998 and March 1999, respectively. The present analysis is based on the E1c data sets listed in Tab. 3.1. The data of the E1b running period were used only for a consistency check, and were not included in the final analysis due to the limited statistics. The analysis has been performed using SEB N-tuple #10 from Pass2x.prod19 "cooking".

Table 3.1: Summary of E1c data set. The reported number of electron events corresponds to the number of reconstructed electrons according to SEB, after the stability check, described in section 3.2

Data set		Total number of electron events
Energy [GeV]	Torus current [A]	x10^6
1.5	1500	131
1.5	2250	51
2.5 (unpolarized beam)	1500	17
2.5	1500	125
2.5 (unpolarized beam)	2250	29
2.5	2250	100
4.0	2250	80
4.2	2250	92
4.4	2250	58

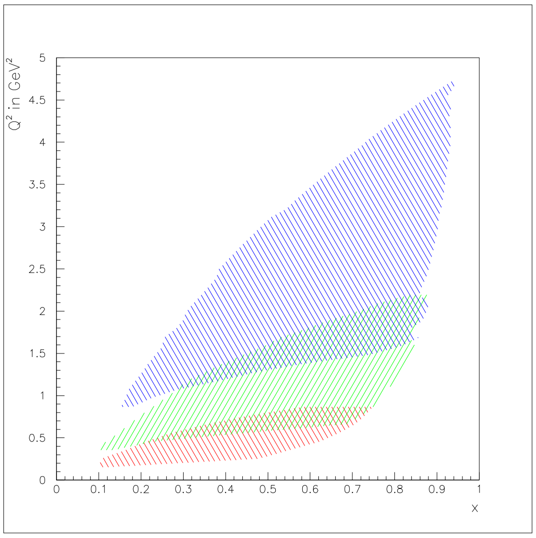

Figure 3.1: Kinematic regions covered by different data sets: red area - $E = 1.5$ GeV; green area - $E = 2.5$ GeV; blue area - $E = 4.0$ GeV.

3.2 Electron rate stability

In the present analysis only the so called “Gold” runs have been used [29]. Nevertheless, among these runs classified as “Gold” significant fluctuations of the inclusive electron rate were observed. To account for this effect, which can be related to target or detector instability the electron rate was monitored for the entire data set. The electron rate was defined as the number of electron events (PID taken from SEB) reconstructed in a safe region of the detector (defined by fiducial cuts described in section 3.4.1), normalized to the Faraday Cup (FC). This rate was evaluated for “block” of electrons corresponding to periods of 10 seconds, i.e. the read-out period of the FC. The FC charge was obtained from the so called “live-gated” signal, where the signal from the Faraday cup is only integrated during the live-time of the data acquisition to correct for its dead-time. An example of the results is shown in Fig. 3.2: at this stage only the blocks within $\pm 2\sigma_{tot}$ from the average have been selected for the analysis. The total width of the electron rate distribution contain also statistical error originated from finite number of events in each block; it is essential to remove that contribution. The remaining error of the electron rate stability was estimated as:

$$\sigma_{rem} = \sqrt{\sigma_{tot}^2 - \sigma_{stat}^2} \tag{3.1}$$

where σ_{stat} and σ_{tot} are averaged statistic error, equal to root square from averaged number of events in block, and r.m.s. deviation, respectively.

The remaining error is obviously related to FC statistical uncertainty. Since at 1 nA current there are about 100 FC clicks per block (10 seconds) and dead time is roughly

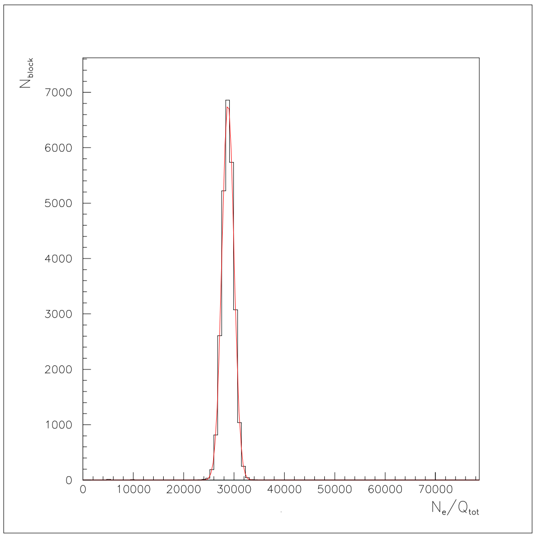

(a) Gaussian fit

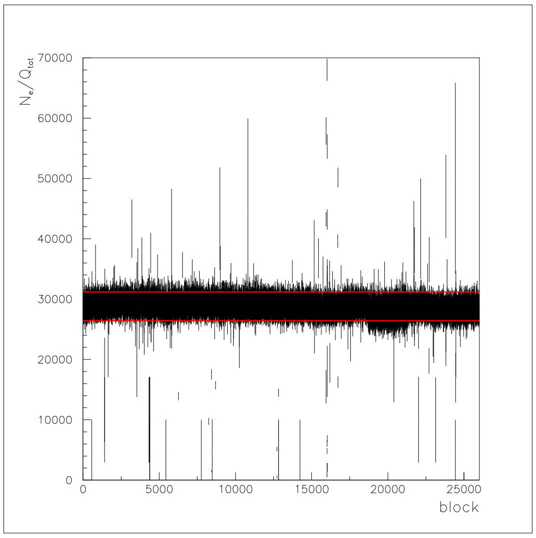

(b) $\pm 2\sigma$ cut

Figure 3.2: Sample of the quality check cut applied to the E1c E=4 GeV 2250A data set; the right plot shows the number of inclusive electron events, collected inside the fiducial region (see chapter 3.4.1), normalized to the total charge evaluated in μC versus number of blocks; the block represents the amount of data taken during 10 seconds: red lines represent $2\sigma_{tot}$ cut applied to the data. The left plot shows gaussian fit of the rate distribution.

Table 3.2: Errors of the electron rate for different data sets.

Data set		Remaining error	Statistical error	Total error
Energy [GeV]	Torus current [A]	[%]	[%]	[%]
1.5	1500	2.9	1.5	3.3
1.5	2250	2.2	1.6	2.8
2.5 (unpolarized beam)	1500	2.4	2.2	3.3
2.5	1500	3	2.1	3.7
2.5 (unpolarized beam)	2250	2	2.7	3.3
2.5	2250	2	2.6	3.3
4.0	2250	3.2	3	4.3
4.2	2250	3.4	2.9	4.5
4.4	2250	1.9	2.8	3.5

estimated as 10% corresponding statistical error of "live-time" scaler is about $\sqrt{10} = 3.3$ clicks, what is equal 3.3% of the measured charge. These very rough estimations appears to be in a good agreement with the remaining error listed in Tab. 3.2.

3.3 Momentum correction

It was observed that different sectors of the CLAS detector give a slightly shifted elastic peak position with respect to each other and to the correct $W = M_p$ position. These shifts are due to a misalignment of the drift chambers and to small inaccuracies in the description of the torus magnetic field, which results in an inaccurate reconstruction of charged particle momentum. Following the procedure developed first by V. Burkert [30], the electron momentum was corrected by a factor, which is a function of θ and ϕ. This was accomplished by making a fit of the elastic peak distributions for different azimuthal and polar angle bins inside each sector, and reconstructing the correct momentum under the assumption that the polar angle was measured precisely. The correction function was parametrized as:

$$P_{corrected} = P_{measured}(C_1 + C_2\phi + C_3\phi^2)\frac{C_4\theta - C_5}{C_6\theta - C_7} \tag{3.2}$$

where C_i are free parameters, $P_{measured,corrected}$ is the scattered electron momentum, θ and ϕ are polar and azimuthal angles, respectively.

These corrections were applied for each sector separately and they resulted in a significant improvement of the elastic peak width (Fig. 3.3).

In order to prove the efficiency of this method the following cross-check was performed for each data set and scattered electron angle: the resonance position in the inclusive spectrum was fitted with a function given by the parameterization [7], leaving mass, width and amplitude of the resonance peak around 1.5 GeV as free parameters. Possible shift in the mass of lowest resonances δ_W can be written as a function of the scattered electron momentum mismatch $\delta_{E'}$:

$$W\delta_W = (M + 2E\sin^2\frac{\theta}{2})\delta_{E'} \tag{3.3}$$

Therefore, the uncertainty of momentum correction should be better seen at lowest W.

The obtained mass of this resonance peak is shown in Fig. 3.4 in comparison with original one, taken from the world data fit [7].

The good agreement of the extracted resonance peak position with the expected value, inside errors which appeared to be much smaller than corresponding bin size (see Tab. 3.3), allow us to conclude that the momentum correction can be applied to the whole W spectrum.

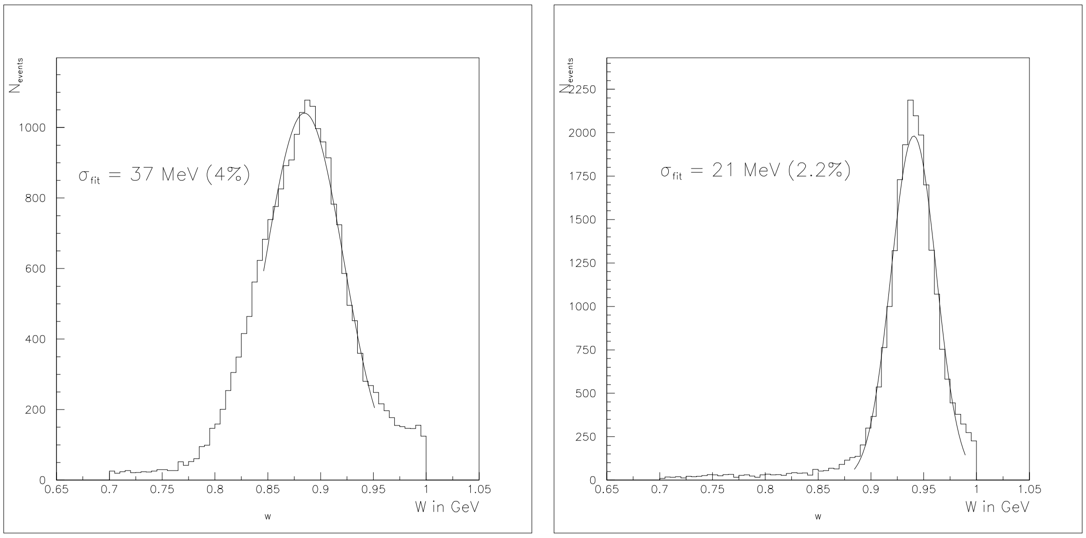

(a) before correction

(b) after correction

Figure 3.3: The Gaussian fit of the elastic peak distribution for sector 4.

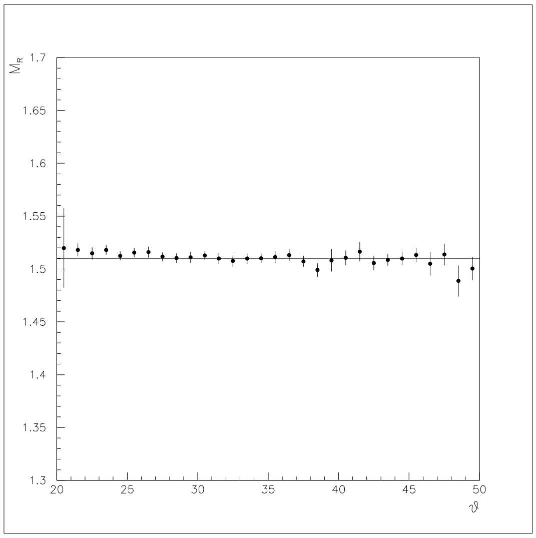

Figure 3.4: Extracted mass of the second resonance peak of inclusive spectrum as a function of θ at $E = 2.5$ GeV; the line represents the value given by the world data fit [7].

In order to estimate the systematic error on the cross section coming from possible mismatch in the measured W, the following quantity was computed using the model of

Table 3.3: Systematic uncertainties of the momentum correction δ_W in comparison with W bin size ΔW. δ_W represents the systematic deviation of measured second resonance peak position from one obtained from world data fit [7], while δ_W^{MINUIT} is error evaluated by the MINUIT [31] fitting program from the simultaneous fit of whole θ range available for one data set in the limited W region around second resonance peak ($1.45 < W < 1.65$).

Data set		δ_W	δ_W^{MINUIT}	$\Delta W(\theta = 29.5°)$
Energy [GeV]	Torus current [A]	[MeV]	[MeV]	[MeV]
1.5	1500	2.3	0.79	12
1.5	2250	2.2	0.96	12
2.5 (unpolarized beam)	1500	3.8	1.1	20
2.5	1500	2.6	0.75	20
2.5 (unpolarized beam)	2250	3.3	0.85	20
2.5	2250	2.1	0.75	20
4.0	2250	7.1	1.4	30
4.2	2250	7.4	1.7	32
4.4	2250	7.6	2.0	33

Ref. [7]:

$$\delta_{mom}(W, Q^2) = \frac{|\sigma^B(W - \delta_W/2, Q^2) - \sigma^B(W + \delta_W/2, Q^2)|}{\sigma^B(W, Q^2)} \tag{3.4}$$

The obtained systematic error for $E = 2.5$ GeV and $Q^2 = 0.8$ GeV^2 is shown in Fig. 3.5.

This systematic error accounts for the precision of the given beam energy, the measured momentum and angle of the scattered electron; possible mismatches of Q^2 which would result in a change of the absolute normalization were estimated in the comparison of measured elastic scattering cross section with the world data fit [32], described in section 3.6.2.

Exactly the same procedure was applied to the simulation results since the shift of the elastic peak position has been also observed in the Monte Carlo simulations. Fortunately, the correction was found to be constant over all ϕ, θ, beam energy and torus field settings ($\delta_W^{GSIM} = 5.7 \pm 2 MeV$).

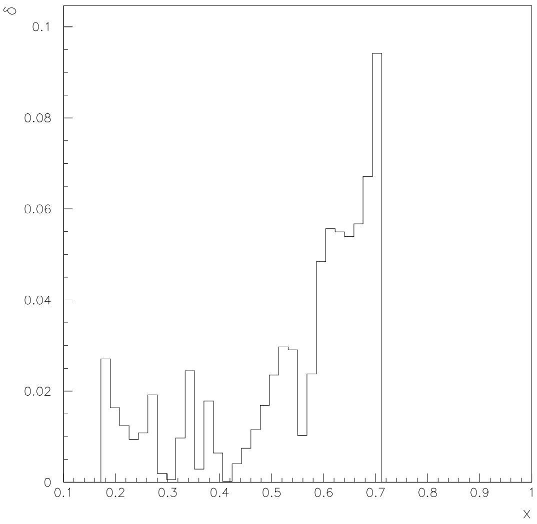

Figure 3.5: Systematic error on the inclusive cross section due to the momentum corrections at $E = 2.5$ GeV and $Q^2 = 0.8$ GeV^2; the error strongly rises in the x region where the cross section is rapidly varying (i.e. on the resonance slopes), while is very small in the resonance peak and in the regions where the cross section is smooth.

3.4 Cuts

Only three type of cuts were applied to the data. First of all, electrons were required to be detected inside the so called "fiducial" region of the detector. The second cut, based on the signals detected in CLAS (DC, CC, TOF, EC), was applied in order to improve the electron identification. The third cut, on the part of the scattered electron energy deposited in the inner EC, reduces the pion contamination discussed below.

3.4.1 Fiducial cuts

The fiducial cuts define the high efficiency regions of the detector, rejecting events whose hits were close to the drift chamber, calorimeter, or Cherenkov edges. These cuts are functions of the scattered electron momentum and angles. In the present analysis the acceptance function developed by V. Burkert has been used, this is given by:

$$A_c(p,\theta,\phi) = \begin{cases} \frac{2\pi}{\Delta\phi}\delta_\phi(p,\theta)\sin\theta, & \theta \in (\theta_{min}, 50^\circ) \text{ and } |\phi - \phi_{sec}| < \delta_\phi(p,\theta) \\ 0, & \theta \notin (\theta_{min}, 50^\circ) \text{ or } |\phi - \phi_{sec}| > \delta_\phi(p,\theta) \end{cases} \tag{3.5}$$

where the function $\delta_\phi(p,\theta)$ is

$$\delta_\phi(p,\theta) = \phi_0 \sin\left(\theta - \theta_{min}(p)\right)^{C\zeta^{\frac{1}{3}}} \tag{3.6}$$

and

$$\theta_{min}(p) = \theta_0 + \frac{\theta_{ac}}{p_{shift} + \zeta} \tag{3.7}$$

The variables are θ, ϕ, p are polar, azimuthal angles and momentum of the scattered electron, respectively, $\zeta = p\frac{T_{max}}{T}$ is the momentum of the scattered electron normalized to the value of torus magnetic field. The additional parameters are: the half of the sector width $\Delta\phi = 30°$, $\phi_0 = 20°$, $C = 0.35$, $\theta_0 = 15.5°$, $\theta_{ac} = 15°$, $p_{shift} = 0.05$; T is the torus current; $T_{max} = 3375$; ϕ_{sec} is the azimuthal angle of the center of current sector.

For very forward electrons ($\theta < \theta_{min}$) $\delta_\phi(p,\theta)$ has form:

$$\delta_\phi(p,\theta) = \phi_{0_f} \sin\left(\theta - \theta_{min}(p)\right)^{C_f \zeta^{\frac{1}{3}}} \tag{3.8}$$

and

$$\theta_{min}(p) = \theta_{0_f} - \theta_f + \frac{\theta_{ac}}{p_{shift} + \zeta} \tag{3.9}$$

where $\phi_{0_f} = 20°$, $C_f = 0.5$ and $\theta_f = 2°$.

The cuts are mainly based on the phenomenological formula relating the polar angle θ and the angle identifying the hit position on the Cherenkov plane $\theta - \theta_{min}(p)$ (see Eq. 3.7).

The regions of CLAS where the function of Eq. 3.5 is greater than zero ($A_c(p,\theta,\phi) > 0$) were assumed to be "safe".

Since standard fiducial cuts, described above, were not sufficient in all sectors to remove all the low efficiency regions, and systematic inconsistencies were observed related to either dead wires and scintillators and so on, it is an important task of the analysis to select only properly working regions of the detector in the whole interesting kinematic domain.

In order to avoid missing TOF paddles, dead wires and etc. ϕ-distributions of the electron rate were studied and holes in the fiducial region described above were identified by difference between averaged over ϕ number of events with one corresponding to a particular bin (see Fig. 3.7):

$$s(E', \theta, \phi) = \frac{\overline{N} - N}{\sqrt{N}} \tag{3.10}$$

where N is the number of events in this particular bin and $\overline{N}$ is average value over the whole ϕ range at fixed scattered electron angle and momentum.

Due to the huge statistics collected during E1 experiment, the statistic errors of the inclusive cross section are very small (for example, see Fig. 3.23) and systematic uncertainties dominate. Thus, the fiducial cuts were constructed in a way to completely exclude the unstable regions from the analysis even loosing some small part of the statistics.

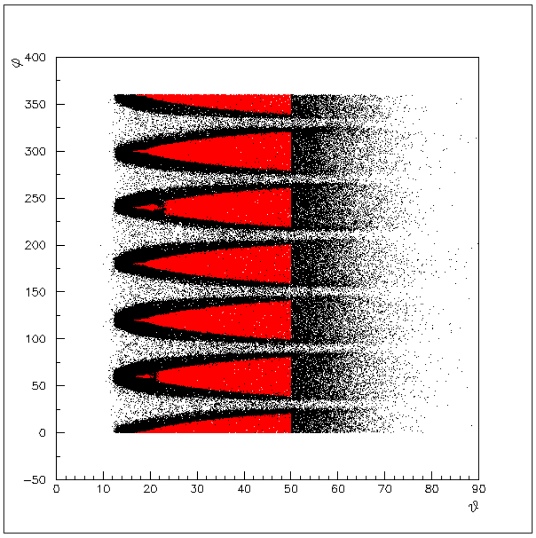

(a) angular behavior

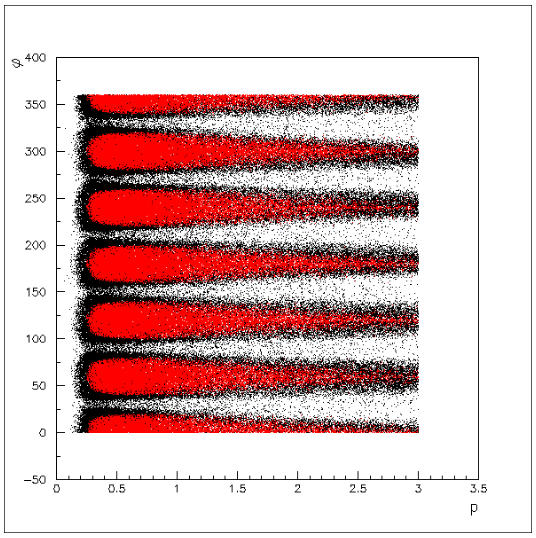

(b) energy behavior

Figure 3.6: Fiducial cut effect: the black points are reconstructed event candidates; while the red points represent event candidates inside the fiducial cuts.

In conclusion four cuts were added in sectors 2, 3 and 5 (see Fig. 3.9). They were derived by studying the central position of the hole on the θ, E' plane. The central position of each hole was fitted by Eq. 3.5 leaving θ_{ac} and p_{shift} as free parameters (for example see Fig. 3.8). The resulted parameters and cuts are shown in Tab. 3.4 and Fig. 3.9, respectively.

Table 3.4: Parameters obtained from the fit described in text.

	θ_{ac}	p_{shift}
	[°]	[GeV]
sector 2	17.093	0.4692
sector 3 (1)	15.0	0.05
sector 3 (2)	17.093	0.4692
sector 5	17.093	0.4692

The final expressions are the following: $4.8 < (\theta - \theta_{min}) < 8$ for the hole in sector 2; $(\theta - \theta_{min}) < 6.9$ for hole 1 in sector 3; $20 < (\theta - \theta_{min}) < 23$ for hole 2 in sector 3; $(\theta - \theta_{min}) < 10$ for the hole in sector 5, where θ_{min} is given by Eq. 3.9 with the parameters from Tab. 3.4.

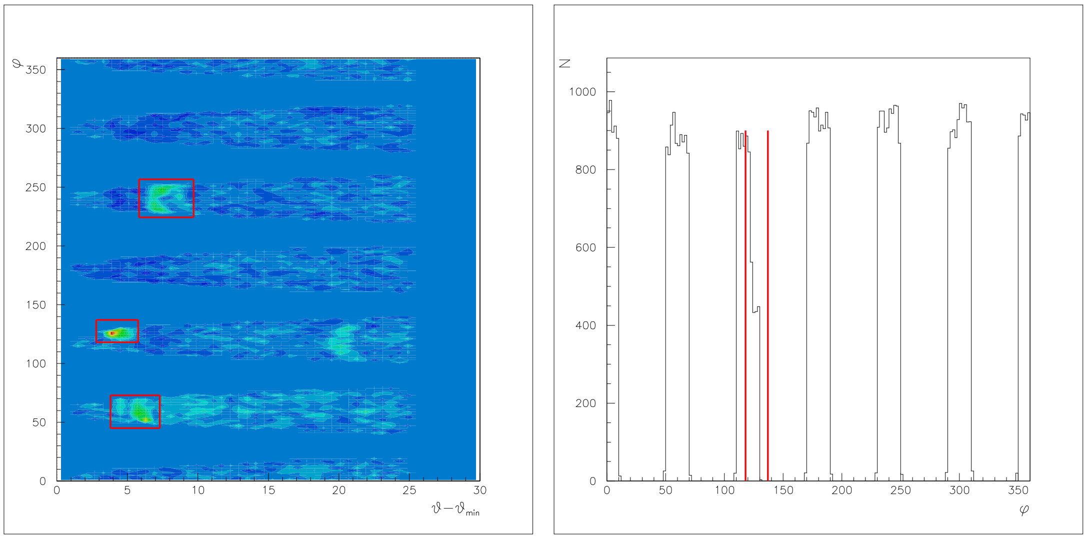

(a) bidimensional distribution (b) slice at $\theta - \theta_{min} = 4°$

Figure 3.7: Dead regions remaining after applying the standard fiducial cuts: left panel shows bidimensional distribution of the difference s (see Eq. 3.10) in ϕ and θ at fixed electron momentum $P = 1.5$ GeV; right panel represents the slice at $\theta - \theta_{min} = 4°$ of of the electron rate; the additional cuts are shown by red lines.

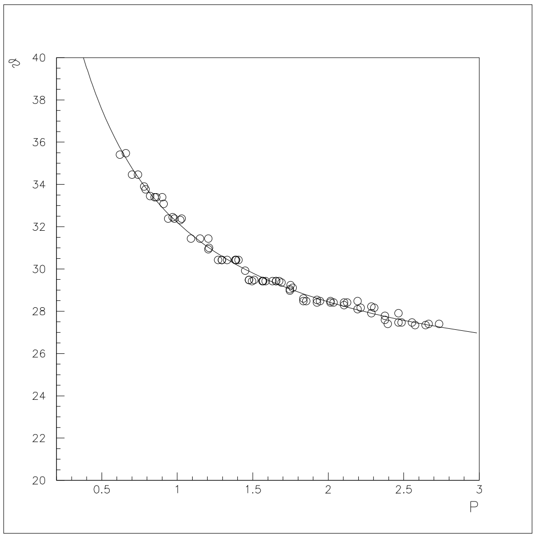

Figure 3.8: Fit of the central position of the hole in sector 5 by expression $\theta - \theta_{min}$, where θ_{min} is described in Eq. 3.9 and θ_{ac}, p_{shift} are free parameters.

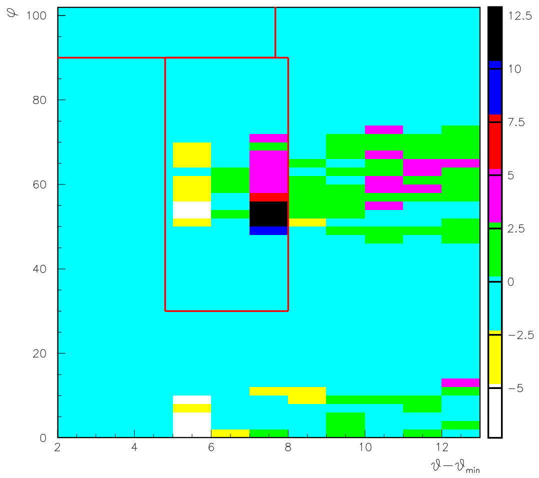

(a) $E = 2.5$ GeV, $E' = 0.73$ GeV

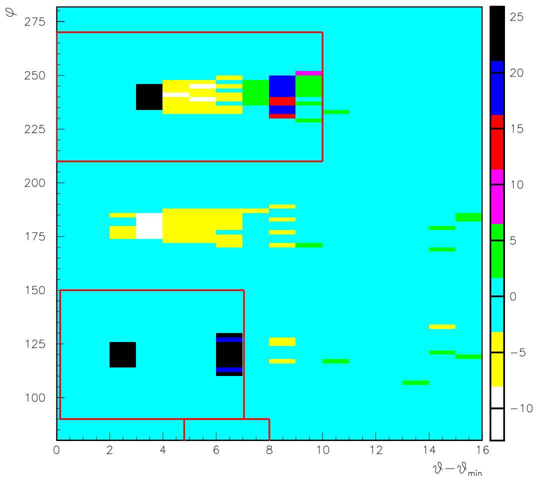

(b) $E = 2.5$ GeV, $E' = 1.09$ GeV

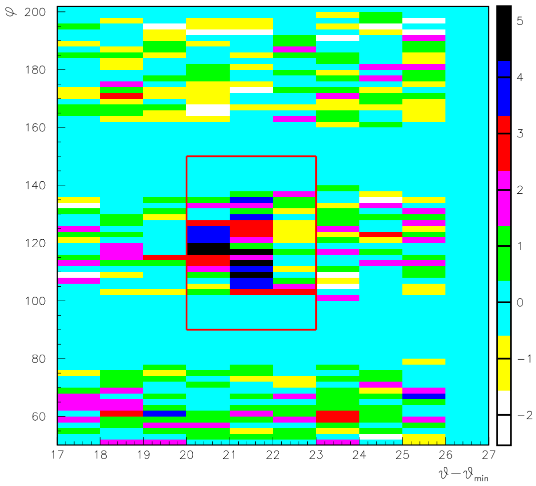

(c) $E = 4.0$ GeV, $E' = 1.15$ GeV

Figure 3.9: s-distributions (see Eq. 3.10). The additional fiducial cuts are shown by red solid line.

3.4.2 Event status cut

Only electron event candidates with signals in all the four systems (DC, CC, TOF, EC) of the CLAS during the reconstruction procedure have been selected. Such a cut strongly decreases the probability of a pion to be misunderstood as an electron, particularly at large momentum transfer. In the safe regions of the detector, defined by fiducial cuts, only the requirement of the CC response rejected a significant amount of event candidates (see Fig. 3.10), but the CC information is necessary for good electron-pion separation.

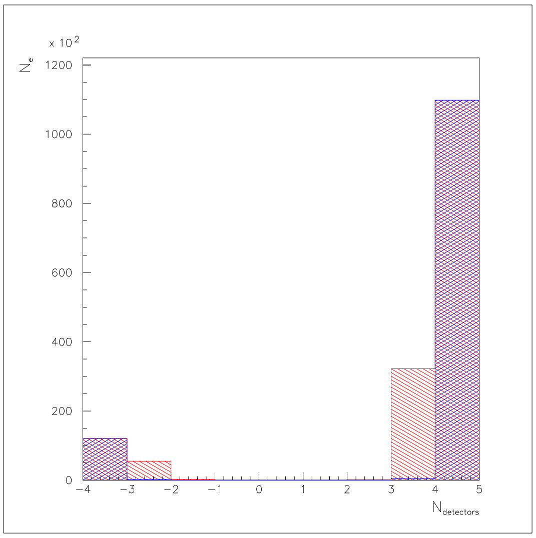

Figure 3.10: Event status distribution at $E = 4$ GeV (number of the detectors (DC, CC, TOF, EC) involved in the event selection); the fiducial cuts were applied; red area - all events; blue area - CC signal is required. The negative numbers correspond to inconsistent information from different detectors.

Since a pion, as a Minimum Ionizing Particle (MIP), deposits a smaller part of its energy in the calorimeter than an electron, the lower deposited energy peak on Fig. 3.11(a) is related to pions misidentified as electrons. Applying the "good event status" cut one can drastically reduce this peak (see Fig. 3.11(b)). But, unfortunately, this cut is not sufficient to avoid residual contamination among event candidates with zero energy deposited in the outer EC.

The Cherenkov gas counter provides additional information about the number of photoelectrons in the photomultiplier produced by the Cherenkov radiation of a particle, which can be used for a better electron-pion separation. The residual pion contamination can be easily seen on Fig. 3.12 as the large peak at $N_{phe} < 2.5$ and $\frac{EC_in}{P} < 0.15$.

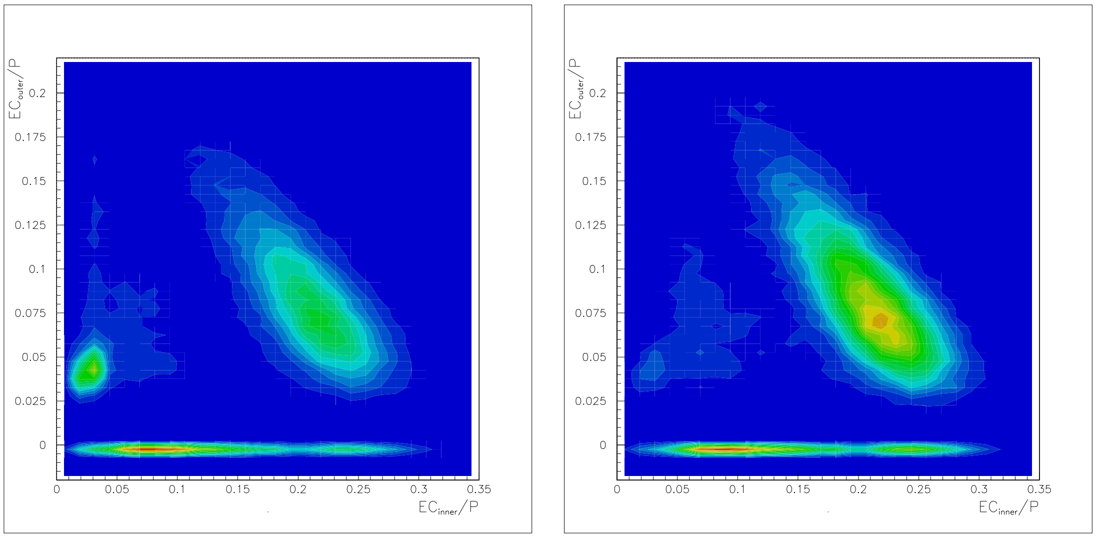

(a) before the cut

(b) after the cut

Figure 3.11: Part of the scattered electron energy deposited in inner EC versus outer one.

3.4.3 Calorimeter cut

Since the photoelectron distribution strongly depends on kinematics the contaminating pion peak cannot be completely removed avoiding large efficiency losses (about 30%) in some particular regions (see Fig. 3.12(b)). As a compromise solution a cut on the part of scattered electron energy deposited in the EC, shown on Fig. 3.12, was applied. It leads to a sizable reduction of the photoelectron correction described below while simultaneously saving reasonable efficiency; and therefore reducing systematic uncertainty.

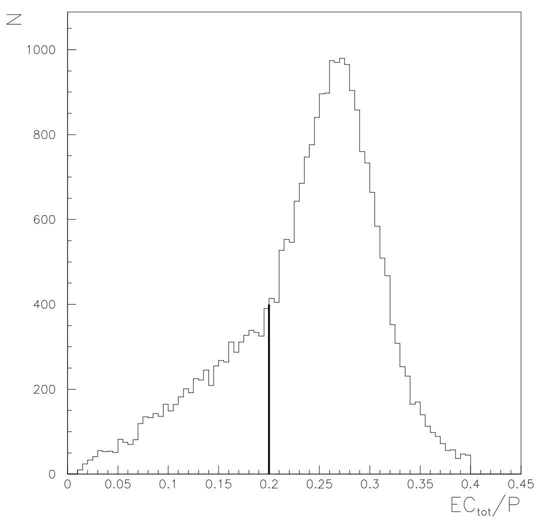

(a) $E = 4$ GeV 2250 A

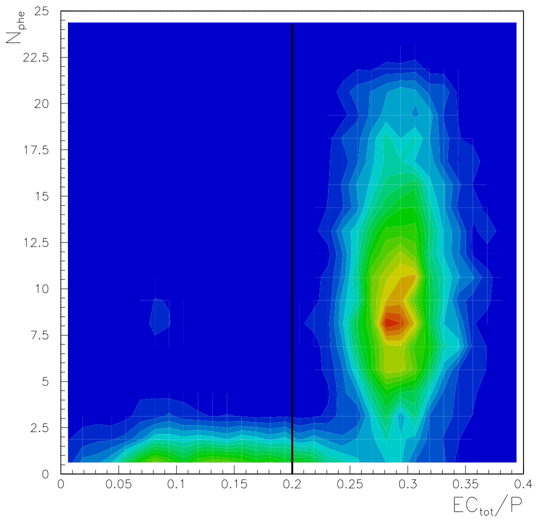

(b) $E = 2.5$ GeV 2250 A

Figure 3.12: Part of the scattered electron energy deposited in EC (a) and this versus number of photoelectrons in CC (b) inside fiducial cuts, after the event status cut has been applied; black line represents the calorimeter cut ($EC_{tot} > 0.2$).

3.5 Background

The extracted spectra suffer from various backgrounds. These are the negative pions misidentified as the electrons, e^+e^- pair production, fast knock-on electron contamination (δ rays) and the contribution of the scattering off target cell walls.

3.5.1 Photoelectron corrections

The Cherenkov gas detector, installed for the purpose of electron-pion separation, appears to be not efficient enough at large momentum transfer ($Q^2 \sim 3 \div 5$ GeV^2). In order to remove the residual pion contamination discussed in chapters 3.4.3 and 3.4.2, the photoelectron corrections were studied.

The electron inclusive cross section requires only the number of scattered electron events for each kinematic point, and it makes no difference which particles have been really detected, electrons or pions. Therefore, because the cuts were not sufficient, one could correct the final cross section, just multiplying it by a correction factor equal to the ratio of real electrons over the total number of event candidates in each kinematic bin.

In order to find the correction function in the whole kinematic range covered by the experimental data, fits of the photoelectron distributions have been performed separately for different values of the scattered electron energy and angle. Since the mean number of photoelectrons produced by pions is very close to zero, while electrons produce more photoelectrons, it is possible to separate pions and electrons making a combined fit of the measured photoelectron distribution with two Poisson distributions convoluted with a Gaussian function, corresponding to the finite photo-multiplier resolution. The fitting function is given by:

$$
\begin{aligned}
f(x) \;=\; & \left[A_\pi \sum_{k=1}^{100} e^{-\lambda_\pi} \frac{\lambda_\pi^k}{k!} \frac{1}{\sqrt{2\pi\sigma^2}} e^{-\frac{(x-k)^2}{2\sigma^2}} + \right. \\
& \left. A_e \sum_{k=1}^{100} e^{-\lambda_e} \frac{\lambda_e^k}{k!} \frac{1}{\sqrt{2\pi(\sigma+\sigma_r)^2}} e^{-\frac{(x-k)^2}{2(\sigma+\sigma_r)^2}} \right] \left\{ \begin{array}{ll} e^{-\frac{(x-x_0)^2}{b^2}} & (x < x_0) \\ 1 & (x \geq x_0) \end{array} \right.
\end{aligned}
\tag{3.11}
$$

where x is the number of photoelectrons, λ_e, σ_r, A_π and A_e are free parameters, and $\lambda_\pi = \frac{\lambda_e}{270}$, $\sigma = 0.45$, $b = 0.65$ and $x_0 = 0.37$ are fixed. Fixed parameters were free at the beginning, but it was found that in the case of pronounced pion peaks, like in Fig. 3.15(c), they were very similar in different kinematics and only when the pion peak was not clearly observed, as in Fig. 3.15(a), they introduced ambiguities. The first term in Eq. 3.11 represents the pion contamination peak, the second term is the peak of electrons, and the Gaussian overall normalization factor (right bracket) was introduced in order to take into account the photomultiplier threshold effect.

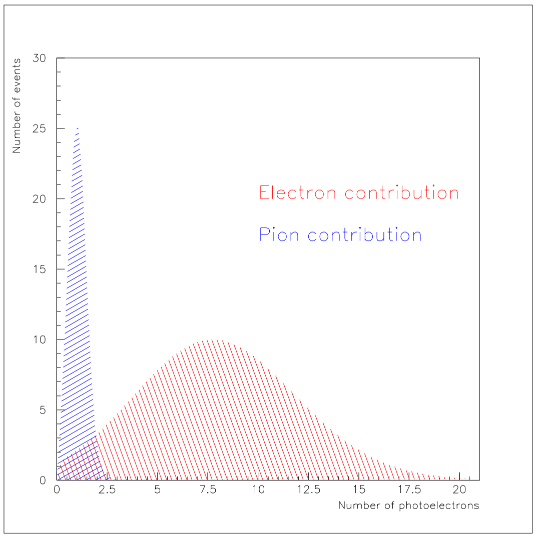

Figure 3.13: The electron - pion separation in the photoelectron distribution; red area - electrons; blue area - pions.

It was found that the shape of the pion peak does not depend on any kinematic variable, only the amplitude can vary (see Fig. 3.14). For this reason the shape of the pion peak was fixed using the distributions where this peak is more pronounced and has a clear form for fitting; the only free parameter related to the pion contribution is therefore the amplitude A_π. On the contrary, the electron peak has a few free parameters: the mean value - λ_e; the additional width σ_r, corresponding to the kinematic bin size, and the amplitude A_e. The additional width σ_r of the electron peak was introduced in order to account for the fact that λ_e is changing inside large kinematic bins, as described below. The pion peak does not require an additional width, because it is situated very close to zero and any possible shift would be irrelevant. The described function, as one can see on Fig. 3.15, provides a reasonable fit of the photoelectron spectra in the interesting kinematic domain. The average value of χ^2 per degree of freedom in this fit was about unity.

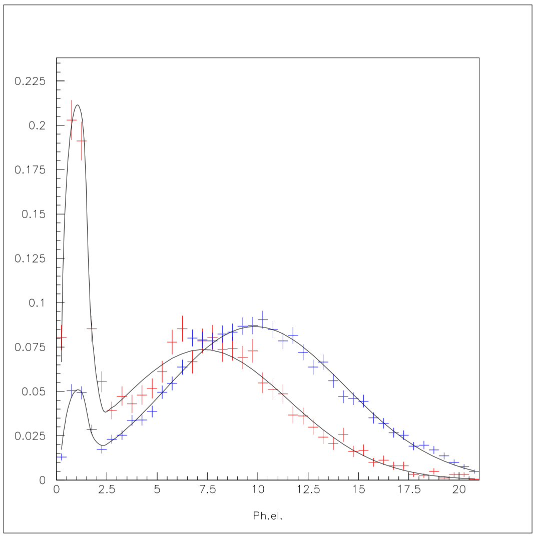

Figure 3.14: The photoelectron distribution for different kinematics: red points - $E = 4$ GeV, $\theta = 41°$, $E' \sim 1$ GeV; blue points - $E = 2.5$ GeV, $\theta = 31°$, $E' \sim 1.2$ GeV.

The final value of the correction function is the area of the electron peak (red area in Fig. 3.13) divided by the total one:

$$C_{photo-el} = \frac{A_e}{A_e + A_\pi} \tag{3.12}$$

The systematic uncertainty related to this correction was estimated as:

$$\delta_{photo-el} = \left[\frac{(A_e \delta_{A_\pi})^2 + (A_\pi \delta_{A_e})^2 - 2A_\pi A_e cov(A_\pi, A_e)}{(A_e + A_\pi)^4} \right]^{\frac{1}{2}} \tag{3.13}$$

where δ_{A_e} and δ_{A_π} represent the errors on the parameters A_e and A_π, respectively, and $cov(A_\pi, A_e)$ is the covariance of the corresponding parameters obtained from the error

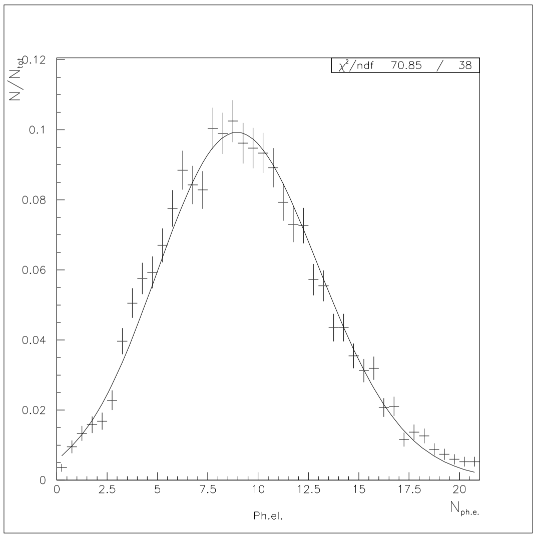

(a) $\theta = 25°$, $E' = 2$ GeV

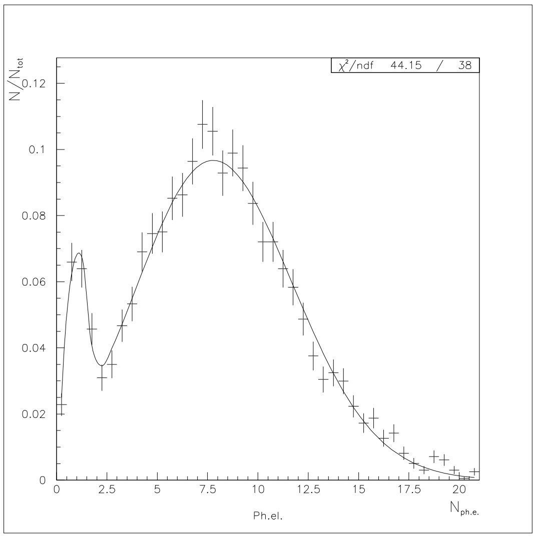

(b) $\theta = 35°$, $E' = 1.5$ GeV

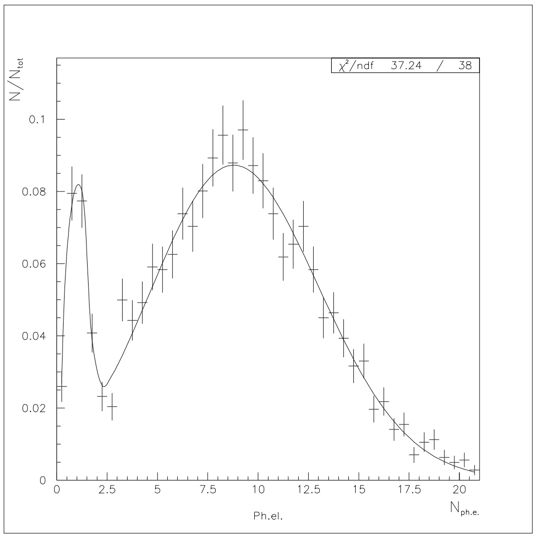

(c) $\theta = 45°$, $E' = 1$ GeV

Figure 3.15: Fit of the photoelectron distribution at $E = 4$ GeV.

matrix. The covariance varies from 0.5 in the region of largest correction (small E') to practically zero at large E'.

Fits described in this chapter were performed for the whole analyzed kinematics ($\theta = 20° \div 50°$ and $W = M_p \div 2.2$ GeV), separately for each sector, because different sectors at fixed θ and W have quite different photoelectron distribution (Fig. 3.16).

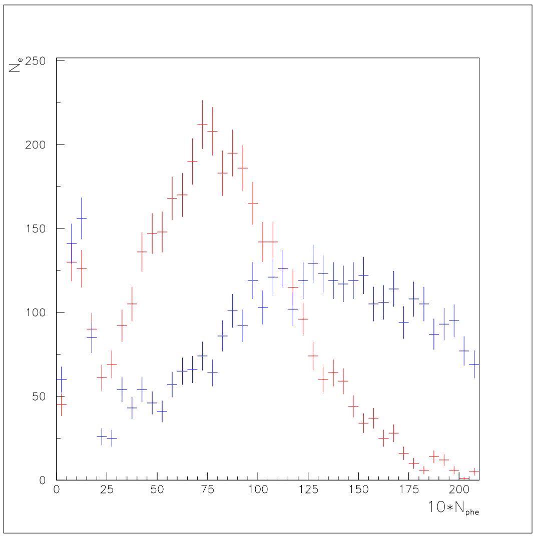

Figure 3.16: The photoelectron distributions of two sectors at E = 4 GeV, $\theta = 30°$, $E' = 1.3$ GeV; red points - sector 4; blue points - sector 6.

Due to insufficient statistics the fit of the photoelectron distributions was performed over relatively large bins ($d\theta = 2°$ and $dE' \sim 0.1$ GeV). Further, in order to apply the correction to the measured cross section obtained in smaller bins ($d\theta = 1°$ and $dE' \sim 0.05$ GeV) the values of the correction were fitted with a polynomial kinematic function:

$$F_{phe}(\theta, \nu) = 1 + A(\nu - \nu_0) + (B + C\theta)(\nu - \nu_0)^2 \tag{3.14}$$

where A, B, C and ν_0 are free parameters.

The results of this fit are shown in Fig. 3.17.

In order to estimate systematic uncertainty of this correction a fit of systematic errors give by Eq. 3.13 was performed using the same function as for the correction values (see Eq. 3.14). Total relative systematic error of this correction $\delta_{F_{phe}}/F_{phe}$ is kinematic dependent, but it appears to be always smaller than 2%.

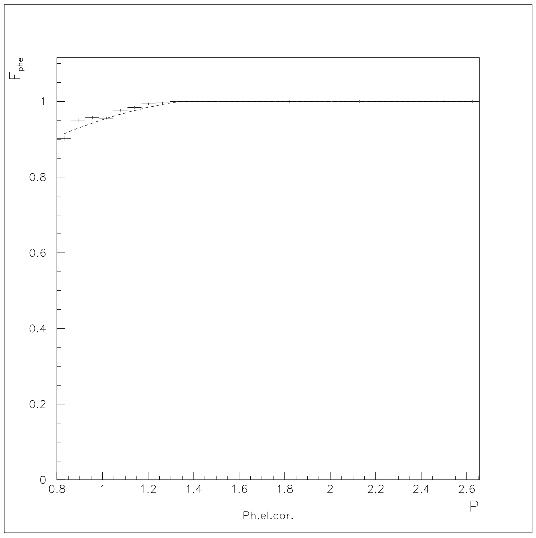

(a) $\theta = 25°$

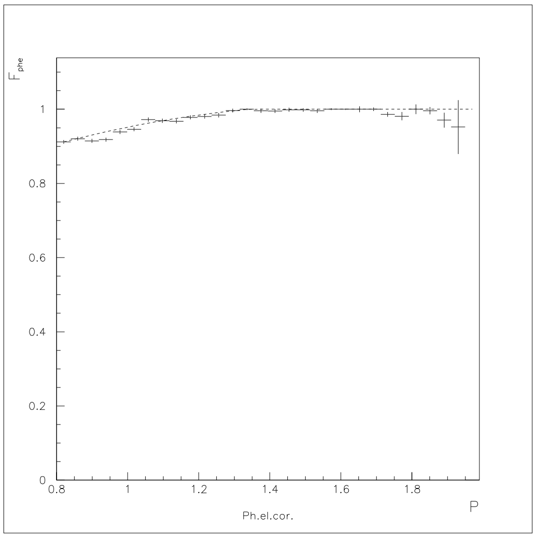

(b) $\theta = 35°$

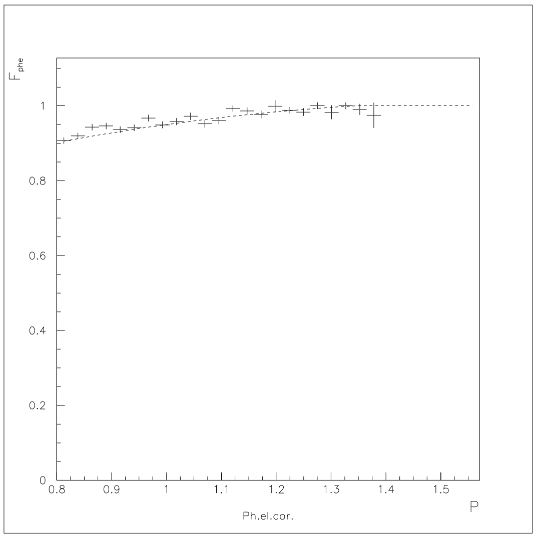

(c) $\theta = 45°$

Figure 3.17: Fit of the photoelectron correction at $E = 4$ GeV: dashed line - fitting function Eq. 3.14; points- values of the correction with errors.

3.5.2 e^+e^- pair production subtraction

Since positron data in the same kinematics as electron one, required the inverse magnetic field, are not available, the pair production background processes were estimated according to P. Bosted model [33]. The most important source of e^+e^- pairs in the CLAS is π^0 production followed either by Dalitz decay to γe^+e^- or $\gamma\gamma$ by decay with one of the photons converting to e^+e^-. This process was computed using the code developed by P. Bosted, which is based on the Wiser fit from Ref. [34] of the inclusive pion production. This model was carefully checked against the EG1 data [33], and it appeared to be in good agreement with measured positron cross sections. The value of the correction is assumed to be equal to the ratio of the inclusive e^+ production cross section over Bodek's fit [7] including radiative processes (tail from elastic peak, bremsstrahlung and Schwinger correction):

$$F_{e^+e^-}(E,x,Q^2) = \frac{\sigma^B_{rad}(E,x,Q^2)}{\sigma^B_{rad}(E,x,Q^2) + \sigma_{e^+}(E,x,Q^2)} \tag{3.15}$$

where σ_{e^+} is the inclusive e^+ production cross section and σ^B_{rad} is Bodek's fit [7] folded with radiative processes, described in chapter C.

Since the effect of this correction is negligible over the available kinematic range (the case of largest correction is shown in Fig. 3.18, where the maximum contribution is equal to 2%), as expected [35] the correction was applied only to 4.0 and 4.2 GeV data sets. The corresponding systematic error could be written as:

$$\frac{\delta_{F_{e^+e^-}}}{F_{e^+e^-}}(E,x,Q^2) = (1 - F_{e^+e^-}(E,x,Q^2))\sqrt{\left(\frac{\delta_{\sigma_{e^+}}}{\sigma_{e^+}}\right)^2 + \left(\frac{\delta_{\sigma^B_{rad}}}{\sigma^B_{rad}}\right)^2} \tag{3.16}$$

where $\delta_{\sigma_{e^+}}/\sigma_{e^+} = 0.3$ is relative systematic error of the positron rate given by [33] and $\sigma^B_{rad}/\sigma^B_{rad}$ is precision of parametrization [7], which was taken to be equal 10%.

The systematic error is kinematic dependent, but since the correction is very close to unity the systematic error associated with it never exceed 1%.

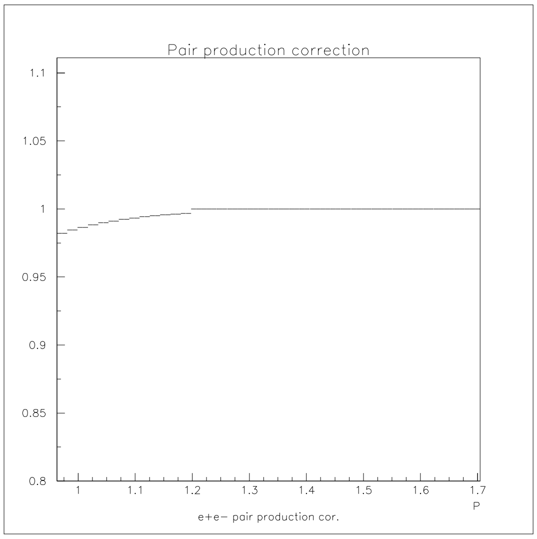

Figure 3.18: e^+e^- pair production correction function at $E = 4.2$ GeV, $\theta = 49.5°$.

3.5.3 Fast knock-on electrons (δ rays)

One possible source of the background originates from a coincidence of a very fast knock-on electron production (δ rays), producing a signal in CC, and a negative pion, giving the track in DC and interacting in EC by a nuclear interaction, in order to satisfy EC cut on deposited energy. Such a contamination may occur if the high energy negative pion, with momentum large enough to have a significant probability of nuclear interaction in EC, produces a knock-on electron, which momentum is above the CC threshold. Therefore, the probability of this coincidence can be written as:

$$P_{e^-p\to\delta AX}(P',\theta,\phi) = P_{e^-p\to\pi^-X}(P',\theta,\phi)P_{\pi^-\to\pi^-\delta}P_{\pi^-A} \tag{3.17}$$

where $P_{e^-p\to\pi^-X}(P',\theta,\phi)$ is the probability of the inclusive π^- production, $P_{\pi^-\to\pi^-\delta}$ is the probability of the knock-on electron production by the pion in the material of the detector and P_{π^-A} is the probability of the nuclear absorption of the pion in EC.

It is convenient to approximate an upper limit for first term in r.h.s. of Eq. 3.17 by the interaction probability derived from the electron inclusive cross section:

$$P_{e^-p\to\pi^-X}(P',\theta,\phi) \leq P_{e^-p\to e^-X}(P',\theta,\phi) * C(P',\theta) \tag{3.18}$$

where factor $C(P',\theta)$ varies from 0 to 50 in the kinematic range of present experiment. This estimation is calculated by a comparison of two fits of inclusive electron [7] and pion production (Wiser fit taken from [33]). For sake of simplicity we consider that $C < 50$ and we will use this maximum value for further estimations.

Thus, dividing both sides of Eq. 3.17 over $P_{e^-p\to e^-X}(P',\theta,\phi)$ we obtain a relative probability of the coincidence of the fast knock-on electron in CC with the nuclear interaction of the pion in EC on each inclusive electron:

$$P_{\delta A} \equiv \frac{P_{e^-p\to\delta AX}}{P_{e^-p\to e^-X}} \leq P_{\pi^-\to\pi^-\delta} P_{\pi^-A} * C \tag{3.19}$$

The knock-on electron production probability is given by [36]:

$$P_{\pi^-\to\pi^-\delta} \equiv \int dTdx \frac{d^2N}{dTdx} \tag{3.20}$$

where the probability distribution $\frac{d^2N}{dTdx}$ is given by:

$$\frac{d^2N}{dTdx} = \frac{1}{2}K\frac{Z}{A}\frac{1}{\beta_\pi^2}\frac{F(T)}{T^2} \tag{3.21}$$

here $x = \rho L$ is amount of the material transversed by the pion in the low magnetic field ($<$ 500 Gauss, otherwise the produced low energy electron will be bent by the magnetic field and it will never achieve CC, at least in the point where reconstruction procedure will assign it to that event), $K = 4\pi N_A r_e^2 m_e c^2 \simeq 0.307 MeV cm^2/g^2$, Z and A are atomic number and mass, respectively; T is the kinetic energy of the created knock-on electron and

$$F(T) = \left\{1 - \beta_\pi^2\frac{T}{T_{max}} + \frac{1}{2}\left(\frac{T}{E_\pi}\right)^2\right\} \tag{3.22}$$

where β_π and E_π are velocity end energy of the pion, respectively and

$$T_{max} = \frac{2m_e c^2\beta_\pi^2\gamma_\pi^2}{1 + 2\gamma_\pi m_e/m_\pi + (m_e/m_\pi)^2} \tag{3.23}$$

is a maximum kinetic energy of the knock-on electron; in present kinematics it is approximately equal 50 MeV. Calculating the integral over knock-on electron kinetic energy from CC threshold (18 MeV) to T_{max} one can obtain:

$$\frac{dN}{dx} = \frac{Z}{A}\left(\frac{4.6\cdot 10^{-3}}{\beta_\pi^2} + \frac{2.3}{\beta_\pi^2 E_\pi^2} - 2.8\cdot 10^{-3}\right) \tag{3.24}$$

In order to estimate the probability of the knock-on electron production one has to integrate Eq. 3.21 over amount of material crossed by the pion in a low magnetic field passing from the target to CC. The total thickness of DC was designed to be less than 0.01 radiation length, therefore roughly the third region of DC has $3\cdot 10^{-3}$ radiation length thickness or about $4\cdot 10^{-2}$ g/cm^2. In addition one can take into account the CC inlet mirror thickness which was estimated as $7 \cdot 10^{-2}$ g/cm^2. Thus, total thickness used in the calculations is equal 0.1 g/cm^2.

The result of such integration gives about $6.5 \cdot 10^{-5}$, taking pion momentum to be equal $p_{\pi^-} = 0.5$ GeV.

The upper limit of the last term in r.h.s. of Eq. 3.17 can be estimated from the total nuclear absorption of pion; which, in the frame of very naive optical model [37, 38], can be written as follows

$$P_{\pi^- A} \simeq \rho N_A L \sigma^A_{\pi^-} \tag{3.25}$$

where P_{π^-} is a probability of total nuclear absorption of pion, L is the path length of the pion in EC, N_A is Avogadro constant; ρ is a density, A is the atomic number, M_A is the molar mass of the EC material and cross section of the total pion absorption is estimated as

$$\sigma^A_{\pi^-} \simeq \frac{25.7 + 47.9A^{2/3}}{M_A} \tag{3.26}$$

the cross section $\sigma^A_{\pi^-}$ is given in mb.

For present EC configuration (40 cm of Bicron BC412 scintillator plus 8 cm of lead) Eq. 3.26 gives an estimate of $P_{\pi^-} \simeq 1$ (as expected, since EC has thickness about one nuclear interaction length).

Finally multiplying results obtained from Eq. 3.21 and Eq. 3.26 the relative contamination probability $P_{\delta A}$ is not more than $3 \cdot 10^{-3}$.

Summarize, upper limit of the relative probability of having the coincidence of the fast knock-on electron in CC with the nuclear interaction of the pion in EC (for definition see Eq. 3.19) is very roughly equal $3 \cdot 10^{-3}$ on each inclusive electron. Therefore, this source of background is completely negligible with respect to statistic and systematic errors of experiment.

3.5.4 Empty target contribution

In order to remove the contribution of scattering on the target walls in the final cross section, the empty target data were analyzed in the same way as the full target ones; then the empty target events normalized to FC charge were subtracted:

$$N_{LH}(E, x, Q^2) = N_{full}(E, x, Q^2) - \frac{Q_{tot_{full}}}{Q_{tot_{empty}}} N_{empty}(E, x, Q^2) \tag{3.27}$$

Any inaccuracy of Z-vertex reconstruction does not affect the extracted cross section because this information was not used in the evaluation procedure.

The uncertainty related to the finite number of empty target events ($\sqrt{N_{empty}}$) was added in quadrature to the cross section statistical error bin by bin.

3.6 Efficiency evaluation

Since most important part of the analysis is evaluation of the electron efficiency this procedure was carefully checked by a comparison of the well known elastic scattering cross section.

3.6.1 Simulations

The simulations were accomplished according following procedure:

1. Events were generated by the random event generator with the probability distribution computed as the ratio of corresponding cross section (elastic or inelastic) to its maximum value in defined kinematic region. The values of elastic and inelastic cross sections were taken from existing fits of world data [32] and [7], respectively. The internal radiative processes contribution were added according to calculations described in appendix C.

2. Then generated events were passed through the standard CLAS GEANT based simulation program GSIM [39] using following form of FFREAD card:

   ```
   AUTO 1
   KINE 1
   CUTS 5.e-3 5.e-3 5.e-3 5.e-3 5.e-3
   CCCUTS 1.e-3 1.e-3 1.e-3 1.e-3 1.e-3
   DCCUTS 1.e-4 1.e-4 1.e-4 1.e-4 1.e-4
   ECCUTS 5.e-4 5.e-4 5.e-4 5.e-4 5.e-4
   SCCUTS 1.e-4 1.e-4 1.e-4 1.e-4 1.e-4
   MAGTYPE 3
   MAGSCALE 0.583 0.75
   PTGIFIELD 0
   GEOM 'ALL'
   NOGEOM 'PTG ' 'ST'
   NOSEC 'OTHE'
   TARGET 'e1b1'
   TGPOS 0.0 -0.030 -0.300
   POSBEAM 0.1115 -0.1346
   SIGBEAM 0.1
   NOMCDATA 'ALL'
   SAVE 'ELMG' 0.01 'HADR' 0.1 'MUON' 0.1
   GRUN 10
   STOP
   ```

3. After that obtained at the previous stage data were analyzed with GSIM Post Processing program GPP to make detector respond more realistic, add some noise, background and introduce registered dead wires and scintillator paddles. The information about the status of different parts of the detector were taken by Perl script gpp.pl written by Kyungseon Joo from on-line MySQL database installed on claspc10.jlab.org. The run number was chosen to be one in the middle of whole data set.

   The parameters responsible for smearing effect in different DC regions were adjusted for each data set separately, in order to reproduce measured elastic peak width.

Table 3.5: Smearing parameters A, B and C corresponding to different DC regions: first, second and third, respectively.

Data set		A	B	C
Energy [GeV]	Torus current [A]			
1.5	1500	1.8	2.3	2.7
1.5	2250	2.1	2.64	3.15
2.5	1500	1.5	1.9	2.2
2.5	2250	1.5	1.9	2.25
4.0	2250	1.1	1.35	1.7
4.2	2250	1.2	1.5	1.8
4.4	2250	1.35	1.7	2.05

4. Finally, the efficiency was calculated in each kinematic bin as a ratio of the number of reconstructed events N_{rec} over the number of events generated N_{gen}:

$$F_{eff}(E, x, Q^2) = \frac{N_{rec}(E, x, Q^2)}{N_{gen}(E, x, Q^2)} \tag{3.28}$$

This complex of program governed by a C-Shell script was run on the JLab and UNH Linux clusters. The speed of the simulations varied from 0.2 seconds per event on very fast Athlon (AMD) systems to 2.5 seconds per event on 300 MHz Pentium II (Intel) machines. Totally 10^8 electron events were generated for each set of beam energy and torus field.

Most important feature of the efficiency obtained from simulations and checked against the elastic scattering in a wide kinematic range shown in Fig. 3.21 is that efficiency appears to be approximately constant (about 97%), varying within 5% interval, inside safe region of the detector defined by fiducial cuts over whole available kinematics.

The fluctuations of the efficiency from the constant appear to be less than actual systematic error.

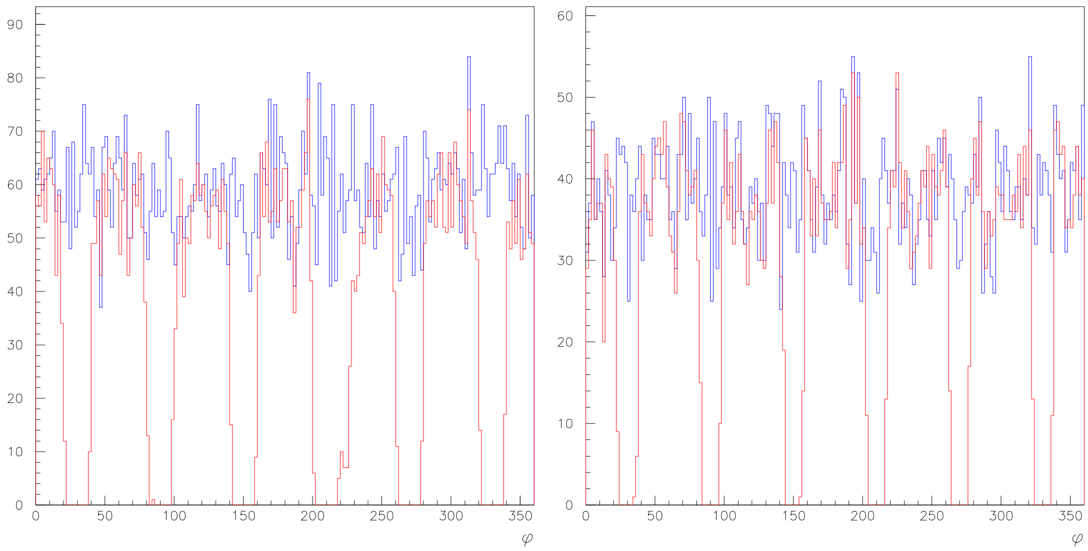

(a) $E = 2.5$ GeV, $I = 1500$, $\theta = 23.5°$ (b) $E = 4.4$ GeV, $I = 2250$, $\theta = 30.5°$

Figure 3.19: A comparison of generated and reconstructed events.

3.6.2 Elastic scattering cross section

In order to check the reliability of the simulation procedure and to evaluate a proper absolute normalization, the well known elastic scattering cross section was measured and compared to the simulated one. Both cross sections appeared to be in a good agreement within statistical and systematic errors (see Fig. 3.20).

The elastic scattering cross section was evaluated as a number of events situated in W-interval from 0.85 to 1.05 GeV multiplied by corresponding luminosity:

$$\frac{d\sigma}{d\Omega}_{exp,rec}(E,\theta) = \frac{L_{sim}}{\rho\frac{N_A}{M_A}LQ_{tot}}\int_{0.85}^{1.05} dW\, N_{exp,rec}(W,\theta) \tag{3.29}$$

where $N_{exp,rec}$ represents the corresponding number of events (in the case of the measured cross section the empty target events were subtracted according to Eq. 3.27).

The kinematic range covered by the measured elastic cross section, and therefore tested simulation efficiency, is shown in Fig. 3.21.

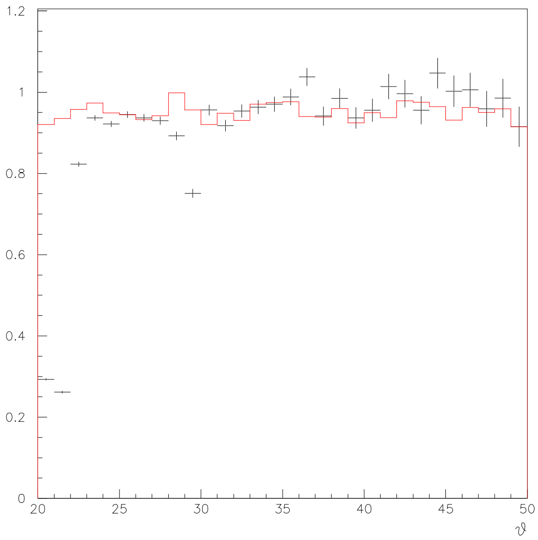

(a) $E = 1.5$ GeV, $\phi = 57°$

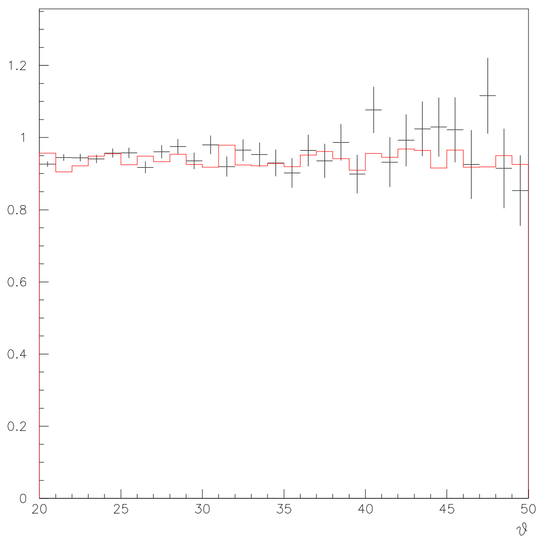

(b) $E = 2.5$ GeV, $\phi = 181°$

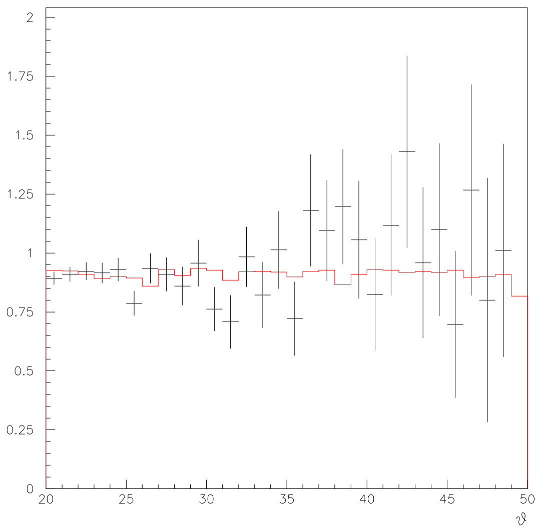

(c) $E = 4.0$ GeV, $\phi = 67°$

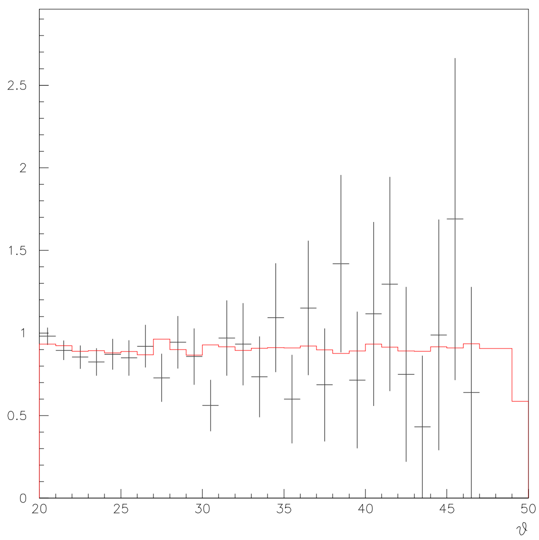

(d) $E = 4.4$ GeV, $\phi = 63°$

Figure 3.20: Ratio of the measured elastic scattering cross section (see Eq. 3.31) corrected by radiative corrections, as described in appendix C, to the parametrization [32] (black points) in comparison to one obtained from the simulations (red line) for a fixed ϕ. Here no efficiency corrections were applied.

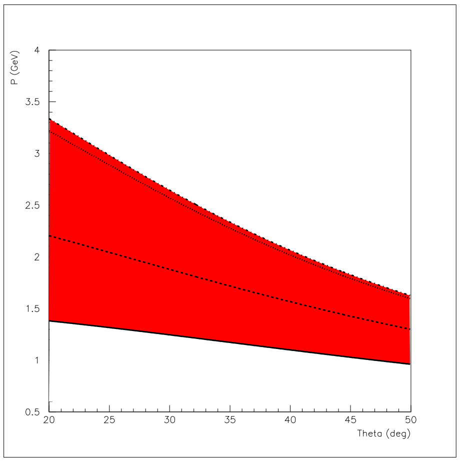

Figure 3.21: Kinematic area covered by the extracted efficiency: solid line - elastic peak position at $E = 1.5$ GeV; dashed line - elastic peak position at $E = 2.5$ GeV; dotted line - elastic peak position at $E = 4.0$ GeV; dashed-dotted line - elastic peak position at $E = 4.2$ GeV.

3.6.3 Systematic uncertainties of the efficiency evaluation

Since the elastic scattering cross section is known with a few percent precision [32] one can obtain the systematic uncertainty of the simulated efficiency by a comparison of the simulated elastic cross section to the measured one. In this comparison it is essential to avoid low efficiency detector regions since they were not used in the analysis.

To this end, the systematic deviation of the experimental cross section from the result of the simulations for each beam energy and scattered electron angle (see Fig. 3.22) was calculated as the following:

$$\delta_{ep}(E,\theta) = \frac{\sqrt{\left(\frac{d\sigma}{d\Omega}_{exp}(E,\theta) - \frac{d\sigma}{d\Omega}_{rec}(E,\theta)\right)^2 - \delta^2_{exp}(E,\theta)}}{\frac{d\sigma}{d\Omega}_{fit}(E,\theta)} \tag{3.30}$$

where $\frac{d\sigma}{d\Omega}_{exp}$ and $\frac{d\sigma}{d\Omega}_{rec}$ are the measured and reconstructed in GSIM simulation procedure elastic scattering cross section, respectively; while $\frac{d\sigma}{d\Omega}_{fit}$ is the parametrization described in Appendix A; δ_{exp} is the statistical error of the measured elastic cross section.

In Eq. 3.30 contribution arises from statistical fluctuation has been removed in order to extract purely systematic difference.

The obtained distributions were averaged out over all beam energies and resulted systematic error is shown in Fig. 3.22.

Finally, the corresponding systematic uncertainty of the overall normalization δ_{eff} has

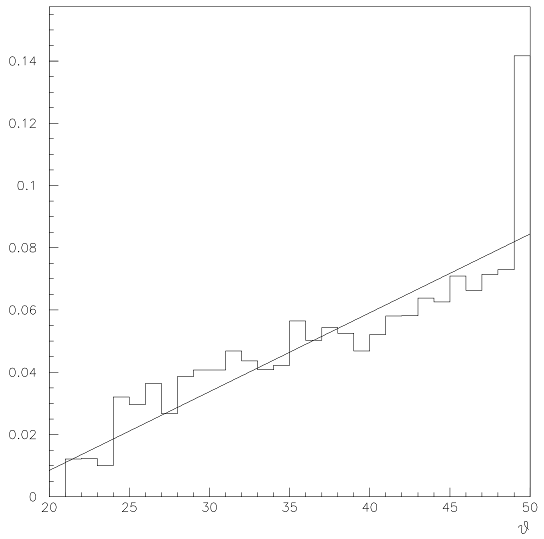

Figure 3.22: Systematic deviation of the GSIM simulated elastic cross section from the measured one. The solid line represents result of the linear fit as a function of θ.

been obtained by the linear fit of the distribution in Fig. 3.22 as the function of scattering electron angle θ.

3.7 Inclusive inelastic cross section

The inclusive inelastic cross section was evaluated for all analyzed data sets using the following equation:

$$\frac{d\sigma^2}{d\Omega dE'}(\theta, E') = \frac{1}{\rho \frac{N_A}{M_A} L Q_{tot}} \frac{N_{LH}(\theta, E')}{\Delta\phi \Delta E' \Delta\theta \sin\theta} F_{eff}(\theta, E') F_{phe}(\theta, E') F_{e^+e^-}(\theta, E') \quad (3.31)$$

where θ, E' are scattered electron angle and energy; ρ is the density of liquid H_2 in the target, N_A is Avogadro constant, M_A is the target particle molar mass, L is the target length, Q_{tot} is total live-gated charge in FC, $N_{LH}(\theta, E')$ is the number of events obtained by Eq. 3.27; $\Delta\theta$, $\Delta\phi$, $\Delta E'$ are corresponding bin sizes; $F_{phe}(\theta, E')$ is the photoelectron correction function described in chapter 3.5.1; $F_{eff}(\theta, E')$ is efficiency function described in chapter 3.6; $F_{e^+e^-}(\theta, E')$ is the pair production correction function described in chapter 3.5.2. The total charge Q_{tot} was obtained, as described in chapter 3.2, already corrected for the data acquisition dead-time. The LH density ρ was evaluated from the density distributions as a function of the temperature and pressure (see Tab. 3.6).

Table 3.6: Target length L and LH density for different data sets.

Data set		L	ρ
Energy [GeV]	Torus current [A]	[cm]	$[\frac{g}{cm^3}]$
1.5	1500	5	0.0705
1.5	2250	5	0.0705
2.5 (unpolarized beam)	1500	3.72	0.0705
2.5	1500	5	0.0705
2.5 (unpolarized beam)	2250	3.72	0.0705
2.5	2250	5	0.0705
4.0	2250	5	0.0715
4.2	2250	5	0.0705
4.4	2250	5	0.0715

In order to apply properly radiative and bin centering corrections, a model cross section σ^B from Ref. [7] was used in the following way:

$$\begin{aligned} \frac{d\sigma^2}{d\Omega dE'}(\theta, E') &= \frac{L_{sim}}{\rho \frac{N_A}{M_A} L Q_{tot}} \frac{N_{LH} - \tilde{N}_{el.rad.}}{N_{rec} - N_{el.rad.}} \\ &\quad \sigma^B(\theta, E') F_{phe}(\theta, E') F_{e^+e^-}(\theta, E') \end{aligned} \quad (3.32)$$

where $N_{el.rad.}$ is the number of reconstructed events related to the radiative tail of the elastic peak, $\tilde{N}_{el.rad.}$ is the same as before but normalized to measured elastic peak cross section:

$$\tilde{N}_{el.rad.} = N_{el.rad.} \frac{\rho \frac{N_A}{M_A} L Q_{tot}}{L_{sim}} \tag{3.33}$$

and

$$L_{sim} = \frac{N_{tot}}{\int d\Omega dE' \sigma^B(\theta, E')} \tag{3.34}$$

is simulations "luminosity" constant.

The corresponding statistical errors were computed as follows:

$$\begin{aligned} \delta_{\frac{d\sigma^2}{d\Omega dE'}}(\theta, E') &= \frac{L_{sim}}{\rho \frac{N_A}{M_A} L Q_{tot}} \frac{\sqrt{N_{LH}}}{N_{rec} - N_{el.rad.}} \\ &\quad \sigma^B(\theta, E') F_{phe}(\theta, E') F_{e^+e^-}(\theta, E') \end{aligned} \tag{3.35}$$

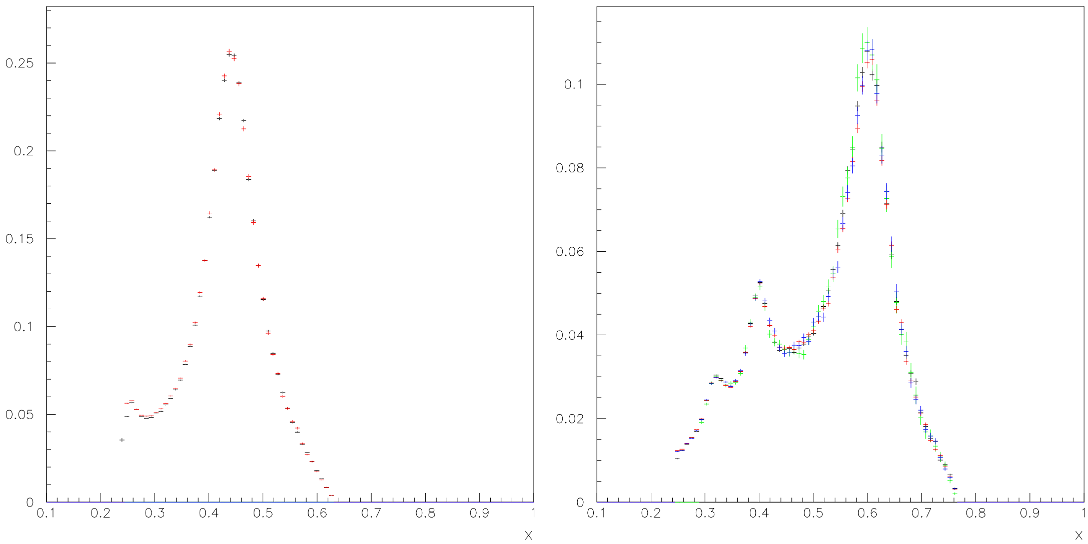

(a) $E = 1.5$ GeV, $Q^2 = 0.48$ GeV^2

(b) $E = 2.5$ GeV, $Q^2 = 0.93$ GeV^2

Figure 3.23: Inclusive inelastic cross section $\frac{d\sigma^2}{d\Omega dE'}$; different colors correspond to different data sets at the same beam energy: black points - torus current 1500 A; red points - torus current 2250 A; green points - unpolarized beam, torus current 1500 A; blue points - unpolarized beam, torus current 2250 A.

3.8 Systematic error of the cross section

All the systematic uncertainties mentioned above were propagated to the final cross section according standard error propagation formula:

$$\sigma_{sys}(\theta, E') = \frac{d\sigma^2}{d\Omega dE'}(\theta, E') \sqrt{\left(\frac{\delta F_{eff}}{F_{eff}}\right)^2 + \left(\frac{\delta F_{phe}}{F_{phe}}\right)^2 + \left(\frac{\delta F_{e^+e^-}}{F_{e^+e^-}}\right)^2 + \delta^2_{mom} + \delta^2_{rad}} \qquad (3.36)$$

where $\delta F_{eff}/F_{eff}$ is the systematic uncertainty of efficiency evaluation, it also contain error on absolute normalization; $\delta F_{phe}/F_{phe}$ is photo-electron correction systematic error, $\delta F_{e^+e^-}/F_{e^+e^-}$ is related to the pair production correction, δ_{mom} is the systematic error of the momentum correction described in section 3.3 and δ_{rad} radiative correction systematic uncertainty (see Appendix C).

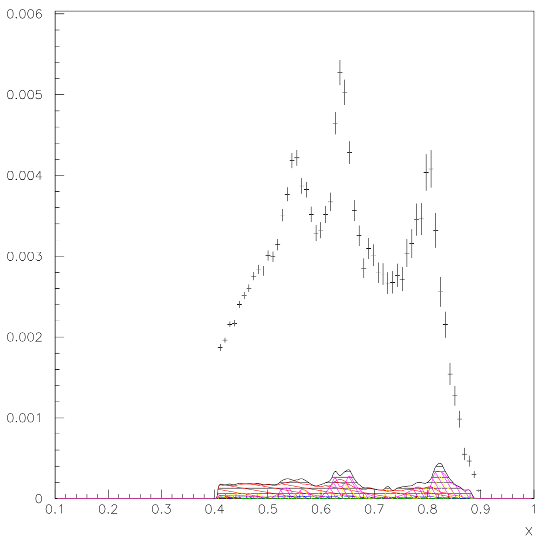

Figure 3.24: The differential cross section at $E = 4$ GeV and $Q^2 = 2.48$ GeV^2 with systematic errors separated by different sources: black area represents the total systematic error; red area corresponds to the efficiency systematic uncertainty δ_{eff}; yellow area shows systematic error of the radiative corrections; pink area is due to uncertainty of the momentum corrections. All other sources of systematic uncertainties shown in Eq. 3.36 are also present on the plot but are not seen due to much smaller absolute values.

3.9 The structure function $F_2(x, Q^2)$

The structure function $F_2(x, Q^2)$ was extracted from the inelastic cross section using the fit of the function $R(x, Q^2) \equiv \sigma_L/\sigma_T$ developed in Ref. [18]:

$$F_2(x, Q^2) = \frac{1}{\sigma_{Mott}} \frac{d^2\sigma}{d\Omega dE'} \frac{\nu}{1 + \frac{1-\epsilon}{\epsilon}\frac{1}{1+R}} \tag{3.37}$$

where the polarization parameter is defined as

$$\epsilon \equiv \left(1 + 2\frac{\nu^2 + Q^2}{Q^2} tan^2\frac{\theta}{2}\right)^{-1} \tag{3.38}$$

The function $R(x, Q^2)$ is not very well known in the resonance region, but fortunately, the structure function F_2 in the interesting kinematic range is not very sensitive to the value of R. In fact even a 100% systematic uncertainty on R gives only few percent uncertainty on F_2 (see Tab. 3.7).

$$\frac{\delta^R_{F_2}}{F_2}(x, Q^2) = \left[\left(\frac{\delta_\sigma}{\sigma}\right)^2 + \left(\frac{1-\epsilon}{1+\epsilon R}\frac{\delta_R}{1+R}\right)^2\right]^{\frac{1}{2}} \tag{3.39}$$

Uncertainties of R given in Ref. [18] were propagated to the resulting F_2, and actual systematic errors introduced by this δ_R were always lower than 3%.

Table 3.7: Samples of the R uncertainties propagation.

E $[GeV]$	Q^2 $[GeV^2]$	x	Error of R [%]	Propagated error of F_2 [%]
2.5	0.65	0.39	77%	1%
4.0	2.62	0.58	166%	3%
4.2	1.66	0.35	50%	2.5%

Actually, the evaluation of the structure function F_2 was performed directly from event rate leaving cross section calculation stage. This was done as follows:

$$F_2(x, Q^2) = \frac{L_{sim}}{\rho\frac{N_A}{M_A}LQ_{tot}} \frac{N_{LH} - \tilde{N}_{el.rad.}}{N_{rec} - N_{el.rad.}} F_2^B(x, Q^2) F_{phe}(x, Q^2) F_{e^+e^-}(x, Q^2) \tag{3.40}$$

and corresponding statistical errors are equal:

$$\delta_{F_2(x,Q^2)}(x, Q^2) = \frac{L_{sim}}{\rho\frac{N_A}{M_A}LQ_{tot}} \frac{\sqrt{N_{LH}}}{N_{rec} - N_{el.rad.}} F_2^B(x, Q^2) F_{phe}(x, Q^2) F_{e^+e^-}(x, Q^2) \tag{3.41}$$

while systematic errors receive an additional contribution from poor knowledge of ratio $R = \sigma_L/\sigma_T$:

$$F_{2_{sys}}(x,Q^2) = F_2(x,Q^2) \sqrt{\left(\frac{\delta F_{eff}}{F_{eff}}\right)^2 + \left(\frac{\delta F_{phe}}{F_{phe}}\right)^2 + \left(\frac{\delta F_{e^+e^-}}{F_{e^+e^-}}\right)^2 + \left(\frac{\delta^R_{F_2}}{F_2}\right)^2 + \delta^2_{mom} + \delta^2_{rad}} \quad (3.42)$$

The extracted structure functions are reported in Table D.5 and in Ref. [40].

Table 3.8: Range of the systematic error variation given separately for each data set, divided by their sources. Values in brackets obtained excluding few extreme points.

Data set		Source of errors						
Beam energy $[GeV]$	Torus current $[A]$	Efficiency [%]	pair prod. [%]	photo-el. [%]	rad. cor. [%]	mom. cor. [%]	$R = \frac{\sigma_L}{\sigma_T}$ [%]	Total [%]
1.5	1500	1-8	0	0.2-0.3	1.5-17 (10)	0.2-5	0.5-4	5-18 (12)
1.5	2250	1.7-9	0	0.1-0.5	1.5-30 (10)	0.1-6	1-3.5	6-35 (15)
2.5 unpol.	1500	1.5-9	0-3	0.2-0.4	1.5-25 (15)	0.1-7	0.6-4	4-27 (19)
2.5	1500	1-8	0-3	0.2-0.4	1.5-30 (14)	0.2-7	0.6-4	3.5-35 (16)
2.5 unpol.	2250	1.5-9	0-2.5	0.1-0.4	1.5-26 (12)	0.1-7	0.7-4	4.5-28 (15)
2.5	2250	1.5-8	0-2.5	0.1-0.4	1.5-30 (15)	0.1-6	0.7-4	4-35 (18)
4.0	2250	1.5-9	0-2	0.5-1	1.5-20 (12)	0.1-15	1-4.5	4-31 (18)
4.2	2250	1.5-9	0-2.2	0.5-0.9	1.5-20 (15)	0.1-15	0.7-4.8	3.5-21 (17)
4.4	2250	1.3-9	0-2.5	0.5-2.2	1.5-15 (15)	0.1-15	0.8-4.9	3.5-25 (18)

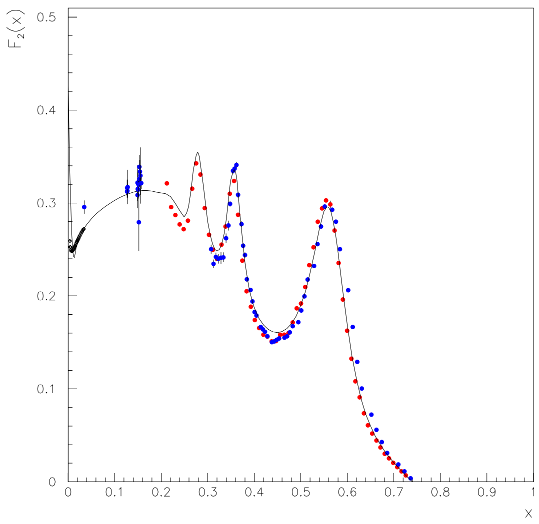

(a) $Q^2 = 0.78$ GeV^2

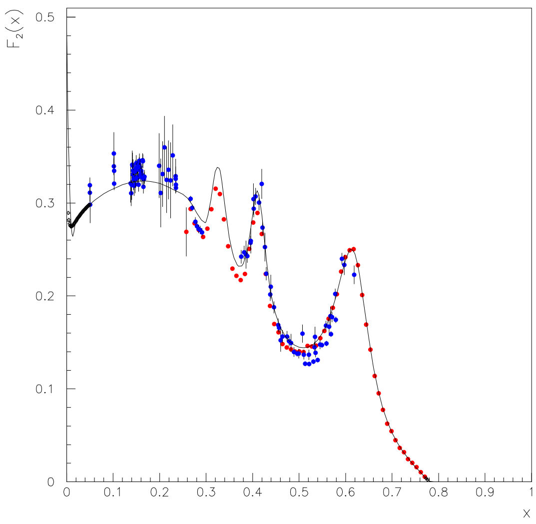

(b) $Q^2 = 0.98$ GeV^2

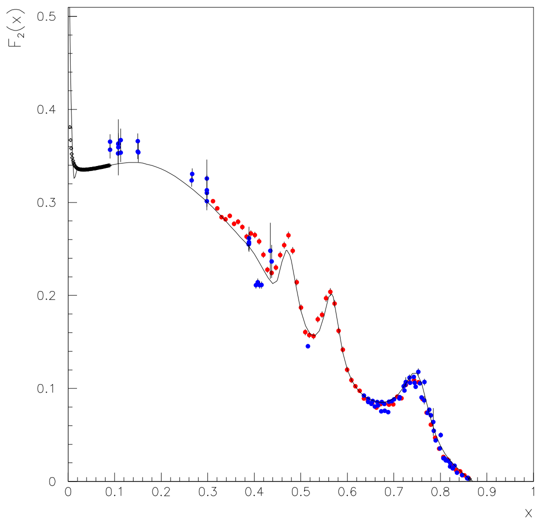

(c) $Q^2 = 1.83$ GeV^2

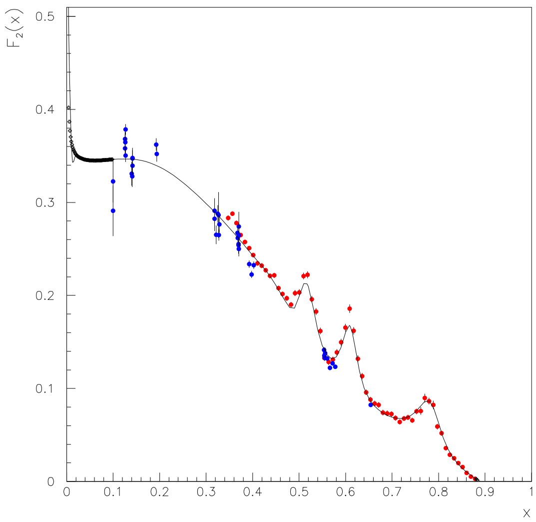

(d) $Q^2 = 2.18$ GeV^2

Figure 3.25: Structure function $F_2(x, Q^2)$; red points - CLAS experimental data; blue points - world experimental data; solid line - global fit [18, 7, 41, 42, 43].

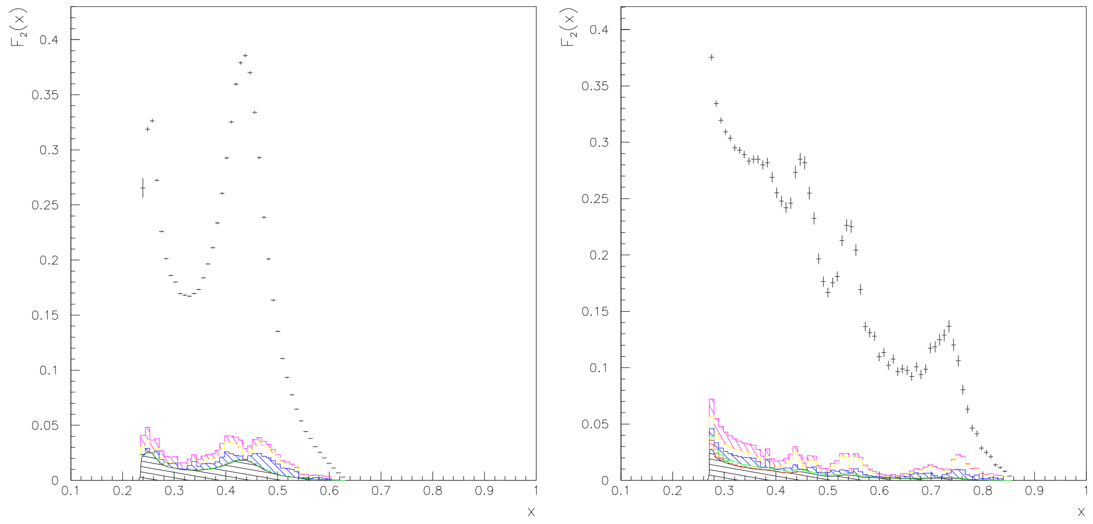

(a) $Q^2 = 0.475$ GeV^2

(b) $Q^2 = 1.675$ GeV^2

Figure 3.26: Structure function $F_2(x, Q^2)$ with systematic errors separated by different sources: black area represents efficiency and absolute normalization systematic error; red - systematic error due to e^+e^--pair production correction; green - photoelectron correction systematic uncertainty; blue - radiative correction systematic error; yellow - systematic error due to momentum correction; pink - systematic error related to $R = \sigma_L/\sigma_T$ uncertainty.

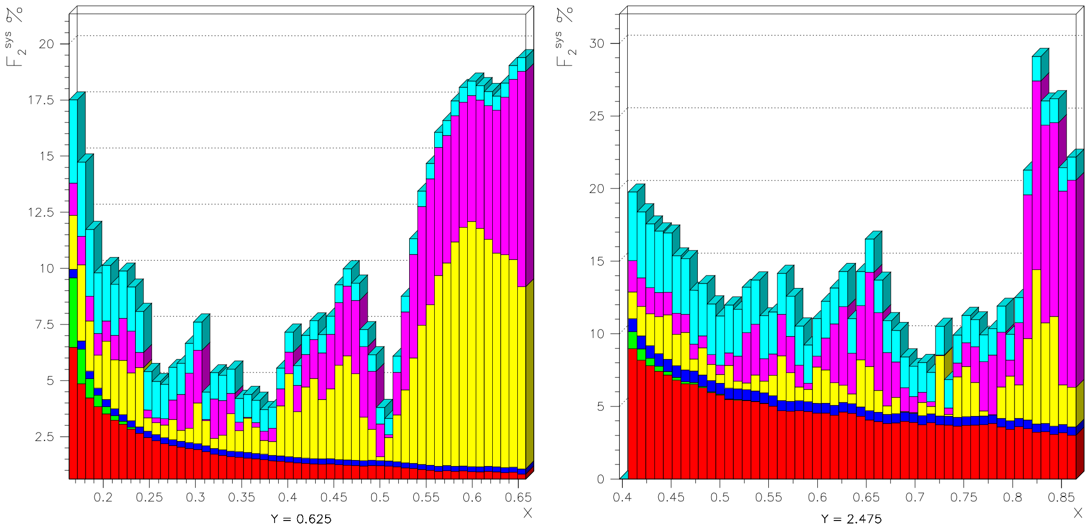

(a) $Q^2 = 0.625$ GeV^2

(b) $Q^2 = 2.475$ GeV^2

Figure 3.27: Systematic errors of the structure function $F_2(x, Q^2)$ separated by different sources: red - efficiency systematic error; green - systematic error due to e^+e^--pair production correction; blue - photoelectron correction systematic uncertainty; yellow - radiative correction systematic error; pink - systematic error due to momentum correction; lilac - systematic error related to $R = \sigma_L/\sigma_T$ uncertainty.

3.10 Moments of structure function F_2

As explained in the introduction, the final goal of this analysis is the evaluation of the Nachtmann moments of the structure function F_2. The evaluation of the latter involves the computation at fixed Q^2 of an integral over x. For this purpose in addition to the results obtained from the CLAS data, world data from [35, 44, 45, 46, 47, 48, 49, 50, 51, 52, 53, 54, 55, 56, 57, 58, 59] have been used to reach an adequate coverage (see Fig. 3.28). Data from [60, 61] were not included in analysis due to their inconsistency with other data sets [60], as described in detail in Ref. [43], and the large experimental uncertainties [61].

The total Nachtmann moments were computed as the sum of the elastic and inelastic ones:

$$M_n^{tot} = M_n^{el} + M_n^{in} \tag{3.43}$$

The contribution originated from the elastic peak was calculated according to the following expression from Ref. [18]:

$$M_n^{el} = \left(\frac{2}{1+r}\right)^{n+1} \frac{3+3(n+1)r+n(n+2)r^2}{(n+2)(n+3)} \frac{G_E^2(Q^2)+\tau G_M^2(Q^2)}{1+\tau} \tag{3.44}$$

where proton form factors $G_E^2(Q^2)$, $G_M^2(Q^2)$ are proton form factors obtained in Appendix A and $\tau = Q^2/4M^2$.

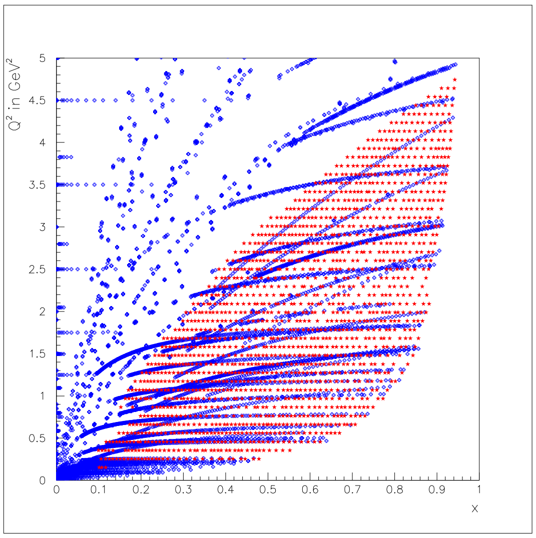

Figure 3.28: Experimental data on the structure function $F_2(x, Q^2)$ used for the moments evaluation: blue points - World data; red points - CLAS data.

However, since the various data sets are really sparse in Q^2 in the resonance region, an interpolation procedure was used. First of all interesting Q^2 range (from 0.05 to 3.75

GeV^2) was divided in 0.05 GeV^2 bins; then all the data within each Q^2 bin were collected and shifted to the central Q^2 bin value, using Q^2-dependence of the fit F_2^B described in Ref. [18]:

$$F_2(x, Q_0^2) = \frac{F_2(x, Q^2)}{F_2^B(x, Q^2)} F_2^B(x, Q_0^2) \tag{3.45}$$

The difference between real and bin-centered data

$$\delta_{F_2}^{cent}(x, Q^2) = F_2(x, Q^2) \left| 1 - \frac{F_2^B(x, Q_0^2)}{F_2^B(x, Q^2)} \right| \quad , \tag{3.46}$$

was added to the systematic errors on F_2 in order to extract the Nachtmann moments.

The inelastic Nachtmann moments have been extracted from CLAS and all available world data using interpolation or extrapolation, if necessary. For the integration the standard trapezoidal method TRAPER [31] was used. Only Q^2 bins containing more than 70% of the experimental data have been kept.

3.10.1 Interpolation

At each fixed $Q^2 = Q_0^2$ an interpolation was assumed to be necessary when the distance between the closest experimental points was greater than Δx, which was chosen equal to $\frac{0.04}{1+\sqrt{\frac{Q^2}{10}}}$ in the resonance region, 0.015 in the low x region and $0.1\{1 + \sqrt{\frac{Q^2}{10}}\}$ in the DIS region. The fit [18] normalized to the experimental data on both edges of the interpolating range has been used. The normalization has been performed in assumption that the shape of the fit is exact and only absolute normalization of the function was allowed to vary in the interpolation range:

$$F_{2_{int}}(x, Q_0^2) = \alpha(Q_0^2) F_2^B(x, Q_0^2) \tag{3.47}$$

Thus the fit function was locally adjusted to the data by a constant factor:

$$\alpha(Q_0^2) = \delta_N^2(Q_0^2) \sum_i^{|x_i - x_{a,b}| < \delta_x} \frac{F_{2_{exp}}(x_i, Q_0^2)/F_2^B(x_i, Q_0^2)}{\left(\delta_{F_{2_{exp}}}(x_i, Q_0^2)/F_2^B(x_i, Q_0^2)\right)^2} \tag{3.48}$$

In present assumption the normalization uncertainty can be written as

$$\delta_N^2(Q_0^2) = \left(\sum_i^{|x_i - x_{a,b}| < \delta_x} \frac{1}{\left(\delta_{F_{2_{exp}}}(x_i, Q_0^2)/F_2^B(x_i, Q_0^2)\right)^2} \right)^{-1} \tag{3.49}$$

where the sums run over x_a and x_b coordinates of the upper and lower edges of the interpolated region, correspondengly; δ_x was chosen equal 0.03 in resonant and very low x regions and 0.05 for DIS region.

In addition, the systematic error related to possible change of slope of the fit function in the interpolation region was evaluated as a difference in the normalization at different edges:

$$\delta_S = \left| \frac{1}{N_i} \sum_{i}^{|x_i - x_a| < \delta_x} \frac{F_{2_{exp}}(x_i, Q_0^2)}{F_2^B(x_i, Q_0^2)} - \frac{1}{N_j} \sum_{j}^{|x_j - x_b| < \delta_x} \frac{F_{2_{exp}}(x_j, Q_0^2)}{F_2^B(x_j, Q_0^2)} \right| \tag{3.50}$$

where N_i and N_j are the number of experimental points situated within the interval δ_x from interpolation region edges x_a and x_b,respectively.

Then, the statistical error of the moments was increased by adding linearly correlated contribution from each interpolation interval as follows:

$$\begin{aligned} \delta_n^{norm}(Q_0^2) = \; & \delta_N \quad (Q_0^2) \int_{x_1}^{x_2} dx \frac{\xi^{n+1}}{x^3} F_2^B(x, Q_0^2) \\ & \frac{3 + 3(n+1)r + n(n+2)r^2}{(n+2)(n+3)} \quad . \end{aligned} \tag{3.51}$$

In order to clarify the statistical error propagation let's consider only one interpolation interval at some fixed Q^2, then:

$$M_n = \sum_i I_n(x_i) w_i + \alpha(Q_0^2) S^{fit} \tag{3.52}$$

where the integrand and the interpolation area can be written as follows:

$$\begin{aligned} I_n(x_i) &= F_2(x_i) \frac{\xi_i^{n+1}}{x_i^3} \frac{3 + 3(n+1)r_i + n(n+2)r_i^2}{(n+2)(n+3)} \\ S^{fit} &= \int_{x_a}^{x_b} dx \frac{\xi^{n+1}}{x^3} \frac{3 + 3(n+1)r + n(n+2)r^2}{(n+2)(n+3)} F_2^B(x) \end{aligned} \tag{3.53}$$

and $w_i = (x_{i+1} - x_{i-1})/2$ is the coefficient in the trapezoidal integration rule, $\alpha(Q_0^2)$ given in Eq. 3.48. Therefore, partial derivative of the n-th moment for the error propagation formula is equal:

$$\frac{\partial M_n}{\partial F_2(x_i)} = \frac{\partial I_n(x_i)}{\partial F_2(x_i)} w_i + \frac{\partial \alpha(Q_0^2)}{\partial F_2(x_i)} S^{fit} \tag{3.54}$$

where

$$\begin{aligned} K_n(x_i) = \frac{\partial I_n(x_i)}{\partial F_2(x_i)} &= \frac{\xi_i^{n+1}}{x_i^3} \frac{3 + 3(n+1)r_i + n(n+2)r_i^2}{(n+2)(n+3)} \\ \frac{\partial \alpha(Q_0^2)}{\partial F_2(x_i)} &= \delta_N^2 \frac{1/F_2^B(x_i)}{(\epsilon_{F_2}(x_i)/F_2^B(x_i))^2} \end{aligned} \tag{3.55}$$

Finally, one obtains following expression for interpolation contribution to the statistical error on the n-th moment:

$$\epsilon_{M_n}^2 = \sum_i \left[\frac{\partial M_n}{\partial F_2(x_i)}\epsilon_{F_2}(x_i)\right]^2 = \sum_i \left[K_n(x_i)w_i + \delta_N^2 \frac{1/F_2^B(x_i)}{(\epsilon_{F_2}(x_i)/F_2^B(x_i))^2} S^{fit}\right]^2 \epsilon_{F_2}^2(x_i) \quad (3.56)$$

or dividing in parts:

$$\epsilon_{M_n}^2 = \epsilon_{integration}^2 + \epsilon_{interpolation}^2 + 2G_n \quad (3.57)$$

where $\epsilon_{integration}^2$ is computed by TRAPER integration routine, $\epsilon_{interpolation} = \delta_n^{norm}$ is given in Eq. 3.51 and the additional term G_n is equal:

$$G_n = \delta_N^2 S^{fit} \sum_i K_n(x_i) w_i F_2^B(x_i) \quad (3.58)$$

where the sum runs over all experimental points used for the interpolation.

The bin centering systematic uncertainty was estimated as follows:

$$\delta_n^C(Q^2) = \sum_i K_n(x_i, Q^2) w_i(Q^2) \delta_{F_2}^{cent}(x_i, Q^2) \quad (3.59)$$

The systematic error introduced in the corresponding moment by the interpolation can be estimated as

$$\delta_n^I(Q^2) = \delta_S \int_{x_1}^{x_2} dx \frac{\xi^{n+1}}{x^3} \frac{3 + 3(n+1)r + n(n+2)r^2}{(n+2)(n+3)} F_2(x, Q^2) \quad (3.60)$$

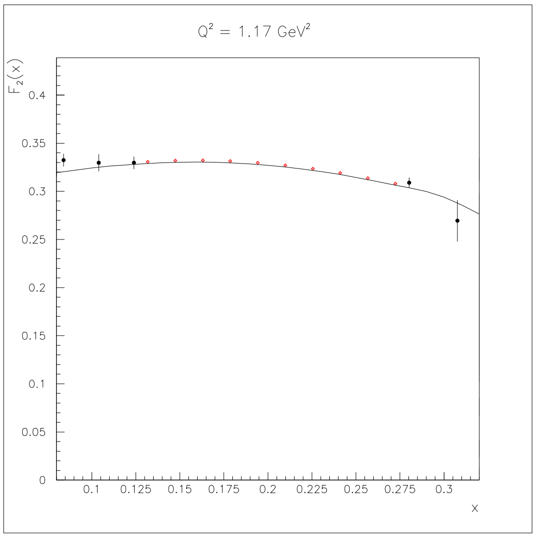

Figure 3.29: Interpolation of the structure function F_2 at $Q^2 = 1.17$ GeV^2; black points - experimental values of F_2; black line - global fit [18, 7, 41, 42, 43]; red points - interpolation (the global fit normalized to the data).

3.10.2 Extrapolation

Following the procedure developed for the interpolation at each fixed $Q^2 = Q_0^2$ an extrapolation was assumed to be necessary when the distance between the closest experimental point and one of the integration limits ($x_a = 0$ and $x_b = 1$) was greater than Δx.

Since local normalization to experimental data in case of extrapolation could introduce unknown systematic errors the original fit function and it's systematic uncertainties given in [18, 7, 41, 42, 43] were used.

At very low x we have performed a test on the functional form dependence comparing moments presented here with ones obtained by using the fitting function from the neural network parametrization of Ref. [62]; the difference appeared to be smaller than other systematic errors (see Fig. 3.31); it is significative only for M_2. The difference was added in quadrature to evaluate total systematic error of the n-th moment.

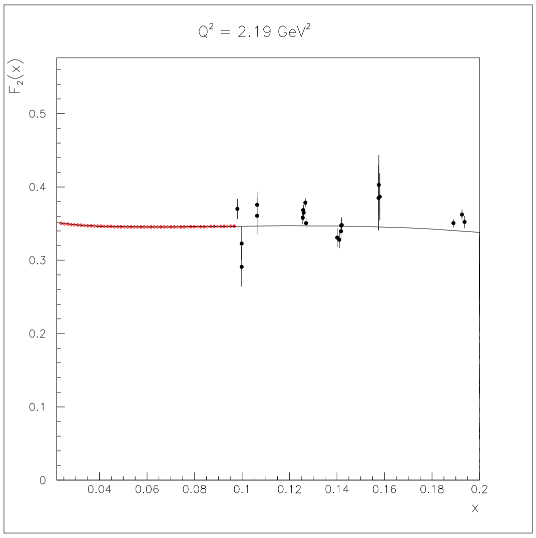

Figure 3.30: Extrapolation of the structure function F_2 at $Q^2 = 4.43$ GeV^2; black points - experimental values of F_2; black line - global fit [18, 7, 41, 42, 43]; red line - extrapolation (the global fit).

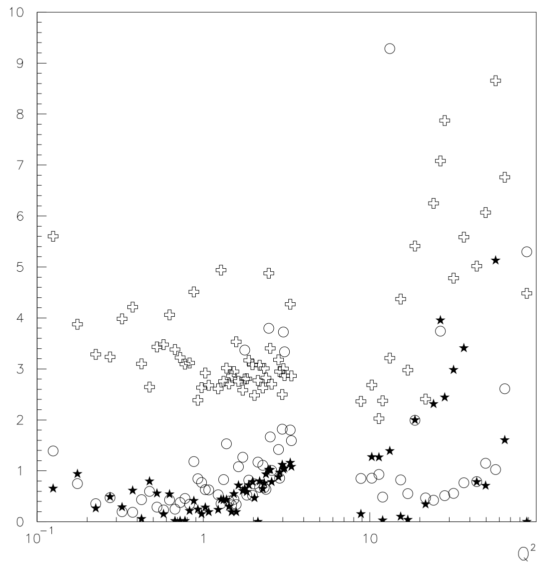

Figure 3.31: Errors of the Inelastic Nachtmann moment M_2 in percentage: empty circles represent statistical errors; empty crosses show summed in quadrature systematic errors given by Eq. 3.62; the difference between inelastic moments extracted using two different F_2 parametrizations [18] and [62] at $W > 2.5$ GeV is shown by stars.

3.10.3 Data systematic errors

Dealing with data systematic errors, one has to understand that there are many data sets measured in different laboratories and at different detectors. Therefore, only systematic errors within one data set could be in some sense correlated, because different experiments are independent.

Following this statement an upper limit of the contribution of one data set systematic errors was evaluated by a simultaneous shift of all experimental points in this set on a value of their systematic error, then the inelastic moments obtained using these distorted data were compared to the original ones, after what the contributions of each data set were summed up in quadrature as independent values:

$$\delta^D(Q^2) = \sqrt{\sum_i^{N_S} (M_n^{i(D)}(Q^2) - \bar{M}_n(Q^2))^2} \tag{3.61}$$

where N_S is a number of available data sets, $M_n^{i(D)}(Q^2)$ is n-th inelastic moment obtained by distorting i-th data set and $\bar{M}_n(Q^2)$ represents original moments, when no disturbations of data were introduced.

Obtained in present procedure error represent upper limit of data systematic errors contribution, because systematic errors in each data set were assumed to be completely correlated.

All systematic errors were summed in quadrature:

$$\delta_n^P(Q^2) = \sqrt{(\delta_n^D(Q^2))^2 + (\delta_n^C(Q^2))^2 + (\delta_n^I(Q^2))^2} \; . \tag{3.62}$$

3.10.4 World data inelastic moments

As an extension of the analysis world data at Q^2 above 5 GeV^2 were analyzed in the same way as described before. The only difference was the Q^2 bin size, which was chosen equal to 5% of Q^2. In addition bins were situated not continuously, but only where data exist. Since at large Q^2 the shape of $F_2(x, Q^2)$ remains almost constant with changing Q^2 the parameters ∇ and Δ were fixed on values 0.01 in the resonance region ($W < 1.8\ GeV$) and 0.1 for DIS. The performed study did not exhibit any significant dependence on the choice of the parameter values. In addition the bins were situated not continuously, but only where data exist.

Chapter 4

Interpretation of the Results

4.1 Extraction of leading and higher twists

The extracted moments are presented in Fig. 4.1. As already shown in Refs. [18] and [63], the extraction of higher twists at large x depends significantly on the effects of high-order radiative corrections; in particular, the use of the well established NLO approximation for the leading twist is known to lead to unreliable results for the higher twists [63]. Hereafter we will follow Ref. [63], where the pQCD corrections beyond the NLO are estimated according to soft gluon resummation (SGR) techniques.

As far as power corrections are concerned, several higher-twist operators exist and mix under the renormalization-group equations. Such mixings are rather involved and in particular the number of mixing operators increases with the order n of the moment. Since a complete calculation of the higher-twist anomalous dimensions is not yet available, we use the same phenomenological ansatz already adopted in Refs. [18] and [63]. Thus, our extracted Nachtmann moments are analyzed in terms of the following twist expansion

$$M_n^N(Q^2) = \mu_n(Q^2) + HT_n(Q^2) \ , \tag{4.1}$$

where $\mu_n(Q^2)$ is the leading twist moment and $HT_n(Q^2)$ is the higher-twist contribution given by [20]

$$\begin{aligned} HT_n(Q^2) = \quad & a_n^{(4)} \left[\frac{\alpha_s(Q^2)}{\alpha_s(\mu^2)} \right]^{\gamma_n^{(4)}} \frac{\mu^2}{Q^2} \\ + \quad & a_n^{(6)} \left[\frac{\alpha_s(Q^2)}{\alpha_s(\mu^2)} \right]^{\gamma_n^{(6)}} \frac{\mu^4}{Q^4} \ , \end{aligned} \tag{4.2}$$

where the logarithmic pQCD evolution of the twist-τ contribution is accounted for by the term $[\alpha_s(Q^2)/\alpha_s(\mu^2)]^{\gamma_n^{(\tau)}}$ (corresponding to the Wilson coefficient $E_{n\tau}(\mu, Q^2)$ in Eq. 1.47)

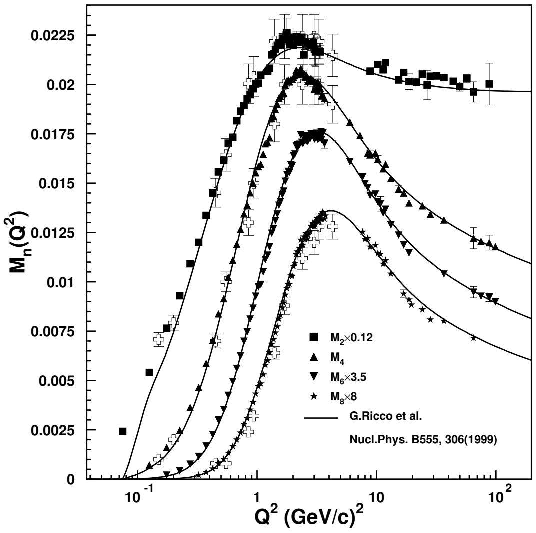

Figure 4.1: The inelastic Nachtman moments extracted from the world data, including the new CLAS results, are shown as the solid shapes. The empty crosses indicate the Nachtman moments determined in Ref. [64]. Errors are statistical only.

with an *effective* anomalous dimension $\gamma_n^{(\tau)}$ and the parameter $a_n^{(\tau)}$ (equal to the matrix element $O_{n\tau}(\mu)$ in Eq. 1.47) represents the overall strength of the twist-τ term at the renormalization scale $Q^2 = \mu^2$.

The twist-2 moment $\mu_n(Q^2)$ is generally given by the sum of non-singlet and singlet terms, leading to three unknown parameters, namely the values of the gluon and quark (non-singlet and singlet) moments at the factorization scale $Q^2 = \mu^2$. However, the decoupling in the pQCD evolution of the singlet quark and gluon densities at large x allows one to consider a pure non-singlet evolution for $n \geq 4$ (cf. [18]): this means that we have only one twist-2 parameter for $n \geq 4$, namely the value of the twist-2 moment $\mu_n(\mu^2)$ at the factorization scale $Q^2 = \mu^2$. The resummation of soft gluons does not introduce any further parameter in the description of the leading twist. Explicitly, for $n \geq 4$ the leading twist moment $\mu_n(Q^2)$ is given by

$$\begin{aligned}
\mu_n(Q^2) \quad = \quad & A_n \left[\frac{\alpha_s(Q^2)}{\alpha_s(\mu^2)}\right]^{\gamma_n^{NS}} \\
& \left\{\left[1 + \frac{\alpha_s(Q^2)}{2\pi} C_{DIS}^{(NLO)}\right] e^{G_n(Q^2)} + \right. \\
& \left. \frac{\alpha_s(Q^2)}{4\pi} R_n^{NS}\right\} \ , \qquad (4.3)
\end{aligned}$$

where the quantities γ_n^{NS}, $C_{DIS}^{(NLO)}$ and R_n^{NS} can be read off from Ref. [63]. In Eq. 4.3 the function $G_n(Q^2)$ is the key quantity of the soft gluon resummation: at next-to-leading-log it reads as

$$G_n(Q^2) = \ln(n) G_1(\lambda_n) + G_2(\lambda_n) + O[\alpha_s^k \ln^{k-1}(n)] \ , \tag{4.4}$$

where $\lambda_n \equiv \beta_0 \alpha_s(Q^2) \ln(n) / 4\pi$ and

$$\begin{aligned} G_1(\lambda) &= C_F \frac{4}{\beta_0 \lambda} \left[\lambda + (1-\lambda) \ln(1-\lambda) \right] \ , \\ G_2(\lambda) &= -C_F \frac{4\gamma_E + 3}{\beta_0} \ln(1-\lambda) \\ &\quad - C_F \frac{8K}{\beta_0^2} \left[\lambda + \ln(1-\lambda) \right] \\ &\quad + C_F \frac{4\beta_1}{\beta_0^3} \left[\lambda + \ln(1-\lambda) + \frac{1}{2} \ln^2(1-\lambda) \right] \ , \end{aligned} \tag{4.5}$$

with $C_F \equiv (N_c^2 - 1)/(2N_c)$, $k = N_c(67/18 - \pi^2/6) - 5N_f/9$, $\beta_0 = 11 - 2N_f/3$, N_c being the number of colors and N_f being the number of active flavors (in this calculations assumed $N_f = 3$). Note that the function $G_2(\lambda)$ is divergent for $\lambda \to 1$; this means that at large n (i.e. large x) the soft gluon resummation cannot be extended to arbitrarily low values of Q^2. Therefore, for a safe use of present SGR techniques we will work far from the above-mentioned divergences by limiting our analyses of low-order moments ($n \leq 8$) to $Q^2 \geq 1$ (GeV/c)^2

All the unknown parameters, namely the twist-2 parameter A_n as well as the higher-twist parameters $a_n^{(4)}, \gamma_n^{(4)}, a_n^{(6)}, \gamma_n^{(6)}$, were simultaneously determined from a χ^2-minimization procedure in the Q^2 range between 1 and 100 (GeV/c)^2. In such a procedure only the statistical errors of the experimental moments were taken into account, as well as the updated Particle Data Group value $\alpha_s(M_Z^2) = 0.118$ [65], and a renormalization scale equal to $\mu^2 = 10$ (GeV/c)^2. The uncertainties of the various twist parameters were then obtained by adding the systematic errors to the experimental moments and by repeating the twist extraction procedure. The parameter values are reported in Table 4.1, where it can be seen that: the leading twist is determined with a few percent uncertainty, while the precision of the extracted higher twists increases with n reaching an overall 10% for $n = 6$ and 8, thanks to the remarkable quality of the CLAS data at large x. Note that the leading twist is directly extracted from the data, which means that no specific functional shape of the parton distributions is assumed in our analysis. The contribution of higher twists to M_2 was too small to be extracted by the present procedure.

Our results, including the uncertainties for each twist term separately, are reported in Fig. 4.2 for $n \geq 2$, while the ratio of the total higher-twist contribution to the leading twist is shown in Fig. 4.3. It can be seen that:

- the extracted twist-2 term yields an important contribution in the whole Q^2-range of the present analysis;

Table 4.1: Extracted parameters of the twist expansion. The contribution of higher twists to M_2 was too small to be extracted by the present procedure.

	M_2	M_4	M_6	M_8
A_2	0.174$\pm$ 0.006	(1.61$\pm$ 0.04)$\times 10^{-2}$	(3.98$\pm$ 0.18)$\times 10^{-3}$	(1.39$\pm$ 0.07)$\times 10^{-3}$
$a^{(4)}$	(1.4 $\pm$ 1.8) $\times 10^{-3}$	(3.6$\pm$ 1.4)$\times 10^{-4}$	(1.9$\pm$ 0.14)$\times 10^{-4}$	(1.69$\pm$ 0.16)$\times 10^{-4}$
$\gamma^{(4)}$	-	5.7 $\pm$ 0.6	7.4 $\pm$ 0.3	6.2 $\pm$ 0.3
$a^{(6)}$	-	(-9.5 $\pm$ 3.4)$\times 10^{-5}$	(-6.57 $\pm$ 0.53)$\times 10^{-5}$	(-5.75 $\pm$ 0.44)$\times 10^{-5}$
$\gamma^{(6)}$	-	4.4 $\pm$ 0.6	5.7 $\pm$ 0.3	4.6 $\pm$ 0.3

- the Q^2-behaviour of the data leaves room for a higher-twist contribution positive at large Q^2 and negative at $Q^2 \sim 1 - 2$ (GeV/c)^2; such a change of sign requires in Eq. 4.2 a twist-6 term with a sign opposite to that of the twist-4. As already noted in Refs. [18, 63], such opposite signs make our total higher-twist contribution smaller than its individual terms;

- the total higher-twist contribution is significant at $Q^2 \approx$ few (GeV/c)^2, but it is less than $\simeq 20\%$ of the leading twist for $Q^2 > 5$ (GeV/c)^2.

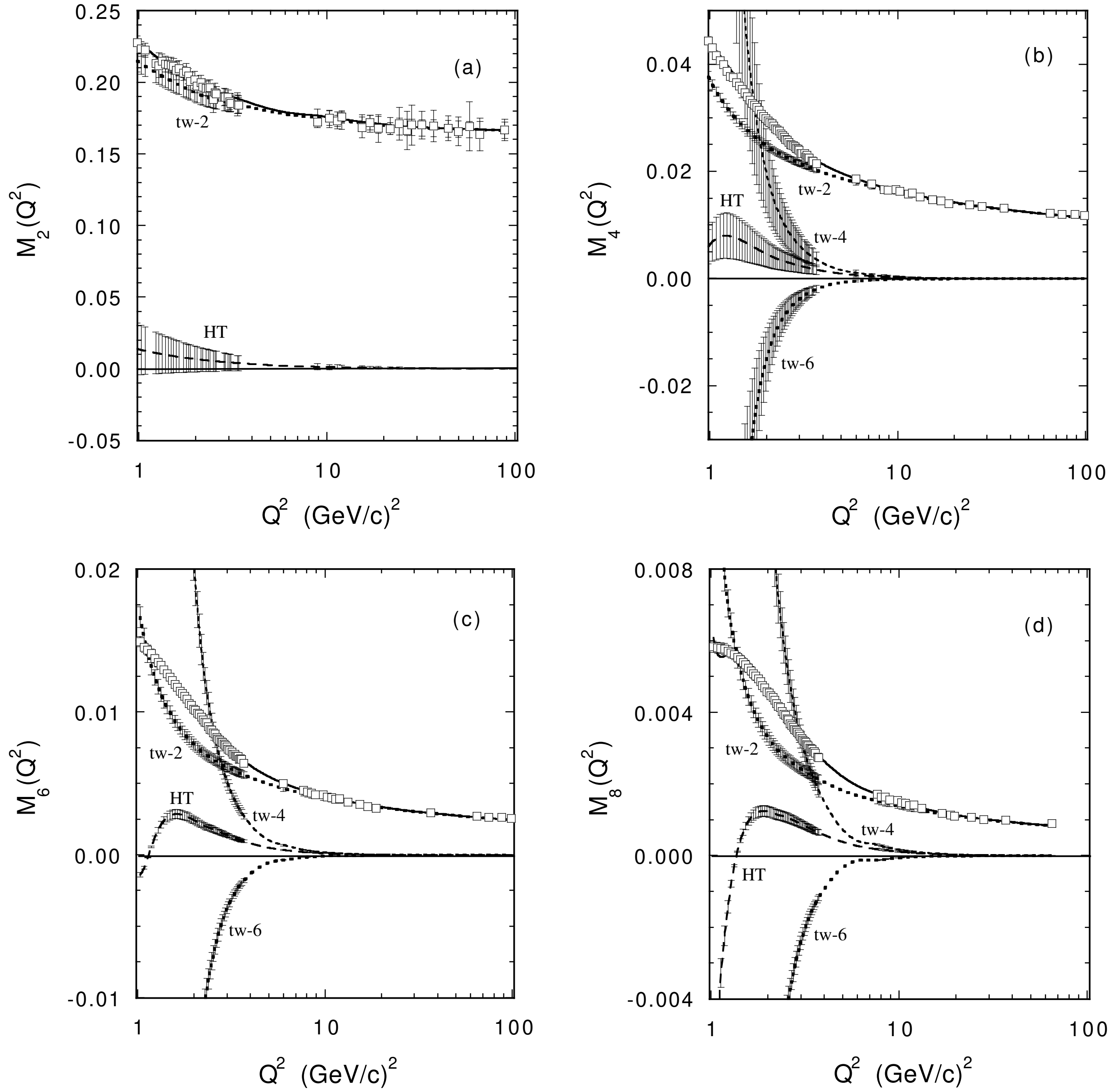

Figure 4.2: Results of the twist analysis. The open squares represent the Nachtman moments obtained in this analysis. The solid line is the fit to the moments using Eq. 4.1 with the parameters listed in Table 4.1. The twist-2, twist-4, twist-6 and higher twist (HT) contributions to the fit are indicated. The twist-2 contribution was calculated using Eq. 4.3.

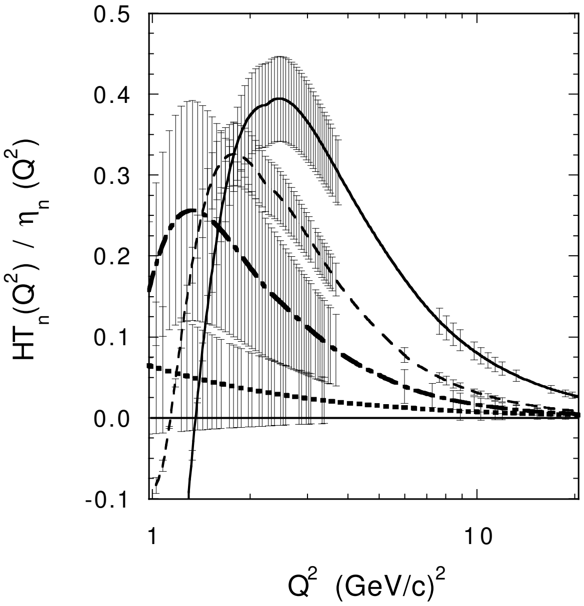

Figure 4.3: Ratio of the total higher-twist (see Eq. 4.2) to the leading twist given in Eq. 4.3. Dotted line - M_2; Dash-dotted line - M_4; dashed line - M_6; continuous line - M_8.

4.2 Conclusions

We extracted the F_2 structure function in a continuous two-dimensional range of Q^2 and x from the inclusive cross section measured with the CLAS detector. Using these data, together with the previously available world data set, we evaluated the Nachtmann moments $M_2(Q^2,x)$, $M_4(Q^2,x)$, $M_6(Q^2,x)$ and $M_8(Q^2,x)$ in the Q^2 range $0.05-100$ (GeV/c)^2. The present data set covers a large interval in x thus reducing the uncertainties in the integration procedure. The Nachtmann moments obtained in this work have been analyzed in terms of a twist expansion in order to simultaneously extract both the leading and the higher twists. The former has not been treated at fixed order in perturbation theory, but higher-order radiative corrections were taken into account by means of soft gluon resummation techniques. Higher twists have been treated phenomenologically by introducing *effective* anomalous dimensions. The range of the analysis was quite large, ranging from 1 to 100 (GeV/c)^2. The leading twist is determined with a few percent uncertainty, while the precision of the higher twists increases with n reaching an overall 10% for $n = 6$ and 8, thanks to the remarkable quality of the experimental moments.

The main results of our twist analysis can be summarized as follows: i) the contribution of the leading twist calculated in the frame of pQCD at NLO remains dominant down to $2Q^2/n \sim 1$ (GeV/c)^2, where n is the moment order. This leads to the conclusion that a pQCD-based description of the proton structure is relevant also at low Q^2, with significant but not crucial corrections; ii) the total contribution of the multi-parton correlation effects is not negligible for $Q^2 < 5$ (GeV/c)^2 and large x corresponding to the resonance region. This can be seen by comparing the higher twist contribution to M_8, which is more heavily weighted in x, to M_2; iii) different higher twist terms tend to compensate each other in such a way that their sum is small even in a Q^2 region where their absolute contributions exceed the leading twist. This cancellation is responsible for the duality phenomena and leads to the prevailing DIS-inspired picture of photon-proton collisions at low Q^2.

Therefore, we demonstrated that a precise determination of higher twists is feasible with the high quality of the new CLAS data. The main limitation of the present analysis is the use of a phenomenological ansatz for the higher twists. In this respect it is necessary to have better theoretical knowledge of the renormalization group behaviour of the relevant higher-twist operators. This would directly test QCD in its non-perturbative regime through the comparison of predictions obtained from lattice simulations with these data.

4.3 Acknowledgments

I wish to express my sincere gratitude to both my scientific advisors Prof. G. Ricco and Prof. B.S. Ishkhanov for their support during the long time of preparation of this thesis, as well as for the guidance given scientific experience.

I would like to acknowledge the essential contribution to this article given by Dr. S. Simula. Special thanks are expressed to Dr. V. Mokeev for his advisory of my undergraduate study at the physics faculty and fruitful discussions afterwards.

Finally, I thank all my colleagues from the Genova section of the Istituto Nazionale di Fisica Nucleare and Skobeltsyn Institute of Nuclear Physics for useful discussions and encourage given to me during my working period.

Bibliography

[1] O. Nachtmann, *Nucl. Phys.* **B63**, 237 (1973).

[2] R.G. Roberts, *The structure of the proton*, Cambridge University Press (1990).

[3] A. J. Buras, Rev. Mod. Phys. **52**, 199 (1980).

[4] S. Capstick and W. Roberts, nucl-th/0008028.

[5] N. Isgur and G. Karl, Phys. Lett. **B72** 109 (1977); Phys. Rev. **D20** 1191 (1979); Phys. Rev. **D23** 155 (1981); Phys. Rev. **D21** 3175 (1980); Phys. Rev. **D18** 4187 (1978).

[6] G. R. Goldstein, TUFTS-TH-G88-5 *Presented at Workshop on Diquarks, Turin, Italy, Oct 24-26, 1988.*

[7] A. Bodek *et al.*, *Phys. Rev.* **D20**, 1471 (1979); S. Stein *et al.*, *Phys. Rev.* **D12**, 1884 (1975).

[8] E. Bloom and F. Gilman, *Phys. Rev. Lett.* **25**, 1140 (1970); *Phys. Rev.* **D4**, 2901 (1971).

[9] I. Niculescu *et al.*, Phys. Rev. Lett. **85**, 1186 (2000).

[10] C. S. Armstrong *et al.*, Phys. Rev. **D63**, 094008 (2001).

[11] N. Isgur, S. Jeschonnek, W. Melnitchouk, J.W. Van Orden, Phys. Rev. **D64**, 054005 (2001).

[12] A. De Rujula, H. Georgi and H. Politzer, *Ann. Phys.* **103**, 315 (1977).

[13] K. G. Wilson, Phys. Rev. **179**, 1499 (1972).

[14] J.M. Cornwall and R.E. Norton, *Phys. Rev.* **177**, 2584 (1969).

[15] G. Altarelli, Phys. Rep. **81**, 1 (1982).

[16] M. Beneke, CERN-TH/98-233; M. Maul *et al.*, *Phys. Lett.* **B401**, 100 (1997); M. Dasgupta and B.R. Webber, *Phys. Lett.* **B382**, 273 (1996); E. Stein *et al.*, *Phys. Lett.* **B376**, 177 (1996).

[17] S. Catani *et al.*, CERN-TH/96-86; M. Cacciari and S. Catani, CERN-TH/2001-174.

[18] G. Ricco *et al.*, *Nucl. Phys.* **B555**, 306 (1999).

[19] E. Stein, M. Maul, L. Mankiewicz and A. Schafer, Nucl. Phys. **B536**, 318 (1998).

[20] X. Ji and P. Unrau, *Phys. Rev.* **D52**, 72 (1995); U.K. Yang and A. Bodek, *Phys. Rev. Lett.* **82**, 2467 (1999).

[21] CEBAF Conceptual Design Report for Experimental Equipment, (1990).

[22] M.D.Mestayer et al., Nucl.Instr. and Meth. A449, 81 (2000).

[23] D.S.Carman et al., Nucl.Instr. and Meth. A419, 315 (1998).

[24] G.Adams et al., Submitted to Nuclear Instruments and Methods:7/28/200.

[25] M.Amarian et al., Submitted to Nuclear Instruments and Methods:9/27/200.

[26] M.Anghinolfi et al., Nucl.Instr. and Meth. A447, 424 (1998).

[27] E.S.Smith et al., Nucl.Instr. and Meth. A432, 265 (1999).

[28] V.Blobel et al., The BOS system for the CLAS detector: Dynamic Memory Management, (1995).

[29] http://www.jlab.org/ claschef/.

[30] R. De Vita, Ph.D. thesis, INFN sez. di Genova (2000).

[31] http://wwwinfo.cern.ch/asd/cernlib/overview.html.

[32] P.E. Bosted *et al.*, *Phys. Rev.* **C51**, 409 (1995).

[33] P. Bosted, private communication.

[34] D. Wiser, *Ph.D. thesis*, University of Wisconsin (1977).

[35] I. Niculescu *et al.*, *Phys. Rev. Lett.* **85**, 1186 (2000); *Phys. Rev. Lett.* **85**, 1182 (2000).

[36] B. Rossi, *High Energy Particles*, Prentice-Hall, Inc., Englewood Cliffs, NJ, 1952.

[37] M. Crozon *et al.*, Nucl. Phys. **64**, 567 (1965).

[38] F. Binon *et al.*, Nucl. Phys. **B17**, 168 (1970).

[39] http://improv.unh.edu/Maurik/gsim_info.shtml.

[40] M. Osipenko *et al.*, CLAS-NOTE-2003-001, (2003).

[41] L.W. Whitlow et al., Phys. Lett. B282, 475 (1992).

[42] B. Adeva *et al.*, *Phys. Rev.* **D58**, 112001 (1998).

[43] A. Milsztajn *et al.*, *Z. Phys.* **C49**, 527 (1991).

[44] A.C. Benvenuti *et al.*,*Phys. Lett.* **B223**, 485 (1989).

[45] M.R. Adams *et al.*, *Phys. Rev.* **D54**, 3006 (1996).

[46] M. Arneodo *et al.*, *Nucl. Phys.* **B483**, 3 (1997).

[47] I. Abt *et al.*, *Nucl. Phys.* **B407**, 515 (1993).

[48] T. Ahmed *et al.*, *Nucl. Phys.* **B439**, 471 (1995).

[49] T. Ahmed *et al.*, *Nucl. Phys.* **B470**, 3 (1996).

[50] C. Adloff *et al.*, *Nucl. Phys.* **B497**, 3 (1997).

[51] C. Adloff *et al.*, DESY-99-107, (1999).

[52] M. Derrick *et al.*, *Phys. Lett.* **B316**, 412 (1993).

[53] M. Derrick *et al.*, *Z. Phys.* **C65**, 379 (1995).

[54] M. Derrick *et al.*, *Z. Phys.* **C69**, 607 (1995).

[55] M. Derrick *et al.*, *Z. Phys.* **C72**, 399 (1996).

[56] J. Brietweg *et al.*, *Phys. Lett.* **B407**, 432 (1997).

[57] J. Brietweg *et al.*, *Eur. Phys. J.* **C7**, 609 (1999).

[58] L.W. Whitlow *et al.*, *Phys. Lett.* **B282**, 475 (1992).

[59] A. Bodek *et al.*, *Phys. Rev.* **D20**, 1471 (1979); M. Mestayer, SLAC-214, (1978); W.B. Atwood *et al.*, *Phys. Lett.* **B64**, 479 (1976); S. Stein *et al.*, *Phys. Rev.* **D12**, 1884 (1975); E.M. Riordan *et al.*, SLAC-PUB-1634, (1975); A. Bodek *et al.*, *Phys. Rev. Lett.* **30**, 1087 (1973); J.S. Poucher *et al.*, *Phys. Rev. Lett.* **32**, 118 (1974); G. Miller *Phys. Rev.* **D5**, 528 (1972); E.D. Bloom *et al.*, SLAC-PUB-653, (1971); M. Breidendach, MIT-2098-635, (1970).

[60] J.J. Aubert *et al.*, *Nucl. Phys.* **B259**, 189 (1985).

[61] D. Allasia *et al.*, *Z. Phys.* **C28**, 321 (1991).

[62] S. Forte *et al.*, hep-ph/0204232, (2002).

[63] S. Simula, *Phys. Lett.* **B493**, 325 (2000).

[64] C.S. Armstrong *et al.*, *Phys. Rev.* **D63**, 094008 (2001).

[65] Particle Data Group, D.E. Groom *et al.*, *Eur. Phys. Jour.* **C15**, 1 (2000).

[66] M.K. Jones *et al.*, *Phys. Rev. Lett.* **84**, 1398 (2000).

[67] L.W. Whitlow *et al.*, *Phys. Lett.* **B250**, 193 (1990).

[68] J. Bartelski *et al.*, hep-ph/9804415, (1998).

[69] V. Burkert, CEBAF-PR-93-035, (1993).

[70] J. Drees *et al.*, *Z. Phys.* **C7**, 183 (1981).

[71] L.M. Stuart *et al.*, *Phys. Rev.* **D58**, 032003 (1998).

[72] L.W. Mo and Y.S. Tsai, *Rev. Mod. Phys.* **41**, 205 (1969); Yung-Su and Tsai, *Phys. Rev.* **122**, 1898 (1961).

[73] I. Akushevich *et al.*, *Acta Phys. Polon.* **B28**, 563 (1997).

[74] T. Kukhto, N. Shumeiko, Nucl. Phys. **B219**, 412 (1983).

[75] I. V. Akushevich, N. M. Shumeiko, J. Phys. **G20**, 513 (1994).

[76] D. Bardin, N. Shumeiko, Nucl. Phys. **B127**, 242 (1977).

[77] S.I. Bilenkaya *et al.*, *JETP Lett.* **19**, 317 (1974).

[78] F.W. Brasse *et al.*, *Nucl. Phys.* **B110**, 413 (1976).

Appendix A

Fit of the proton form factors

Since precision of the proton form factors is crucial for the present analysis, recent high precision TJNAF Hall A data on the ratio $\frac{G_E}{G_M}$ [66] force us to modify the existing parametrization [32]. The magnetic form factor G_M is very well established (see Fig. A.1(a)), whereas G_E is not. Therefore, the electric form factor G_E from the parametrization [32] was adjusted to accommodate the new data. This was accomplished by making a polynomial fit to the data as follow:

$$\frac{G_E}{G_M}(Q^2) = \frac{G_{E_{Bosted}}(Q^2)(1-(A+BQ^2))}{G_{M_{Bosted}}(Q^2)} \tag{A.1}$$

where A and B are free parameters. The resulting function $G_E(Q^2)$, shown in Fig. A.1(b), was computed as:

$$G_E(Q^2) = G_{E_{Bosted}}(Q^2)\left(1 - 0.2\frac{Q^2-0.4}{1.6}\right) \tag{A.2}$$

We stress that the elastic cross section in the interesting kinematic region is not very sensitive to this correction and the difference is much lower than the precision of the parametrization [32].

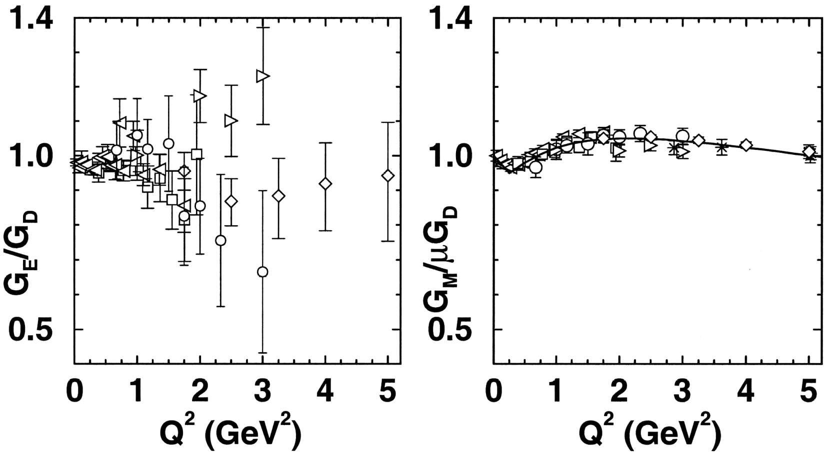

(a) World data for G_E/G_D and G_M/G_D. Solid curve is a fit to G_M data [32].

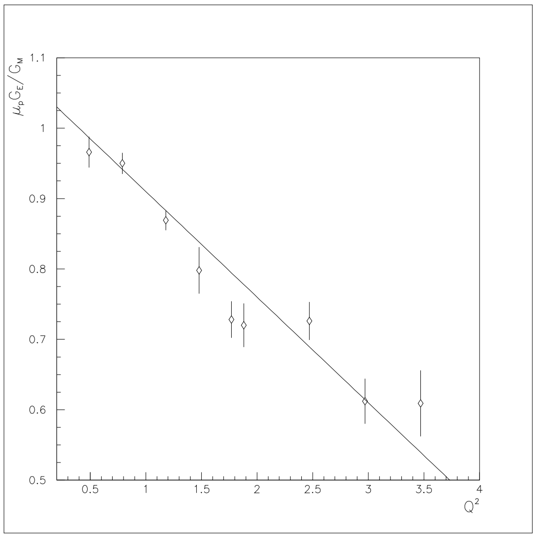

(b) The fit of ratio $\frac{G_E}{G_M}$.

Figure A.1: The elastic proton form factors.

Appendix B

Fit of the ratio $R \equiv \sigma_L/\sigma_T$

The function $R(x, Q^2)$ was described as follows:

$$R(x,Q^2) = \begin{cases} \frac{(1-x)^3}{(1-x_{th})^3}\left(0.041\frac{\xi_{th}}{\log\frac{Q^2}{0.04}} + \frac{0.592}{Q^2} - \frac{0.331}{(0.09+Q^4)}\right) & W < 2.5 \\ 0.041\frac{\xi}{\log\frac{Q^2}{0.04}} + \frac{0.592}{Q^2} - \frac{0.331}{(0.09+Q^4)} & W > 2.5 \end{cases} \tag{B.1}$$

This parametrization of $R(x, Q^2)$ consists of two different parts: the fit for the DIS region ($W > 2.5$ GeV) [67, 68] and the function, adjusted to scarce data at small Q^2 [69, 70, 71], in the resonance region ($W < 2.5$ GeV). The systematic error on this parametrization was estimated according to Ref. [18] as follows:

$$\delta_R = \begin{cases} 0.08 & W < 2.5\ , \\ \frac{0.006\xi}{\zeta} + \frac{0.01}{Q^2} - \frac{0.01}{(0.09+Q^4)} & W > 2.5 \end{cases} \tag{B.2}$$

where

$$\begin{aligned} \zeta &= \log\frac{Q^2}{0.04} \\ \xi &= 1 + 12\frac{Q^2}{1+Q^2}\frac{0.015625}{0.015625+x^2} \\ \xi_{th} &= \xi(W = 2.5) \\ x_{th} &= x(W = 2.5) \end{aligned} \tag{B.3}$$

All dimensional variables are given in GeV.

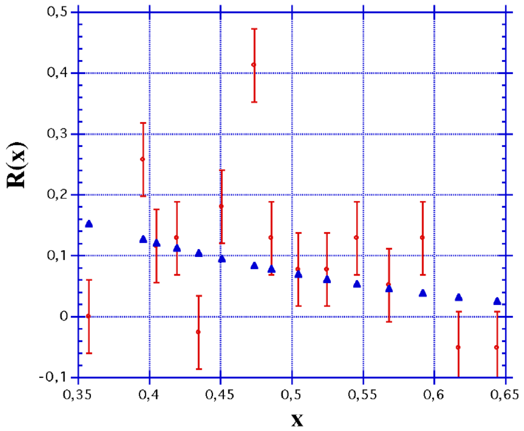

(a) $Q^2 = 1.1GeV^2$

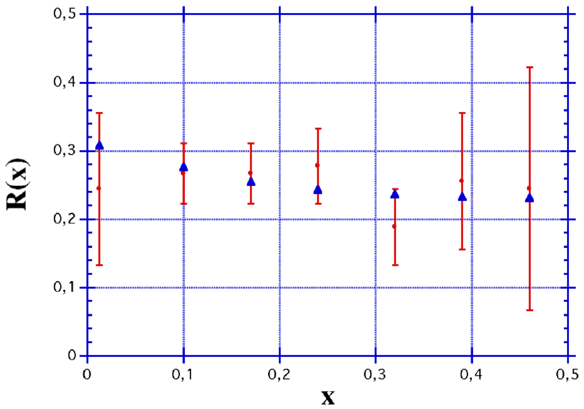

(b) $Q^2 = 2GeV^2$

Figure B.1: The fit of ratio R at small Q^2: red points - experimental data [69, 70, 71]; blue points - fit developed in [18].

Appendix C

Radiative corrections

One of the important tasks of the analysis is the evaluation of the radiative corrections. The radiative corrections to the elastic and inelastic inclusive electron scattering on the proton were applied according to [72].

C.1 Correction to the elastic cross section

The corrected elastic ep cross section was evaluated as:

$$\frac{d\sigma}{d\Omega}_{cor} = \frac{d\sigma}{d\Omega}_{exp} \exp\left(-\delta - \delta_t\right) \tag{C.1}$$

where $\frac{d\sigma}{d\Omega}_{exp}$ is the measured elastic cross section, $\frac{d\sigma}{d\Omega}_{cor}$ is the corrected cross section and:

$$
\begin{aligned}
\delta \;=\;& -\frac{\alpha}{\pi}\Bigg(\frac{28}{9}-\frac{13}{6}\ln\left(\frac{-q^2}{m_e^2}\right)+\left(\ln\left(\frac{-q^2}{m_e^2}\right)-1+2Z\ln\eta\right)\left(2\ln\frac{E_1}{\Delta E}-3\ln\eta\right)- \\
& \Phi\left(\frac{E_3-E_1}{E_3}\right)-Z^2\ln\frac{E_4}{M}+Z^2\ln\frac{M}{\eta\Delta E}\left(\frac{1}{\beta_4}\ln\frac{1+\beta_4}{1-\beta_4}-2\right)+ \\
& \frac{Z^2}{\beta_4}\left\{\frac{1}{2}\ln\frac{1+\beta_4}{1-\beta_4}\ln\frac{E_4+M}{2M}-\Phi\left[-\left(\frac{E_4-M}{E_4+M}\right)^{\frac{1}{2}}\left(\frac{1+\beta_4}{1-\beta_4}\right)^{\frac{1}{2}}\right]\right\}+ \\
& Z\Bigg[\Phi\left(-\frac{M-E_3}{E_1}\right)-\Phi\left(\frac{M(M-E_3)}{2E_3E_4-ME_1}\right)+\Phi\left(\frac{2E_3(M-E_3)}{2E_3E_4-ME_1}\right)+ \\
& \ln\left|\frac{2E_3E_4-ME_1}{E_1(M-2E_3)}\right|\ln\left(\frac{M}{2E_3}\right)\Bigg]- \\
& Z\Bigg[\Phi\left(-\frac{E_4-E_3}{E_3}\right)-\Phi\left(\frac{M(E_4-E_3)}{2E_1E_4-ME_3}\right)+\Phi\left(\frac{2E_1(E_4-E_3)}{2E_1E_4-ME_3}\right)+ \\
& \ln\left|\frac{2E_1E_4-ME_3}{E_3(M-2E_1)}\right|\ln\left(\frac{M}{2E_1}\right)\Bigg]- \\
& Z\Bigg[\Phi\left(-\frac{M-E_1}{E_1}\right)-\Phi\left(\frac{M-E_1}{E_1}\right)+\Phi\left(\frac{2(M-E_1)}{M}\right)+ \\
& \ln\left|\frac{M}{2E_1-M}\right|\ln\left(\frac{M}{2E_1}\right)\Bigg]+ \\
& Z\Bigg[\Phi\left(-\frac{M-E_3}{E_3}\right)-\Phi\left(\frac{M-E_3}{E_3}\right)+\Phi\left(\frac{2(M-E_3)}{M}\right)+ \\
& \ln\left|\frac{M}{2E_3-M}\right|\ln\left(\frac{M}{2E_3}\right)\Bigg]\Bigg)- \\
& \frac{\alpha}{\pi}\Bigg(-\Phi\left(\frac{E_1-E_3}{E_1}\right)-\frac{Z^2}{\beta_4}\Bigg\{\Phi\left[\left(\frac{E_4-M}{E_4+M}\right)^{\frac{1}{2}}\left(\frac{1-\beta_4}{1+\beta_4}\right)^{\frac{1}{2}}\right]- \\
& \Phi\left[\left(\frac{E_4-M}{E_4+M}\right)^{\frac{1}{2}}\right]+\Phi\left[-\left(\frac{E_4-M}{E_4+M}\right)^{\frac{1}{2}}\right]\Bigg\}\Bigg) \qquad \text{(C.2)}
\end{aligned}
$$

represents the Schwinger correction and:

$$
\delta_t=-\left\{\left[b_w t_{iw}+\frac{1}{2}bT\right]\ln\left(\frac{E_1}{\eta^2\Delta E}\right)+\left[b_w t_{fw}+\frac{1}{2}bT\right]\ln\left(\frac{E_3}{\Delta E}\right)\right\} \qquad \text{(C.3)}
$$

is related to the straggling effect in the target. Due to the very small value of the target thickness the contribution of the straggling correction is negligible. Functions, variables and constants used in Eq. C.2 and Eq. C.3 were defined as: $\Phi(x)$ is the Spence function, E_1, E_3, E_4 are energies of incident electron, scattered electron and the recoil nucleon, respectively; β_4 is the velocity of the recoil particle in units of the velocity of light; $\eta = \frac{E_1}{E_3}$ and $\Delta E = \Delta E_3 = E_{3_{peak}} - E_{3_{min}}$ is related to energy resolution of detector;

$$b = \frac{4}{3}\left\{1 + \frac{1}{9}\frac{\frac{Z+1}{Z+\xi}}{\ln 183 Z^{-\frac{1}{3}}}\right\} \tag{C.4}$$

$$\xi = \frac{\ln 1440 Z^{-\frac{2}{3}}}{\ln 183 Z^{-\frac{1}{3}}} \tag{C.5}$$

here Z is the atomic number of the target particle; in the case of the E1c run period: $T = 0.0056$, $t_{iw} = 0.00023$ and $t_{fw} = 0.00012$ - the target input and exit windows thickness, respectively, in units of radiation length.

C.2 Correction to the inelastic cross section

The radiative corrections to the inelastic inclusive *ep* cross section were accomplished following the unfolding procedure developed by Mo and Tsai [72], and the corresponding code was developed.

The procedure can be divided in two stages: first of all one has to remove the elastic peak tail from the inelastic spectrum. It is essential to use the exact formula to calculate the elastic radiative tail, which is usually the most dominant background to the inelastic electron scattering, because the peaking approximation can be in error by as much as 30% to 40% when the energy of the scattered electron is $E' < E_{elastic}$. The radiative tail from the elastic peak was computed as:

$$
\begin{aligned}
\frac{d\sigma^2}{d\Omega dp} &= \frac{\alpha^3}{(2\pi)^2}\left(\frac{E_p}{E_s}\right)\frac{1}{M}\int_{-1}^{1}\frac{\omega d(\cos\theta_k)}{2q^4(u_0-|u|\cos\theta_k)} \\
&\Bigg(M^2F_j(q^2)\Bigg\{-\frac{2\pi a m_e^2}{(a^2-b^2)^{\frac{3}{2}}}\left[2E_s(E_p+\omega)+\frac{q^2}{2}\right]- \\
&\frac{2\pi a' m_e^2}{(a'^2-b'^2)^{\frac{3}{2}}}\left[2E_p(E_s-\omega)+\frac{q^2}{2}\right]-4\pi+ \\
&4\pi\left(\frac{\nu}{(a^2-b^2)^{\frac{1}{2}}}-\frac{\nu'}{(a'^2-b'^2)^{\frac{1}{2}}}\right)\{m_e^2(sp-\omega^2)+ \\
&(sp)[2E_sE_p-(sp)+\omega(E_s-E_p)]\}+ \\
&\frac{2\pi}{(a^2-b^2)^{\frac{1}{2}}}\left[2(E_sE_p+E_s\omega+E_p^2)+\frac{q^2}{2}-(sp)-m_e^2\right]- \\
&\frac{2\pi}{(a'^2-b'^2)^{\frac{1}{2}}}\left[2(E_sE_p-E_p\omega+E_s^2)+\frac{q^2}{2}-(sp)-m_e^2\right]\Bigg\}+ \\
&G_j(q^2)\Bigg[\left(\frac{2\pi a}{(a^2-b^2)^{\frac{3}{2}}}+\frac{2\pi a'}{(a'^2-b'^2)^{\frac{3}{2}}}\right)m_e^2(2m_e^2+q^2)+8\pi- \\
&8\pi\left(\frac{\nu}{(a^2-b^2)^{\frac{1}{2}}}-\frac{\nu'}{(a'^2-b'^2)^{\frac{1}{2}}}\right)(sp)(sp-2m_e^2)+ \\
&2\pi[\frac{1}{(a^2-b^2)^{\frac{1}{2}}}-\frac{1}{(a'^2-b'^2)^{\frac{1}{2}}}](2sp+2m_e^2-q^2)\Bigg]\Bigg)
\end{aligned}
\tag{C.6}
$$

where the proton form-factors $F_j(q^2)$ and $G_j(q^2)$ were obtained from the parametrization [32], already mentioned above, as:

$$
\begin{aligned}
F_j(q^2) &= 4\frac{G_E^2(Q^2)+\tau G_M^2(Q^2)}{1+\tau} \\
G_j(q^2) &= Q^2G_M^2(Q^2)
\end{aligned}
\tag{C.7}
$$

where

$$
\tau = \frac{Q^2}{4M^2}
\tag{C.8}
$$

The kinematic variables in Eq. C.6 are defined as following: $s=(E_s,s)$, $p=(E_p,p)$, $k=(\omega,k)$ are four momenta of incident, outgoing electron and real photon emitted, respectively; $u = (u_0, u) \equiv s + p_i - p = p_f + k$, where $p_i = (M, 0)$ is the four momentum of the target particle; $p_f = s + p_i - p - k$ is the four momentum of the final hadronic system, $q^2 = (s - p - k)^2 = (p_f - p_i)^2$ is the four momentum transfer, and:

$$\begin{aligned}
\omega &= \frac{1}{2}\frac{u^2 - M_f^2}{u_0 - |u|\cos\theta_k} \\
q^2 &= 2m_e^2 - 2E_sE_p + 2|s||p|\cos\theta + 2M^2 - 2\omega(E_s - E_p) + 2\omega|u|\cos\theta_k \\
\nu &= \frac{-|p|\sin\theta_p}{\omega[E_p|s|\sin\theta_s - E_s|p|\sin\theta_p + |s||p|\sin\theta\cos\theta_k]} \\
\nu' &= \frac{-|s|\sin\theta_s}{\omega[E_p|s|\sin\theta_s - E_s|p|\sin\theta_p + |s||p|\sin\theta\cos\theta_k]} \\
a &= \omega(E_p - |p|\cos\theta_p\cos\theta_k) \\
b &= -\omega|p|\sin\theta_p\sin\theta_k \\
a' &= \omega(E_s - |s|\cos\theta_s\cos\theta_k) \\
b' &= -\omega|s|\sin\theta_s\sin\theta_k
\end{aligned} \tag{C.9}$$

where θ is the scattering electron angle; θ_k is angle between u and k; θ_s is angle between u and s; θ_p is angle between u and p.

The effect of straggling on the radiative tail from the elastic peak was computed as:

$$\begin{aligned}
\frac{d\sigma_t^2}{d\Omega dE_p}(E_s, E_p, T) &= I_b(E_s, E_p\eta_1, \frac{1}{2}T)\eta_1^2\frac{d\sigma_0}{d\Omega}(E_p\eta_1) + \\
& I_b(\frac{E_s}{\eta_2}, E_p, \frac{1}{2}T)\frac{d\sigma_0}{d\Omega}(E_s)
\end{aligned} \tag{C.10}$$

where

$$\begin{aligned}
\eta_1 &= \frac{1}{1 - \frac{E_p}{M}(1 - \cos\theta)} \\
\eta_2 &= 1 + \frac{E_s}{M}(1 - \cos\theta)
\end{aligned} \tag{C.11}$$

$$I_b(E_0, E, t) = \frac{1}{E_0}\frac{[\ln(\frac{E_0}{E})]^{bt-1}}{\Gamma(bt)} \tag{C.12}$$

On the second stage, when the radiative tail from the elastic peak has already been subtracted from the measured cross section, one can express the corrected cross section as following:

$$
\begin{aligned}
\frac{d\sigma^2}{d\Omega dE_p}(E_s,\theta,E_p) &= \exp\left(-\delta_t-\delta_r\right)\left[\frac{d\sigma^2_{exp}}{d\Omega dE_p}(E_s,\theta,E_p)-\right.\\
&\left(\frac{\Delta}{E_p}\right)^{\frac{f_p}{2}}\int_{E_{s_{min}}(E_p)}^{E_s-\Delta}\frac{dE'_s}{E_s-E'_s}\psi(x_s)\frac{d\sigma^2}{d\Omega dE_p}(E'_s,\theta,E_p)-\\
&\left.\left(\frac{\Delta}{E_s}\right)^{\frac{f_s}{2}}\int_{E_p+\Delta}^{E_{p_{max}}(E_s)}\frac{dE'_p}{E'_p-E_p}\psi(x_p)\frac{d\sigma^2}{d\Omega dE'_p}(E_s,\theta,E'_p)\right] \quad \text{(C.13)}
\end{aligned}
$$

where $\frac{d\sigma^2}{d\Omega dE_p}$ is the desired corrected cross section; $\frac{d\sigma^2_{exp}}{d\Omega dE_p}$ is the measured cross section after elastic radiative tail subtraction and functions:

$$
\begin{aligned}
\psi(x_s) &= \{t_s+(b_w t_{iw}+\frac{1}{2}bT)[x_s+\frac{3}{4}(1-x_s)^2]\}(\ln\frac{1}{x_s})^{f_s}\\
\psi(x_p) &= \{t_p+(b_w t_{fw}+\frac{1}{2}bT)[x_p+\frac{3}{4}(1-x_p)^2]\}(\ln\frac{1}{x_p})^{f_p}\\
\delta_t &= -\left[\left(b_w t_{iw}\right)\ln\frac{E_s}{\Delta}+[b_w t_{fw}+\frac{1}{2}bT]\ln\frac{E_p}{\Delta}\right]\\
\delta_r &= -\frac{\alpha}{\pi}\left[\frac{28}{9}-\frac{13}{6}\ln\frac{2sp}{m_e^2}+\left(\ln\frac{E_s}{\Delta}+\ln\frac{E_p}{\Delta}\right)\left(\ln\frac{2sp}{m_e^2}-1\right)-\right.\\
&\left.\Phi\left(-\frac{E_s-E_p}{E_p}\right)-\Phi\left(\frac{E_s-E_p}{E_s}\right)\right] \quad \text{(C.14)}
\end{aligned}
$$

$$
\begin{aligned}
f_s &= bt_r + b_w t_{iw} + \frac{1}{2}bT \\
f_p &= bt_r + b_w t_{fw} + \frac{1}{2}bT \\
t_r &= \frac{\alpha}{\pi b}[\ln\frac{2sp}{m_e^2} - 1] \\
t_{s,p} &= \frac{\alpha}{\pi}\{\frac{1}{2}(1+x_{s,p}^2)\ln\frac{2sp}{m_e^2} - x_{s,p}\} \\
x_s &= \frac{E'_s}{E_s} \\
x_p &= \frac{E_p}{E'_p} \\
E_{s_{min}}(E_p) &= \frac{m_\pi^2 + 2M_p m_\pi + 2M_p E_p}{2M_p - 2E_p(1-\cos\theta)} \\
E_{p_{max}}(E_s) &= \frac{2M_p E_s - 2M_p m_\pi - m_\pi^2}{2M_p + 2E_s(1-\cos\theta)}
\end{aligned}
\tag{C.15}
$$

The first term in Eq. C.13 represents the Schwinger correction contribution and the two integrals correspond to the bremsstrahlung of the initial and scattered electron, respectively. Since the bremsstrahlung processes require corrected inelastic cross sections to be known, one should use all available experimental information in order to estimate this correction. In the present analysis contribution of the bremsstrahlung of the scattered electron was evaluated precisely based only on experimental inclusive cross sections obtained here. This was accomplished for each E' spectrum at fixed θ by starting from the first point in the neighborhood of the pion threshold, where this correction obviously equals to zero, going toward increasing W point by point, using already corrected experimental points to compute the integral. Unfortunately, the bremsstrahlung of the initial electron cannot be computed precisely in the present analysis due to limitations on the available kinematic region. The method (interpolation or extrapolation along the equimissing mass line) described by Mo and Tsai [72] intended for the calculation of this integral requires a similar W-range at fixed θ to be covered by data at many different beam energies. To estimate the contribution from this process, Bodek's fit of the SLAC data [7] was used; before making this integral, fit [7] folded with the radiative corrections was compared with uncorrected data and it appeared to agree within few percent (see figure C.1). Since the contribution of this integral to the cross section in the present kinematics is not more than 10% and the average deviation of the fit [7] from our data is not more than 10%, the total systematic uncertainty related to the bremsstrahlung of the initial electron is very small (less than 1%).

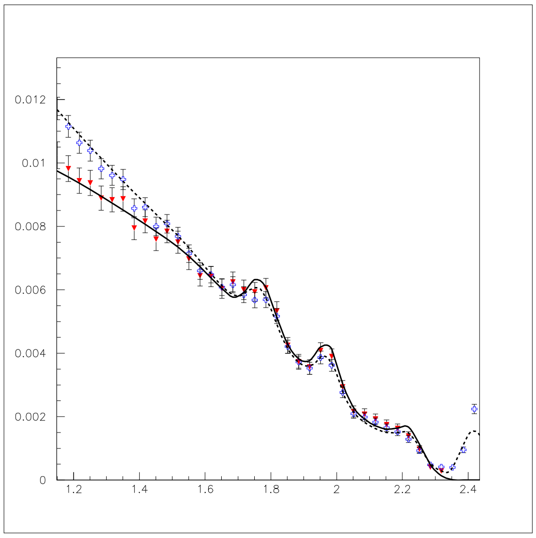

Figure C.1: Corrected and uncorrected data in comparison to "radiated" and pure Bodek's fit; at $E = 4.0$ GeV and $\theta = 30°$; blue open circles - measured cross section, red filled triangles - corrected data, solid line - Bodek's fit [7], dashed line - Bodek's fit with radiative processes (Schwinger correction, bremsstrahlung and straggling).

An accurate check of the radiative correction code was performed, reproducing all the samples given in [72] (see tables C.1, C.2, C.3, C.4, C.5, C.6, and figures C.2, C.3, C.4, C.5).

Table C.1: Example A. Radiative correction for e^-p elastic scattering, $E_1 = 0.9GeV$, $E_3 = 0.327GeV$, $\theta = 145°$; [72] formula II.6; data from [72] chapter IV

	δ_{Tsai}	δ_{prog}
η	2.75	2.752
E_4	1.511	1.5111
β_4	0.783	0.7839
Q^2	1.075	1.07075
δ	-0.15	-0.14335

In order to test the inelastic radiative correction procedure a comparison of the present method against recently developed code POLRAD 2.0 [73] has been performed. This code is based on a very detailed theoretical framework [74, 75, 76] where exact calculations of radiative tails at one-loop level are included. The advantage of exact calculation is absent of the soft photon cut-off parameter ΔE.

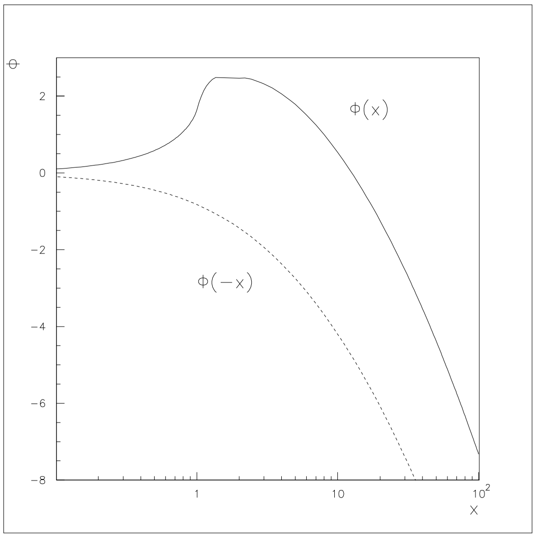

Figure C.2: Spence function $\Phi(x)$; solid line - $\Phi(x)$, dashed line - $\Phi(-x)$; compared to [72] Fig. 5.

Table C.2: Example B. Radiative correction for $e^{-}p$ elastic scattering, $E_1 = 5GeV$, $E_3 = 0.5GeV$, $\theta = 133°$; [72] formula II.6; data from [72] chapter IV

	δ_{Tsai}	δ_{prog}
η	10	10
E_4		5.438
β_4	0.975	0.985
Q^2		8.4417
δ	-0.21	-0.2284

Table C.3: Radiative corrections for $e^{-}\ {}^{48}Ca$ elastic scattering; $E_1 = 0.5GeV$ ($\Delta E_3/E_3 = 1\%$); data from [72] Tab.II (Tsai row)

E_3	θ	δ_{Tsai}	δ_{prog}
0.4993	30°	-0.1912	-0.1921
0.4972	60°	-0.2170	-0.2212
0.4945	90°	-0.2341	-0.2423
0.4918	120°	-0.2465	-0.2586

The difference between these two approaches (see Fig. C.6 and Fig. C.7) was calculated

Table C.4: Radiative corrections for e^-p elastic scattering ($\Delta E_3/E_3 = 1\%$); data from [72] Tab.I (row called "by Tsai")

E_1	E_3	θ	δ_{Tsai}	δ_{prog}
2.206	2.022	15.999°	-0.2195	-0.2197
2.201	1.455	38.601°	-0.2507	-0.2513
6.032	4.687	17.186°	-0.2606	-0.2626
10.723	8.005	14.0°	-0.2769	-0.2806
11.999	7.997	16.082°	-0.2880	-0.2922
13.329	8.006	17.6°	-0.2965	-0.3009
14.649	7.992	18.8°	-0.3034	-0.3078
15.999	8.007	19.7°	-0.3090	-0.3134
17.314	3.975	35.1°	-0.3271	-0.3270

Table C.5: Radiative tail from elastic e^-p scattering at 5°; data from [72] Tab.III (Exact row)

E_s $[GeV]$	E_p $[GeV]$	$Tail_{Tsai}$ $\left[\frac{mcbn}{GeV sr}\right]$	$Tail_{prog}$ $\left[\frac{mcbn}{GeV sr}\right]$	$\frac{d\sigma_0}{d\Omega}_{Tsai}$ $\left[\frac{mcbn}{GeV sr}\right]$	$\frac{d\sigma_0}{d\Omega}_{prog}$ $\left[\frac{mcbn}{GeV sr}\right]$
20	18.4	$15.85 * 10^{-3}$	$15.93 * 10^{-3}$	$22.0 * 10^{-3}$	$22.0 * 10^{-3}$
	17.5	$1.884 * 10^{-3}$	$1.886 * 10^{-3}$		
	16.5	$1.246 * 10^{-3}$	$1.247 * 10^{-3}$		
	10.0	$5.011 * 10^{-3}$	$5.017 * 10^{-3}$		
	5.0	$42.70 * 10^{-3}$	$42.75 * 10^{-3}$		
	1.5	$581.9 * 10^{-3}$	$583.0 * 10^{-3}$		
5	4.8	17.26	17.28	29.6	29.6
	4.5	4.533	4.538		
	4.0	2.250	2.252		
	2.5	1.665	1.666		
	1.0	5.69	5.70		
1	0.98	$3.733 * 10^3$	$3.737 * 10^3$	$1.38 * 10^3$	$1.38 * 10^3$
	0.9	$0.6244 * 10^3$	$0.6251 * 10^3$		
	0.7	$0.2275 * 10^3$	$0.2278 * 10^3$		
	0.5	$0.1934 * 10^3$	$0.1938 * 10^3$		
	0.3	$0.3048 * 10^3$	$0.3081 * 10^3$		
	0.2	$0.5435 * 10^3$	$0.5615 * 10^3$		

Table C.6: Radiative tail from continuous spectra; data from [72] Tab.IV (Exact row)

E_s $[GeV]$	E_p $[GeV]$	$Tail_{Tsai}$ $\left[\frac{mcbn}{GeV\,sr}\right]$	$Tail_{prog}$ $\left[\frac{mcbn}{GeV\,sr}\right]$	$\frac{d\sigma_0}{d\Omega}_{Tsai}$ $\left[\frac{mcbn}{GeV\,sr}\right]$	$\frac{d\sigma_0}{d\Omega}_{prog}$ $\left[\frac{mcbn}{GeV\,sr}\right]$
20	17.5	$1.94 * 10^{-3}$	$1.93 * 10^{-3}$	$16.1 * 10^{-3}$	$16.1 * 10^{-3}$
	16.5	$1.032 * 10^{-3}$	$1.010 * 10^{-3}$		
	10.0	$2.373 * 10^{-3}$	$2.265 * 10^{-3}$		
	5.0	$8.916 * 10^{-3}$	$9.38 * 10^{-3}$		
	1.5	$17.15 * 10^{-3}$	$18.0 * 10^{-3}$		
5	4.5	8.246	8.250	8.59	8.61
	4.0	0.8624	0.8629		
	2.5	0.2229	0.2239		
	1.0	0.1182	0.1155		
1	0.6	15.17	15.24	19.7	20.0
	0.5	4.264	4.304		
	0.3	1.307	1.326		
	0.2	0.8596	0.8740		

for each kinematic point and since these two approaches use different parameterizations of the elastic ([32] and [77]) and inelastic ([7] and [78]) cross sections and different calculation techniques it was assumed to be systematic error of the radiative correction procedure.

$$\delta_{rad}(E, x, Q^2) = |r_{TSAI}(E, x, Q^2) - r_{POLRAD}(E, x, Q^2)| \tag{C.16}$$

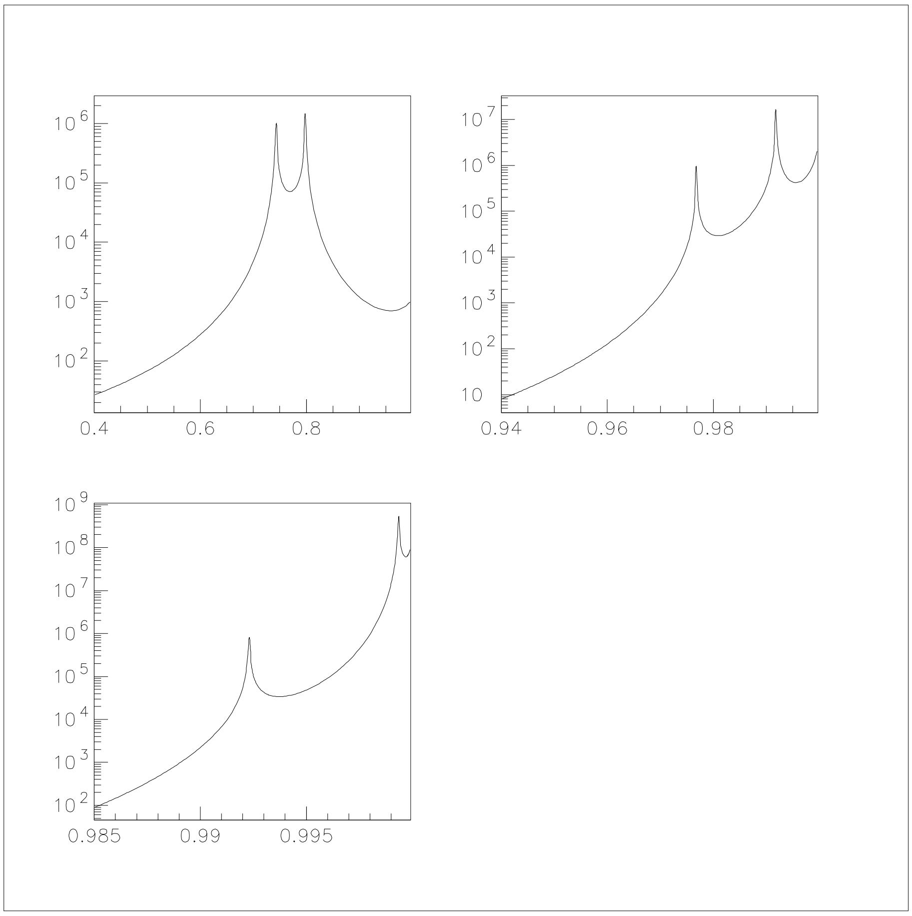

Figure C.3: Integrands in Eq. B.5 [72], to be compared with [72] Fig. 11 a,b,c.

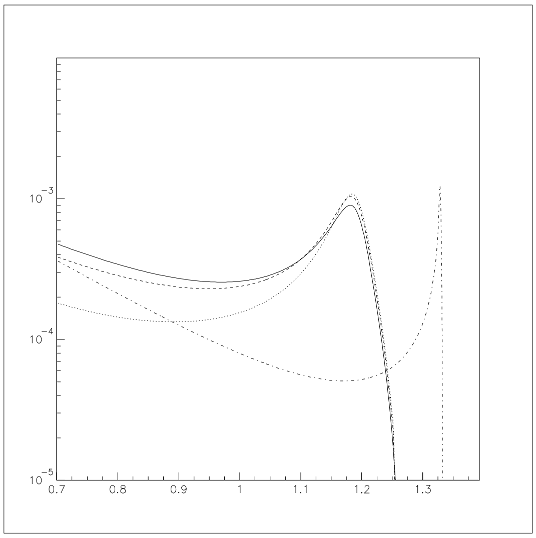

(a) $E_s = 3$ GeV, $\theta = 52.6°$

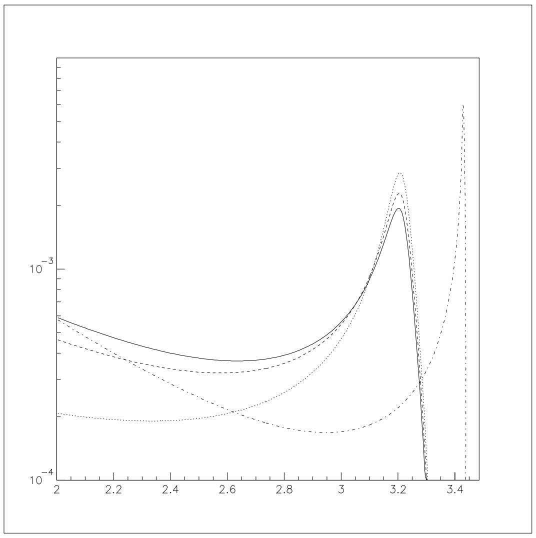

(b) $E_s = 5$ GeV, $\theta = 23.9°$

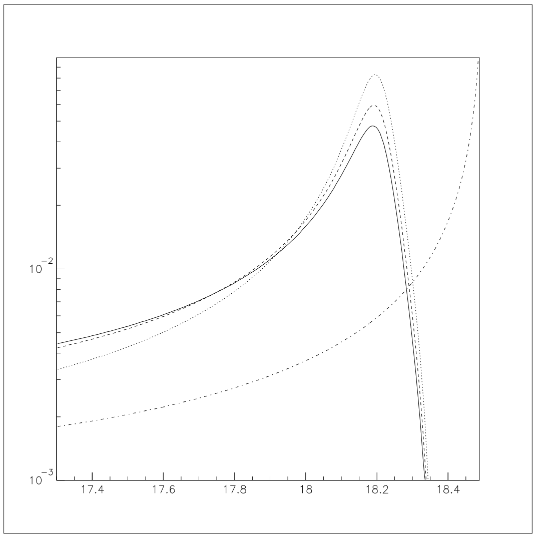

(c) $E_s = 20$ GeV, $\theta = 5°$

Figure C.4: Change of P33(1232) resonance due to radiative corrections and straggling. Compare with [72] Fig. 2c; solid line - all corrections included; dashed line - without straggling (zero target thickness); dotted line - non-radiative cross section; dashed-dotted line - radiative tail from elastic peak.

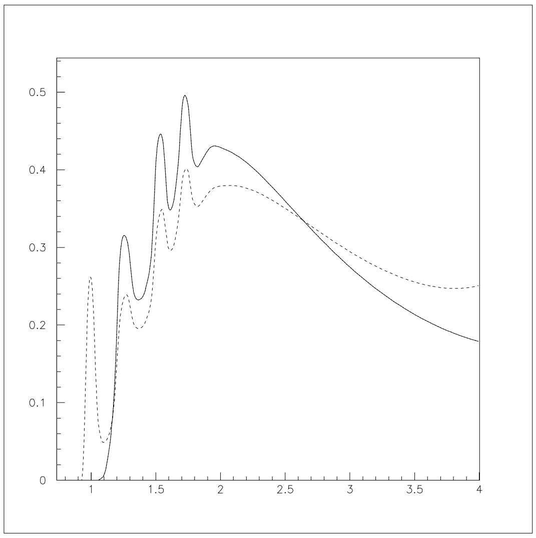

Figure C.5: Applying complete radiative correction procedure to quasi-experimental data at $E_s = 13.5$ GeV, $\theta = 6°$; solid line - radiatively corrected data, dashed line raw data, as quasi-experimental data Bodek fit was used; compare to [72] Fig. 5c.

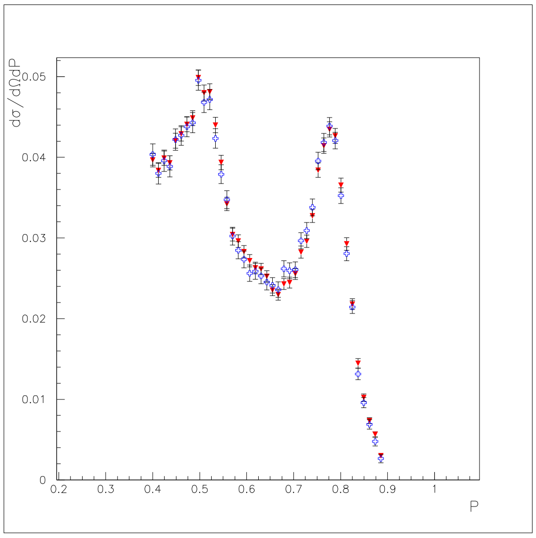

(a) $E_s = 1.5$ GeV, $\theta = 47.5°$

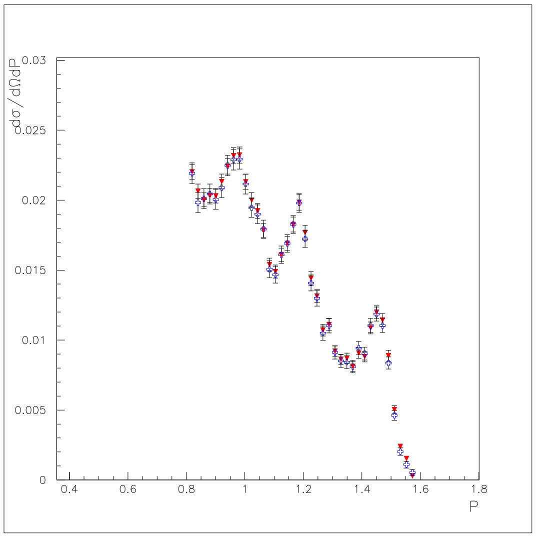

(b) $E_s = 2.5$ GeV, $\theta = 36.5°$

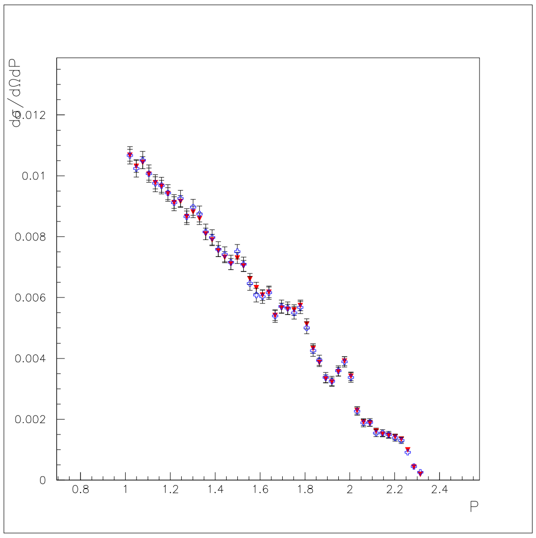

(c) $E_s = 4.0$ GeV, $\theta = 32.5°$

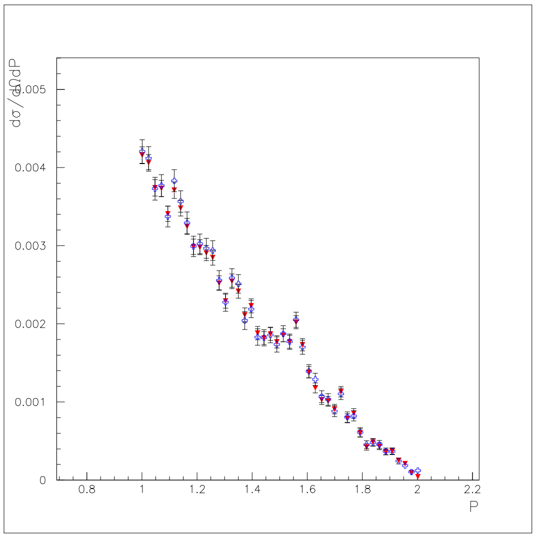

(d) $E_s = 4.2$ GeV, $\theta = 39.5°$

Figure C.6: A comparison of obtained cross sections corrected with present method of the radiative corrections (blue points) and POLRAD 2.0 [73] (red points).

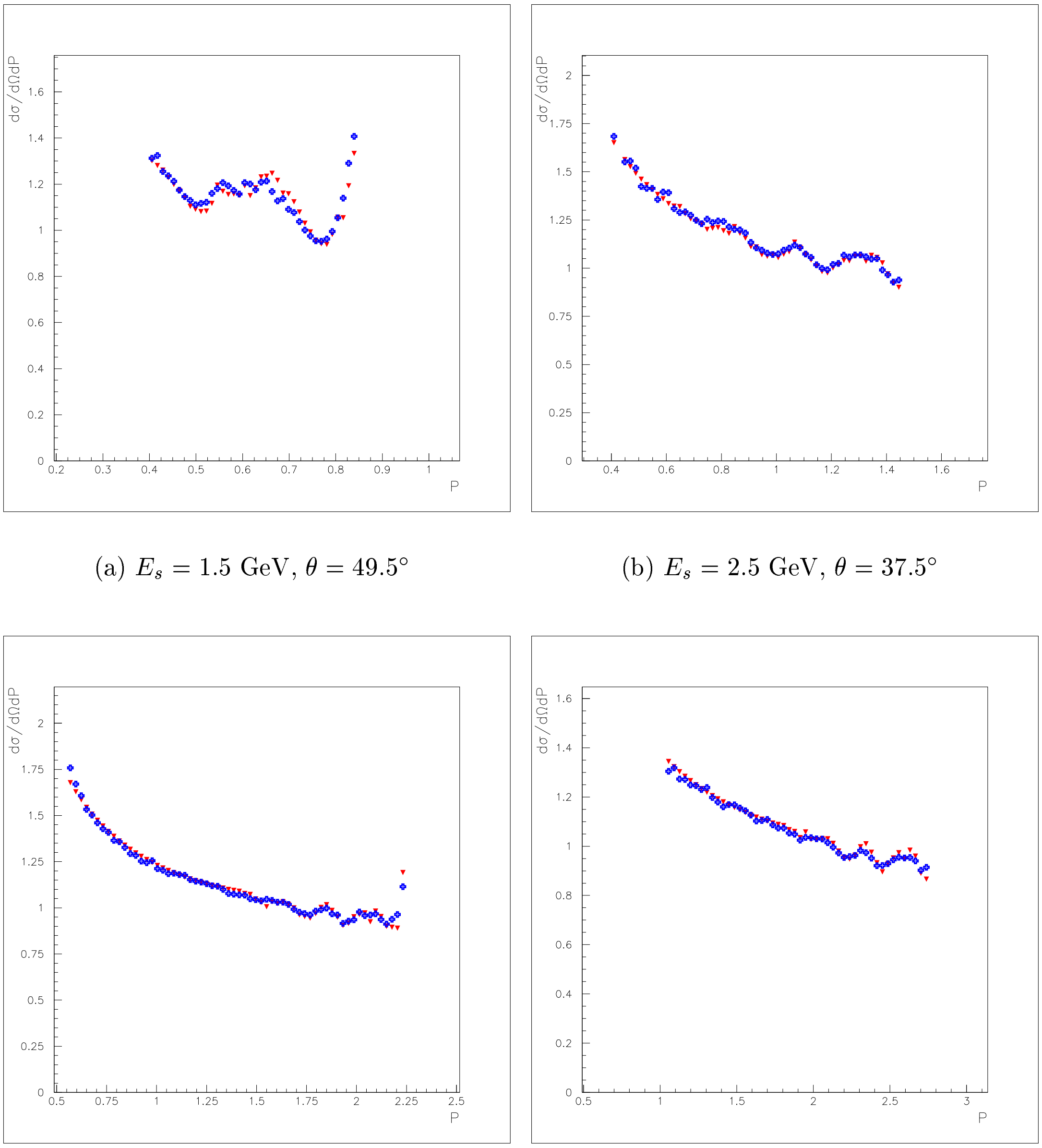

(a) $E_s = 1.5$ GeV, $\theta = 49.5°$

(b) $E_s = 2.5$ GeV, $\theta = 37.5°$

(c) $E_s = 4.0$ GeV, $\theta = 33.5°$

(d) $E_s = 4.2$ GeV, $\theta = 25.5°$

Figure C.7: A comparison of the correction factor calculated according to present method of the radiative corrections (blue points) and POLRAD 2.0 [73] (red points).

Appendix D

The obtained Nachtmann moments

The obtained inelastic Nachtmann moments with different percentage of coverage by experimental data are shown in Fig. D.1 and corresponding values are listed in Tab. D.1D.2D.3D.4.

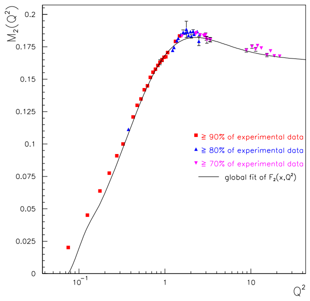

(a) M_2^{in}

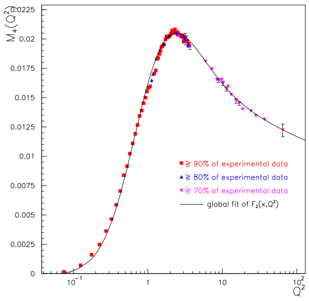

(b) M_4^{in}

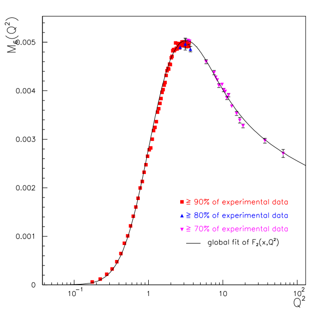

(c) M_6^{in}

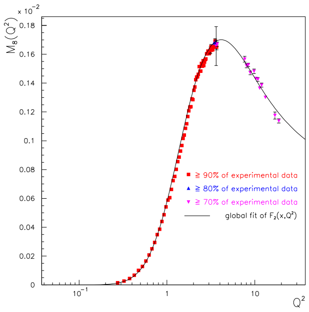

(d) M_8^{in}

Figure D.1: Inelastic Nachtmann moments. The errors are statistic only.

Table D.1: The inelastic Nachtmann moment M_2^{in}.

Q^2	$M_2^{in}(Q^2)$	$\delta^{stat}_{M_2^{in}}$	$\delta^{sys}_{M_2^{in}}$
[GeV^2]	x10^{-1}	x10^{-1}	x10^{-1}
0.075	0.202	0.002	0.009
0.125	0.451	0.006	0.025
0.175	0.638	0.005	0.025
0.225	0.775	0.003	0.026
0.275	0.910	0.004	0.030
0.325	1.000	0.002	0.040
0.375	1.114	0.002	0.047
0.425	1.209	0.005	0.037
0.475	1.298	0.008	0.036
0.525	1.347	0.004	0.047
0.575	1.419	0.003	0.049
0.625	1.444	0.006	0.059
0.675	1.514	0.004	0.051
0.725	1.554	0.006	0.050
0.775	1.578	0.007	0.049
0.825	1.606	0.006	0.050
0.875	1.625	0.019	0.074
0.925	1.649	0.014	0.040
0.975	1.669	0.013	0.044
1.025	1.673	0.011	0.049
1.075	1.706	0.011	0.046
1.225	1.722	0.009	0.045
1.275	1.736	0.006	0.086
1.325	1.792	0.015	0.050
1.375	1.798	0.027	0.055
1.425	1.815	0.007	0.049
1.475	1.833	0.006	0.053
1.525	1.844	0.008	0.055
1.575	1.833	0.006	0.065
1.625	1.862	0.020	0.053

Q^2	$M_2^{in}(Q^2)$	$\delta^{stat}_{M_2^{in}}$	$\delta^{sys}_{M_2^{in}}$
[GeV^2]	x10^{-1}	x10^{-1}	x10^{-1}
1.725	1.857	0.023	0.049
1.775	1.884	0.063	0.054
1.825	1.862	0.010	0.053
1.875	1.837	0.015	0.060
1.975	1.866	0.010	0.059
2.025	1.831	0.014	0.046
2.125	1.870	0.022	0.052
2.175	1.846	0.013	0.059
2.275	1.852	0.020	0.050
2.325	1.859	0.012	0.058
2.375	1.867	0.012	0.055
2.475	1.793	0.068	0.089
2.525	1.845	0.031	0.066
2.575	1.841	0.019	0.052
2.825	1.836	0.026	0.061
2.875	1.839	0.016	0.057
2.975	1.843	0.033	0.050
3.025	1.816	0.068	0.058
3.075	1.804	0.060	0.055
3.325	1.808	0.033	0.080
3.375	1.804	0.029	0.055
8.857	1.723	0.015	0.041
10.267	1.752	0.015	0.052
11.345	1.731	0.016	0.041
11.939	1.759	0.008	0.042
15.310	1.686	0.014	0.074
16.902	1.718	0.010	0.051
18.697	1.679	0.033	0.097
21.625	1.677	0.008	0.041

Table D.2: The inelastic Nachtmann moment M_4^{in}.

Q^2	$M_4^{in}(Q^2)$	$\delta^{stat}_{M_4^{in}}$	$\delta^{sys}_{M_4^{in}}$
[GeV^2]	x10^{-2}	x10^{-2}	x10^{-2}
0.075	0.016	0.0005	0.001
0.125	0.072	0.002	0.004
0.175	0.162	0.002	0.007
0.225	0.248	0.001	0.008
0.275	0.364	0.002	0.015
0.325	0.465	0.0005	0.026
0.375	0.587	0.0005	0.033
0.425	0.704	0.001	0.034
0.475	0.839	0.003	0.023
0.525	0.916	0.003	0.038
0.575	1.023	0.002	0.050
0.625	1.110	0.003	0.041
0.675	1.191	0.001	0.062
0.725	1.267	0.001	0.059
0.775	1.345	0.002	0.053
0.825	1.389	0.002	0.066
0.875	1.452	0.005	0.065
0.925	1.500	0.005	0.058
0.975	1.553	0.005	0.058
1.025	1.584	0.004	0.061
1.075	1.597	0.004	0.067
1.125	1.648	0.003	0.076
1.175	1.701	0.004	0.055
1.225	1.706	0.005	0.066
1.275	1.732	0.005	0.060
1.325	1.828	0.004	0.076
1.375	1.839	0.004	0.082
1.425	1.873	0.004	0.073
1.475	1.899	0.004	0.073
1.525	1.931	0.004	0.082
1.575	1.940	0.004	0.096
1.625	1.953	0.005	0.091
1.675	1.957	0.005	0.083
1.725	1.998	0.005	0.075
1.775	2.020	0.011	0.072
1.825	2.024	0.006	0.072
1.875	2.014	0.006	0.101
1.925	2.026	0.006	0.093
1.975	2.027	0.007	0.091
2.025	2.037	0.007	0.092
2.075	2.046	0.008	0.084
2.125	2.074	0.008	0.092
2.175	2.064	0.010	0.098
2.225	2.053	0.012	0.089
2.275	2.062	0.008	0.095
2.325	2.081	0.009	0.108
2.375	2.060	0.008	0.101
2.425	2.051	0.008	0.107
2.475	2.056	0.010	0.082
2.525	2.035	0.010	0.110
2.575	2.050	0.010	0.103
2.625	2.035	0.011	0.122
2.675	2.018	0.009	0.024
2.725	2.028	0.011	0.099
2.775	2.028	0.017	0.107
2.825	2.031	0.014	0.118
2.875	2.019	0.013	0.108
2.925	2.023	0.016	0.112
2.975	2.018	0.014	0.102
3.025	1.978	0.016	0.104
3.075	1.992	0.022	0.114
3.175	2.011	0.031	0.141
3.225	1.968	0.021	0.112
3.275	2.007	0.022	0.116
3.325	1.979	0.014	0.096
3.375	1.981	0.016	0.086
3.475	1.943	0.013	0.064
3.525	1.951	0.021	0.088
3.675	1.930	0.024	0.040
5.967	1.810	0.015	0.116
7.268	1.743	0.011	0.044
8.434	1.653	0.014	0.084
8.857	1.645	0.019	0.027
9.781	1.653	0.010	0.061
10.267	1.622	0.019	0.031
11.345	1.573	0.018	0.035
11.939	1.596	0.013	0.031
13.185	1.525	0.016	0.021
15.310	1.471	0.019	0.032
16.902	1.450	0.017	0.025
18.697	1.401	0.013	0.027
24.192	1.385	0.008	0.024
28.192	1.344	0.007	0.037
36.750	1.314	0.009	0.057
64.884	1.222	0.053	0.044

Table D.3: The inelastic Nachtmann moment M_6^{in}.

Q^2	$M_6^{in}(Q^2)$	$\delta^{stat}_{M_6^{in}}$	$\delta^{sys}_{M_6^{in}}$
[GeV^2]	x10^{-3}	x10^{-3}	x10^{-3}
0.075	0.0019	0.0001	0.0001
0.125	0.017	0.001	0.001
0.175	0.060	0.001	0.003
0.225	0.119	0.001	0.004
0.275	0.218	0.002	0.010
0.325	0.328	0.0005	0.020
0.375	0.478	0.0005	0.030
0.425	0.644	0.001	0.038
0.475	0.858	0.003	0.024
0.525	1.010	0.005	0.046
0.575	1.215	0.002	0.068
0.625	1.413	0.005	0.057
0.675	1.603	0.002	0.098
0.725	1.785	0.002	0.102
0.775	1.996	0.002	0.087
0.825	2.130	0.003	0.117
0.875	2.320	0.004	0.122
0.925	2.476	0.005	0.119
0.975	2.651	0.007	0.113
1.025	2.785	0.011	0.116
1.075	2.820	0.005	0.140
1.125	3.002	0.005	0.150
1.175	3.179	0.007	0.117
1.225	3.245	0.009	0.154
1.275	3.364	0.012	0.126
1.325	3.561	0.011	0.178
1.375	3.630	0.008	0.189
1.425	3.741	0.011	0.173
1.475	3.839	0.010	0.154
1.525	3.968	0.012	0.187
1.575	4.022	0.010	0.249
1.625	4.116	0.010	0.252
1.675	4.170	0.011	0.231
1.725	4.316	0.013	0.218
1.775	4.412	0.012	0.194
1.825	4.459	0.015	0.168
1.875	4.446	0.015	0.256
1.925	4.551	0.015	0.243
1.975	4.539	0.018	0.253
2.025	4.677	0.020	0.263
2.075	4.699	0.022	0.232
2.125	4.825	0.022	0.269
2.175	4.850	0.024	0.282
2.225	4.825	0.024	0.267
2.275	4.852	0.023	0.271
2.325	4.984	0.025	0.291
2.375	4.876	0.023	0.275
2.425	4.860	0.023	0.257
2.475	4.971	0.020	0.234
2.525	4.899	0.018	0.260
2.575	4.972	0.021	0.280
2.625	4.884	0.024	0.293
2.675	4.896	0.022	0.277
2.725	4.933	0.025	0.283
2.775	4.931	0.029	0.293
2.825	5.004	0.028	0.326
2.875	4.976	0.027	0.309
2.925	5.007	0.033	0.303
2.975	4.983	0.027	0.294
3.025	4.926	0.027	0.314
3.075	4.942	0.040	0.352
3.125	5.002	0.064	0.372
3.175	4.916	0.040	0.358
3.225	4.985	0.043	0.351
3.275	4.944	0.032	0.332
3.325	4.976	0.031	0.312
3.375	5.034	0.035	0.325
3.425	4.915	0.032	0.253
3.475	4.999	0.052	0.316
3.525	5.021	0.043	0.268
3.575	4.857	0.063	0.310
3.675	4.597	0.044	0.553
5.967	4.374	0.044	0.098
8.027	4.279	0.027	0.135
8.433	4.223	0.032	0.109
8.857	4.108	0.042	0.109
9.781	4.130	0.034	0.146
10.267	4.016	0.035	0.095
10.793	3.987	0.106	0.761
11.344	3.853	0.041	0.140
11.939	3.910	0.040	0.111
13.184	3.681	0.029	0.067
15.310	3.533	0.044	0.133
16.902	3.392	0.058	0.073
18.697	3.275	0.039	0.088
36.750	2.971	0.027	0.313
64.884	2.708	0.082	0.193

Table D.4: The inelastic Nachtmann moment M_8^{in}.

Q^2	$M_8^{in}(Q^2)$	$\delta^{stat}_{M_8^{in}}$	$\delta^{sys}_{M_8^{in}}$
[GeV^2]	x10^{-3}	x10^{-3}	x10^{-3}
0.175	0.0025	0.0001	0.0001
0.225	0.0064	0.0001	0.0002
0.275	0.0146	0.0001	0.0007
0.325	0.0259	0.00005	0.0017
0.375	0.0439	0.00005	0.0029
0.425	0.0670	0.0001	0.0043
0.475	0.1002	0.0004	0.0030
0.525	0.1279	0.0008	0.0062
0.575	0.1660	0.0003	0.0101
0.625	0.2079	0.0009	0.0090
0.675	0.2507	0.0005	0.0168
0.725	0.2946	0.0004	0.0190
0.775	0.3484	0.0005	0.0160
0.825	0.3860	0.0006	0.0233
0.875	0.4393	0.0008	0.0254
0.925	0.4866	0.0010	0.0264
0.975	0.5416	0.0015	0.0254
1.025	0.5887	0.0030	0.0248
1.075	0.6048	0.0012	0.0322
1.125	0.6627	0.0013	0.0370
1.175	0.7236	0.0018	0.0298
1.225	0.7525	0.0020	0.0402
1.275	0.8021	0.0036	0.0309
1.325	0.8556	0.0033	0.0475
1.375	0.8864	0.0024	0.0516
1.425	0.9280	0.0032	0.0492
1.475	0.9669	0.0031	0.0397
1.525	1.0158	0.0042	0.0488
1.575	1.0395	0.0033	0.0725
1.625	1.0859	0.0034	0.0772
1.675	1.1173	0.0036	0.0740
1.725	1.1680	0.0043	0.0726
1.775	1.2081	0.0043	0.0628
1.825	1.2338	0.0050	0.0462
1.875	1.2363	0.0046	0.0798
1.925	1.2903	0.0047	0.0755
1.975	1.2857	0.0058	0.0824
2.025	1.3480	0.0069	0.0867
2.075	1.3694	0.0084	0.0750
2.125	1.4239	0.0082	0.0903
2.175	1.4421	0.0092	0.0945
2.225	1.4442	0.0093	0.0912
2.275	1.4606	0.0092	0.0917
2.325	1.5149	0.0098	0.0959
2.375	1.4832	0.0091	0.0921
2.425	1.4835	0.0089	0.0850
2.475	1.5362	0.0079	0.0796
2.525	1.5176	0.0063	0.0751
2.575	1.5556	0.0078	0.0915
2.625	1.5218	0.0087	0.0933
2.675	1.5457	0.0091	0.0988
2.725	1.5634	0.0094	0.0970
2.775	1.5677	0.0096	0.0989
2.825	1.6030	0.0098	0.1081
2.875	1.6032	0.0098	0.1036
2.925	1.6219	0.0104	0.0970
2.975	1.6145	0.0092	0.0941
3.025	1.6042	0.0090	0.1057
3.075	1.6136	0.0119	0.1222
3.125	1.6293	0.0118	0.1491
3.175	1.6524	0.0159	0.1310
3.225	1.6289	0.0122	0.1315
3.275	1.6478	0.0127	0.1304
3.325	1.6321	0.0120	0.1264
3.375	1.6543	0.0119	0.1243
3.425	1.6787	0.0125	0.1285
3.475	1.6489	0.0118	0.1079
3.525	1.6918	0.0168	0.1238
3.575	1.6858	0.0142	0.1049
3.675	1.6493	0.0197	0.1199
3.725	1.6698	0.0160	0.1276
7.645	1.5659	0.0202	0.0396
8.027	1.5205	0.0107	0.0642
8.433	1.5264	0.0122	0.0419
8.857	1.4712	0.0138	0.0566
9.781	1.4818	0.0167	0.0666
10.267	1.4321	0.0113	0.0367
10.793	1.4256	0.0175	0.1103
11.344	1.3644	0.0176	0.0793
11.939	1.3860	0.0181	0.0574
13.184	1.3011	0.0091	0.0336
16.902	1.1752	0.0252	0.0283
18.697	1.1377	0.0147	0.0346

Table D.5: $F_2(x, Q^2)$ with statistical and systematic errors extracted from CLAS data.

Q^2 [GeV^2]	x	F_2	δ_{stat}	δ_{sys}
0.225	0.1315	3.009E-01	6.194E-04	1.573E-02
	0.1405	3.228E-01	7.125E-04	1.276E-02
	0.1495	2.487E-01	6.064E-04	8.952E-03
	0.1585	2.053E-01	5.748E-04	8.110E-03
	0.1675	1.876E-01	6.007E-04	7.170E-03
	0.1765	1.794E-01	6.436E-04	5.482E-03
	0.1855	1.746E-01	6.930E-04	5.291E-03
	0.1945	1.754E-01	7.588E-04	1.812E-02
	0.2035	1.795E-01	8.352E-04	9.854E-03
	0.2125	1.955E-01	9.521E-04	1.002E-02
	0.2215	2.221E-01	1.125E-03	9.431E-03
	0.2305	2.509E-01	1.326E-03	9.521E-03
	0.2395	2.994E-01	1.605E-03	1.947E-02
	0.2485	3.569E-01	1.953E-03	1.771E-02
	0.2575	4.087E-01	2.277E-03	1.487E-02
	0.2665	4.449E-01	2.542E-03	1.228E-02
	0.2755	4.366E-01	2.634E-03	9.806E-03
	0.2845	3.924E-01	2.525E-03	1.473E-02
	0.2935	3.307E-01	2.310E-03	1.746E-02
	0.3025	2.666E-01	2.108E-03	1.779E-02
	0.3115	2.094E-01	1.921E-03	1.858E-02
	0.3205	1.627E-01	1.731E-03	1.664E-02
	0.3295	1.314E-01	1.588E-03	1.456E-02
	0.3385	1.086E-01	1.483E-03	1.206E-02
	0.3475	8.573E-02	1.361E-03	9.559E-03
	0.3565	7.021E-02	1.242E-03	7.885E-03
	0.3655	6.022E-02	1.200E-03	6.846E-03
	0.3745	4.947E-02	1.107E-03	5.729E-03
	0.3835	4.178E-02	9.795E-04	4.970E-03
	0.3925	3.158E-02	8.371E-04	3.911E-03
	0.4015	2.401E-02	7.294E-04	3.157E-03
	0.4105	1.820E-02	5.855E-04	2.625E-03
	0.4195	1.394E-02	4.567E-04	2.446E-04
	0.4285	9.111E-03	3.274E-04	1.601E-04
	0.4375	5.100E-03	1.969E-04	8.887E-05
0.275	0.1495	2.671E-01	5.785E-04	1.693E-02
	0.1585	2.989E-01	6.506E-04	1.778E-02
	0.1675	3.124E-01	7.372E-04	1.490E-02
	0.1765	2.466E-01	6.528E-04	1.095E-02
	0.1855	2.091E-01	6.134E-04	9.663E-03
	0.1945	1.866E-01	5.909E-04	8.040E-03
	0.2035	1.754E-01	5.857E-04	6.597E-03
	0.2125	1.699E-01	5.897E-04	6.205E-03
	0.2215	1.798E-01	9.046E-04	1.105E-02
	0.2305	1.825E-01	9.676E-04	1.439E-02
	0.2395	1.898E-01	1.056E-03	9.907E-03
	0.2485	1.994E-01	7.086E-04	9.994E-03
	0.2575	2.230E-01	7.751E-04	9.784E-03
	0.2665	2.579E-01	1.564E-03	1.075E-02
	0.2755	2.917E-01	9.690E-04	1.630E-02
	0.2845	3.383E-01	1.100E-03	1.954E-02
	0.2935	3.830E-01	1.227E-03	1.614E-02
	0.3025	4.224E-01	1.362E-03	1.536E-02
	0.3115	4.273E-01	1.406E-03	1.234E-02
	0.3205	4.028E-01	1.393E-03	1.317E-02
	0.3295	3.557E-01	1.312E-03	1.966E-02
	0.3385	2.951E-01	1.185E-03	1.923E-02
	0.3475	2.400E-01	1.060E-03	1.988E-02
	0.3565	1.936E-01	9.485E-04	2.117E-02
	0.3655	1.581E-01	8.540E-04	1.551E-02
	0.3745	1.267E-01	7.642E-04	7.740E-03
	0.3835	1.055E-01	6.979E-04	7.099E-03
	0.3925	8.593E-02	6.194E-04	8.069E-03
	0.4015	7.009E-02	5.533E-04	3.987E-03
	0.4105	5.922E-02	5.047E-04	6.099E-03
	0.4195	4.934E-02	4.480E-04	5.715E-03
	0.4285	3.952E-02	3.934E-04	4.675E-03
	0.4375	3.130E-02	3.272E-04	3.447E-03
	0.4465	2.616E-02	2.867E-04	3.341E-03
	0.4555	2.094E-02	2.396E-04	2.870E-03
	0.4645	1.557E-02	1.903E-04	2.384E-03
	0.4735	1.102E-02	1.415E-04	2.304E-04
	0.4825	7.099E-03	9.318E-05	1.480E-04
	0.4915	3.491E-03	4.758E-05	7.150E-05
0.325	0.1675	2.677E-01	6.312E-04	2.072E-02
	0.1765	2.774E-01	5.607E-04	1.968E-02
	0.1855	3.328E-01	7.284E-04	2.148E-02
	0.1945	3.061E-01	7.060E-04	1.693E-02
	0.2035	2.449E-01	6.278E-04	1.264E-02
	0.2125	2.104E-01	5.991E-04	1.099E-02
	0.2215	1.947E-01	5.941E-04	9.598E-03
	0.2305	1.832E-01	5.918E-04	8.462E-03
	0.2395	1.761E-01	5.962E-04	7.713E-03
	0.2485	1.745E-01	6.097E-04	7.482E-03
	0.2575	1.779E-01	6.306E-04	1.664E-02
	0.2665	1.838E-01	6.586E-04	9.538E-03
	0.2755	1.956E-01	6.960E-04	1.031E-02
	0.2845	2.128E-01	7.470E-04	1.057E-02
	0.2935	2.372E-01	8.109E-04	1.084E-02
	0.3025	2.660E-01	8.880E-04	1.248E-02
	0.3115	3.016E-01	9.841E-04	1.811E-02
	0.3205	3.411E-01	1.088E-03	1.922E-02
	0.3295	3.837E-01	1.202E-03	1.759E-02
	0.3385	4.156E-01	1.300E-03	1.699E-02
	0.3475	4.213E-01	1.342E-03	1.450E-02
	0.3565	4.007E-01	1.330E-03	1.424E-02
	0.3655	3.556E-01	1.248E-03	1.768E-02
	0.3745	3.006E-01	1.141E-03	1.936E-02
	0.3835	2.498E-01	1.032E-03	1.924E-02
	0.3925	1.998E-01	9.159E-04	1.969E-02
	0.4015	1.617E-01	8.124E-04	1.736E-02
	0.4105	1.328E-01	7.316E-04	1.092E-02
	0.4195	1.104E-01	6.594E-04	7.761E-03
	0.4285	8.960E-02	5.898E-04	8.538E-03
	0.4375	7.374E-02	5.308E-04	7.482E-03
	0.4465	6.189E-02	4.727E-04	3.550E-03
	0.4555	5.165E-02	4.221E-04	5.076E-03
	0.4645	4.195E-02	3.637E-04	4.910E-03
	0.4735	3.451E-02	3.203E-04	3.512E-03
	0.4825	2.811E-02	2.786E-04	2.097E-03
	0.4915	2.305E-02	2.352E-04	1.956E-03
	0.5005	1.744E-02	1.879E-04	1.754E-03
	0.5095	1.320E-02	1.445E-04	3.080E-04
	0.5185	9.079E-03	1.055E-04	2.129E-04
	0.5275	5.396E-03	6.490E-05	1.227E-04
0.375	0.1855	2.899E-01	9.834E-04	2.785E-02
	0.1945	2.710E-01	7.085E-04	2.241E-02
	0.2035	3.188E-01	6.721E-04	2.525E-02
	0.2125	3.318E-01	6.955E-04	2.221E-02
	0.2215	2.792E-01	6.402E-04	1.754E-02
	0.2305	2.300E-01	5.966E-04	1.354E-02
	0.2395	2.044E-01	5.975E-04	1.186E-02
	0.2485	1.910E-01	6.122E-04	1.080E-02
	0.2575	1.805E-01	6.210E-04	9.577E-03
	0.2665	1.749E-01	6.390E-04	8.815E-03
	0.2755	1.734E-01	6.587E-04	8.547E-03
	0.2845	1.765E-01	6.934E-04	1.514E-02
	0.2935	1.807E-01	7.163E-04	9.987E-03
	0.3025	1.900E-01	7.485E-04	1.046E-02
	0.3115	2.050E-01	7.942E-04	1.116E-02
	0.3205	2.259E-01	8.555E-04	1.159E-02
	0.3295	2.529E-01	9.262E-04	1.298E-02
	0.3385	2.820E-01	1.011E-03	1.617E-02
	0.3475	3.180E-01	1.109E-03	2.083E-02
	0.3565	3.577E-01	1.220E-03	1.941E-02
	0.3655	3.940E-01	1.324E-03	1.952E-02
	0.3745	4.155E-01	1.394E-03	1.828E-02
	0.3835	4.177E-01	1.430E-03	1.652E-02
	0.3925	3.913E-01	1.390E-03	1.692E-02
	0.4015	3.423E-01	1.299E-03	1.937E-02
	0.4105	2.912E-01	1.190E-03	1.998E-02
	0.4195	2.398E-01	1.065E-03	1.924E-02
	0.4285	1.964E-01	9.574E-04	1.897E-02
	0.4375	1.606E-01	8.560E-04	1.603E-02
	0.4465	1.296E-01	7.614E-04	1.077E-02
	0.4555	1.090E-01	6.918E-04	8.836E-03
	0.4645	8.955E-02	6.179E-04	9.146E-03

	0.4735	7.492E-02	5.521E-04	7.587E-03
	0.4825	6.016E-02	4.831E-04	3.568E-03
	0.4915	5.082E-02	4.350E-04	4.029E-03
	0.5005	4.219E-02	3.778E-04	4.042E-03
	0.5095	3.438E-02	3.319E-04	2.660E-03
	0.5185	2.870E-02	2.839E-04	2.324E-03
	0.5275	2.265E-02	2.371E-04	1.945E-03
	0.5365	1.805E-02	1.943E-04	1.821E-03
	0.5455	1.302E-02	1.476E-04	3.496E-04
	0.5545	8.736E-03	1.051E-04	2.319E-04
	0.5635	5.430E-03	6.415E-05	1.384E-04
0.425	0.2035	2.719E-01	5.669E-03	2.930E-02
	0.2125	2.698E-01	1.422E-03	2.592E-02
	0.2215	3.122E-01	8.332E-04	2.879E-02
	0.2305	3.427E-01	7.837E-04	2.796E-02
	0.2395	3.111E-01	7.051E-04	2.243E-02
	0.2485	2.538E-01	6.181E-04	1.797E-02
	0.2575	2.169E-01	5.823E-04	1.445E-02
	0.2665	1.980E-01	5.733E-04	1.258E-02
	0.2755	1.854E-01	5.723E-04	1.205E-02
	0.2845	1.772E-01	5.757E-04	1.031E-02
	0.2935	1.730E-01	5.865E-04	9.782E-03
	0.3025	1.694E-01	6.065E-04	9.380E-03
	0.3115	1.727E-01	6.350E-04	1.394E-02
	0.3205	1.781E-01	6.738E-04	1.019E-02
	0.3295	1.864E-01	7.141E-04	1.090E-02
	0.3385	2.011E-01	7.709E-04	1.204E-02
	0.3475	2.156E-01	8.318E-04	1.214E-02
	0.3565	2.375E-01	9.052E-04	1.332E-02
	0.3655	2.683E-01	1.008E-03	1.632E-02
	0.3745	3.034E-01	1.122E-03	2.037E-02
	0.3835	3.375E-01	1.241E-03	1.972E-02
	0.3925	3.726E-01	1.356E-03	2.074E-02
	0.4015	3.991E-01	1.460E-03	2.045E-02
	0.4105	4.056E-01	1.521E-03	1.883E-02
	0.4195	3.892E-01	1.523E-03	1.759E-02
	0.4285	3.512E-01	1.450E-03	1.924E-02
	0.4375	2.996E-01	1.323E-03	1.986E-02
	0.4465	2.504E-01	1.198E-03	1.902E-02
	0.4555	2.047E-01	1.079E-03	1.804E-02
	0.4645	1.673E-01	9.657E-04	1.618E-02
	0.4735	1.398E-01	8.743E-04	1.254E-02
	0.4825	1.153E-01	7.883E-04	1.079E-02
	0.4915	9.549E-02	7.118E-04	9.319E-03
	0.5005	7.831E-02	6.340E-04	8.463E-03
	0.5095	6.627E-02	5.771E-04	5.185E-03
	0.5185	5.667E-02	5.219E-04	3.540E-03
	0.5275	4.697E-02	4.647E-04	3.515E-03
	0.5365	3.972E-02	4.088E-04	2.941E-03
	0.5455	3.214E-02	3.539E-04	2.498E-03
	0.5545	2.597E-02	3.024E-04	2.381E-03
	0.5635	2.135E-02	2.559E-04	2.135E-03
	0.5725	1.620E-02	2.018E-04	1.886E-03
	0.5815	1.168E-02	1.508E-04	3.815E-04
	0.5905	7.465E-03	9.938E-05	2.352E-04
	0.5995	3.713E-03	4.946E-05	1.169E-04
0.475	0.1405	2.715E-01	1.141E-03	1.539E-02
	0.1495	2.690E-01	1.197E-03	1.325E-02
	0.1585	2.623E-01	1.260E-03	1.052E-02
	0.1675	2.685E-01	1.426E-03	1.063E-02
	0.1765	2.858E-01	1.719E-03	1.217E-02
	0.1855	3.420E-01	2.316E-03	1.377E-02
	0.1945	3.670E-01	2.870E-03	1.335E-02
	0.2035	3.282E-01	3.140E-03	8.464E-03
	0.2125	2.994E-01	3.735E-03	7.350E-03
	0.2215	2.895E-01	4.649E-03	7.052E-03
	0.2305	2.950E-01	5.937E-03	7.906E-03
	0.2395	2.654E-01	8.881E-03	2.605E-02
	0.2485	3.435E-01	1.300E-03	3.275E-02
	0.2575	3.297E-01	1.009E-03	2.731E-02
	0.2665	2.724E-01	8.002E-04	2.198E-02
	0.2755	2.278E-01	6.802E-04	1.689E-02
	0.2845	2.038E-01	6.311E-04	1.446E-02
	0.2935	1.878E-01	6.159E-04	1.308E-02
	0.3025	1.803E-01	6.112E-04	1.261E-02
	0.3115	1.718E-01	6.093E-04	1.120E-02
	0.3205	1.696E-01	6.133E-04	1.072E-02

	0.3295	1.693E-01	6.227E-04	1.100E-02
	0.3385	1.705E-01	6.405E-04	1.276E-02
	0.3475	1.744E-01	6.628E-04	1.075E-02
	0.3565	1.861E-01	7.010E-04	1.193E-02
	0.3655	1.976E-01	7.367E-04	1.253E-02
	0.3745	2.129E-01	7.856E-04	1.303E-02
	0.3835	2.356E-01	8.502E-04	1.462E-02
	0.3925	2.605E-01	9.191E-04	1.734E-02
	0.4015	2.949E-01	1.017E-03	2.104E-02
	0.4105	3.256E-01	1.102E-03	2.109E-02
	0.4195	3.618E-01	1.206E-03	2.189E-02
	0.4285	3.809E-01	1.279E-03	2.151E-02
	0.4375	3.870E-01	1.326E-03	2.014E-02
	0.4465	3.687E-01	1.312E-03	1.863E-02
	0.4555	3.338E-01	1.259E-03	1.922E-02
	0.4645	2.896E-01	1.167E-03	1.977E-02
	0.4735	2.398E-01	1.060E-03	1.847E-02
	0.4825	2.004E-01	9.634E-04	1.734E-02
	0.4915	1.634E-01	8.668E-04	1.510E-02
	0.5005	1.356E-01	7.908E-04	1.268E-02
	0.5095	1.099E-01	7.121E-04	9.572E-03
	0.5185	9.296E-02	6.570E-04	9.243E-03
	0.5275	7.803E-02	5.952E-04	8.388E-03
	0.5365	6.359E-02	5.326E-04	6.678E-03
	0.5455	5.375E-02	4.797E-04	3.464E-03
	0.5545	4.465E-02	4.282E-04	3.051E-03
	0.5635	3.903E-02	3.891E-04	2.683E-03
	0.5725	3.080E-02	3.374E-04	2.646E-03
	0.5815	2.503E-02	2.848E-04	2.578E-03
	0.5905	2.035E-02	2.382E-04	2.200E-03
	0.5995	1.522E-02	1.894E-04	1.848E-03
	0.6085	1.094E-02	1.415E-04	3.679E-04
	0.6175	6.843E-03	9.403E-05	2.239E-04
	0.6265	3.123E-03	4.382E-05	1.013E-04
0.525	0.1495	2.889E-01	1.181E-03	1.750E-02
	0.1585	2.822E-01	1.365E-03	1.466E-02
	0.1675	2.740E-01	1.425E-03	1.212E-02
	0.1765	2.655E-01	1.443E-03	1.131E-02
	0.1855	2.650E-01	1.476E-03	1.113E-02
	0.1945	2.926E-01	1.652E-03	1.333E-02
	0.2035	3.325E-01	1.932E-03	1.312E-02
	0.2125	3.337E-01	2.061E-03	1.143E-02
	0.2215	2.972E-01	2.029E-03	8.161E-03
	0.2305	2.710E-01	2.065E-03	7.069E-03
	0.2395	2.598E-01	2.171E-03	6.760E-03
	0.2485	2.733E-01	2.425E-03	7.700E-03
	0.2575	3.117E-01	2.909E-03	1.043E-02
	0.2665	3.502E-01	2.498E-03	2.016E-02
	0.2755	3.577E-01	2.769E-03	1.586E-02
	0.2845	2.986E-01	2.228E-03	1.689E-02
	0.2935	2.463E-01	1.869E-03	1.308E-02
	0.3025	2.212E-01	1.912E-03	1.114E-02
	0.3115	2.024E-01	1.935E-03	9.696E-03
	0.3205	1.909E-01	2.019E-03	9.881E-03
	0.3295	1.783E-01	2.053E-03	8.285E-03
	0.3385	1.744E-01	2.197E-03	7.893E-03
	0.3475	1.778E-01	2.477E-03	7.804E-03
	0.3565	1.747E-01	2.565E-03	1.102E-02
	0.3655	1.748E-01	2.809E-03	9.984E-03
	0.3745	1.839E-01	3.257E-03	1.014E-02
	0.3835	1.955E-01	3.686E-03	1.192E-02
	0.3925	2.084E-01	4.158E-03	1.342E-02
	0.4015	2.149E-01	8.544E-04	1.445E-02
	0.4105	2.346E-01	9.117E-04	1.631E-02
	0.4195	2.634E-01	9.920E-04	1.944E-02
	0.4285	2.930E-01	1.081E-03	2.178E-02
	0.4375	3.235E-01	1.163E-03	2.215E-02
	0.4465	3.488E-01	1.242E-03	2.274E-02
	0.4555	3.704E-01	1.308E-03	2.268E-02
	0.4645	3.677E-01	1.326E-03	2.122E-02
	0.4735	3.456E-01	1.290E-03	1.952E-02
	0.4825	3.076E-01	1.214E-03	1.963E-02
	0.4915	2.657E-01	1.121E-03	1.955E-02
	0.5005	2.220E-01	1.010E-03	1.786E-02
	0.5095	1.845E-01	9.219E-04	1.619E-02
	0.5185	1.499E-01	8.200E-04	1.336E-02
	0.5275	1.222E-01	7.367E-04	1.079E-02

	0.5365	1.020E-01	6.666E-04	9.335E-03
	0.5455	8.578E-02	6.059E-04	8.993E-03
	0.5545	7.133E-02	5.454E-04	7.432E-03
	0.5635	5.830E-02	4.863E-04	4.528E-03
	0.5725	4.923E-02	4.349E-04	3.258E-03
	0.5815	4.115E-02	3.931E-04	2.829E-03
	0.5905	3.419E-02	3.471E-04	2.487E-03
	0.5995	2.885E-02	3.037E-04	3.611E-03
	0.6085	2.366E-02	2.644E-04	2.689E-03
	0.6175	1.842E-02	2.181E-04	2.182E-03
	0.6265	1.456E-02	1.739E-04	5.856E-04
	0.6355	9.979E-03	1.263E-04	3.916E-04
	0.6445	5.694E-03	7.385E-05	2.212E-04
0.575	0.1585	3.016E-01	1.170E-03	2.124E-02
	0.1675	2.839E-01	1.195E-03	1.674E-02
	0.1765	2.920E-01	8.992E-04	1.549E-02
	0.1855	2.833E-01	9.793E-04	1.466E-02
	0.1945	2.807E-01	1.042E-03	1.250E-02
	0.2035	2.894E-01	1.095E-03	1.301E-02
	0.2125	3.296E-01	1.262E-03	1.535E-02
	0.2215	3.618E-01	1.429E-03	1.515E-02
	0.2305	3.420E-01	1.457E-03	1.105E-02
	0.2395	3.008E-01	1.430E-03	9.154E-03
	0.2485	2.740E-01	1.465E-03	7.949E-03
	0.2575	2.677E-01	1.577E-03	7.766E-03
	0.2665	2.849E-01	1.806E-03	8.826E-03
	0.2755	3.000E-01	2.456E-03	1.054E-02
	0.2845	3.330E-01	2.799E-03	1.223E-02
	0.2935	3.518E-01	3.253E-03	1.926E-02
	0.3025	2.974E-01	2.171E-03	1.531E-02
	0.3115	2.476E-01	1.924E-03	1.207E-02
	0.3205	2.187E-01	1.840E-03	1.016E-02
	0.3295	1.952E-01	1.688E-03	1.039E-02
	0.3385	1.847E-01	1.462E-03	9.976E-03
	0.3475	1.785E-01	1.470E-03	9.041E-03
	0.3565	1.726E-01	1.485E-03	8.686E-03
	0.3655	1.742E-01	1.561E-03	8.489E-03
	0.3745	1.700E-01	1.552E-03	1.057E-02
	0.3835	1.759E-01	1.647E-03	1.079E-02
	0.3925	1.799E-01	1.692E-03	9.558E-03
	0.4015	1.905E-01	1.852E-03	1.121E-02
	0.4105	2.007E-01	1.947E-03	1.206E-02
	0.4195	2.173E-01	2.136E-03	1.260E-02
	0.4285	2.326E-01	2.253E-03	1.331E-02
	0.4375	2.597E-01	2.486E-03	1.807E-02
	0.4465	2.802E-01	2.616E-03	2.188E-02
	0.4555	3.149E-01	2.959E-03	1.769E-02
	0.4645	3.360E-01	1.682E-03	2.015E-02
	0.4735	3.421E-01	1.349E-03	2.373E-02
	0.4825	3.556E-01	1.402E-03	2.320E-02
	0.4915	3.417E-01	1.383E-03	2.128E-02
	0.5005	3.170E-01	1.334E-03	2.049E-02
	0.5095	2.869E-01	1.745E-03	1.904E-02
	0.5185	2.415E-01	1.611E-03	1.868E-02
	0.5275	1.991E-01	1.441E-03	1.713E-02
	0.5365	1.639E-01	1.314E-03	1.489E-02
	0.5455	1.353E-01	1.221E-03	1.268E-02
	0.5545	1.111E-01	1.065E-03	1.110E-02
	0.5635	9.399E-02	1.036E-03	9.982E-03
	0.5725	7.814E-02	9.323E-04	9.259E-03
	0.5815	6.274E-02	7.964E-04	6.265E-03
	0.5905	5.392E-02	7.447E-04	4.697E-03
	0.5995	4.621E-02	7.059E-04	4.054E-03
	0.6085	3.889E-02	6.312E-04	3.508E-03
	0.6175	3.207E-02	5.660E-04	3.515E-03
	0.6265	2.731E-02	5.110E-04	3.421E-03
	0.6355	2.128E-02	4.278E-04	2.766E-03
	0.6445	1.612E-02	3.346E-04	2.221E-03
	0.6535	1.244E-02	2.770E-04	4.112E-04
	0.6625	7.554E-03	1.713E-04	2.384E-04
0.625	0.1675	3.193E-01	1.481E-03	2.731E-02
	0.1765	3.153E-01	8.482E-04	2.319E-02
	0.1855	2.952E-01	8.674E-04	1.729E-02
	0.1945	2.887E-01	9.528E-04	1.470E-02
	0.2035	2.786E-01	1.014E-03	1.425E-02
	0.2125	2.771E-01	1.101E-03	1.284E-02
	0.2215	2.949E-01	1.226E-03	1.414E-02

	0.2305	3.341E-01	1.407E-03	1.491E-02
	0.2395	3.493E-01	1.496E-03	1.476E-02
	0.2485	3.159E-01	1.417E-03	1.070E-02
	0.2575	2.758E-01	1.322E-03	8.897E-03
	0.2665	2.530E-01	1.277E-03	7.841E-03
	0.2755	2.534E-01	1.306E-03	7.875E-03
	0.2845	2.669E-01	1.393E-03	8.839E-03
	0.2935	2.960E-01	1.545E-03	1.112E-02
	0.3025	3.328E-01	1.753E-03	1.256E-02
	0.3115	3.391E-01	1.855E-03	9.104E-03
	0.3205	2.891E-01	1.716E-03	9.051E-03
	0.3295	2.417E-01	1.601E-03	7.169E-03
	0.3385	2.157E-01	1.532E-03	9.811E-03
	0.3475	1.992E-01	1.346E-03	7.692E-03
	0.3565	1.843E-01	1.297E-03	7.003E-03
	0.3655	1.760E-01	1.318E-03	6.462E-03
	0.3745	1.700E-01	2.090E-03	7.140E-03
	0.3835	1.679E-01	1.283E-03	7.282E-03
	0.3925	1.698E-01	1.304E-03	8.163E-03
	0.4015	1.720E-01	1.352E-03	9.922E-03
	0.4105	1.766E-01	1.436E-03	8.907E-03
	0.4195	1.819E-01	1.524E-03	1.003E-02
	0.4285	1.862E-01	1.594E-03	1.163E-02
	0.4375	1.990E-01	1.724E-03	1.162E-02
	0.4465	2.159E-01	1.876E-03	1.320E-02
	0.4555	2.339E-01	1.985E-03	1.598E-02
	0.4645	2.601E-01	1.281E-03	1.991E-02
	0.4735	2.847E-01	1.379E-03	2.084E-02
	0.4825	3.072E-01	1.475E-03	2.030E-02
	0.4915	3.358E-01	1.606E-03	2.094E-02
	0.5005	3.465E-01	1.678E-03	1.973E-02
	0.5095	3.458E-01	1.709E-03	1.830E-02
	0.5185	3.204E-01	1.656E-03	1.839E-02
	0.5275	2.795E-01	1.539E-03	1.845E-02
	0.5365	2.404E-01	1.427E-03	1.843E-02
	0.5455	1.992E-01	1.279E-03	1.721E-02
	0.5545	1.662E-01	1.161E-03	1.493E-02
	0.5635	1.373E-01	1.052E-03	1.274E-02
	0.5725	1.135E-01	9.678E-04	1.104E-02
	0.5815	9.385E-02	8.717E-04	9.987E-03
	0.5905	7.804E-02	7.849E-04	8.536E-03
	0.5995	6.488E-02	7.160E-04	6.718E-03
	0.6085	5.535E-02	6.612E-04	5.102E-03
	0.6175	4.640E-02	5.922E-04	4.144E-03
	0.6265	4.007E-02	5.398E-04	3.687E-03
	0.6355	3.614E-02	1.451E-03	4.091E-03
	0.6445	2.763E-02	4.171E-04	3.525E-03
	0.6535	2.187E-02	3.420E-04	2.817E-03
	0.6625	1.708E-02	2.811E-04	2.345E-03
	0.6715	1.242E-02	2.190E-04	4.312E-04
	0.6805	7.478E-03	1.382E-04	2.522E-04
	0.6895	2.930E-03	5.661E-05	9.417E-05
0.675	0.1855	3.055E-01	1.283E-03	2.373E-02
	0.1945	2.939E-01	8.127E-04	1.859E-02
	0.2035	2.907E-01	9.155E-04	1.651E-02
	0.2125	2.812E-01	9.917E-04	1.586E-02
	0.2215	2.779E-01	1.064E-03	1.450E-02
	0.2305	2.823E-01	1.141E-03	1.388E-02
	0.2395	3.205E-01	1.337E-03	1.644E-02
	0.2485	3.472E-01	1.516E-03	1.562E-02
	0.2575	3.382E-01	1.577E-03	1.363E-02
	0.2665	2.996E-01	1.521E-03	1.083E-02
	0.2755	2.650E-01	1.452E-03	9.196E-03
	0.2845	2.507E-01	1.437E-03	8.476E-03
	0.2935	2.509E-01	1.443E-03	8.546E-03
	0.3025	2.662E-01	1.514E-03	9.702E-03
	0.3115	2.949E-01	1.656E-03	1.189E-02
	0.3205	3.280E-01	1.834E-03	1.241E-02
	0.3295	3.259E-01	1.845E-03	9.596E-03
	0.3385	2.771E-01	1.670E-03	9.313E-03
	0.3475	2.306E-01	1.515E-03	7.218E-03
	0.3565	2.014E-01	1.424E-03	5.756E-03
	0.3655	1.844E-01	1.394E-03	4.913E-03
	0.3745	1.764E-01	1.399E-03	4.632E-03
	0.3835	1.692E-01	1.479E-03	7.210E-03
	0.3925	1.640E-01	1.256E-03	6.846E-03
	0.4015	1.635E-01	1.231E-03	6.608E-03

	0.4105	1.596E-01	1.224E-03	6.564E-03
	0.4195	1.657E-01	1.270E-03	7.941E-03
	0.4285	1.691E-01	1.319E-03	7.243E-03
	0.4375	1.744E-01	1.297E-03	9.959E-03
	0.4465	1.815E-01	1.250E-03	1.045E-02
	0.4555	1.955E-01	1.326E-03	1.102E-02
	0.4645	2.098E-01	1.215E-03	1.276E-02
	0.4735	2.264E-01	1.296E-03	1.511E-02
	0.4825	2.444E-01	1.388E-03	1.728E-02
	0.4915	2.718E-01	1.518E-03	1.829E-02
	0.5005	2.994E-01	1.655E-03	1.817E-02
	0.5095	3.242E-01	1.835E-03	1.753E-02
	0.5185	3.373E-01	1.919E-03	1.623E-02
	0.5275	3.318E-01	1.938E-03	1.457E-02
	0.5365	3.117E-01	1.922E-03	1.552E-02
	0.5455	2.738E-01	1.792E-03	1.778E-02
	0.5545	2.347E-01	1.674E-03	1.816E-02
	0.5635	1.974E-01	1.521E-03	1.662E-02
	0.5725	1.594E-01	1.365E-03	1.274E-02
	0.5815	1.331E-01	1.250E-03	1.236E-02
	0.5905	1.093E-01	1.151E-03	1.084E-02
	0.5995	9.015E-02	1.025E-03	9.718E-03
	0.6085	7.398E-02	9.209E-04	8.280E-03
	0.6175	6.246E-02	8.799E-04	6.756E-03
	0.6265	5.174E-02	7.931E-04	5.270E-03
	0.6355	4.234E-02	6.766E-04	4.083E-03
	0.6445	3.723E-02	6.476E-04	3.926E-03
	0.6535	2.969E-02	5.382E-04	3.286E-03
	0.6625	2.592E-02	5.126E-04	3.138E-03
	0.6715	1.887E-02	3.911E-04	2.373E-03
	0.6805	1.528E-02	3.361E-04	2.187E-03
	0.6895	1.061E-02	2.315E-04	3.362E-04
	0.6985	6.291E-03	1.410E-04	2.036E-04
0.725	0.1945	3.259E-01	1.666E-03	2.939E-02
	0.2035	3.019E-01	8.193E-04	2.164E-02
	0.2125	2.923E-01	8.673E-04	1.860E-02
	0.2215	2.810E-01	9.270E-04	1.651E-02
	0.2305	2.757E-01	1.006E-03	1.477E-02
	0.2395	2.787E-01	1.107E-03	1.775E-02
	0.2485	2.994E-01	1.243E-03	1.600E-02
	0.2575	3.360E-01	1.429E-03	1.686E-02
	0.2665	3.470E-01	1.537E-03	1.644E-02
	0.2755	3.200E-01	1.526E-03	1.299E-02
	0.2845	2.778E-01	1.468E-03	1.076E-02
	0.2935	2.570E-01	1.479E-03	9.550E-03
	0.3025	2.449E-01	1.488E-03	9.000E-03
	0.3115	2.505E-01	1.584E-03	9.342E-03
	0.3205	2.693E-01	1.696E-03	1.082E-02
	0.3295	3.029E-01	1.898E-03	1.299E-02
	0.3385	3.327E-01	2.099E-03	1.222E-02
	0.3475	3.124E-01	2.017E-03	1.035E-02
	0.3565	2.646E-01	1.832E-03	9.542E-03
	0.3655	2.191E-01	1.639E-03	7.243E-03
	0.3745	1.983E-01	1.573E-03	6.040E-03
	0.3835	1.833E-01	1.506E-03	5.366E-03
	0.3925	1.706E-01	1.452E-03	5.024E-03
	0.4015	1.632E-01	1.425E-03	4.554E-03
	0.4105	1.566E-01	1.396E-03	4.322E-03
	0.4195	1.579E-01	1.439E-03	4.396E-03
	0.4285	1.565E-01	1.432E-03	4.336E-03
	0.4375	1.638E-01	1.504E-03	9.602E-03
	0.4465	1.606E-01	1.329E-03	8.390E-03
	0.4555	1.671E-01	1.350E-03	8.862E-03
	0.4645	1.737E-01	1.168E-03	1.009E-02
	0.4735	1.844E-01	1.207E-03	1.049E-02
	0.4825	1.980E-01	1.263E-03	1.150E-02
	0.4915	2.132E-01	1.344E-03	1.371E-02
	0.5005	2.338E-01	1.522E-03	1.680E-02
	0.5095	2.554E-01	1.432E-03	1.758E-02
	0.5185	2.770E-01	1.479E-03	1.750E-02
	0.5275	3.049E-01	1.571E-03	1.739E-02
	0.5365	3.145E-01	1.627E-03	1.595E-02
	0.5455	3.127E-01	1.642E-03	1.459E-02
	0.5545	2.892E-01	1.578E-03	1.537E-02
	0.5635	2.605E-01	1.506E-03	1.767E-02
	0.5725	2.220E-01	1.396E-03	1.772E-02
	0.5815	1.815E-01	1.243E-03	1.591E-02

	0.5905	1.465E-01	1.104E-03	1.278E-02
	0.5995	1.250E-01	1.031E-03	1.032E-02
	0.6085	1.018E-01	9.241E-04	9.357E-03
	0.6175	8.451E-02	8.487E-04	9.024E-03
	0.6265	7.143E-02	7.716E-04	7.519E-03
	0.6355	6.029E-02	7.382E-04	5.421E-03
	0.6445	4.987E-02	6.373E-04	3.665E-03
	0.6535	4.267E-02	5.733E-04	4.010E-03
	0.6625	3.564E-02	5.181E-04	3.472E-03
	0.6715	2.894E-02	4.562E-04	3.315E-03
	0.6805	2.436E-02	3.956E-04	2.895E-03
	0.6895	1.976E-02	3.298E-04	2.522E-03
	0.6985	1.371E-02	2.497E-04	4.641E-04
	0.7075	9.400E-03	1.756E-04	3.213E-04
	0.7165	4.780E-03	9.028E-05	1.622E-04
0.775	0.2125	3.210E-01	8.198E-04	2.761E-02
	0.2215	2.955E-01	8.917E-04	2.074E-02
	0.2305	2.869E-01	9.301E-04	1.826E-02
	0.2395	2.770E-01	9.621E-04	1.658E-02
	0.2485	2.717E-01	1.014E-03	1.699E-02
	0.2575	2.811E-01	1.118E-03	1.596E-02
	0.2665	3.154E-01	1.312E-03	1.770E-02
	0.2755	3.426E-01	1.493E-03	1.718E-02
	0.2845	3.307E-01	1.536E-03	1.522E-02
	0.2935	2.945E-01	1.480E-03	1.275E-02
	0.3025	2.658E-01	1.449E-03	1.103E-02
	0.3115	2.499E-01	1.449E-03	1.007E-02
	0.3205	2.397E-01	1.481E-03	9.559E-03
	0.3295	2.551E-01	1.606E-03	1.047E-02
	0.3385	2.745E-01	1.741E-03	1.204E-02
	0.3475	3.101E-01	1.982E-03	1.405E-02
	0.3565	3.236E-01	2.126E-03	1.177E-02
	0.3655	2.872E-01	1.996E-03	1.071E-02
	0.3745	2.380E-01	1.816E-03	8.970E-03
	0.3835	2.049E-01	1.688E-03	7.129E-03
	0.3925	1.883E-01	1.660E-03	6.146E-03
	0.4015	1.742E-01	1.634E-03	5.498E-03
	0.4105	1.654E-01	1.599E-03	5.494E-03
	0.4195	1.584E-01	1.590E-03	4.878E-03
	0.4285	1.564E-01	1.605E-03	4.736E-03
	0.4375	1.511E-01	1.558E-03	4.552E-03
	0.4465	1.515E-01	1.578E-03	4.836E-03
	0.4555	1.583E-01	1.650E-03	5.109E-03
	0.4645	1.583E-01	1.324E-03	4.891E-03
	0.4735	1.599E-01	1.334E-03	6.577E-03
	0.4825	1.716E-01	1.402E-03	7.757E-03
	0.4915	1.868E-01	2.017E-03	1.341E-02
	0.5005	1.918E-01	1.533E-03	1.368E-02
	0.5095	2.097E-01	1.506E-03	1.475E-02
	0.5185	2.332E-01	1.562E-03	1.626E-02
	0.5275	2.522E-01	1.605E-03	1.617E-02
	0.5365	2.800E-01	1.722E-03	1.558E-02
	0.5455	2.941E-01	1.782E-03	1.514E-02
	0.5545	3.026E-01	1.837E-03	1.358E-02
	0.5635	2.984E-01	4.111E-03	1.563E-02
	0.5725	2.704E-01	1.871E-03	1.567E-02
	0.5815	2.353E-01	1.545E-03	1.722E-02
	0.5905	1.962E-01	1.326E-03	1.641E-02
	0.5995	1.627E-01	1.169E-03	1.454E-02
	0.6085	1.325E-01	1.027E-03	1.162E-02
	0.6175	1.081E-01	9.178E-04	8.982E-03
	0.6265	9.094E-02	8.383E-04	9.535E-03
	0.6355	7.384E-02	7.340E-04	7.990E-03
	0.6445	6.072E-02	6.453E-04	6.086E-03
	0.6535	5.191E-02	5.964E-04	4.311E-03
	0.6625	4.437E-02	5.485E-04	3.332E-03
	0.6715	3.708E-02	4.832E-04	3.023E-03
	0.6805	3.028E-02	4.137E-04	3.291E-03
	0.6895	2.538E-02	3.708E-04	3.279E-03
	0.6985	2.051E-02	3.197E-04	2.811E-03
	0.7075	1.581E-02	2.528E-04	2.398E-03
	0.7165	1.120E-02	1.887E-04	3.991E-04
	0.7255	6.836E-03	1.195E-04	2.302E-04
0.825	0.2215	3.387E-01	1.074E-03	3.414E-02
	0.2305	3.009E-01	7.975E-04	2.341E-02
	0.2395	2.878E-01	9.662E-04	2.024E-02
	0.2485	2.769E-01	9.909E-04	1.822E-02

	0.2575	2.700E-01	1.016E-03	1.634E-02
	0.2665	2.743E-01	1.072E-03	1.697E-02
	0.2755	2.958E-01	1.186E-03	1.774E-02
	0.2845	3.249E-01	1.331E-03	1.772E-02
	0.2935	3.320E-01	1.437E-03	1.729E-02
	0.3025	2.992E-01	1.417E-03	1.414E-02
	0.3115	2.656E-01	1.402E-03	1.206E-02
	0.3205	2.466E-01	1.413E-03	1.082E-02
	0.3295	2.367E-01	1.430E-03	1.025E-02
	0.3385	2.417E-01	1.503E-03	1.051E-02
	0.3475	2.557E-01	1.611E-03	1.149E-02
	0.3565	2.860E-01	1.799E-03	1.366E-02
	0.3655	3.160E-01	2.011E-03	1.433E-02
	0.3745	3.188E-01	2.098E-03	1.216E-02
	0.3835	2.732E-01	1.966E-03	1.125E-02
	0.3925	2.254E-01	1.772E-03	8.833E-03
	0.4015	2.004E-01	1.722E-03	7.376E-03
	0.4105	1.844E-01	1.674E-03	6.501E-03
	0.4195	1.637E-01	1.583E-03	5.550E-03
	0.4285	1.620E-01	1.623E-03	5.659E-03
	0.4375	1.576E-01	1.649E-03	5.206E-03
	0.4465	1.532E-01	1.636E-03	5.016E-03
	0.4555	1.523E-01	1.689E-03	4.942E-03
	0.4645	1.462E-01	1.285E-03	4.969E-03
	0.4735	1.464E-01	1.296E-03	4.769E-03
	0.4825	1.529E-01	1.349E-03	5.297E-03
	0.4915	1.583E-01	1.391E-03	6.980E-03
	0.5005	1.629E-01	1.427E-03	7.626E-03
	0.5095	1.782E-01	1.537E-03	8.052E-03
	0.5185	1.885E-01	1.606E-03	9.462E-03
	0.5275	1.991E-01	1.678E-03	1.177E-02
	0.5365	2.255E-01	1.843E-03	1.187E-02
	0.5455	2.412E-01	1.966E-03	1.199E-02
	0.5545	2.672E-01	2.123E-03	1.145E-02
	0.5635	2.840E-01	2.252E-03	1.817E-02
	0.5725	2.838E-01	2.084E-03	1.416E-02
	0.5815	2.717E-01	1.975E-03	1.267E-02
	0.5905	2.477E-01	1.835E-03	1.590E-02
	0.5995	2.144E-01	1.652E-03	1.575E-02
	0.6085	1.755E-01	1.449E-03	1.467E-02
	0.6175	1.439E-01	1.293E-03	1.247E-02
	0.6265	1.185E-01	1.154E-03	9.408E-03
	0.6355	9.740E-02	1.036E-03	8.285E-03
	0.6445	8.168E-02	9.366E-04	8.461E-03
	0.6535	6.735E-02	8.995E-04	7.110E-03
	0.6625	5.604E-02	7.138E-04	5.060E-03
	0.6715	4.751E-02	6.224E-04	3.730E-03
	0.6805	3.975E-02	5.373E-04	3.143E-03
	0.6895	3.237E-02	4.662E-04	3.116E-03
	0.6985	2.713E-02	4.051E-04	3.461E-03
	0.7075	2.277E-02	3.581E-04	3.042E-03
	0.7165	1.646E-02	2.768E-04	2.392E-03
	0.7255	1.274E-02	2.174E-04	4.494E-04
	0.7345	8.128E-03	1.413E-04	2.846E-04
	0.7435	3.853E-03	6.837E-05	1.294E-04
0.875	0.2305	2.869E-01	2.305E-03	2.938E-02
	0.2395	3.117E-01	9.260E-04	2.748E-02
	0.2485	2.902E-01	8.550E-04	2.238E-02
	0.2575	2.778E-01	8.683E-04	1.976E-02
	0.2665	2.704E-01	1.060E-03	1.787E-02
	0.2755	2.664E-01	1.083E-03	1.876E-02
	0.2845	2.840E-01	1.173E-03	1.833E-02
	0.2935	3.166E-01	1.324E-03	2.027E-02
	0.3025	3.266E-01	1.406E-03	1.829E-02
	0.3115	3.066E-01	1.397E-03	1.578E-02
	0.3205	2.726E-01	1.333E-03	1.349E-02
	0.3295	2.448E-01	1.300E-03	1.161E-02
	0.3385	2.302E-01	1.317E-03	1.070E-02
	0.3475	2.292E-01	1.389E-03	1.052E-02
	0.3565	2.361E-01	1.483E-03	1.102E-02
	0.3655	2.626E-01	1.658E-03	1.294E-02
	0.3745	2.942E-01	1.871E-03	1.491E-02
	0.3835	3.118E-01	2.023E-03	1.357E-02
	0.3925	2.892E-01	1.960E-03	1.225E-02
	0.4015	2.454E-01	1.806E-03	1.066E-02
	0.4105	2.059E-01	1.671E-03	8.357E-03
	0.4195	1.895E-01	1.637E-03	7.301E-03

	0.4285	1.710E-01	1.583E-03	6.350E-03
	0.4375	1.644E-01	1.586E-03	5.999E-03
	0.4465	1.551E-01	1.578E-03	5.593E-03
	0.4555	1.536E-01	1.612E-03	5.502E-03
	0.4645	1.495E-01	1.420E-03	5.308E-03
	0.4735	1.474E-01	1.431E-03	5.180E-03
	0.4825	1.467E-01	1.427E-03	5.136E-03
	0.4915	1.480E-01	1.452E-03	5.252E-03
	0.5005	1.492E-01	1.451E-03	5.928E-03
	0.5095	1.543E-01	1.486E-03	7.249E-03
	0.5185	1.640E-01	1.561E-03	7.898E-03
	0.5275	1.739E-01	1.628E-03	8.044E-03
	0.5365	1.856E-01	1.714E-03	1.031E-02
	0.5455	2.037E-01	1.817E-03	1.170E-02
	0.5545	2.207E-01	1.931E-03	1.196E-02
	0.5635	2.406E-01	2.069E-03	1.149E-02
	0.5725	2.622E-01	2.219E-03	1.087E-02
	0.5815	2.763E-01	2.311E-03	9.811E-03
	0.5905	2.704E-01	2.324E-03	8.484E-03
	0.5995	2.593E-01	2.284E-03	9.778E-03
	0.6085	2.293E-01	2.128E-03	1.431E-02
	0.6175	1.926E-01	1.951E-03	1.423E-02
	0.6265	1.573E-01	2.546E-03	1.566E-02
	0.6355	1.288E-01	1.636E-03	1.207E-02
	0.6445	1.057E-01	1.315E-03	9.452E-03
	0.6535	8.786E-02	1.120E-03	8.194E-03
	0.6625	7.220E-02	9.839E-04	7.353E-03
	0.6715	5.898E-02	8.576E-04	5.564E-03
	0.6805	4.840E-02	7.557E-04	3.839E-03
	0.6895	4.183E-02	6.756E-04	3.243E-03
	0.6985	3.501E-02	5.954E-04	3.161E-03
	0.7075	2.812E-02	5.056E-04	3.477E-03
	0.7165	2.284E-02	4.357E-04	2.990E-03
	0.7255	1.818E-02	3.657E-04	2.561E-03
	0.7345	1.408E-02	2.988E-04	1.494E-03
	0.7435	9.134E-03	1.961E-04	3.098E-04
	0.7525	4.720E-03	1.028E-04	1.717E-04
0.925	0.2485	3.231E-01	1.280E-03	3.252E-02
	0.2575	2.909E-01	9.236E-04	2.452E-02
	0.2665	2.809E-01	9.163E-04	2.162E-02
	0.2755	2.700E-01	9.248E-04	1.944E-02
	0.2845	2.657E-01	9.488E-04	2.010E-02
	0.2935	2.721E-01	1.185E-03	1.809E-02
	0.3025	3.019E-01	1.319E-03	1.948E-02
	0.3115	3.225E-01	1.423E-03	1.961E-02
	0.3205	3.118E-01	1.437E-03	1.812E-02
	0.3295	2.786E-01	1.377E-03	1.486E-02
	0.3385	2.484E-01	1.319E-03	1.274E-02
	0.3475	2.282E-01	1.303E-03	1.140E-02
	0.3565	2.207E-01	1.298E-03	1.085E-02
	0.3655	2.232E-01	1.342E-03	1.097E-02
	0.3745	2.418E-01	1.475E-03	1.232E-02
	0.3835	2.694E-01	1.646E-03	1.421E-02
	0.3925	2.925E-01	1.825E-03	1.477E-02
	0.4015	2.956E-01	1.910E-03	1.299E-02
	0.4105	2.538E-01	1.790E-03	1.168E-02
	0.4195	2.144E-01	1.660E-03	9.574E-03
	0.4285	1.910E-01	1.598E-03	8.079E-03
	0.4375	1.718E-01	1.538E-03	6.929E-03
	0.4465	1.613E-01	1.521E-03	6.391E-03
	0.4555	1.544E-01	1.520E-03	6.228E-03
	0.4645	1.493E-01	1.432E-03	5.702E-03
	0.4735	1.472E-01	1.439E-03	5.674E-03
	0.4825	1.449E-01	1.456E-03	5.479E-03
	0.4915	1.428E-01	1.441E-03	5.343E-03
	0.5005	1.450E-01	1.492E-03	5.434E-03
	0.5095	1.473E-01	1.529E-03	5.574E-03
	0.5185	1.494E-01	1.547E-03	6.905E-03
	0.5275	1.547E-01	1.604E-03	7.779E-03
	0.5365	1.671E-01	1.705E-03	8.225E-03
	0.5455	1.753E-01	1.767E-03	8.235E-03
	0.5545	1.923E-01	1.919E-03	1.192E-02
	0.5635	2.097E-01	2.041E-03	1.224E-02
	0.5725	2.219E-01	2.137E-03	1.160E-02
	0.5815	2.423E-01	2.325E-03	1.127E-02
	0.5905	2.571E-01	2.443E-03	1.035E-02
	0.5995	2.660E-01	2.560E-03	9.401E-03

	0.6085	2.554E-01	2.508E-03	8.812E-03
	0.6175	2.308E-01	2.360E-03	1.118E-02
	0.6265	1.915E-01	2.108E-03	1.290E-02
	0.6355	1.623E-01	1.914E-03	1.306E-02
	0.6445	1.331E-01	1.726E-03	1.082E-02
	0.6535	1.031E-01	1.479E-03	7.239E-03
	0.6625	8.755E-02	1.341E-03	6.899E-03
	0.6715	7.142E-02	1.200E-03	7.749E-03
	0.6805	5.883E-02	1.065E-03	5.593E-03
	0.6895	5.117E-02	9.866E-04	3.822E-03
	0.6985	4.121E-02	8.662E-04	2.855E-03
	0.7075	3.385E-02	7.508E-04	2.739E-03
	0.7165	2.906E-02	7.746E-04	3.732E-03
	0.7255	2.438E-02	5.739E-04	3.185E-03
	0.7345	1.898E-02	4.523E-04	2.663E-03
	0.7435	1.443E-02	3.369E-04	2.271E-03
	0.7525	1.061E-02	2.482E-04	4.184E-04
	0.7615	5.558E-03	1.333E-04	2.147E-04
0.975	0.2575	2.689E-01	2.631E-02	2.470E-02
	0.2665	2.935E-01	1.188E-03	2.710E-02
	0.2755	2.780E-01	9.813E-04	2.326E-02
	0.2845	2.709E-01	9.729E-04	2.118E-02
	0.2935	2.635E-01	9.830E-04	1.977E-02
	0.3025	2.724E-01	1.042E-03	1.936E-02
	0.3115	2.932E-01	1.354E-03	2.031E-02
	0.3205	3.153E-01	1.458E-03	2.144E-02
	0.3295	3.097E-01	1.485E-03	1.867E-02
	0.3385	2.823E-01	1.427E-03	1.620E-02
	0.3475	2.535E-01	1.365E-03	1.401E-02
	0.3565	2.294E-01	1.321E-03	1.231E-02
	0.3655	2.215E-01	1.331E-03	1.174E-02
	0.3745	2.171E-01	1.359E-03	1.138E-02
	0.3835	2.238E-01	1.416E-03	1.186E-02
	0.3925	2.507E-01	1.564E-03	1.388E-02
	0.4015	2.791E-01	1.736E-03	1.547E-02
	0.4105	2.892E-01	1.820E-03	1.400E-02
	0.4195	2.666E-01	1.754E-03	1.280E-02
	0.4285	2.236E-01	1.602E-03	1.074E-02
	0.4375	1.892E-01	1.502E-03	8.675E-03
	0.4465	1.697E-01	1.447E-03	7.375E-03
	0.4555	1.609E-01	1.442E-03	6.805E-03
	0.4645	1.483E-01	1.236E-03	6.178E-03
	0.4735	1.447E-01	1.273E-03	5.938E-03
	0.4825	1.425E-01	1.320E-03	5.778E-03
	0.4915	1.401E-01	1.339E-03	5.682E-03
	0.5005	1.403E-01	1.369E-03	5.664E-03
	0.5095	1.395E-01	1.414E-03	5.641E-03
	0.5185	1.462E-01	1.509E-03	6.005E-03
	0.5275	1.456E-01	1.515E-03	6.396E-03
	0.5365	1.465E-01	1.549E-03	7.437E-03
	0.5455	1.545E-01	1.630E-03	7.954E-03
	0.5545	1.624E-01	1.722E-03	7.426E-03
	0.5635	1.755E-01	1.840E-03	1.034E-02
	0.5725	1.872E-01	1.948E-03	1.149E-02
	0.5815	2.018E-01	2.071E-03	1.117E-02
	0.5905	2.264E-01	2.264E-03	1.134E-02
	0.5995	2.416E-01	2.383E-03	1.069E-02
	0.6085	2.490E-01	2.481E-03	9.767E-03
	0.6175	2.504E-01	2.564E-03	9.134E-03
	0.6265	2.330E-01	2.464E-03	1.019E-02
	0.6355	2.011E-01	2.287E-03	1.246E-02
	0.6445	1.691E-01	2.067E-03	1.370E-02
	0.6535	1.421E-01	1.862E-03	1.337E-02
	0.6625	1.138E-01	1.656E-03	8.358E-03
	0.6715	9.518E-02	1.524E-03	6.972E-03
	0.6805	7.756E-02	1.374E-03	7.418E-03
	0.6895	6.261E-02	1.184E-03	6.150E-03
	0.6985	5.449E-02	1.120E-03	4.178E-03
	0.7075	4.490E-02	9.964E-04	3.103E-03
	0.7165	3.634E-02	8.647E-04	2.859E-03
	0.7255	3.187E-02	8.036E-04	3.499E-03
	0.7345	2.449E-02	6.611E-04	3.081E-03
	0.7435	2.052E-02	5.634E-04	2.778E-03
	0.7525	1.576E-02	4.620E-04	2.432E-03
	0.7615	1.025E-02	3.124E-04	2.836E-04
	0.7705	5.477E-03	1.711E-04	1.431E-04
1.025	0.2755	2.925E-01	7.867E-03	2.951E-02

	0.2845	2.706E-01	1.232E-03	2.417E-02
	0.2935	2.663E-01	1.040E-03	2.224E-02
	0.3025	2.643E-01	1.034E-03	2.078E-02
	0.3115	2.649E-01	1.065E-03	2.032E-02
	0.3205	2.836E-01	1.149E-03	2.125E-02
	0.3295	3.064E-01	1.246E-03	2.266E-02
	0.3385	3.095E-01	1.542E-03	2.016E-02
	0.3475	2.826E-01	1.490E-03	1.761E-02
	0.3565	2.515E-01	1.410E-03	1.493E-02
	0.3655	2.292E-01	1.365E-03	1.316E-02
	0.3745	2.156E-01	1.346E-03	1.213E-02
	0.3835	2.120E-01	1.372E-03	1.171E-02
	0.3925	2.198E-01	1.426E-03	1.227E-02
	0.4015	2.382E-01	1.540E-03	1.377E-02
	0.4105	2.638E-01	1.698E-03	1.562E-02
	0.4195	2.829E-01	1.836E-03	1.527E-02
	0.4285	2.727E-01	1.828E-03	1.370E-02
	0.4375	2.335E-01	1.670E-03	1.201E-02
	0.4465	1.925E-01	1.509E-03	9.450E-03
	0.4555	1.725E-01	1.447E-03	8.055E-03
	0.4645	1.599E-01	1.218E-03	7.293E-03
	0.4735	1.479E-01	1.192E-03	6.602E-03
	0.4825	1.410E-01	1.171E-03	6.197E-03
	0.4915	1.370E-01	1.187E-03	6.028E-03
	0.5005	1.333E-01	1.192E-03	5.707E-03
	0.5095	1.354E-01	1.238E-03	5.755E-03
	0.5185	1.345E-01	1.264E-03	5.729E-03
	0.5275	1.341E-01	1.283E-03	5.702E-03
	0.5365	1.305E-01	1.277E-03	5.489E-03
	0.5455	1.391E-01	1.375E-03	7.117E-03
	0.5545	1.412E-01	1.421E-03	7.550E-03
	0.5635	1.516E-01	1.522E-03	7.725E-03
	0.5725	1.596E-01	1.596E-03	9.088E-03
	0.5815	1.721E-01	1.720E-03	1.091E-02
	0.5905	1.914E-01	1.884E-03	1.117E-02
	0.5995	2.064E-01	2.030E-03	1.096E-02
	0.6085	2.278E-01	2.207E-03	1.080E-02
	0.6175	2.401E-01	2.367E-03	1.041E-02
	0.6265	2.423E-01	2.440E-03	9.581E-03
	0.6355	2.282E-01	2.379E-03	9.431E-03
	0.6445	2.029E-01	2.282E-03	1.171E-02
	0.6535	1.713E-01	2.062E-03	1.267E-02
	0.6625	1.363E-01	1.823E-03	1.156E-02
	0.6715	1.090E-01	1.631E-03	8.248E-03
	0.6805	8.875E-02	1.475E-03	6.205E-03
	0.6895	7.419E-02	1.322E-03	6.625E-03
	0.6985	6.082E-02	1.207E-03	6.068E-03
	0.7075	5.014E-02	1.066E-03	4.722E-03
	0.7165	3.960E-02	9.276E-04	2.688E-03
	0.7255	3.405E-02	8.407E-04	2.663E-03
	0.7345	2.879E-02	7.503E-04	3.129E-03
	0.7435	2.290E-02	6.468E-04	2.881E-03
	0.7525	2.013E-02	5.741E-04	2.720E-03
	0.7615	1.485E-02	4.416E-04	2.284E-03
	0.7705	9.887E-03	3.095E-04	2.817E-04
	0.7795	5.734E-03	1.828E-04	1.659E-04
1.075	0.2845	2.786E-01	3.020E-03	3.043E-02
	0.2935	2.723E-01	1.662E-03	2.647E-02
	0.3025	2.621E-01	1.358E-03	2.331E-02
	0.3115	2.571E-01	1.104E-03	2.161E-02
	0.3205	2.584E-01	1.100E-03	2.110E-02
	0.3295	2.781E-01	1.186E-03	2.227E-02
	0.3385	3.015E-01	1.287E-03	2.348E-02
	0.3475	3.051E-01	1.327E-03	2.148E-02
	0.3565	2.845E-01	1.564E-03	1.918E-02
	0.3655	2.543E-01	1.475E-03	1.612E-02
	0.3745	2.276E-01	1.401E-03	1.395E-02
	0.3835	2.080E-01	1.375E-03	1.249E-02
	0.3925	2.063E-01	1.394E-03	1.213E-02
	0.4015	2.087E-01	1.420E-03	1.215E-02
	0.4105	2.259E-01	1.526E-03	1.353E-02
	0.4195	2.468E-01	1.669E-03	1.515E-02
	0.4285	2.741E-01	1.837E-03	1.623E-02
	0.4375	2.768E-01	1.886E-03	1.484E-02
	0.4465	2.403E-01	1.737E-03	1.312E-02
	0.4555	1.994E-01	1.555E-03	1.064E-02
	0.4645	1.728E-01	1.237E-03	8.732E-03

	0.4735	1.571E-01	1.207E-03	7.627E-03
	0.4825	1.481E-01	1.189E-03	7.094E-03
	0.4915	1.390E-01	1.179E-03	6.513E-03
	0.5005	1.344E-01	1.181E-03	6.268E-03
	0.5095	1.308E-01	1.186E-03	5.992E-03
	0.5185	1.289E-01	1.199E-03	5.899E-03
	0.5275	1.258E-01	1.190E-03	5.678E-03
	0.5365	1.285E-01	1.220E-03	5.829E-03
	0.5455	1.259E-01	1.206E-03	5.632E-03
	0.5545	1.302E-01	1.252E-03	6.588E-03
	0.5635	1.350E-01	1.298E-03	7.430E-03
	0.5725	1.400E-01	1.359E-03	7.654E-03
	0.5815	1.487E-01	1.439E-03	8.372E-03
	0.5905	1.574E-01	1.506E-03	1.020E-02
	0.5995	1.693E-01	1.603E-03	1.022E-02
	0.6085	1.861E-01	1.782E-03	1.027E-02
	0.6175	2.065E-01	1.928E-03	1.032E-02
	0.6265	2.171E-01	2.045E-03	1.001E-02
	0.6355	2.220E-01	2.130E-03	9.261E-03
	0.6445	2.138E-01	2.139E-03	9.020E-03
	0.6535	1.916E-01	2.025E-03	1.042E-02
	0.6625	1.611E-01	1.846E-03	1.157E-02
	0.6715	1.347E-01	1.665E-03	1.308E-02
	0.6805	1.080E-01	1.485E-03	8.392E-03
	0.6895	8.943E-02	1.347E-03	6.126E-03
	0.6985	6.960E-02	1.181E-03	5.965E-03
	0.7075	5.838E-02	1.061E-03	5.851E-03
	0.7165	5.082E-02	1.038E-03	4.464E-03
	0.7255	4.153E-02	9.230E-04	2.829E-03
	0.7345	3.407E-02	7.964E-04	2.670E-03
	0.7435	2.765E-02	7.045E-04	3.051E-03
	0.7525	2.289E-02	6.237E-04	2.893E-03
	0.7615	1.758E-02	4.901E-04	2.389E-03
	0.7705	1.375E-02	4.192E-04	2.145E-03
	0.7795	9.585E-03	2.958E-04	3.081E-04
	0.7885	4.853E-03	1.544E-04	1.515E-04
1.125	0.3025	2.741E-01	3.090E-03	2.914E-02
	0.3115	2.576E-01	1.743E-03	2.483E-02
	0.3205	2.495E-01	1.487E-03	2.222E-02
	0.3295	2.523E-01	1.199E-03	2.194E-02
	0.3385	2.665E-01	1.206E-03	2.230E-02
	0.3475	2.928E-01	1.327E-03	2.371E-02
	0.3565	3.048E-01	1.388E-03	2.320E-02
	0.3655	2.848E-01	1.350E-03	2.023E-02
	0.3745	2.538E-01	1.278E-03	1.724E-02
	0.3835	2.280E-01	1.483E-03	1.509E-02
	0.3925	2.033E-01	1.401E-03	1.298E-02
	0.4015	1.988E-01	1.409E-03	1.451E-02
	0.4105	2.003E-01	1.433E-03	1.244E-02
	0.4195	2.096E-01	1.491E-03	1.312E-02
	0.4285	2.338E-01	1.655E-03	1.499E-02
	0.4375	2.613E-01	1.830E-03	1.654E-02
	0.4465	2.649E-01	1.877E-03	1.501E-02
	0.4555	2.431E-01	1.801E-03	1.374E-02
	0.4645	1.998E-01	1.320E-03	1.109E-02
	0.4735	1.734E-01	1.236E-03	9.270E-03
	0.4825	1.599E-01	1.211E-03	8.258E-03
	0.4915	1.459E-01	1.170E-03	7.435E-03
	0.5005	1.369E-01	1.145E-03	6.936E-03
	0.5095	1.317E-01	1.140E-03	6.527E-03
	0.5185	1.261E-01	1.135E-03	6.184E-03
	0.5275	1.252E-01	1.158E-03	6.095E-03
	0.5365	1.245E-01	1.176E-03	6.019E-03
	0.5455	1.241E-01	1.211E-03	5.910E-03
	0.5545	1.219E-01	1.213E-03	5.788E-03
	0.5635	1.248E-01	1.251E-03	6.212E-03
	0.5725	1.283E-01	1.297E-03	7.243E-03
	0.5815	1.325E-01	1.345E-03	7.615E-03
	0.5905	1.414E-01	1.410E-03	8.037E-03
	0.5995	1.515E-01	1.485E-03	9.774E-03
	0.6085	1.612E-01	1.558E-03	9.636E-03
	0.6175	1.732E-01	1.657E-03	9.854E-03
	0.6265	1.891E-01	1.779E-03	1.012E-02
	0.6355	2.037E-01	1.903E-03	1.005E-02
	0.6445	2.147E-01	2.023E-03	9.784E-03
	0.6535	2.086E-01	2.019E-03	9.333E-03
	0.6625	1.815E-01	1.838E-03	9.733E-03
	0.6715	1.568E-01	1.709E-03	1.110E-02
	0.6805	1.289E-01	1.547E-03	1.088E-02
	0.6895	1.004E-01	1.326E-03	8.090E-03
	0.6985	8.345E-02	1.213E-03	5.678E-03
	0.7075	6.772E-02	1.119E-03	5.690E-03
	0.7165	5.569E-02	9.874E-04	5.561E-03
	0.7255	4.570E-02	8.845E-04	3.503E-03
	0.7345	3.729E-02	8.015E-04	2.537E-03
	0.7435	3.124E-02	7.397E-04	3.640E-03
	0.7525	2.548E-02	6.410E-04	2.932E-03
	0.7615	2.022E-02	5.348E-04	2.575E-03
	0.7705	1.709E-02	4.680E-04	2.351E-03
	0.7795	1.281E-02	3.690E-04	2.051E-03
	0.7885	7.427E-03	2.371E-04	2.471E-04
	0.7975	3.316E-03	1.098E-04	1.038E-04
1.175	0.3205	2.590E-01	3.249E-03	2.746E-02
	0.3295	2.542E-01	1.907E-03	2.457E-02
	0.3385	2.506E-01	1.794E-03	2.335E-02
	0.3475	2.610E-01	1.361E-03	2.301E-02
	0.3565	2.855E-01	1.371E-03	2.444E-02
	0.3655	2.971E-01	1.431E-03	2.387E-02
	0.3745	2.859E-01	1.422E-03	2.175E-02
	0.3835	2.554E-01	1.335E-03	1.847E-02
	0.3925	2.268E-01	1.267E-03	1.599E-02
	0.4015	2.041E-01	1.210E-03	1.386E-02
	0.4105	2.004E-01	1.491E-03	1.537E-02
	0.4195	1.975E-01	1.490E-03	1.330E-02
	0.4285	2.029E-01	1.527E-03	1.334E-02
	0.4375	2.198E-01	1.658E-03	1.476E-02
	0.4465	2.427E-01	1.798E-03	1.619E-02
	0.4555	2.597E-01	1.928E-03	1.590E-02
	0.4645	2.396E-01	1.532E-03	1.424E-02
	0.4735	2.052E-01	1.396E-03	1.209E-02
	0.4825	1.705E-01	1.268E-03	9.615E-03
	0.4915	1.556E-01	1.216E-03	8.440E-03
	0.5005	1.429E-01	1.175E-03	7.542E-03
	0.5095	1.361E-01	1.164E-03	7.196E-03
	0.5185	1.268E-01	1.136E-03	6.631E-03
	0.5275	1.220E-01	1.124E-03	6.260E-03
	0.5365	1.188E-01	1.117E-03	6.067E-03
	0.5455	1.189E-01	1.131E-03	6.012E-03
	0.5545	1.214E-01	1.174E-03	6.176E-03
	0.5635	1.220E-01	1.196E-03	6.211E-03
	0.5725	1.214E-01	1.197E-03	6.294E-03
	0.5815	1.239E-01	1.237E-03	7.187E-03
	0.5905	1.288E-01	1.298E-03	7.645E-03
	0.5995	1.329E-01	1.345E-03	7.743E-03
	0.6085	1.436E-01	1.444E-03	9.324E-03
	0.6175	1.534E-01	1.531E-03	9.992E-03
	0.6265	1.632E-01	1.608E-03	9.687E-03
	0.6355	1.797E-01	1.759E-03	1.007E-02
	0.6445	1.930E-01	1.890E-03	1.001E-02
	0.6535	1.959E-01	1.941E-03	9.407E-03
	0.6625	1.922E-01	1.957E-03	8.950E-03
	0.6715	1.756E-01	1.860E-03	9.504E-03
	0.6805	1.503E-01	1.701E-03	1.067E-02
	0.6895	1.231E-01	1.512E-03	1.044E-02
	0.6985	9.747E-02	1.330E-03	7.805E-03
	0.7075	8.153E-02	1.201E-03	5.583E-03
	0.7165	6.345E-02	1.055E-03	5.342E-03
	0.7255	5.136E-02	9.204E-04	5.069E-03
	0.7345	4.207E-02	8.224E-04	3.150E-03
	0.7435	3.689E-02	7.722E-04	2.538E-03
	0.7525	2.934E-02	6.783E-04	3.045E-03
	0.7615	2.358E-02	5.937E-04	2.866E-03
	0.7705	2.068E-02	5.110E-04	2.665E-03
	0.7795	1.479E-02	4.034E-04	2.084E-03
	0.7885	1.168E-02	3.256E-04	1.216E-03
	0.7975	6.940E-03	2.057E-04	2.394E-04
	0.8065	2.452E-03	7.216E-05	8.232E-05
1.225	0.3385	2.471E-01	3.621E-03	2.611E-02
	0.3475	2.476E-01	2.074E-03	2.497E-02
	0.3565	2.521E-01	2.417E-03	2.383E-02
	0.3655	2.786E-01	1.597E-03	2.507E-02
	0.3745	2.865E-01	1.494E-03	2.429E-02
	0.3835	2.776E-01	1.459E-03	2.210E-02
	0.3925	2.493E-01	1.381E-03	1.898E-02

	0.4015	2.212E-01	1.302E-03	1.647E-02
	0.4105	2.050E-01	1.275E-03	1.492E-02
	0.4195	1.950E-01	1.246E-03	1.577E-02
	0.4285	1.930E-01	1.534E-03	1.363E-02
	0.4375	1.988E-01	1.571E-03	1.380E-02
	0.4465	2.126E-01	1.690E-03	1.498E-02
	0.4555	2.341E-01	1.824E-03	1.667E-02
	0.4645	2.506E-01	1.632E-03	1.647E-02
	0.4735	2.435E-01	1.616E-03	1.527E-02
	0.4825	2.018E-01	1.438E-03	1.262E-02
	0.4915	1.706E-01	1.315E-03	1.017E-02
	0.5005	1.507E-01	1.238E-03	8.655E-03
	0.5095	1.362E-01	1.188E-03	7.664E-03
	0.5185	1.311E-01	1.184E-03	7.341E-03
	0.5275	1.260E-01	1.173E-03	6.900E-03
	0.5365	1.228E-01	1.176E-03	6.710E-03
	0.5455	1.189E-01	1.161E-03	6.424E-03
	0.5545	1.147E-01	1.150E-03	6.073E-03
	0.5635	1.138E-01	1.156E-03	6.079E-03
	0.5725	1.142E-01	1.166E-03	5.997E-03
	0.5815	1.135E-01	1.182E-03	5.912E-03
	0.5905	1.181E-01	1.218E-03	6.968E-03
	0.5995	1.224E-01	1.264E-03	7.584E-03
	0.6085	1.257E-01	1.295E-03	7.553E-03
	0.6175	1.346E-01	1.375E-03	8.876E-03
	0.6265	1.433E-01	1.444E-03	9.518E-03
	0.6355	1.550E-01	1.536E-03	9.485E-03
	0.6445	1.718E-01	1.662E-03	9.971E-03
	0.6535	1.832E-01	1.772E-03	9.990E-03
	0.6625	1.873E-01	1.834E-03	9.498E-03
	0.6715	1.826E-01	1.860E-03	9.042E-03
	0.6805	1.735E-01	1.832E-03	9.827E-03
	0.6895	1.406E-01	1.615E-03	1.022E-02
	0.6985	1.178E-01	1.459E-03	1.013E-02
	0.7075	9.405E-02	1.304E-03	7.560E-03
	0.7165	7.420E-02	1.129E-03	5.149E-03
	0.7255	5.858E-02	9.980E-04	5.038E-03
	0.7345	5.107E-02	9.488E-04	4.968E-03
	0.7435	3.991E-02	8.189E-04	2.867E-03
	0.7525	3.331E-02	7.440E-04	2.404E-03
	0.7615	2.721E-02	6.623E-04	2.471E-03
	0.7705	2.218E-02	5.565E-04	2.756E-03
	0.7795	1.777E-02	4.880E-04	2.333E-03
	0.7885	1.417E-02	3.931E-04	2.060E-03
	0.7975	9.812E-03	2.898E-04	3.533E-04
	0.8065	5.707E-03	1.726E-04	2.117E-04
1.275	0.3565	2.459E-01	4.318E-03	2.704E-02
	0.3655	2.515E-01	2.335E-03	2.534E-02
	0.3745	2.819E-01	4.825E-03	2.757E-02
	0.3835	2.799E-01	1.850E-03	2.510E-02
	0.3925	2.689E-01	1.580E-03	2.241E-02
	0.4015	2.381E-01	1.411E-03	1.916E-02
	0.4105	2.134E-01	1.331E-03	1.658E-02
	0.4195	1.954E-01	1.293E-03	1.480E-02
	0.4285	1.857E-01	1.270E-03	1.513E-02
	0.4375	1.882E-01	1.307E-03	1.426E-02
	0.4465	1.949E-01	1.348E-03	1.435E-02
	0.4555	2.088E-01	1.728E-03	1.541E-02
	0.4645	2.325E-01	1.573E-03	1.736E-02
	0.4735	2.468E-01	1.662E-03	1.727E-02
	0.4825	2.331E-01	1.620E-03	1.542E-02
	0.4915	1.993E-01	1.476E-03	1.307E-02
	0.5005	1.697E-01	1.361E-03	1.077E-02
	0.5095	1.495E-01	1.280E-03	9.135E-03
	0.5185	1.349E-01	1.231E-03	8.027E-03
	0.5275	1.263E-01	1.198E-03	7.341E-03
	0.5365	1.204E-01	1.174E-03	6.940E-03
	0.5455	1.148E-01	1.156E-03	6.466E-03
	0.5545	1.108E-01	1.152E-03	6.178E-03
	0.5635	1.115E-01	1.169E-03	6.233E-03
	0.5725	1.103E-01	1.186E-03	6.175E-03
	0.5815	1.097E-01	1.182E-03	6.091E-03
	0.5905	1.129E-01	1.222E-03	6.149E-03
	0.5995	1.147E-01	1.245E-03	6.991E-03
	0.6085	1.173E-01	1.279E-03	7.459E-03
	0.6175	1.227E-01	1.335E-03	7.686E-03
	0.6265	1.300E-01	1.401E-03	8.702E-03

	0.6355	1.391E-01	1.480E-03	9.493E-03
	0.6445	1.491E-01	1.556E-03	9.035E-03
	0.6535	1.641E-01	1.682E-03	9.869E-03
	0.6625	1.698E-01	1.737E-03	9.583E-03
	0.6715	1.795E-01	1.858E-03	9.619E-03
	0.6805	1.724E-01	1.823E-03	8.911E-03
	0.6895	1.585E-01	1.744E-03	9.273E-03
	0.6985	1.365E-01	1.580E-03	1.019E-02
	0.7075	1.088E-01	1.387E-03	1.076E-02
	0.7165	8.914E-02	1.240E-03	7.051E-03
	0.7255	6.837E-02	1.049E-03	4.819E-03
	0.7345	5.600E-02	9.607E-04	5.062E-03
	0.7435	4.663E-02	8.787E-04	4.366E-03
	0.7525	3.804E-02	7.721E-04	2.624E-03
	0.7615	3.151E-02	7.061E-04	2.286E-03
	0.7705	2.572E-02	6.127E-04	2.548E-03
	0.7795	2.239E-02	5.645E-04	2.833E-03
	0.7885	1.656E-02	4.460E-04	2.222E-03
	0.7975	1.255E-02	3.523E-04	1.910E-03
	0.8065	8.005E-03	2.403E-04	3.209E-04
	0.8155	3.878E-03	1.178E-04	1.408E-04
1.325	0.2305	3.492E-01	1.937E-03	2.162E-02
	0.2395	3.445E-01	2.110E-03	1.945E-02
	0.2485	3.338E-01	2.287E-03	1.745E-02
	0.2575	3.330E-01	2.378E-03	1.635E-02
	0.2665	3.314E-01	2.431E-03	1.520E-02
	0.2755	3.248E-01	2.491E-03	1.408E-02
	0.2845	3.249E-01	2.533E-03	1.341E-02
	0.2935	3.223E-01	2.571E-03	1.290E-02
	0.3025	3.214E-01	2.663E-03	1.269E-02
	0.3115	3.180E-01	2.764E-03	1.109E-02
	0.3205	3.096E-01	2.809E-03	1.022E-02
	0.3295	3.032E-01	2.910E-03	1.240E-02
	0.3385	3.019E-01	3.109E-03	8.986E-03
	0.3475	2.942E-01	3.284E-03	8.508E-03
	0.3565	2.916E-01	3.480E-03	8.429E-03
	0.3655	2.904E-01	3.661E-03	9.403E-03
	0.3745	2.917E-01	3.594E-03	2.329E-02
	0.3835	2.997E-01	2.575E-03	2.188E-02
	0.3925	3.068E-01	2.592E-03	1.852E-02
	0.4015	2.932E-01	2.355E-03	1.763E-02
	0.4105	2.621E-01	2.166E-03	1.614E-02
	0.4195	2.344E-01	2.088E-03	1.370E-02
	0.4285	2.111E-01	2.024E-03	1.158E-02
	0.4375	2.007E-01	2.100E-03	1.101E-02
	0.4465	1.991E-01	2.184E-03	1.136E-02
	0.4555	2.076E-01	2.338E-03	1.257E-02
	0.4645	2.185E-01	2.452E-03	1.478E-02
	0.4735	2.311E-01	2.870E-03	1.737E-02
	0.4825	2.606E-01	3.380E-03	1.710E-02
	0.4915	2.401E-01	3.360E-03	1.449E-02
	0.5005	2.177E-01	3.077E-03	1.479E-02
	0.5095	1.733E-01	2.029E-03	1.112E-02
	0.5185	1.569E-01	2.017E-03	9.156E-03
	0.5275	1.371E-01	1.858E-03	7.398E-03
	0.5365	1.211E-01	1.205E-03	7.472E-03
	0.5455	1.268E-01	1.877E-03	6.352E-03
	0.5545	1.213E-01	1.861E-03	5.958E-03
	0.5635	1.203E-01	1.929E-03	5.771E-03
	0.5725	1.169E-01	1.979E-03	5.579E-03
	0.5815	1.127E-01	1.840E-03	5.321E-03
	0.5905	1.102E-01	1.940E-03	5.285E-03
	0.5995	1.119E-01	1.972E-03	5.540E-03
	0.6085	1.174E-01	2.089E-03	7.182E-03
	0.6175	1.181E-01	2.089E-03	7.895E-03
	0.6265	1.258E-01	2.298E-03	8.660E-03
	0.6355	1.300E-01	2.371E-03	8.588E-03
	0.6445	1.317E-01	1.472E-03	9.097E-03
	0.6535	1.472E-01	2.685E-03	9.541E-03
	0.6625	1.569E-01	3.052E-03	9.898E-03
	0.6715	1.711E-01	3.389E-03	9.890E-03
	0.6805	1.662E-01	1.816E-03	9.237E-03
	0.6895	1.693E-01	3.753E-03	9.285E-03
	0.6985	1.484E-01	1.718E-03	9.022E-03
	0.7075	1.271E-01	3.551E-03	1.194E-02
	0.7165	1.084E-01	3.362E-03	1.188E-02
	0.7255	8.137E-02	1.199E-03	6.339E-03

	0.7345	6.560E-02	1.062E-03	4.786E-03
	0.7435	5.167E-02	9.340E-04	5.011E-03
	0.7525	4.331E-02	8.435E-04	3.788E-03
	0.7615	3.472E-02	7.471E-04	2.373E-03
	0.7705	2.807E-02	6.511E-04	2.171E-03
	0.7795	2.350E-02	5.890E-04	2.622E-03
	0.7885	1.891E-02	5.109E-04	2.442E-03
	0.7975	1.497E-02	4.146E-04	2.082E-03
	0.8065	1.070E-02	3.166E-04	1.723E-03
	0.8155	6.752E-03	2.048E-04	2.721E-04
	0.8245	2.195E-03	7.080E-05	8.707E-05
1.375	0.2395	3.394E-01	2.100E-03	1.984E-02
	0.2485	3.327E-01	2.175E-03	1.795E-02
	0.2575	3.328E-01	2.320E-03	1.668E-02
	0.2665	3.418E-01	2.610E-03	1.623E-02
	0.2755	3.291E-01	2.561E-03	1.566E-02
	0.2845	3.207E-01	2.579E-03	1.432E-02
	0.2935	3.194E-01	2.669E-03	1.369E-02
	0.3025	3.140E-01	2.664E-03	1.300E-02
	0.3115	3.129E-01	2.698E-03	1.272E-02
	0.3205	3.106E-01	2.753E-03	1.117E-02
	0.3295	3.194E-01	2.914E-03	1.098E-02
	0.3385	2.993E-01	2.903E-03	1.324E-02
	0.3475	2.875E-01	2.925E-03	8.860E-03
	0.3565	2.800E-01	2.968E-03	8.312E-03
	0.3655	2.746E-01	3.082E-03	8.127E-03
	0.3745	2.747E-01	3.234E-03	9.144E-03
	0.3835	2.927E-01	3.638E-03	1.372E-02
	0.3925	2.996E-01	5.383E-03	2.394E-02
	0.4015	3.069E-01	2.740E-03	1.952E-02
	0.4105	2.901E-01	2.512E-03	1.668E-02
	0.4195	2.538E-01	2.525E-03	1.624E-02
	0.4285	2.287E-01	1.959E-03	1.411E-02
	0.4375	2.038E-01	1.879E-03	1.163E-02
	0.4465	1.824E-01	1.596E-03	1.252E-02
	0.4555	1.937E-01	1.933E-03	1.152E-02
	0.4645	1.989E-01	2.028E-03	1.236E-02
	0.4735	2.100E-01	2.124E-03	1.460E-02
	0.4825	2.341E-01	2.373E-03	1.766E-02
	0.4915	2.575E-01	2.662E-03	1.605E-02
	0.5005	2.437E-01	2.576E-03	1.365E-02
	0.5095	2.086E-01	2.359E-03	1.471E-02
	0.5185	1.776E-01	2.232E-03	1.177E-02
	0.5275	1.528E-01	2.055E-03	8.828E-03
	0.5365	1.394E-01	2.002E-03	7.236E-03
	0.5455	1.320E-01	2.041E-03	6.280E-03
	0.5545	1.175E-01	2.125E-03	6.114E-03
	0.5635	1.127E-01	2.145E-03	5.755E-03
	0.5725	1.161E-01	2.105E-03	5.128E-03
	0.5815	1.159E-01	2.236E-03	5.116E-03
	0.5905	1.081E-01	2.301E-03	5.377E-03
	0.5995	1.038E-01	1.217E-03	6.304E-03
	0.6085	1.111E-01	2.469E-03	6.161E-03
	0.6175	1.010E-01	1.224E-03	6.558E-03
	0.6265	1.073E-01	1.886E-03	6.901E-03
	0.6355	1.110E-01	1.341E-03	7.358E-03
	0.6445	1.140E-01	1.363E-03	7.909E-03
	0.6535	1.351E-01	2.339E-03	9.899E-03
	0.6625	1.313E-01	1.534E-03	8.467E-03
	0.6715	1.399E-01	1.608E-03	8.765E-03
	0.6805	1.531E-01	1.756E-03	9.317E-03
	0.6895	1.608E-01	1.844E-03	9.113E-03
	0.6985	1.541E-01	1.815E-03	8.744E-03
	0.7075	1.392E-01	1.723E-03	9.177E-03
	0.7165	1.143E-01	1.504E-03	9.212E-03
	0.7255	9.648E-02	1.374E-03	8.811E-03
	0.7345	7.864E-02	1.831E-03	8.013E-03
	0.7435	5.907E-02	1.574E-03	6.143E-03
	0.7525	4.883E-02	1.432E-03	5.847E-03
	0.7615	3.964E-02	1.306E-03	4.056E-03
	0.7705	3.378E-02	1.272E-03	3.257E-03
	0.7795	2.723E-02	1.143E-03	2.931E-03
	0.7885	2.372E-02	1.017E-03	3.339E-03
	0.7975	1.858E-02	8.865E-04	2.926E-03
	0.8065	1.288E-02	6.556E-04	2.252E-03
	0.8155	9.423E-03	5.209E-04	3.185E-04
	0.8245	4.789E-03	2.580E-04	1.661E-04

1.425	0.2485	3.312E-01	2.185E-03	1.956E-02
	0.2575	3.332E-01	2.307E-03	1.818E-02
	0.2665	3.261E-01	2.326E-03	1.673E-02
	0.2755	3.328E-01	2.491E-03	1.603E-02
	0.2845	3.231E-01	2.590E-03	1.479E-02
	0.2935	3.266E-01	2.734E-03	1.424E-02
	0.3025	3.208E-01	2.821E-03	1.345E-02
	0.3115	3.161E-01	2.890E-03	1.294E-02
	0.3205	3.131E-01	2.985E-03	1.224E-02
	0.3295	3.085E-01	3.106E-03	1.089E-02
	0.3385	3.202E-01	3.506E-03	1.065E-02
	0.3475	3.131E-01	3.929E-03	1.331E-02
	0.3565	3.115E-01	4.424E-03	9.473E-03
	0.3655	2.751E-01	2.981E-03	8.567E-03
	0.3745	2.713E-01	3.012E-03	8.386E-03
	0.3835	2.686E-01	3.086E-03	9.305E-03
	0.3925	2.798E-01	3.298E-03	1.352E-02
	0.4015	3.008E-01	3.638E-03	1.444E-02
	0.4105	3.123E-01	3.961E-03	1.006E-02
	0.4195	2.839E-01	2.903E-03	1.761E-02
	0.4285	2.480E-01	2.306E-03	1.561E-02
	0.4375	2.224E-01	2.155E-03	1.304E-02
	0.4465	1.938E-01	1.845E-03	1.188E-02
	0.4555	1.867E-01	1.763E-03	1.140E-02
	0.4645	1.882E-01	1.791E-03	1.173E-02
	0.4735	1.928E-01	1.879E-03	1.229E-02
	0.4825	1.995E-01	1.773E-03	1.517E-02
	0.4915	2.277E-01	2.225E-03	1.749E-02
	0.5005	2.384E-01	2.153E-03	1.684E-02
	0.5095	2.250E-01	2.123E-03	1.458E-02
	0.5185	2.015E-01	2.249E-03	1.457E-02
	0.5275	1.734E-01	2.106E-03	1.181E-02
	0.5365	1.462E-01	1.944E-03	8.838E-03
	0.5455	1.383E-01	1.948E-03	7.454E-03
	0.5545	1.278E-01	1.925E-03	6.365E-03
	0.5635	1.222E-01	1.926E-03	5.862E-03
	0.5725	1.155E-01	1.864E-03	5.350E-03
	0.5815	1.163E-01	1.951E-03	5.307E-03
	0.5905	1.139E-01	1.927E-03	5.136E-03
	0.5995	1.099E-01	1.891E-03	4.994E-03
	0.6085	1.088E-01	1.956E-03	4.952E-03
	0.6175	1.070E-01	1.745E-03	5.698E-03
	0.6265	1.094E-01	2.011E-03	6.784E-03
	0.6355	1.106E-01	2.041E-03	7.554E-03
	0.6445	1.138E-01	2.236E-03	7.399E-03
	0.6535	1.233E-01	2.413E-03	8.544E-03
	0.6625	1.251E-01	2.613E-03	8.605E-03
	0.6715	1.328E-01	2.798E-03	8.897E-03
	0.6805	1.404E-01	1.686E-03	9.036E-03
	0.6895	1.446E-01	1.748E-03	9.036E-03
	0.6985	1.465E-01	1.792E-03	8.622E-03
	0.7075	1.394E-01	1.740E-03	8.120E-03
	0.7165	1.285E-01	3.088E-03	1.062E-02
	0.7255	1.025E-01	1.426E-03	8.693E-03
	0.7345	8.212E-02	2.364E-03	9.075E-03
	0.7435	6.712E-02	2.109E-03	6.765E-03
	0.7525	5.876E-02	1.985E-03	7.102E-03
	0.7615	4.692E-02	1.730E-03	6.014E-03
	0.7705	3.823E-02	1.508E-03	4.272E-03
	0.7795	3.175E-02	1.283E-03	3.538E-03
	0.7885	2.257E-02	6.213E-04	2.241E-03
	0.7975	1.841E-02	9.775E-04	2.770E-03
	0.8065	1.569E-02	7.002E-04	2.581E-03
	0.8155	1.067E-02	3.468E-04	1.645E-03
	0.8245	7.043E-03	3.533E-04	2.439E-04
	0.8335	2.880E-03	1.354E-04	1.061E-04
1.475	0.2305	3.510E-01	3.794E-03	2.351E-02
	0.2395	3.457E-01	2.557E-03	2.292E-02
	0.2485	3.413E-01	2.149E-03	2.246E-02
	0.2575	3.333E-01	2.256E-03	1.998E-02
	0.2665	3.265E-01	2.391E-03	1.805E-02
	0.2755	3.210E-01	2.422E-03	1.685E-02
	0.2845	3.210E-01	2.502E-03	1.581E-02
	0.2935	3.200E-01	2.636E-03	1.504E-02
	0.3025	3.137E-01	2.724E-03	1.411E-02
	0.3115	3.177E-01	2.856E-03	1.373E-02
	0.3205	3.096E-01	2.902E-03	1.319E-02

	0.3295	3.093E-01	3.028E-03	1.221E-02
	0.3385	3.052E-01	3.098E-03	1.147E-02
	0.3475	2.999E-01	3.151E-03	1.029E-02
	0.3565	2.864E-01	3.170E-03	1.136E-02
	0.3655	2.756E-01	3.250E-03	8.591E-03
	0.3745	2.735E-01	3.410E-03	8.305E-03
	0.3835	2.614E-01	3.525E-03	7.699E-03
	0.3925	2.576E-01	3.644E-03	9.090E-03
	0.4015	2.862E-01	4.093E-03	1.431E-02
	0.4105	3.121E-01	4.574E-03	1.469E-02
	0.4195	3.300E-01	5.070E-03	1.001E-02
	0.4285	2.997E-01	4.973E-03	8.966E-03
	0.4375	2.488E-01	3.633E-03	1.804E-02
	0.4465	2.133E-01	2.196E-03	1.318E-02
	0.4555	1.912E-01	1.986E-03	1.091E-02
	0.4645	1.783E-01	2.548E-03	1.245E-02
	0.4735	1.782E-01	1.748E-03	1.221E-02
	0.4825	1.807E-01	1.736E-03	1.226E-02
	0.4915	1.970E-01	1.872E-03	1.445E-02
	0.5005	2.207E-01	2.078E-03	1.739E-02
	0.5095	2.330E-01	2.228E-03	1.516E-02
	0.5185	2.313E-01	2.281E-03	1.389E-02
	0.5275	1.934E-01	2.051E-03	1.441E-02
	0.5365	1.631E-01	1.932E-03	1.132E-02
	0.5455	1.473E-01	1.881E-03	9.134E-03
	0.5545	1.348E-01	1.834E-03	7.483E-03
	0.5635	1.260E-01	1.824E-03	6.612E-03
	0.5725	1.191E-01	1.844E-03	5.942E-03
	0.5815	1.140E-01	1.817E-03	5.369E-03
	0.5905	1.110E-01	1.793E-03	5.394E-03
	0.5995	1.072E-01	1.824E-03	5.019E-03
	0.6085	1.054E-01	1.614E-03	5.813E-03
	0.6175	1.064E-01	1.887E-03	5.048E-03
	0.6265	1.024E-01	1.640E-03	5.728E-03
	0.6355	1.007E-01	1.575E-03	6.683E-03
	0.6445	1.074E-01	1.931E-03	7.175E-03
	0.6535	1.100E-01	1.769E-03	7.512E-03
	0.6625	1.189E-01	2.121E-03	8.914E-03
	0.6715	1.205E-01	2.213E-03	8.976E-03
	0.6805	1.334E-01	2.357E-03	9.045E-03
	0.6895	1.389E-01	2.240E-03	9.017E-03
	0.6985	1.464E-01	2.329E-03	8.679E-03
	0.7075	1.471E-01	2.451E-03	7.710E-03
	0.7165	1.427E-01	2.715E-03	1.017E-02
	0.7255	1.211E-01	2.219E-03	1.090E-02
	0.7345	9.783E-02	2.192E-03	1.188E-02
	0.7435	8.250E-02	1.970E-03	1.033E-02
	0.7525	6.064E-02	1.686E-03	7.046E-03
	0.7615	4.687E-02	1.461E-03	5.805E-03
	0.7705	3.326E-02	1.225E-03	3.520E-03
	0.7795	3.137E-02	1.302E-03	3.486E-03
	0.7885	2.509E-02	9.675E-04	2.609E-03
	0.7975	2.074E-02	1.026E-03	2.965E-03
	0.8065	1.412E-02	6.546E-04	2.069E-03
	0.8155	1.257E-02	5.668E-04	2.190E-03
	0.8245	8.727E-03	4.345E-04	3.138E-04
	0.8335	5.125E-03	2.433E-04	1.848E-04
1.525	0.2485	3.377E-01	2.469E-03	2.230E-02
	0.2575	3.298E-01	2.082E-03	2.186E-02
	0.2665	3.283E-01	2.325E-03	1.998E-02
	0.2755	3.232E-01	2.432E-03	1.830E-02
	0.2845	3.185E-01	2.570E-03	1.693E-02
	0.2935	3.174E-01	2.631E-03	1.602E-02
	0.3025	3.116E-01	2.645E-03	1.494E-02
	0.3115	3.155E-01	2.778E-03	1.456E-02
	0.3205	3.147E-01	2.889E-03	1.415E-02
	0.3295	3.093E-01	2.986E-03	1.378E-02
	0.3385	3.037E-01	2.993E-03	1.185E-02
	0.3475	2.983E-01	3.105E-03	1.176E-02
	0.3565	3.026E-01	3.243E-03	1.075E-02
	0.3655	2.860E-01	3.245E-03	1.041E-02
	0.3745	2.721E-01	3.232E-03	8.801E-03
	0.3835	2.644E-01	3.282E-03	8.329E-03
	0.3925	2.500E-01	3.274E-03	7.621E-03
	0.4015	2.588E-01	3.464E-03	9.581E-03
	0.4105	2.738E-01	3.837E-03	1.440E-02
	0.4195	2.986E-01	4.264E-03	1.382E-02
	0.4285	2.980E-01	4.405E-03	8.851E-03
	0.4375	2.834E-01	4.378E-03	9.142E-03
	0.4465	2.601E-01	4.367E-03	1.029E-02
	0.4555	2.317E-01	6.863E-03	1.535E-02
	0.4645	2.008E-01	2.870E-03	1.078E-02
	0.4735	1.835E-01	2.658E-03	9.783E-03
	0.4825	1.782E-01	2.654E-03	1.037E-02
	0.4915	1.802E-01	2.058E-03	1.316E-02
	0.5005	1.956E-01	1.916E-03	1.515E-02
	0.5095	2.155E-01	2.054E-03	1.743E-02
	0.5185	2.292E-01	2.202E-03	1.528E-02
	0.5275	2.173E-01	2.165E-03	1.409E-02
	0.5365	1.834E-01	1.943E-03	1.398E-02
	0.5455	1.496E-01	1.729E-03	1.059E-02
	0.5545	1.340E-01	1.664E-03	8.587E-03
	0.5635	1.237E-01	1.608E-03	7.067E-03
	0.5725	1.228E-01	2.492E-03	5.941E-03
	0.5815	1.183E-01	2.419E-03	5.390E-03
	0.5905	1.121E-01	2.403E-03	4.941E-03
	0.5995	1.057E-01	2.338E-03	4.929E-03
	0.6085	1.040E-01	2.347E-03	4.617E-03
	0.6175	1.087E-01	2.540E-03	4.779E-03
	0.6265	1.087E-01	2.617E-03	4.807E-03
	0.6355	1.100E-01	2.793E-03	5.721E-03
	0.6445	1.055E-01	2.883E-03	6.960E-03
	0.6535	1.095E-01	1.936E-03	7.458E-03
	0.6625	1.090E-01	1.743E-03	7.732E-03
	0.6715	1.095E-01	1.760E-03	8.322E-03
	0.6805	1.184E-01	1.896E-03	8.502E-03
	0.6895	1.284E-01	2.035E-03	8.906E-03
	0.6985	1.370E-01	2.174E-03	9.048E-03
	0.7075	1.416E-01	2.224E-03	8.290E-03
	0.7165	1.338E-01	2.203E-03	7.639E-03
	0.7255	1.224E-01	2.151E-03	9.083E-03
	0.7345	1.087E-01	2.012E-03	1.054E-02
	0.7435	8.982E-02	1.838E-03	1.059E-02
	0.7525	6.866E-02	1.694E-03	8.306E-03
	0.7615	5.555E-02	1.500E-03	6.407E-03
	0.7705	4.566E-02	2.024E-03	6.313E-03
	0.7795	3.379E-02	1.145E-03	3.809E-03
	0.7885	2.631E-02	1.575E-03	3.118E-03
	0.7975	2.106E-02	8.602E-04	2.587E-03
	0.8065	1.512E-02	7.133E-04	2.276E-03
	0.8155	1.221E-02	7.032E-04	2.271E-03
	0.8245	9.313E-03	4.983E-04	2.173E-03
	0.8335	6.232E-03	3.397E-04	1.478E-04
	0.8425	1.777E-03	1.214E-04	4.230E-05
1.575	0.2665	3.259E-01	2.019E-03	2.184E-02
	0.2755	3.210E-01	2.339E-03	1.981E-02
	0.2845	3.188E-01	2.491E-03	1.838E-02
	0.2935	3.143E-01	2.614E-03	1.705E-02
	0.3025	3.145E-01	2.765E-03	1.622E-02
	0.3115	3.068E-01	2.768E-03	1.516E-02
	0.3205	3.069E-01	2.799E-03	1.453E-02
	0.3295	3.048E-01	2.881E-03	1.408E-02
	0.3385	3.020E-01	3.004E-03	1.421E-02
	0.3475	2.990E-01	3.073E-03	1.203E-02
	0.3565	2.882E-01	3.101E-03	1.185E-02
	0.3655	2.865E-01	3.170E-03	1.038E-02
	0.3745	2.748E-01	3.209E-03	9.575E-03
	0.3835	2.689E-01	3.222E-03	9.094E-03
	0.3925	2.631E-01	3.296E-03	8.637E-03
	0.4015	2.495E-01	3.295E-03	8.023E-03
	0.4105	2.613E-01	3.441E-03	1.030E-02
	0.4195	2.762E-01	3.694E-03	1.542E-02
	0.4285	2.977E-01	4.041E-03	1.341E-02
	0.4375	2.986E-01	4.340E-03	8.660E-03
	0.4465	2.671E-01	4.145E-03	9.256E-03
	0.4555	2.397E-01	3.951E-03	9.734E-03
	0.4645	2.147E-01	3.867E-03	7.154E-03
	0.4735	1.984E-01	3.769E-03	5.463E-03
	0.4825	1.878E-01	3.219E-03	1.137E-02
	0.4915	1.819E-01	2.623E-03	1.144E-02
	0.5005	1.821E-01	2.586E-03	1.159E-02
	0.5095	2.004E-01	2.885E-03	1.450E-02
	0.5185	2.113E-01	2.199E-03	1.779E-02
	0.5275	2.305E-01	2.971E-03	1.348E-02

	0.5365	2.104E-01	2.118E-03	1.457E-02
	0.5455	1.766E-01	1.889E-03	1.393E-02
	0.5545	1.506E-01	2.457E-03	1.049E-02
	0.5635	1.292E-01	1.667E-03	8.407E-03
	0.5725	1.206E-01	2.280E-03	6.539E-03
	0.5815	1.122E-01	1.550E-03	6.258E-03
	0.5905	1.078E-01	1.544E-03	5.733E-03
	0.5995	1.014E-01	1.514E-03	5.465E-03
	0.6085	1.000E-01	1.536E-03	5.112E-03
	0.6175	1.003E-01	2.213E-03	4.527E-03
	0.6265	9.845E-02	1.532E-03	5.330E-03
	0.6355	9.785E-02	1.598E-03	5.169E-03
	0.6445	1.025E-01	1.673E-03	5.868E-03
	0.6535	1.013E-01	1.685E-03	6.821E-03
	0.6625	1.046E-01	1.735E-03	7.155E-03
	0.6715	1.049E-01	1.740E-03	7.441E-03
	0.6805	1.112E-01	2.504E-03	8.084E-03
	0.6895	1.184E-01	2.017E-03	8.432E-03
	0.6985	1.322E-01	2.222E-03	9.227E-03
	0.7075	1.331E-01	2.147E-03	9.002E-03
	0.7165	1.413E-01	2.466E-03	7.534E-03
	0.7255	1.314E-01	2.213E-03	8.310E-03
	0.7345	1.164E-01	2.110E-03	9.514E-03
	0.7435	9.750E-02	2.045E-03	1.109E-02
	0.7525	7.627E-02	2.720E-03	1.019E-02
	0.7615	5.966E-02	1.527E-03	6.848E-03
	0.7705	4.890E-02	2.361E-03	6.225E-03
	0.7795	3.559E-02	1.108E-03	4.550E-03
	0.7885	3.115E-02	1.032E-03	3.392E-03
	0.7975	2.572E-02	9.300E-04	2.886E-03
	0.8065	1.911E-02	7.943E-04	2.746E-03
	0.8155	1.490E-02	6.293E-04	2.357E-03
	0.8245	1.097E-02	4.833E-04	2.014E-03
	0.8335	7.307E-03	3.601E-04	5.163E-04
	0.8425	3.680E-03	1.940E-04	1.217E-04
1.625	0.2755	3.238E-01	1.981E-03	2.187E-02
	0.2845	3.175E-01	2.263E-03	1.988E-02
	0.2935	3.149E-01	2.533E-03	1.840E-02
	0.3025	3.094E-01	2.639E-03	1.715E-02
	0.3115	3.099E-01	2.793E-03	1.633E-02
	0.3205	3.007E-01	2.870E-03	1.520E-02
	0.3295	3.055E-01	2.914E-03	1.496E-02
	0.3385	2.984E-01	2.934E-03	1.430E-02
	0.3475	2.920E-01	2.961E-03	1.410E-02
	0.3565	2.926E-01	3.077E-03	1.210E-02
	0.3655	2.932E-01	3.190E-03	1.158E-02
	0.3745	2.817E-01	3.259E-03	1.062E-02
	0.3835	2.591E-01	3.153E-03	9.282E-03
	0.3925	2.601E-01	3.209E-03	8.963E-03
	0.4015	2.458E-01	3.179E-03	8.322E-03
	0.4105	2.491E-01	3.266E-03	8.708E-03
	0.4195	2.567E-01	3.450E-03	1.087E-02
	0.4285	2.772E-01	3.764E-03	1.560E-02
	0.4375	2.906E-01	3.978E-03	1.265E-02
	0.4465	2.801E-01	3.992E-03	8.322E-03
	0.4555	2.631E-01	3.914E-03	9.796E-03
	0.4645	2.291E-01	3.736E-03	9.493E-03
	0.4735	1.987E-01	3.586E-03	6.672E-03
	0.4825	1.913E-01	3.696E-03	5.393E-03
	0.4915	1.841E-01	3.740E-03	4.973E-03
	0.5005	1.797E-01	3.701E-03	6.783E-03
	0.5095	1.852E-01	2.875E-03	1.283E-02
	0.5185	1.951E-01	2.740E-03	1.501E-02
	0.5275	2.142E-01	2.918E-03	1.673E-02
	0.5365	2.171E-01	3.029E-03	1.149E-02
	0.5455	1.990E-01	2.650E-03	1.405E-02
	0.5545	1.662E-01	2.340E-03	1.310E-02
	0.5635	1.423E-01	2.197E-03	1.001E-02
	0.5725	1.244E-01	2.055E-03	7.736E-03
	0.5815	1.192E-01	2.094E-03	6.617E-03
	0.5905	1.073E-01	2.249E-03	6.178E-03
	0.5995	1.091E-01	2.107E-03	5.294E-03
	0.6085	1.030E-01	2.068E-03	5.030E-03
	0.6175	9.547E-02	1.524E-03	5.088E-03
	0.6265	9.878E-02	2.179E-03	4.688E-03
	0.6355	9.336E-02	2.100E-03	4.568E-03
	0.6445	9.333E-02	1.535E-03	5.065E-03
	0.6535	9.338E-02	1.550E-03	5.700E-03
	0.6625	9.397E-02	1.548E-03	6.511E-03
	0.6715	9.460E-02	1.596E-03	6.656E-03
	0.6805	9.940E-02	1.679E-03	7.217E-03
	0.6895	1.081E-01	1.796E-03	8.099E-03
	0.6985	1.143E-01	1.859E-03	8.145E-03
	0.7075	1.214E-01	2.006E-03	8.508E-03
	0.7165	1.354E-01	2.172E-03	8.389E-03
	0.7255	1.267E-01	2.277E-03	7.709E-03
	0.7345	1.211E-01	2.140E-03	8.386E-03
	0.7435	1.061E-01	2.002E-03	1.039E-02
	0.7525	8.786E-02	1.788E-03	1.101E-02
	0.7615	6.794E-02	1.547E-03	8.435E-03
	0.7705	5.372E-02	1.904E-03	6.630E-03
	0.7795	3.972E-02	1.472E-03	5.223E-03
	0.7885	3.326E-02	1.016E-03	3.882E-03
	0.7975	2.622E-02	1.244E-03	3.088E-03
	0.8065	2.083E-02	1.040E-03	2.667E-03
	0.8155	1.716E-02	7.030E-04	2.665E-03
	0.8245	1.304E-02	5.807E-04	2.273E-03
	0.8335	1.046E-02	4.651E-04	2.275E-03
	0.8425	5.588E-03	2.833E-04	1.933E-04
	0.8515	2.011E-03	9.284E-05	6.766E-05
1.675	0.2845	3.192E-01	1.992E-03	2.179E-02
	0.2935	3.099E-01	2.174E-03	1.969E-02
	0.3025	3.063E-01	2.444E-03	1.828E-02
	0.3115	3.107E-01	2.713E-03	1.757E-02
	0.3205	3.019E-01	2.807E-03	1.626E-02
	0.3295	3.032E-01	2.973E-03	1.565E-02
	0.3385	2.949E-01	3.044E-03	1.483E-02
	0.3475	2.884E-01	3.087E-03	1.433E-02
	0.3565	2.921E-01	3.106E-03	1.394E-02
	0.3655	2.817E-01	3.084E-03	1.192E-02
	0.3745	2.785E-01	3.157E-03	1.124E-02
	0.3835	2.803E-01	3.259E-03	1.275E-02
	0.3925	2.673E-01	3.289E-03	9.956E-03
	0.4015	2.554E-01	3.310E-03	9.198E-03
	0.4105	2.403E-01	3.229E-03	8.439E-03
	0.4195	2.385E-01	3.285E-03	8.748E-03
	0.4285	2.448E-01	3.349E-03	1.113E-02
	0.4375	2.668E-01	3.641E-03	1.420E-02
	0.4465	2.743E-01	3.828E-03	1.135E-02
	0.4555	2.771E-01	3.970E-03	8.624E-03
	0.4645	2.460E-01	3.818E-03	9.767E-03
	0.4735	2.217E-01	3.639E-03	9.337E-03
	0.4825	1.950E-01	3.488E-03	6.565E-03
	0.4915	1.846E-01	3.427E-03	5.360E-03
	0.5005	1.665E-01	3.268E-03	4.832E-03
	0.5095	1.792E-01	3.607E-03	6.979E-03
	0.5185	1.816E-01	3.805E-03	8.755E-03
	0.5275	2.116E-01	4.270E-03	1.349E-02
	0.5365	2.126E-01	3.195E-03	1.689E-02
	0.5455	2.222E-01	3.273E-03	1.159E-02
	0.5545	1.887E-01	2.850E-03	1.399E-02
	0.5635	1.562E-01	2.579E-03	1.241E-02
	0.5725	1.310E-01	2.081E-03	1.034E-02
	0.5815	1.192E-01	1.945E-03	8.319E-03
	0.5905	1.145E-01	1.954E-03	6.618E-03
	0.5995	1.015E-01	1.796E-03	5.581E-03
	0.6085	9.954E-02	1.868E-03	5.255E-03
	0.6175	9.766E-02	1.889E-03	4.913E-03
	0.6265	9.812E-02	1.993E-03	4.613E-03
	0.6355	9.347E-02	1.950E-03	4.607E-03
	0.6445	9.601E-02	2.036E-03	4.798E-03
	0.6535	9.214E-02	1.971E-03	4.633E-03
	0.6625	9.797E-02	2.146E-03	5.946E-03
	0.6715	8.892E-02	2.149E-03	6.184E-03
	0.6805	9.482E-02	1.650E-03	6.677E-03
	0.6895	9.929E-02	2.225E-03	7.225E-03
	0.6985	1.075E-01	1.800E-03	7.927E-03
	0.7075	1.111E-01	2.518E-03	7.815E-03
	0.7165	1.254E-01	2.088E-03	8.771E-03
	0.7255	1.197E-01	1.933E-03	7.999E-03
	0.7345	1.270E-01	2.159E-03	7.433E-03
	0.7435	1.104E-01	2.011E-03	8.962E-03
	0.7525	9.248E-02	1.802E-03	1.006E-02
	0.7615	7.306E-02	1.539E-03	9.551E-03

	0.7705	5.786E-02	1.356E-03	6.781E-03
	0.7795	4.830E-02	1.947E-03	6.212E-03
	0.7885	3.446E-02	1.030E-03	4.611E-03
	0.7975	2.810E-02	8.948E-04	2.987E-03
	0.8065	2.380E-02	1.211E-03	2.902E-03
	0.8155	1.825E-02	7.195E-04	2.591E-03
	0.8245	1.480E-02	8.198E-04	2.549E-03
	0.8335	1.076E-02	4.473E-04	2.026E-03
	0.8425	7.522E-03	3.377E-04	2.956E-04
	0.8515	3.701E-03	1.726E-04	1.458E-04
1.725	0.2935	3.162E-01	2.051E-03	2.177E-02
	0.3025	3.069E-01	2.163E-03	1.976E-02
	0.3115	3.067E-01	2.376E-03	1.860E-02
	0.3205	3.008E-01	2.622E-03	1.733E-02
	0.3295	2.929E-01	2.790E-03	1.612E-02
	0.3385	2.879E-01	2.874E-03	1.529E-02
	0.3475	2.942E-01	3.070E-03	1.515E-02
	0.3565	2.852E-01	3.152E-03	1.462E-02
	0.3655	2.873E-01	3.280E-03	1.344E-02
	0.3745	2.831E-01	3.293E-03	1.251E-02
	0.3835	2.693E-01	3.157E-03	1.121E-02
	0.3925	2.630E-01	3.178E-03	1.169E-02
	0.4015	2.511E-01	3.171E-03	9.587E-03
	0.4105	2.504E-01	3.244E-03	9.346E-03
	0.4195	2.398E-01	3.277E-03	8.831E-03
	0.4285	2.320E-01	3.317E-03	9.114E-03
	0.4375	2.410E-01	3.473E-03	1.190E-02
	0.4465	2.566E-01	3.710E-03	1.317E-02
	0.4555	2.669E-01	3.854E-03	1.028E-02
	0.4645	2.547E-01	3.777E-03	8.479E-03
	0.4735	2.327E-01	3.644E-03	9.801E-03
	0.4825	2.036E-01	3.441E-03	8.441E-03
	0.4915	1.865E-01	3.330E-03	6.300E-03
	0.5005	1.765E-01	3.316E-03	5.244E-03
	0.5095	1.683E-01	3.314E-03	5.528E-03
	0.5185	1.767E-01	3.472E-03	7.209E-03
	0.5275	1.868E-01	3.669E-03	9.587E-03
	0.5365	2.129E-01	4.132E-03	1.402E-02
	0.5455	2.229E-01	4.505E-03	1.253E-02
	0.5545	2.137E-01	4.576E-03	1.255E-02
	0.5635	1.786E-01	2.945E-03	1.436E-02
	0.5725	1.503E-01	2.584E-03	1.220E-02
	0.5815	1.283E-01	2.373E-03	9.339E-03
	0.5905	1.116E-01	2.152E-03	7.408E-03
	0.5995	1.078E-01	2.042E-03	6.917E-03
	0.6085	9.730E-02	1.803E-03	6.353E-03
	0.6175	9.498E-02	1.818E-03	5.505E-03
	0.6265	9.146E-02	1.817E-03	4.795E-03
	0.6355	8.873E-02	1.811E-03	4.695E-03
	0.6445	8.690E-02	1.787E-03	4.542E-03
	0.6535	8.502E-02	1.773E-03	4.494E-03
	0.6625	8.331E-02	1.702E-03	4.565E-03
	0.6715	9.243E-02	1.951E-03	5.835E-03
	0.6805	9.211E-02	1.932E-03	6.316E-03
	0.6895	9.608E-02	2.161E-03	6.852E-03
	0.6985	9.797E-02	2.130E-03	7.270E-03
	0.7075	1.071E-01	2.292E-03	7.632E-03
	0.7165	1.156E-01	2.539E-03	8.180E-03
	0.7255	1.190E-01	2.582E-03	7.763E-03
	0.7345	1.134E-01	2.770E-03	6.790E-03
	0.7435	1.187E-01	2.820E-03	7.516E-03
	0.7525	1.008E-01	2.558E-03	9.668E-03
	0.7615	8.281E-02	2.221E-03	1.053E-02
	0.7705	6.056E-02	1.810E-03	8.472E-03
	0.7795	5.020E-02	1.650E-03	6.141E-03
	0.7885	3.897E-02	1.415E-03	5.277E-03
	0.7975	3.229E-02	1.334E-03	4.171E-03
	0.8065	2.493E-02	1.192E-03	2.892E-03
	0.8155	2.125E-02	1.104E-03	2.908E-03
	0.8245	1.559E-02	9.903E-04	2.603E-03
	0.8335	1.206E-02	5.400E-04	2.295E-03
	0.8425	8.162E-03	5.772E-04	2.042E-03
	0.8515	4.176E-03	2.187E-04	1.364E-04
1.775	0.3025	3.090E-01	2.076E-03	2.154E-02
	0.3115	3.002E-01	2.163E-03	1.965E-02
	0.3205	2.991E-01	2.320E-03	1.843E-02
	0.3295	2.916E-01	2.501E-03	1.715E-02
	0.3385	2.875E-01	2.723E-03	1.610E-02
	0.3475	2.833E-01	2.905E-03	1.544E-02
	0.3565	2.757E-01	2.972E-03	1.466E-02
	0.3655	2.706E-01	3.071E-03	1.451E-02
	0.3745	2.757E-01	3.203E-03	1.302E-02
	0.3835	2.796E-01	3.427E-03	1.295E-02
	0.3925	2.734E-01	3.451E-03	1.160E-02
	0.4015	2.603E-01	3.391E-03	1.059E-02
	0.4105	2.507E-01	3.269E-03	9.829E-03
	0.4195	2.367E-01	3.204E-03	8.999E-03
	0.4285	2.374E-01	3.293E-03	8.811E-03
	0.4375	2.335E-01	3.347E-03	9.715E-03
	0.4465	2.539E-01	3.585E-03	1.379E-02
	0.4555	2.622E-01	3.863E-03	1.336E-02
	0.4645	2.704E-01	4.064E-03	9.906E-03
	0.4735	2.501E-01	3.895E-03	9.242E-03
	0.4825	2.154E-01	3.633E-03	9.722E-03
	0.4915	1.884E-01	3.361E-03	7.566E-03
	0.5005	1.713E-01	3.211E-03	5.799E-03
	0.5095	1.631E-01	3.184E-03	4.931E-03
	0.5185	1.658E-01	3.229E-03	6.206E-03
	0.5275	1.654E-01	3.346E-03	7.116E-03
	0.5365	1.845E-01	3.604E-03	1.016E-02
	0.5455	2.041E-01	4.011E-03	1.368E-02
	0.5545	2.223E-01	4.389E-03	1.086E-02
	0.5635	2.207E-01	4.464E-03	8.553E-03
	0.5725	1.803E-01	3.958E-03	1.332E-02
	0.5815	1.412E-01	3.337E-03	1.210E-02
	0.5905	1.210E-01	2.315E-03	8.765E-03
	0.5995	1.147E-01	2.247E-03	8.021E-03
	0.6085	1.016E-01	2.060E-03	6.098E-03
	0.6175	1.014E-01	2.158E-03	5.981E-03
	0.6265	9.352E-02	1.979E-03	6.897E-03
	0.6355	9.076E-02	1.851E-03	6.386E-03
	0.6445	8.685E-02	1.801E-03	4.916E-03
	0.6535	8.760E-02	1.845E-03	5.087E-03
	0.6625	9.122E-02	1.935E-03	4.871E-03
	0.6715	8.235E-02	1.820E-03	4.784E-03
	0.6805	8.615E-02	1.884E-03	5.861E-03
	0.6895	8.411E-02	1.831E-03	5.811E-03
	0.6985	9.094E-02	2.036E-03	6.442E-03
	0.7075	9.407E-02	2.078E-03	6.943E-03
	0.7165	1.008E-01	2.188E-03	7.266E-03
	0.7255	1.109E-01	2.457E-03	7.964E-03
	0.7345	1.151E-01	2.527E-03	7.202E-03
	0.7435	1.170E-01	2.674E-03	6.197E-03
	0.7525	1.069E-01	2.547E-03	8.223E-03
	0.7615	9.213E-02	2.390E-03	1.032E-02
	0.7705	6.909E-02	1.893E-03	9.750E-03
	0.7795	5.481E-02	1.632E-03	7.259E-03
	0.7885	4.284E-02	1.340E-03	5.180E-03
	0.7975	3.373E-02	1.329E-03	4.829E-03
	0.8065	2.774E-02	1.184E-03	3.304E-03
	0.8155	2.211E-02	1.005E-03	2.719E-03
	0.8245	1.797E-02	9.324E-04	2.795E-03
	0.8335	1.248E-02	7.051E-04	2.216E-03
	0.8425	1.002E-02	5.992E-04	2.205E-03
	0.8515	6.169E-03	3.502E-04	2.023E-04
	0.8605	2.238E-03	1.112E-04	7.220E-05
1.825	0.3115	3.013E-01	2.099E-03	2.121E-02
	0.3205	2.936E-01	2.206E-03	1.946E-02
	0.3295	2.840E-01	2.239E-03	1.785E-02
	0.3385	2.819E-01	2.411E-03	1.689E-02
	0.3475	2.855E-01	2.642E-03	1.642E-02
	0.3565	2.771E-01	2.809E-03	1.539E-02
	0.3655	2.791E-01	3.043E-03	1.526E-02
	0.3745	2.734E-01	3.123E-03	1.498E-02
	0.3835	2.633E-01	3.152E-03	1.277E-02
	0.3925	2.667E-01	3.381E-03	1.219E-02
	0.4015	2.650E-01	3.444E-03	1.148E-02
	0.4105	2.581E-01	3.500E-03	1.084E-02
	0.4195	2.436E-01	3.484E-03	9.930E-03
	0.4285	2.275E-01	3.333E-03	8.990E-03
	0.4375	2.241E-01	3.282E-03	8.832E-03
	0.4465	2.300E-01	3.301E-03	1.024E-02
	0.4555	2.435E-01	3.543E-03	1.429E-02
	0.4645	2.541E-01	3.783E-03	1.242E-02

	0.4735	2.647E-01	3.992E-03	9.487E-03
	0.4825	2.481E-01	3.912E-03	1.007E-02
	0.4915	2.143E-01	3.706E-03	1.022E-02
	0.5005	1.869E-01	3.466E-03	7.353E-03
	0.5095	1.605E-01	3.290E-03	5.413E-03
	0.5185	1.576E-01	3.210E-03	4.937E-03
	0.5275	1.562E-01	3.238E-03	6.265E-03
	0.5365	1.744E-01	3.455E-03	7.908E-03
	0.5455	1.793E-01	3.657E-03	1.058E-02
	0.5545	1.969E-01	3.901E-03	1.313E-02
	0.5635	2.038E-01	4.165E-03	8.038E-03
	0.5725	1.911E-01	4.021E-03	1.006E-02
	0.5815	1.619E-01	3.686E-03	1.225E-02
	0.5905	1.417E-01	3.506E-03	8.990E-03
	0.5995	1.202E-01	3.204E-03	5.806E-03
	0.6085	1.090E-01	3.039E-03	7.862E-03
	0.6175	1.023E-01	2.193E-03	6.504E-03
	0.6265	9.760E-02	2.041E-03	6.499E-03
	0.6355	8.926E-02	1.964E-03	5.834E-03
	0.6445	8.662E-02	2.000E-03	5.553E-03
	0.6535	8.473E-02	1.967E-03	5.202E-03
	0.6625	7.949E-02	1.690E-03	6.208E-03
	0.6715	8.322E-02	1.789E-03	6.106E-03
	0.6805	8.336E-02	1.799E-03	6.002E-03
	0.6895	8.248E-02	1.827E-03	6.108E-03
	0.6985	8.281E-02	1.877E-03	5.813E-03
	0.7075	9.125E-02	2.067E-03	6.619E-03
	0.7165	8.951E-02	1.992E-03	6.549E-03
	0.7255	1.037E-01	2.259E-03	7.543E-03
	0.7345	1.068E-01	1.833E-03	7.847E-03
	0.7435	1.090E-01	1.908E-03	6.913E-03
	0.7525	1.067E-01	2.458E-03	6.583E-03
	0.7615	8.869E-02	2.194E-03	8.204E-03
	0.7705	7.412E-02	2.009E-03	9.343E-03
	0.7795	6.102E-02	1.718E-03	8.613E-03
	0.7885	4.705E-02	1.544E-03	5.775E-03
	0.7975	3.534E-02	1.337E-03	4.736E-03
	0.8065	2.652E-02	1.095E-03	3.388E-03
	0.8155	2.363E-02	1.135E-03	2.847E-03
	0.8245	1.705E-02	8.155E-04	2.353E-03
	0.8335	1.242E-02	7.381E-04	2.144E-03
	0.8425	1.081E-02	4.732E-04	2.038E-03
	0.8515	6.697E-03	4.024E-04	7.948E-04
	0.8605	3.801E-03	2.261E-04	1.392E-04
1.875	0.3025	3.101E-01	2.604E-03	2.325E-02
	0.3115	3.081E-01	2.019E-03	2.369E-02
	0.3205	2.994E-01	2.133E-03	2.159E-02
	0.3295	2.913E-01	2.248E-03	1.959E-02
	0.3385	2.873E-01	2.334E-03	1.837E-02
	0.3475	2.763E-01	2.380E-03	1.688E-02
	0.3565	2.770E-01	2.564E-03	1.626E-02
	0.3655	2.729E-01	2.740E-03	1.549E-02
	0.3745	2.756E-01	2.929E-03	1.545E-02
	0.3835	2.604E-01	3.063E-03	1.394E-02
	0.3925	2.591E-01	3.192E-03	1.292E-02
	0.4015	2.569E-01	3.248E-03	1.188E-02
	0.4105	2.506E-01	3.326E-03	1.206E-02
	0.4195	2.382E-01	3.306E-03	1.024E-02
	0.4285	2.333E-01	3.391E-03	9.746E-03
	0.4375	2.371E-01	3.536E-03	9.794E-03
	0.4465	2.190E-01	3.498E-03	9.139E-03
	0.4555	2.252E-01	3.531E-03	1.090E-02
	0.4645	2.400E-01	3.734E-03	1.386E-02
	0.4735	2.521E-01	3.850E-03	1.156E-02
	0.4825	2.554E-01	3.938E-03	9.170E-03
	0.4915	2.294E-01	3.715E-03	1.004E-02
	0.5005	2.067E-01	3.555E-03	9.895E-03
	0.5095	1.860E-01	3.422E-03	7.322E-03
	0.5185	1.666E-01	3.344E-03	5.723E-03
	0.5275	1.630E-01	3.421E-03	5.423E-03
	0.5365	1.582E-01	3.409E-03	6.702E-03
	0.5455	1.626E-01	3.531E-03	7.885E-03
	0.5545	1.741E-01	3.678E-03	1.098E-02
	0.5635	1.931E-01	4.064E-03	1.237E-02
	0.5725	1.963E-01	4.097E-03	6.283E-03
	0.5815	1.787E-01	3.967E-03	1.161E-02
	0.5905	1.497E-01	3.529E-03	1.111E-02
	0.5995	1.250E-01	3.225E-03	7.399E-03
	0.6085	1.114E-01	3.037E-03	5.079E-03
	0.6175	9.714E-02	2.966E-03	3.587E-03
	0.6265	9.592E-02	2.943E-03	3.077E-03
	0.6355	1.034E-01	3.318E-03	8.153E-03
	0.6445	8.778E-02	2.124E-03	6.570E-03
	0.6535	8.217E-02	1.903E-03	5.444E-03
	0.6625	8.189E-02	1.872E-03	5.575E-03
	0.6715	8.377E-02	1.938E-03	5.710E-03
	0.6805	7.989E-02	1.951E-03	5.369E-03
	0.6895	7.788E-02	1.752E-03	7.137E-03
	0.6985	8.091E-02	1.746E-03	7.271E-03
	0.7075	8.239E-02	1.773E-03	7.653E-03
	0.7165	9.035E-02	1.590E-03	7.717E-03
	0.7255	8.983E-02	1.618E-03	7.063E-03
	0.7345	9.599E-02	1.712E-03	7.398E-03
	0.7435	1.023E-01	1.849E-03	7.282E-03
	0.7525	1.035E-01	2.413E-03	6.018E-03
	0.7615	9.330E-02	1.808E-03	7.220E-03
	0.7705	8.246E-02	2.215E-03	9.082E-03
	0.7795	6.260E-02	1.719E-03	8.655E-03
	0.7885	5.006E-02	1.594E-03	6.641E-03
	0.7975	4.010E-02	1.406E-03	5.051E-03
	0.8065	3.037E-02	1.222E-03	4.291E-03
	0.8155	2.485E-02	1.052E-03	2.944E-03
	0.8245	2.123E-02	1.011E-03	2.695E-03
	0.8335	1.444E-02	7.675E-04	2.339E-03
	0.8425	1.157E-02	6.485E-04	2.167E-03
	0.8515	7.396E-03	4.394E-04	1.660E-03
	0.8605	4.624E-03	2.339E-04	1.853E-04
1.925	0.3115	3.005E-01	2.645E-03	2.256E-02
	0.3205	2.995E-01	2.055E-03	2.313E-02
	0.3295	2.959E-01	2.161E-03	2.142E-02
	0.3385	2.862E-01	2.260E-03	1.953E-02
	0.3475	2.766E-01	2.340E-03	1.793E-02
	0.3565	2.693E-01	2.378E-03	1.674E-02
	0.3655	2.640E-01	2.471E-03	1.585E-02
	0.3745	2.648E-01	2.639E-03	1.551E-02
	0.3835	2.608E-01	2.787E-03	1.519E-02
	0.3925	2.547E-01	2.914E-03	1.366E-02
	0.4015	2.568E-01	3.127E-03	1.318E-02
	0.4105	2.506E-01	3.252E-03	1.233E-02
	0.4195	2.363E-01	3.298E-03	1.113E-02
	0.4285	2.282E-01	3.269E-03	1.001E-02
	0.4375	2.234E-01	3.310E-03	9.531E-03
	0.4465	2.205E-01	3.396E-03	9.302E-03
	0.4555	2.183E-01	3.489E-03	9.615E-03
	0.4645	2.370E-01	3.773E-03	1.269E-02
	0.4735	2.468E-01	3.998E-03	1.358E-02
	0.4825	2.496E-01	4.168E-03	1.075E-02
	0.4915	2.334E-01	3.975E-03	9.024E-03
	0.5005	2.169E-01	3.737E-03	1.035E-02
	0.5095	1.915E-01	3.465E-03	8.885E-03
	0.5185	1.722E-01	3.273E-03	6.639E-03
	0.5275	1.587E-01	3.232E-03	5.531E-03
	0.5365	1.440E-01	3.048E-03	5.261E-03
	0.5455	1.527E-01	3.319E-03	6.791E-03
	0.5545	1.733E-01	3.637E-03	9.199E-03
	0.5635	1.842E-01	3.952E-03	1.222E-02
	0.5725	2.049E-01	4.349E-03	1.185E-02
	0.5815	2.012E-01	4.400E-03	6.919E-03
	0.5905	1.689E-01	3.945E-03	1.240E-02
	0.5995	1.388E-01	3.529E-03	9.840E-03
	0.6085	1.165E-01	3.153E-03	6.449E-03
	0.6175	1.084E-01	3.075E-03	4.688E-03
	0.6265	9.671E-02	2.962E-03	3.470E-03
	0.6355	1.011E-01	3.024E-03	3.239E-03
	0.6445	9.644E-02	3.031E-03	2.885E-03
	0.6535	8.340E-02	2.791E-03	2.398E-03
	0.6625	8.501E-02	2.852E-03	2.412E-03
	0.6715	8.271E-02	2.191E-03	6.733E-03
	0.6805	8.133E-02	1.975E-03	5.943E-03
	0.6895	7.850E-02	1.884E-03	6.026E-03
	0.6985	8.298E-02	1.986E-03	6.848E-03
	0.7075	7.621E-02	1.949E-03	6.562E-03
	0.7165	8.372E-02	2.024E-03	7.358E-03
	0.7255	8.469E-02	1.883E-03	8.032E-03

	0.7345	8.960E-02	1.927E-03	8.560E-03
	0.7435	9.485E-02	2.072E-03	8.800E-03
	0.7525	1.034E-01	2.229E-03	6.637E-03
	0.7615	9.153E-02	2.162E-03	5.796E-03
	0.7705	8.667E-02	2.084E-03	8.244E-03
	0.7795	7.169E-02	1.893E-03	9.083E-03
	0.7885	5.339E-02	1.600E-03	7.735E-03
	0.7975	3.941E-02	1.304E-03	4.773E-03
	0.8065	3.143E-02	1.182E-03	4.301E-03
	0.8155	2.598E-02	1.002E-03	3.242E-03
	0.8245	2.153E-02	9.876E-04	2.596E-03
	0.8335	1.422E-02	8.458E-04	2.034E-03
	0.8425	1.404E-02	7.248E-04	2.551E-03
	0.8515	1.061E-02	5.823E-04	2.234E-03
	0.8605	6.514E-03	3.766E-04	2.458E-04
	0.8695	2.506E-03	1.234E-04	1.125E-04
1.975	0.3295	2.964E-01	2.128E-03	2.305E-02
	0.3385	2.892E-01	2.187E-03	2.121E-02
	0.3475	2.777E-01	2.274E-03	1.930E-02
	0.3565	2.687E-01	2.338E-03	1.771E-02
	0.3655	2.651E-01	2.432E-03	1.681E-02
	0.3745	2.675E-01	2.526E-03	1.645E-02
	0.3835	2.528E-01	2.532E-03	1.518E-02
	0.3925	2.624E-01	2.750E-03	1.570E-02
	0.4015	2.489E-01	2.850E-03	1.351E-02
	0.4105	2.531E-01	3.007E-03	1.298E-02
	0.4195	2.484E-01	3.158E-03	1.202E-02
	0.4285	2.365E-01	3.286E-03	1.154E-02
	0.4375	2.266E-01	3.289E-03	1.030E-02
	0.4465	2.154E-01	3.300E-03	9.429E-03
	0.4555	2.091E-01	3.310E-03	8.915E-03
	0.4645	2.045E-01	3.424E-03	9.540E-03
	0.4735	2.221E-01	3.630E-03	1.298E-02
	0.4825	2.399E-01	3.915E-03	1.288E-02
	0.4915	2.572E-01	4.362E-03	1.055E-02
	0.5005	2.330E-01	4.241E-03	1.010E-02
	0.5095	2.059E-01	3.938E-03	1.054E-02
	0.5185	1.813E-01	3.698E-03	8.059E-03
	0.5275	1.614E-01	3.375E-03	6.124E-03
	0.5365	1.457E-01	3.218E-03	5.067E-03
	0.5455	1.522E-01	3.254E-03	6.462E-03
	0.5545	1.555E-01	3.358E-03	7.187E-03
	0.5635	1.684E-01	3.606E-03	9.701E-03
	0.5725	1.746E-01	3.774E-03	1.190E-02
	0.5815	1.864E-01	4.093E-03	8.956E-03
	0.5905	1.888E-01	4.228E-03	9.500E-03
	0.5995	1.486E-01	3.681E-03	1.154E-02
	0.6085	1.328E-01	3.517E-03	8.833E-03
	0.6175	1.128E-01	3.201E-03	5.843E-03
	0.6265	1.013E-01	3.077E-03	4.187E-03
	0.6355	9.799E-02	3.050E-03	3.482E-03
	0.6445	9.674E-02	3.103E-03	3.113E-03
	0.6535	8.604E-02	2.994E-03	2.654E-03
	0.6625	8.937E-02	3.011E-03	2.623E-03
	0.6715	8.253E-02	2.886E-03	2.412E-03
	0.6805	7.985E-02	2.871E-03	3.117E-03
	0.6895	8.200E-02	2.912E-03	2.536E-03
	0.6985	7.973E-02	2.843E-03	3.549E-03
	0.7075	7.970E-02	2.081E-03	7.120E-03
	0.7165	7.915E-02	2.001E-03	7.141E-03
	0.7255	8.245E-02	2.082E-03	7.203E-03
	0.7345	8.096E-02	2.079E-03	7.020E-03
	0.7435	9.326E-02	2.365E-03	8.137E-03
	0.7525	9.672E-02	2.466E-03	8.714E-03
	0.7615	8.940E-02	2.172E-03	7.441E-03
	0.7705	8.502E-02	2.052E-03	8.358E-03
	0.7795	7.504E-02	1.879E-03	9.866E-03
	0.7885	5.656E-02	1.509E-03	7.931E-03
	0.7975	4.333E-02	1.347E-03	5.637E-03
	0.8065	3.434E-02	1.178E-03	4.303E-03
	0.8155	2.614E-02	1.002E-03	3.633E-03
	0.8245	2.337E-02	9.296E-04	2.809E-03
	0.8335	1.852E-02	8.142E-04	2.458E-03
	0.8425	1.208E-02	6.262E-04	2.037E-03
	0.8515	8.903E-03	4.940E-04	1.660E-03
	0.8605	6.630E-03	3.793E-04	7.012E-04
	0.8695	3.250E-03	2.017E-04	1.277E-04

2.025	0.3385	2.845E-01	2.156E-03	2.235E-02
	0.3475	2.825E-01	2.221E-03	2.091E-02
	0.3565	2.732E-01	2.286E-03	1.931E-02
	0.3655	2.701E-01	2.374E-03	1.813E-02
	0.3745	2.622E-01	2.476E-03	1.687E-02
	0.3835	2.574E-01	2.537E-03	1.612E-02
	0.3925	2.537E-01	2.624E-03	1.562E-02
	0.4015	2.524E-01	2.696E-03	1.508E-02
	0.4105	2.453E-01	2.780E-03	1.363E-02
	0.4195	2.399E-01	2.908E-03	1.226E-02
	0.4285	2.359E-01	2.979E-03	1.163E-02
	0.4375	2.249E-01	3.031E-03	1.092E-02
	0.4465	2.234E-01	3.264E-03	1.038E-02
	0.4555	2.101E-01	3.301E-03	9.589E-03
	0.4645	2.046E-01	3.274E-03	9.401E-03
	0.4735	2.027E-01	3.342E-03	1.022E-02
	0.4825	2.221E-01	3.677E-03	1.387E-02
	0.4915	2.315E-01	3.931E-03	1.173E-02
	0.5005	2.361E-01	4.086E-03	9.537E-03
	0.5095	2.226E-01	3.982E-03	1.043E-02
	0.5185	2.045E-01	3.841E-03	1.072E-02
	0.5275	1.691E-01	3.544E-03	7.407E-03
	0.5365	1.644E-01	3.676E-03	6.321E-03
	0.5455	1.477E-01	3.459E-03	5.431E-03
	0.5545	1.458E-01	3.491E-03	6.633E-03
	0.5635	1.437E-01	3.502E-03	7.061E-03
	0.5725	1.662E-01	3.729E-03	1.040E-02
	0.5815	1.756E-01	3.959E-03	1.167E-02
	0.5905	1.959E-01	4.258E-03	7.256E-03
	0.5995	1.701E-01	3.853E-03	1.118E-02
	0.6085	1.387E-01	3.425E-03	1.067E-02
	0.6175	1.253E-01	3.258E-03	7.808E-03
	0.6265	1.086E-01	3.086E-03	5.284E-03
	0.6355	9.597E-02	2.992E-03	3.857E-03
	0.6445	9.496E-02	3.068E-03	3.429E-03
	0.6535	8.263E-02	2.896E-03	2.714E-03
	0.6625	7.808E-02	2.842E-03	2.444E-03
	0.6715	8.167E-02	2.995E-03	2.503E-03
	0.6805	7.550E-02	2.827E-03	2.701E-03
	0.6895	8.074E-02	3.017E-03	2.486E-03
	0.6985	7.605E-02	2.916E-03	2.728E-03
	0.7075	7.859E-02	2.988E-03	3.935E-03
	0.7165	7.629E-02	2.936E-03	3.997E-03
	0.7255	7.866E-02	3.010E-03	4.382E-03
	0.7345	8.296E-02	3.200E-03	4.670E-03
	0.7435	9.573E-02	3.451E-03	5.620E-03
	0.7525	9.213E-02	2.341E-03	8.521E-03
	0.7615	9.232E-02	2.447E-03	7.123E-03
	0.7705	8.878E-02	2.444E-03	6.837E-03
	0.7795	7.776E-02	2.293E-03	8.585E-03
	0.7885	5.999E-02	1.877E-03	8.677E-03
	0.7975	4.859E-02	1.487E-03	7.578E-03
	0.8065	3.811E-02	1.236E-03	5.554E-03
	0.8155	2.720E-02	9.939E-04	4.152E-03
	0.8245	2.101E-02	8.691E-04	3.054E-03
	0.8335	1.659E-02	7.877E-04	2.373E-03
	0.8425	1.444E-02	6.828E-04	2.339E-03
	0.8515	9.610E-03	5.188E-04	1.700E-03
	0.8605	8.440E-03	4.430E-04	1.883E-03
	0.8695	3.934E-03	2.349E-04	1.705E-04
2.075	0.3475	2.835E-01	2.226E-03	2.246E-02
	0.3565	2.784E-01	2.271E-03	2.094E-02
	0.3655	2.653E-01	2.305E-03	1.893E-02
	0.3745	2.611E-01	2.357E-03	1.784E-02
	0.3835	2.557E-01	2.495E-03	1.674E-02
	0.3925	2.534E-01	2.589E-03	1.620E-02
	0.4015	2.419E-01	2.596E-03	1.546E-02
	0.4105	2.451E-01	2.682E-03	1.428E-02
	0.4195	2.385E-01	2.703E-03	1.349E-02
	0.4285	2.375E-01	2.846E-03	1.290E-02
	0.4375	2.233E-01	2.900E-03	1.138E-02
	0.4465	2.139E-01	2.902E-03	1.041E-02
	0.4555	2.056E-01	2.956E-03	9.748E-03
	0.4645	2.091E-01	3.159E-03	9.775E-03
	0.4735	1.996E-01	3.202E-03	9.538E-03
	0.4825	2.061E-01	3.453E-03	1.148E-02
	0.4915	2.231E-01	3.745E-03	1.288E-02

	0.5005	2.259E-01	3.945E-03	1.068E-02
	0.5095	2.130E-01	3.890E-03	8.920E-03
	0.5185	2.015E-01	3.865E-03	1.050E-02
	0.5275	1.779E-01	3.494E-03	9.020E-03
	0.5365	1.594E-01	3.443E-03	6.816E-03
	0.5455	1.556E-01	3.466E-03	6.055E-03
	0.5545	1.352E-01	3.287E-03	5.314E-03
	0.5635	1.377E-01	3.356E-03	6.591E-03
	0.5725	1.612E-01	3.830E-03	8.702E-03
	0.5815	1.642E-01	3.984E-03	1.102E-02
	0.5905	1.772E-01	4.291E-03	1.062E-02
	0.5995	1.787E-01	4.434E-03	6.661E-03
	0.6085	1.495E-01	3.914E-03	1.137E-02
	0.6175	1.214E-01	3.410E-03	8.778E-03
	0.6265	1.097E-01	3.150E-03	6.284E-03
	0.6355	9.595E-02	2.856E-03	4.350E-03
	0.6445	8.701E-02	2.858E-03	3.394E-03
	0.6535	8.038E-02	2.686E-03	2.878E-03
	0.6625	8.440E-02	2.787E-03	2.823E-03
	0.6715	8.409E-02	2.861E-03	2.731E-03
	0.6805	7.994E-02	2.896E-03	2.588E-03
	0.6895	7.636E-02	2.899E-03	3.362E-03
	0.6985	7.177E-02	2.788E-03	2.347E-03
	0.7075	7.585E-02	2.934E-03	3.253E-03
	0.7165	7.995E-02	3.034E-03	4.156E-03
	0.7255	7.607E-02	3.118E-03	4.103E-03
	0.7345	7.447E-02	3.053E-03	4.107E-03
	0.7435	8.760E-02	3.426E-03	4.940E-03
	0.7525	8.916E-02	3.545E-03	5.191E-03
	0.7615	8.844E-02	3.672E-03	4.358E-03
	0.7705	8.961E-02	3.781E-03	3.293E-03
	0.7795	9.477E-02	3.924E-03	6.632E-03
	0.7885	6.821E-02	2.082E-03	9.231E-03
	0.7975	5.329E-02	1.784E-03	8.462E-03
	0.8065	4.075E-02	1.486E-03	6.225E-03
	0.8155	2.873E-02	1.256E-03	4.393E-03
	0.8245	2.373E-02	1.080E-03	3.578E-03
	0.8335	1.875E-02	8.564E-04	2.644E-03
	0.8425	1.317E-02	6.867E-04	2.035E-03
	0.8515	1.139E-02	5.958E-04	2.053E-03
	0.8605	8.229E-03	4.595E-04	1.758E-03
	0.8695	5.205E-03	3.266E-04	2.279E-04
	0.8785	2.067E-03	1.242E-04	8.325E-05
2.125	0.3565	2.746E-01	2.280E-03	2.208E-02
	0.3655	2.624E-01	2.268E-03	1.976E-02
	0.3745	2.607E-01	2.328E-03	1.888E-02
	0.3835	2.539E-01	2.386E-03	1.765E-02
	0.3925	2.471E-01	2.431E-03	1.651E-02
	0.4015	2.408E-01	2.524E-03	1.573E-02
	0.4105	2.355E-01	2.625E-03	1.532E-02
	0.4195	2.312E-01	2.650E-03	1.370E-02
	0.4285	2.285E-01	2.705E-03	1.306E-02
	0.4375	2.285E-01	2.773E-03	1.220E-02
	0.4465	2.214E-01	2.822E-03	1.162E-02
	0.4555	2.093E-01	2.859E-03	1.043E-02
	0.4645	2.055E-01	2.980E-03	1.002E-02
	0.4735	1.873E-01	2.903E-03	8.828E-03
	0.4825	1.950E-01	3.060E-03	9.919E-03
	0.4915	2.045E-01	3.293E-03	1.253E-02
	0.5005	2.223E-01	3.687E-03	1.266E-02
	0.5095	2.275E-01	3.990E-03	1.030E-02
	0.5185	2.166E-01	3.988E-03	1.009E-02
	0.5275	1.843E-01	3.659E-03	1.016E-02
	0.5365	1.647E-01	3.444E-03	7.824E-03
	0.5455	1.469E-01	3.282E-03	6.171E-03
	0.5545	1.373E-01	3.265E-03	5.379E-03
	0.5635	1.371E-01	3.338E-03	6.339E-03
	0.5725	1.452E-01	3.489E-03	7.150E-03
	0.5815	1.451E-01	3.579E-03	8.621E-03
	0.5905	1.745E-01	4.184E-03	1.213E-02
	0.5995	1.871E-01	4.478E-03	9.191E-03
	0.6085	1.725E-01	4.419E-03	9.665E-03
	0.6175	1.427E-01	3.924E-03	1.140E-02
	0.6265	1.233E-01	3.776E-03	8.285E-03
	0.6355	1.041E-01	3.350E-03	5.507E-03
	0.6445	9.251E-02	3.200E-03	3.983E-03
	0.6535	8.540E-02	3.033E-03	3.261E-03
	0.6625	8.715E-02	3.043E-03	3.091E-03
	0.6715	8.358E-02	2.937E-03	2.852E-03
	0.6805	8.273E-02	2.928E-03	2.775E-03
	0.6895	7.810E-02	2.849E-03	2.815E-03
	0.6985	7.733E-02	2.839E-03	2.810E-03
	0.7075	7.169E-02	2.787E-03	2.433E-03
	0.7165	7.590E-02	2.851E-03	3.745E-03
	0.7255	7.006E-02	2.772E-03	3.779E-03
	0.7345	7.582E-02	3.097E-03	4.117E-03
	0.7435	8.112E-02	3.224E-03	4.409E-03
	0.7525	8.023E-02	3.262E-03	4.652E-03
	0.7615	9.823E-02	3.883E-03	5.431E-03
	0.7705	8.522E-02	3.867E-03	3.807E-03
	0.7795	8.122E-02	4.692E-03	4.230E-03
	0.7885	7.532E-02	3.559E-03	7.742E-03
	0.7975	5.588E-02	2.835E-03	8.732E-03
	0.8065	4.921E-02	1.878E-03	8.136E-03
	0.8155	3.601E-02	1.460E-03	5.535E-03
	0.8245	2.607E-02	1.139E-03	4.143E-03
	0.8335	1.951E-02	1.011E-03	2.753E-03
	0.8425	1.595E-02	8.534E-04	2.448E-03
	0.8515	1.155E-02	6.750E-04	2.076E-03
	0.8605	8.105E-03	5.153E-04	1.671E-03
	0.8695	5.237E-03	3.706E-04	4.734E-04
	0.8785	2.361E-03	1.673E-04	8.863E-05
2.175	0.3475	2.833E-01	2.944E-03	2.337E-02
	0.3565	2.879E-01	2.371E-03	2.542E-02
	0.3655	2.779E-01	2.365E-03	2.247E-02
	0.3745	2.649E-01	2.369E-03	2.021E-02
	0.3835	2.573E-01	2.395E-03	1.888E-02
	0.3925	2.509E-01	2.432E-03	1.776E-02
	0.4015	2.434E-01	2.459E-03	1.666E-02
	0.4105	2.344E-01	2.493E-03	1.576E-02
	0.4195	2.321E-01	2.641E-03	1.503E-02
	0.4285	2.271E-01	2.684E-03	1.364E-02
	0.4375	2.211E-01	2.729E-03	1.246E-02
	0.4465	2.215E-01	2.802E-03	1.192E-02
	0.4555	2.078E-01	2.749E-03	1.114E-02
	0.4645	2.015E-01	2.753E-03	1.038E-02
	0.4735	1.969E-01	2.833E-03	9.860E-03
	0.4825	1.902E-01	2.910E-03	9.468E-03
	0.4915	2.026E-01	3.194E-03	1.099E-02
	0.5005	2.033E-01	3.326E-03	1.330E-02
	0.5095	2.209E-01	3.615E-03	1.196E-02
	0.5185	2.222E-01	3.706E-03	1.003E-02
	0.5275	1.959E-01	3.639E-03	1.027E-02
	0.5365	1.827E-01	3.622E-03	1.023E-02
	0.5455	1.618E-01	3.510E-03	7.529E-03
	0.5545	1.327E-01	3.163E-03	5.640E-03
	0.5635	1.285E-01	3.139E-03	5.126E-03
	0.5725	1.310E-01	3.260E-03	6.339E-03
	0.5815	1.387E-01	3.409E-03	7.226E-03
	0.5905	1.497E-01	3.713E-03	9.742E-03
	0.5995	1.654E-01	4.078E-03	1.104E-02
	0.6085	1.858E-01	4.473E-03	7.234E-03
	0.6175	1.620E-01	4.135E-03	1.177E-02
	0.6265	1.320E-01	3.630E-03	1.023E-02
	0.6355	1.132E-01	3.380E-03	7.071E-03
	0.6445	9.594E-02	3.107E-03	4.764E-03
	0.6535	8.795E-02	3.098E-03	3.662E-03
	0.6625	8.384E-02	3.050E-03	3.153E-03
	0.6715	8.240E-02	3.143E-03	2.918E-03
	0.6805	7.403E-02	3.004E-03	2.526E-03
	0.6895	7.322E-02	3.000E-03	2.463E-03
	0.6985	7.256E-02	3.025E-03	3.394E-03
	0.7075	6.817E-02	2.844E-03	2.314E-03
	0.7165	6.402E-02	2.722E-03	2.704E-03
	0.7255	6.782E-02	2.809E-03	3.527E-03
	0.7345	6.878E-02	2.823E-03	3.671E-03
	0.7435	6.571E-02	2.725E-03	3.480E-03
	0.7525	7.541E-02	2.985E-03	4.227E-03
	0.7615	7.586E-02	4.093E-03	4.337E-03
	0.7705	8.966E-02	4.781E-03	4.296E-03
	0.7795	8.644E-02	3.585E-03	3.562E-03
	0.7885	8.231E-02	4.625E-03	6.295E-03
	0.7975	5.898E-02	2.930E-03	8.021E-03
	0.8065	5.186E-02	2.719E-03	9.016E-03

	0.8155	3.588E-02	2.252E-03	5.634E-03
	0.8245	2.884E-02	1.928E-03	4.814E-03
	0.8335	2.487E-02	1.726E-03	3.720E-03
	0.8425	1.994E-02	1.566E-03	2.987E-03
	0.8515	1.617E-02	9.294E-04	2.845E-03
	0.8605	9.150E-03	6.172E-04	1.797E-03
	0.8695	5.537E-03	4.127E-04	1.363E-03
	0.8785	2.890E-03	2.225E-04	1.185E-04
2.225	0.3655	2.744E-01	2.378E-03	2.386E-02
	0.3745	2.660E-01	2.413E-03	2.168E-02
	0.3835	2.533E-01	2.389E-03	1.968E-02
	0.3925	2.547E-01	2.448E-03	1.887E-02
	0.4015	2.461E-01	2.472E-03	1.771E-02
	0.4105	2.359E-01	2.504E-03	1.653E-02
	0.4195	2.314E-01	2.515E-03	1.595E-02
	0.4285	2.261E-01	2.583E-03	1.452E-02
	0.4375	2.262E-01	2.694E-03	1.400E-02
	0.4465	2.176E-01	2.754E-03	1.261E-02
	0.4555	2.092E-01	2.767E-03	1.164E-02
	0.4645	2.013E-01	2.749E-03	1.077E-02
	0.4735	1.941E-01	2.762E-03	1.017E-02
	0.4825	1.878E-01	2.739E-03	9.738E-03
	0.4915	1.907E-01	2.838E-03	1.001E-02
	0.5005	1.994E-01	3.052E-03	1.191E-02
	0.5095	2.054E-01	3.291E-03	1.245E-02
	0.5185	2.136E-01	3.520E-03	1.070E-02
	0.5275	2.061E-01	3.541E-03	9.763E-03
	0.5365	1.850E-01	3.383E-03	1.062E-02
	0.5455	1.617E-01	3.151E-03	8.627E-03
	0.5545	1.490E-01	3.288E-03	6.894E-03
	0.5635	1.390E-01	3.213E-03	5.961E-03
	0.5725	1.263E-01	3.155E-03	5.525E-03
	0.5815	1.299E-01	3.294E-03	6.482E-03
	0.5905	1.381E-01	3.517E-03	7.903E-03
	0.5995	1.568E-01	3.761E-03	1.084E-02
	0.6085	1.699E-01	4.156E-03	9.725E-03
	0.6175	1.642E-01	4.231E-03	7.751E-03
	0.6265	1.374E-01	3.642E-03	1.109E-02
	0.6355	1.091E-01	3.339E-03	7.809E-03
	0.6445	9.453E-02	3.017E-03	5.417E-03
	0.6535	8.452E-02	2.939E-03	3.975E-03
	0.6625	8.430E-02	3.025E-03	3.523E-03
	0.6715	7.471E-02	2.880E-03	2.863E-03
	0.6805	8.077E-02	3.157E-03	2.955E-03
	0.6895	7.490E-02	3.039E-03	2.672E-03
	0.6985	7.047E-02	2.852E-03	2.576E-03
	0.7075	7.707E-02	3.115E-03	3.164E-03
	0.7165	7.388E-02	3.075E-03	2.579E-03
	0.7255	6.678E-02	2.903E-03	3.229E-03
	0.7345	7.233E-02	3.270E-03	3.783E-03
	0.7435	7.140E-02	3.337E-03	3.682E-03
	0.7525	7.184E-02	3.270E-03	3.791E-03
	0.7615	7.781E-02	3.333E-03	4.528E-03
	0.7705	8.569E-02	3.651E-03	4.674E-03
	0.7795	8.080E-02	4.784E-03	3.489E-03
	0.7885	8.087E-02	4.955E-03	4.301E-03
	0.7975	6.154E-02	2.976E-03	6.933E-03
	0.8065	4.877E-02	2.570E-03	8.006E-03
	0.8155	3.420E-02	2.025E-03	5.701E-03
	0.8245	2.724E-02	1.689E-03	4.266E-03
	0.8335	2.217E-02	1.571E-03	3.525E-03
	0.8425	1.824E-02	1.371E-03	2.655E-03
	0.8515	1.284E-02	1.114E-03	2.217E-03
	0.8605	9.892E-03	1.039E-03	2.121E-03
	0.8695	9.260E-03	8.117E-04	2.489E-03
	0.8785	4.108E-03	5.103E-04	9.951E-05
	0.8875	1.201E-03	1.558E-04	2.764E-05
2.275	0.3475	2.915E-01	5.050E-03	2.543E-02
	0.3565	2.836E-01	3.101E-03	2.548E-02
	0.3655	2.734E-01	3.936E-03	2.595E-02
	0.3745	2.641E-01	2.412E-03	2.302E-02
	0.3835	2.619E-01	2.464E-03	2.166E-02
	0.3925	2.497E-01	2.468E-03	1.961E-02
	0.4015	2.444E-01	2.482E-03	1.825E-02
	0.4105	2.363E-01	2.502E-03	1.721E-02
	0.4195	2.282E-01	2.524E-03	1.635E-02
	0.4285	2.249E-01	2.546E-03	1.570E-02

	0.4375	2.232E-01	2.596E-03	1.430E-02
	0.4465	2.142E-01	2.610E-03	1.382E-02
	0.4555	2.104E-01	2.714E-03	1.237E-02
	0.4645	2.001E-01	2.735E-03	1.168E-02
	0.4735	1.886E-01	2.726E-03	1.032E-02
	0.4825	1.884E-01	2.751E-03	1.005E-02
	0.4915	1.832E-01	2.769E-03	9.538E-03
	0.5005	1.834E-01	2.826E-03	1.020E-02
	0.5095	1.970E-01	3.039E-03	1.298E-02
	0.5185	2.061E-01	3.196E-03	1.221E-02
	0.5275	2.077E-01	3.446E-03	1.011E-02
	0.5365	1.845E-01	3.231E-03	9.552E-03
	0.5455	1.689E-01	3.174E-03	1.004E-02
	0.5545	1.486E-01	3.066E-03	7.520E-03
	0.5635	1.345E-01	2.974E-03	6.153E-03
	0.5725	1.255E-01	2.942E-03	5.445E-03
	0.5815	1.238E-01	2.967E-03	6.394E-03
	0.5905	1.322E-01	3.172E-03	6.973E-03
	0.5995	1.410E-01	3.453E-03	9.019E-03
	0.6085	1.515E-01	3.850E-03	1.062E-02
	0.6175	1.707E-01	4.393E-03	7.654E-03
	0.6265	1.560E-01	4.119E-03	1.068E-02
	0.6355	1.231E-01	3.474E-03	9.919E-03
	0.6445	1.035E-01	3.186E-03	6.776E-03
	0.6535	9.344E-02	3.118E-03	4.890E-03
	0.6625	7.916E-02	2.917E-03	3.519E-03
	0.6715	8.277E-02	3.085E-03	3.377E-03
	0.6805	7.598E-02	2.850E-03	2.875E-03
	0.6895	8.138E-02	3.042E-03	3.008E-03
	0.6985	6.761E-02	2.835E-03	2.471E-03
	0.7075	6.810E-02	2.883E-03	3.453E-03
	0.7165	6.961E-02	2.901E-03	2.520E-03
	0.7255	6.399E-02	2.855E-03	2.763E-03
	0.7345	6.478E-02	2.852E-03	3.404E-03
	0.7435	6.128E-02	2.879E-03	3.183E-03
	0.7525	6.746E-02	3.042E-03	3.426E-03
	0.7615	7.172E-02	3.296E-03	4.052E-03
	0.7705	7.699E-02	3.592E-03	4.422E-03
	0.7795	7.703E-02	3.595E-03	3.814E-03
	0.7885	8.183E-02	3.973E-03	3.539E-03
	0.7975	6.881E-02	3.500E-03	6.056E-03
	0.8065	4.863E-02	2.838E-03	7.108E-03
	0.8155	4.441E-02	2.725E-03	7.801E-03
	0.8245	3.178E-02	2.116E-03	4.899E-03
	0.8335	2.385E-02	1.661E-03	3.982E-03
	0.8425	1.990E-02	1.591E-03	2.827E-03
	0.8515	1.443E-02	1.339E-03	2.263E-03
	0.8605	1.036E-02	9.075E-04	2.118E-03
	0.8695	7.183E-03	7.673E-04	1.716E-03
	0.8785	5.332E-03	7.432E-04	2.310E-04
	0.8875	1.326E-03	2.111E-04	3.006E-05
2.325	0.3565	2.755E-01	5.070E-03	2.437E-02
	0.3655	2.765E-01	3.164E-03	2.491E-02
	0.3745	2.668E-01	5.195E-03	2.575E-02
	0.3835	2.541E-01	2.463E-03	2.232E-02
	0.3925	2.491E-01	2.458E-03	2.068E-02
	0.4015	2.466E-01	2.528E-03	1.963E-02
	0.4105	2.369E-01	2.528E-03	1.810E-02
	0.4195	2.317E-01	2.531E-03	1.720E-02
	0.4285	2.256E-01	2.582E-03	1.648E-02
	0.4375	2.233E-01	2.612E-03	1.558E-02
	0.4465	2.127E-01	2.596E-03	1.383E-02
	0.4555	2.070E-01	2.598E-03	1.274E-02
	0.4645	1.992E-01	2.634E-03	1.176E-02
	0.4735	1.940E-01	2.681E-03	1.129E-02
	0.4825	1.921E-01	2.788E-03	1.078E-02
	0.4915	1.775E-01	2.711E-03	9.786E-03
	0.5005	1.738E-01	2.775E-03	9.561E-03
	0.5095	1.806E-01	2.876E-03	1.084E-02
	0.5185	1.993E-01	3.149E-03	1.314E-02
	0.5275	2.020E-01	3.227E-03	1.132E-02
	0.5365	1.981E-01	3.211E-03	9.919E-03
	0.5455	1.837E-01	3.147E-03	1.086E-02
	0.5545	1.494E-01	2.850E-03	8.647E-03
	0.5635	1.349E-01	2.862E-03	6.698E-03
	0.5725	1.200E-01	2.711E-03	5.488E-03
	0.5815	1.177E-01	2.795E-03	5.215E-03

	0.5905	1.215E-01	2.937E-03	6.420E-03
	0.5995	1.339E-01	3.200E-03	7.641E-03
	0.6085	1.481E-01	3.415E-03	1.030E-02
	0.6175	1.563E-01	3.249E-03	1.017E-02
	0.6265	1.646E-01	4.081E-03	7.344E-03
	0.6355	1.375E-01	3.690E-03	1.123E-02
	0.6445	1.066E-01	3.328E-03	8.033E-03
	0.6535	9.706E-02	3.164E-03	5.810E-03
	0.6625	8.217E-02	2.998E-03	4.052E-03
	0.6715	7.442E-02	2.715E-03	3.227E-03
	0.6805	7.816E-02	2.933E-03	3.146E-03
	0.6895	7.421E-02	2.940E-03	2.851E-03
	0.6985	6.092E-02	2.607E-03	2.248E-03
	0.7075	6.909E-02	2.870E-03	2.746E-03
	0.7165	7.073E-02	3.024E-03	3.232E-03
	0.7255	5.946E-02	2.732E-03	2.222E-03
	0.7345	6.163E-02	2.872E-03	3.057E-03
	0.7435	6.574E-02	2.944E-03	3.502E-03
	0.7525	6.175E-02	2.968E-03	3.117E-03
	0.7615	6.750E-02	3.075E-03	3.620E-03
	0.7705	6.909E-02	3.121E-03	4.002E-03
	0.7795	8.193E-02	4.712E-03	4.488E-03
	0.7885	7.743E-02	3.564E-03	3.423E-03
	0.7975	6.859E-02	3.487E-03	4.576E-03
	0.8065	6.334E-02	3.326E-03	8.008E-03
	0.8155	4.452E-02	2.588E-03	7.634E-03
	0.8245	3.341E-02	2.362E-03	5.453E-03
	0.8335	3.020E-02	2.108E-03	4.874E-03
	0.8425	1.788E-02	1.712E-03	2.646E-03
	0.8515	1.540E-02	1.443E-03	2.318E-03
	0.8605	9.091E-03	1.125E-03	1.747E-03
	0.8695	1.003E-02	1.027E-03	2.243E-03
	0.8785	7.703E-03	9.688E-04	2.800E-04
	0.8875	2.802E-03	4.050E-04	7.883E-05
2.375	0.3655	2.811E-01	3.513E-03	2.770E-02
	0.3745	2.672E-01	3.198E-03	2.413E-02
	0.3835	2.735E-01	8.536E-03	2.706E-02
	0.3925	2.531E-01	2.580E-03	2.243E-02
	0.4015	2.431E-01	2.495E-03	2.044E-02
	0.4105	2.355E-01	2.567E-03	1.906E-02
	0.4195	2.280E-01	2.529E-03	1.781E-02
	0.4285	2.172E-01	2.515E-03	1.640E-02
	0.4375	2.155E-01	2.579E-03	1.611E-02
	0.4465	2.138E-01	2.609E-03	1.480E-02
	0.4555	2.074E-01	2.634E-03	1.445E-02
	0.4645	1.990E-01	2.612E-03	1.244E-02
	0.4735	1.942E-01	2.653E-03	1.186E-02
	0.4825	1.829E-01	2.606E-03	1.070E-02
	0.4915	1.764E-01	2.619E-03	1.000E-02
	0.5005	1.745E-01	2.702E-03	9.727E-03
	0.5095	1.728E-01	2.763E-03	9.973E-03
	0.5185	1.794E-01	2.931E-03	1.179E-02
	0.5275	1.965E-01	3.181E-03	1.238E-02
	0.5365	1.902E-01	3.210E-03	9.986E-03
	0.5455	1.854E-01	3.185E-03	9.922E-03
	0.5545	1.625E-01	2.958E-03	1.014E-02
	0.5635	1.501E-01	2.880E-03	8.194E-03
	0.5725	1.304E-01	2.723E-03	6.392E-03
	0.5815	1.202E-01	2.698E-03	5.558E-03
	0.5905	1.124E-01	2.657E-03	5.936E-03
	0.5995	1.175E-01	2.857E-03	6.305E-03
	0.6085	1.304E-01	3.203E-03	8.256E-03
	0.6175	1.397E-01	3.353E-03	1.001E-02
	0.6265	1.518E-01	3.715E-03	7.849E-03
	0.6355	1.352E-01	3.492E-03	9.028E-03
	0.6445	1.206E-01	3.234E-03	1.006E-02
	0.6535	1.004E-01	3.030E-03	6.895E-03
	0.6625	9.079E-02	2.869E-03	5.065E-03
	0.6715	7.630E-02	2.638E-03	3.638E-03
	0.6805	6.926E-02	2.654E-03	2.985E-03
	0.6895	7.255E-02	2.821E-03	2.922E-03
	0.6985	6.708E-02	2.774E-03	2.658E-03
	0.7075	6.219E-02	2.642E-03	2.420E-03
	0.7165	6.155E-02	2.651E-03	3.291E-03
	0.7255	6.101E-02	2.607E-03	2.314E-03
	0.7345	6.443E-02	3.019E-03	2.898E-03
	0.7435	5.651E-02	2.577E-03	2.960E-03
	0.7525	6.028E-02	2.752E-03	3.208E-03
	0.7615	6.275E-02	3.100E-03	3.206E-03
	0.7705	6.261E-02	2.974E-03	3.551E-03
	0.7795	6.804E-02	3.193E-03	3.881E-03
	0.7885	7.020E-02	3.381E-03	3.510E-03
	0.7975	6.731E-02	3.423E-03	3.454E-03
	0.8065	6.472E-02	3.284E-03	6.698E-03
	0.8155	5.189E-02	2.902E-03	8.316E-03
	0.8245	3.174E-02	2.030E-03	5.412E-03
	0.8335	2.831E-02	1.913E-03	4.474E-03
	0.8425	1.985E-02	1.644E-03	3.107E-03
	0.8515	1.496E-02	1.254E-03	2.221E-03
	0.8605	1.103E-02	1.004E-03	1.940E-03
	0.8695	9.324E-03	9.447E-04	1.992E-03
	0.8785	5.643E-03	8.559E-04	1.636E-03
	0.8875	3.893E-03	4.793E-04	1.188E-04
2.425	0.3925	2.449E-01	3.283E-03	2.096E-02
	0.4015	2.400E-01	2.704E-03	2.155E-02
	0.4105	2.382E-01	2.521E-03	2.020E-02
	0.4195	2.324E-01	2.580E-03	1.899E-02
	0.4285	2.246E-01	2.603E-03	1.772E-02
	0.4375	2.173E-01	2.613E-03	1.676E-02
	0.4465	2.108E-01	2.593E-03	1.567E-02
	0.4555	2.099E-01	2.668E-03	1.445E-02
	0.4645	2.067E-01	2.710E-03	1.365E-02
	0.4735	1.990E-01	2.666E-03	1.271E-02
	0.4825	1.804E-01	2.616E-03	1.139E-02
	0.4915	1.814E-01	2.638E-03	1.081E-02
	0.5005	1.738E-01	2.642E-03	1.018E-02
	0.5095	1.706E-01	2.639E-03	9.937E-03
	0.5185	1.731E-01	2.814E-03	1.065E-02
	0.5275	1.830E-01	3.051E-03	1.307E-02
	0.5365	1.990E-01	3.266E-03	1.201E-02
	0.5455	1.891E-01	3.267E-03	9.869E-03
	0.5545	1.737E-01	3.116E-03	1.054E-02
	0.5635	1.548E-01	2.950E-03	9.639E-03
	0.5725	1.310E-01	2.711E-03	6.964E-03
	0.5815	1.210E-01	2.632E-03	5.966E-03
	0.5905	1.183E-01	2.626E-03	5.687E-03
	0.5995	1.132E-01	2.687E-03	6.315E-03
	0.6085	1.154E-01	2.784E-03	6.660E-03
	0.6175	1.257E-01	3.014E-03	8.720E-03
	0.6265	1.482E-01	3.548E-03	9.900E-03
	0.6355	1.528E-01	3.777E-03	6.972E-03
	0.6445	1.246E-01	3.285E-03	1.026E-02
	0.6535	1.122E-01	3.176E-03	8.734E-03
	0.6625	8.890E-02	2.814E-03	5.565E-03
	0.6715	8.641E-02	2.873E-03	4.527E-03
	0.6805	7.014E-02	2.603E-03	3.237E-03
	0.6895	7.112E-02	2.610E-03	3.062E-03
	0.6985	6.509E-02	2.637E-03	2.717E-03
	0.7075	6.664E-02	2.681E-03	2.658E-03
	0.7165	6.155E-02	2.590E-03	2.698E-03
	0.7255	6.398E-02	2.706E-03	2.895E-03
	0.7345	6.376E-02	2.704E-03	2.547E-03
	0.7435	5.463E-02	2.550E-03	2.735E-03
	0.7525	5.660E-02	2.686E-03	2.959E-03
	0.7615	6.574E-02	2.970E-03	3.277E-03
	0.7705	6.081E-02	2.853E-03	3.280E-03
	0.7795	5.907E-02	3.052E-03	3.432E-03
	0.7885	6.148E-02	3.057E-03	3.376E-03
	0.7975	6.621E-02	3.395E-03	2.988E-03
	0.8065	5.550E-02	2.834E-03	4.504E-03
	0.8155	5.415E-02	3.040E-03	7.817E-03
	0.8245	3.771E-02	2.305E-03	6.569E-03
	0.8335	2.820E-02	1.962E-03	4.517E-03
	0.8425	1.842E-02	1.421E-03	3.098E-03
	0.8515	1.373E-02	1.291E-03	1.971E-03
	0.8605	1.286E-02	1.136E-03	2.091E-03
	0.8695	1.035E-02	8.799E-04	2.160E-03
	0.8785	6.164E-03	5.957E-04	1.597E-03
	0.8875	4.046E-03	3.878E-04	1.199E-04
2.475	0.3745	2.614E-01	5.590E-03	2.447E-02
	0.3835	2.556E-01	3.761E-03	2.495E-02
	0.3925	2.523E-01	3.269E-03	2.297E-02
	0.4015	2.430E-01	3.391E-03	2.102E-02
	0.4105	2.424E-01	2.975E-03	2.184E-02

	0.4195	2.320E-01	2.524E-03	1.982E-02
	0.4285	2.229E-01	2.578E-03	1.846E-02
	0.4375	2.205E-01	2.667E-03	1.768E-02
	0.4465	2.111E-01	2.625E-03	1.670E-02
	0.4555	2.088E-01	2.661E-03	1.529E-02
	0.4645	2.014E-01	2.664E-03	1.461E-02
	0.4735	1.939E-01	2.674E-03	1.303E-02
	0.4825	1.874E-01	2.680E-03	1.227E-02
	0.4915	1.765E-01	2.638E-03	1.099E-02
	0.5005	1.753E-01	2.643E-03	1.072E-02
	0.5095	1.681E-01	2.639E-03	9.951E-03
	0.5185	1.654E-01	2.652E-03	9.995E-03
	0.5275	1.739E-01	2.805E-03	1.165E-02
	0.5365	1.787E-01	2.986E-03	1.192E-02
	0.5455	1.870E-01	3.186E-03	1.065E-02
	0.5545	1.829E-01	3.247E-03	1.021E-02
	0.5635	1.566E-01	2.995E-03	1.019E-02
	0.5725	1.455E-01	2.848E-03	8.510E-03
	0.5815	1.287E-01	2.753E-03	6.826E-03
	0.5905	1.155E-01	2.641E-03	5.733E-03
	0.5995	1.098E-01	2.581E-03	5.841E-03
	0.6085	1.125E-01	2.682E-03	6.376E-03
	0.6175	1.173E-01	2.767E-03	7.428E-03
	0.6265	1.443E-01	3.278E-03	1.061E-02
	0.6355	1.486E-01	3.444E-03	8.171E-03
	0.6445	1.420E-01	3.473E-03	9.493E-03
	0.6535	1.125E-01	3.079E-03	9.568E-03
	0.6625	9.439E-02	2.780E-03	6.683E-03
	0.6715	8.225E-02	2.701E-03	4.724E-03
	0.6805	7.813E-02	2.746E-03	3.844E-03
	0.6895	7.508E-02	2.623E-03	3.471E-03
	0.6985	6.478E-02	2.456E-03	2.860E-03
	0.7075	6.939E-02	2.660E-03	2.901E-03
	0.7165	6.422E-02	2.582E-03	2.732E-03
	0.7255	5.773E-02	2.405E-03	3.261E-03
	0.7345	5.398E-02	2.378E-03	2.181E-03
	0.7435	5.854E-02	2.603E-03	2.781E-03
	0.7525	5.777E-02	2.665E-03	3.104E-03
	0.7615	6.268E-02	2.887E-03	3.221E-03
	0.7705	6.150E-02	2.891E-03	3.229E-03
	0.7795	6.296E-02	3.041E-03	3.652E-03
	0.7885	6.793E-02	3.361E-03	3.873E-03
	0.7975	7.084E-02	3.445E-03	3.562E-03
	0.8065	7.085E-02	3.452E-03	4.345E-03
	0.8155	5.252E-02	2.851E-03	6.419E-03
	0.8245	3.495E-02	2.134E-03	5.965E-03
	0.8335	3.207E-02	2.071E-03	5.173E-03
	0.8425	2.232E-02	1.498E-03	3.555E-03
	0.8515	1.636E-02	1.497E-03	2.366E-03
	0.8605	1.276E-02	1.236E-03	1.954E-03
	0.8695	6.718E-03	8.362E-04	1.318E-03
	0.8785	5.357E-03	5.953E-04	1.244E-03
	0.8875	3.325E-03	3.549E-04	8.973E-05
	0.8965	1.387E-03	1.979E-04	4.575E-05
2.525	0.3655	2.639E-01	8.412E-03	2.988E-02
	0.3745	2.692E-01	5.620E-03	2.712E-02
	0.3835	2.609E-01	5.780E-03	2.435E-02
	0.3925	2.517E-01	4.003E-03	2.452E-02
	0.4015	2.439E-01	3.306E-03	2.229E-02
	0.4105	2.348E-01	3.408E-03	2.032E-02
	0.4195	2.400E-01	3.447E-03	2.219E-02
	0.4285	2.185E-01	2.565E-03	1.889E-02
	0.4375	2.096E-01	2.555E-03	1.745E-02
	0.4465	2.072E-01	2.627E-03	1.702E-02
	0.4555	2.052E-01	2.685E-03	1.630E-02
	0.4645	1.997E-01	2.662E-03	1.449E-02
	0.4735	2.005E-01	2.730E-03	1.448E-02
	0.4825	1.903E-01	2.732E-03	1.284E-02
	0.4915	1.791E-01	2.644E-03	1.240E-02
	0.5005	1.766E-01	2.683E-03	1.124E-02
	0.5095	1.632E-01	2.615E-03	1.004E-02
	0.5185	1.602E-01	2.647E-03	9.817E-03
	0.5275	1.648E-01	2.724E-03	1.050E-02
	0.5365	1.762E-01	2.898E-03	1.289E-02
	0.5455	1.806E-01	3.025E-03	1.163E-02
	0.5545	1.763E-01	3.062E-03	9.883E-03
	0.5635	1.649E-01	2.990E-03	1.015E-02

	0.5725	1.430E-01	2.831E-03	9.373E-03
	0.5815	1.262E-01	2.683E-03	7.132E-03
	0.5905	1.157E-01	2.637E-03	5.958E-03
	0.5995	1.049E-01	2.552E-03	5.278E-03
	0.6085	1.064E-01	2.625E-03	6.230E-03
	0.6175	1.166E-01	2.755E-03	6.982E-03
	0.6265	1.166E-01	2.842E-03	8.210E-03
	0.6355	1.356E-01	3.199E-03	9.465E-03
	0.6445	1.365E-01	3.251E-03	6.640E-03
	0.6535	1.257E-01	3.134E-03	1.057E-02
	0.6625	1.004E-01	2.724E-03	8.024E-03
	0.6715	8.805E-02	2.625E-03	5.684E-03
	0.6805	7.866E-02	2.513E-03	4.197E-03
	0.6895	6.750E-02	2.436E-03	3.243E-03
	0.6985	6.040E-02	2.339E-03	2.702E-03
	0.7075	6.590E-02	2.517E-03	2.854E-03
	0.7165	6.343E-02	2.557E-03	2.717E-03
	0.7255	6.091E-02	2.568E-03	3.074E-03
	0.7345	5.633E-02	2.406E-03	2.558E-03
	0.7435	5.568E-02	2.531E-03	2.381E-03
	0.7525	5.871E-02	2.543E-03	3.043E-03
	0.7615	5.431E-02	2.201E-03	2.962E-03
	0.7705	5.845E-02	2.702E-03	2.967E-03
	0.7795	5.830E-02	2.372E-03	3.428E-03
	0.7885	5.995E-02	2.465E-03	3.536E-03
	0.7975	6.474E-02	3.131E-03	3.494E-03
	0.8065	5.761E-02	2.603E-03	2.957E-03
	0.8155	5.619E-02	2.915E-03	5.699E-03
	0.8245	4.418E-02	2.539E-03	7.209E-03
	0.8335	3.130E-02	2.053E-03	5.420E-03
	0.8425	2.237E-02	1.697E-03	3.528E-03
	0.8515	1.733E-02	1.325E-03	2.594E-03
	0.8605	1.308E-02	1.152E-03	1.933E-03
	0.8695	1.086E-02	9.604E-04	1.990E-03
	0.8785	6.372E-03	7.144E-04	1.430E-03
	0.8875	4.476E-03	4.602E-04	1.508E-04
	0.8965	1.753E-03	1.956E-04	5.323E-05
2.575	0.3745	2.648E-01	8.440E-03	2.953E-02
	0.3835	2.731E-01	5.809E-03	2.759E-02
	0.3925	2.501E-01	5.892E-03	2.336E-02
	0.4015	2.471E-01	4.359E-03	2.444E-02
	0.4105	2.380E-01	3.364E-03	2.186E-02
	0.4195	2.320E-01	3.473E-03	2.026E-02
	0.4285	2.343E-01	4.227E-03	2.178E-02
	0.4375	2.223E-01	2.696E-03	1.950E-02
	0.4465	2.066E-01	2.586E-03	1.753E-02
	0.4555	2.013E-01	2.674E-03	1.680E-02
	0.4645	2.030E-01	2.763E-03	1.597E-02
	0.4735	2.012E-01	2.760E-03	1.516E-02
	0.4825	1.927E-01	2.745E-03	1.373E-02
	0.4915	1.798E-01	2.663E-03	1.231E-02
	0.5005	1.739E-01	2.688E-03	1.160E-02
	0.5095	1.638E-01	2.642E-03	1.073E-02
	0.5185	1.574E-01	2.632E-03	9.998E-03
	0.5275	1.567E-01	2.643E-03	9.995E-03
	0.5365	1.619E-01	2.749E-03	1.111E-02
	0.5455	1.702E-01	2.898E-03	1.187E-02
	0.5545	1.799E-01	3.122E-03	1.095E-02
	0.5635	1.680E-01	2.978E-03	9.767E-03
	0.5725	1.492E-01	2.851E-03	1.012E-02
	0.5815	1.353E-01	2.706E-03	8.258E-03
	0.5905	1.195E-01	2.604E-03	6.656E-03
	0.5995	1.172E-01	2.653E-03	6.130E-03
	0.6085	1.053E-01	2.593E-03	5.766E-03
	0.6175	1.066E-01	2.665E-03	6.227E-03
	0.6265	1.088E-01	2.681E-03	7.060E-03
	0.6355	1.257E-01	3.025E-03	9.423E-03
	0.6445	1.320E-01	3.264E-03	7.750E-03
	0.6535	1.300E-01	3.290E-03	9.060E-03
	0.6625	1.046E-01	2.894E-03	9.111E-03
	0.6715	9.212E-02	2.597E-03	6.659E-03
	0.6805	7.771E-02	2.496E-03	4.595E-03
	0.6895	7.591E-02	2.468E-03	3.972E-03
	0.6985	6.693E-02	2.307E-03	3.185E-03
	0.7075	6.257E-02	2.310E-03	2.876E-03
	0.7165	5.605E-02	2.205E-03	2.423E-03
	0.7255	6.082E-02	2.466E-03	2.637E-03

	0.7345	5.851E-02	2.477E-03	3.319E-03
	0.7435	5.360E-02	2.390E-03	2.362E-03
	0.7525	5.194E-02	2.332E-03	2.576E-03
	0.7615	5.361E-02	2.440E-03	2.908E-03
	0.7705	5.919E-02	2.616E-03	3.025E-03
	0.7795	5.628E-02	2.693E-03	3.094E-03
	0.7885	5.955E-02	2.757E-03	3.518E-03
	0.7975	6.270E-02	3.193E-03	3.663E-03
	0.8065	5.843E-02	2.560E-03	3.239E-03
	0.8155	5.248E-02	2.397E-03	4.290E-03
	0.8245	4.022E-02	2.508E-03	5.959E-03
	0.8335	3.681E-02	2.215E-03	6.440E-03
	0.8425	2.355E-02	1.587E-03	3.668E-03
	0.8515	1.868E-02	1.459E-03	2.959E-03
	0.8605	1.283E-02	1.257E-03	1.869E-03
	0.8695	9.324E-03	9.109E-04	1.601E-03
	0.8785	7.016E-03	7.739E-04	1.459E-03
	0.8875	3.983E-03	4.595E-04	1.179E-03
	0.8965	2.649E-03	3.963E-04	9.020E-05
2.625	0.3835	2.748E-01	8.699E-03	3.017E-02
	0.3925	2.641E-01	5.813E-03	2.664E-02
	0.4015	2.447E-01	6.002E-03	2.301E-02
	0.4105	2.542E-01	4.979E-03	2.553E-02
	0.4195	2.291E-01	3.397E-03	2.112E-02
	0.4285	2.214E-01	3.468E-03	1.944E-02
	0.4375	2.268E-01	6.157E-03	2.209E-02
	0.4465	2.147E-01	2.773E-03	1.925E-02
	0.4555	1.990E-01	2.586E-03	1.712E-02
	0.4645	1.891E-01	2.611E-03	1.592E-02
	0.4735	1.962E-01	2.745E-03	1.512E-02
	0.4825	1.883E-01	2.725E-03	1.474E-02
	0.4915	1.780E-01	2.721E-03	1.263E-02
	0.5005	1.726E-01	2.671E-03	1.248E-02
	0.5095	1.675E-01	2.692E-03	1.126E-02
	0.5185	1.602E-01	2.632E-03	1.069E-02
	0.5275	1.474E-01	2.564E-03	9.504E-03
	0.5365	1.573E-01	2.739E-03	1.059E-02
	0.5455	1.607E-01	2.831E-03	1.224E-02
	0.5545	1.753E-01	3.036E-03	1.196E-02
	0.5635	1.731E-01	3.090E-03	1.018E-02
	0.5725	1.597E-01	2.946E-03	1.032E-02
	0.5815	1.402E-01	2.762E-03	9.523E-03
	0.5905	1.224E-01	2.607E-03	7.267E-03
	0.5995	1.089E-01	2.483E-03	6.016E-03
	0.6085	1.059E-01	2.541E-03	5.653E-03
	0.6175	1.045E-01	2.586E-03	6.381E-03
	0.6265	1.050E-01	2.664E-03	6.418E-03
	0.6355	1.152E-01	2.879E-03	8.331E-03
	0.6445	1.270E-01	3.181E-03	9.031E-03
	0.6535	1.329E-01	3.280E-03	6.729E-03
	0.6625	1.172E-01	3.090E-03	1.018E-02
	0.6715	9.652E-02	2.755E-03	7.830E-03
	0.6805	8.367E-02	2.575E-03	5.469E-03
	0.6895	7.034E-02	2.388E-03	3.867E-03
	0.6985	6.785E-02	2.353E-03	3.396E-03
	0.7075	6.297E-02	2.306E-03	3.032E-03
	0.7165	6.068E-02	2.289E-03	2.778E-03
	0.7255	5.413E-02	2.166E-03	2.482E-03
	0.7345	5.571E-02	2.226E-03	3.210E-03
	0.7435	5.363E-02	2.217E-03	2.323E-03
	0.7525	5.404E-02	2.391E-03	2.494E-03
	0.7615	4.842E-02	2.292E-03	2.562E-03
	0.7705	5.157E-02	2.337E-03	2.741E-03
	0.7795	4.839E-02	2.301E-03	2.574E-03
	0.7885	5.275E-02	2.529E-03	3.064E-03
	0.7975	5.217E-02	2.651E-03	3.132E-03
	0.8065	5.551E-02	2.745E-03	3.034E-03
	0.8155	5.169E-02	2.674E-03	3.304E-03
	0.8245	4.693E-02	2.578E-03	5.857E-03
	0.8335	3.226E-02	2.006E-03	5.539E-03
	0.8425	2.548E-02	1.714E-03	4.044E-03
	0.8515	1.762E-02	1.364E-03	2.893E-03
	0.8605	1.267E-02	1.256E-03	1.817E-03
	0.8695	8.883E-03	9.976E-04	1.432E-03
	0.8785	8.058E-03	9.034E-04	1.632E-03
	0.8875	4.325E-03	5.229E-04	1.183E-03
	0.8965	2.139E-03	2.549E-04	6.215E-05

2.675	0.4015	2.429E-01	5.723E-03	2.430E-02
	0.4105	2.288E-01	6.026E-03	2.148E-02
	0.4195	2.291E-01	5.403E-03	2.245E-02
	0.4285	2.241E-01	3.465E-03	2.084E-02
	0.4375	2.137E-01	3.477E-03	1.907E-02
	0.4465	2.045E-01	3.581E-03	1.743E-02
	0.4555	1.998E-01	2.913E-03	1.817E-02
	0.4645	1.950E-01	2.623E-03	1.722E-02
	0.4735	1.891E-01	2.645E-03	1.561E-02
	0.4825	1.831E-01	2.732E-03	1.454E-02
	0.4915	1.803E-01	2.749E-03	1.367E-02
	0.5005	1.731E-01	2.719E-03	1.264E-02
	0.5095	1.608E-01	2.634E-03	1.141E-02
	0.5185	1.594E-01	2.614E-03	1.093E-02
	0.5275	1.509E-01	2.629E-03	1.015E-02
	0.5365	1.501E-01	2.658E-03	1.021E-02
	0.5455	1.526E-01	2.743E-03	1.103E-02
	0.5545	1.667E-01	2.960E-03	1.213E-02
	0.5635	1.636E-01	3.009E-03	1.062E-02
	0.5725	1.634E-01	3.030E-03	1.010E-02
	0.5815	1.413E-01	2.806E-03	1.003E-02
	0.5905	1.245E-01	2.611E-03	7.997E-03
	0.5995	1.076E-01	2.453E-03	6.468E-03
	0.6085	1.023E-01	2.417E-03	5.661E-03
	0.6175	9.966E-02	2.435E-03	5.768E-03
	0.6265	1.011E-01	2.520E-03	6.185E-03
	0.6355	1.096E-01	2.713E-03	7.367E-03
	0.6445	1.228E-01	3.019E-03	9.431E-03
	0.6535	1.292E-01	3.316E-03	7.638E-03
	0.6625	1.167E-01	3.163E-03	8.705E-03
	0.6715	1.000E-01	2.851E-03	8.812E-03
	0.6805	7.924E-02	2.455E-03	5.741E-03
	0.6895	6.934E-02	2.342E-03	4.262E-03
	0.6985	6.877E-02	2.453E-03	3.792E-03
	0.7075	6.116E-02	2.342E-03	3.103E-03
	0.7165	6.230E-02	2.330E-03	3.002E-03
	0.7255	6.013E-02	2.311E-03	2.837E-03
	0.7345	5.323E-02	2.150E-03	2.595E-03
	0.7435	5.246E-02	2.177E-03	2.957E-03
	0.7525	4.998E-02	2.083E-03	2.264E-03
	0.7615	4.554E-02	2.058E-03	2.379E-03
	0.7705	5.210E-02	2.296E-03	2.798E-03
	0.7795	4.634E-02	2.136E-03	2.374E-03
	0.7885	5.123E-02	2.327E-03	2.900E-03
	0.7975	5.682E-02	2.606E-03	3.358E-03
	0.8065	5.508E-02	2.697E-03	3.343E-03
	0.8155	5.316E-02	2.492E-03	3.134E-03
	0.8245	4.715E-02	2.640E-03	4.995E-03
	0.8335	3.981E-02	2.269E-03	6.621E-03
	0.8425	2.446E-02	1.612E-03	4.141E-03
	0.8515	2.048E-02	1.489E-03	3.297E-03
	0.8605	1.862E-02	1.508E-03	2.699E-03
	0.8695	1.036E-02	1.122E-03	1.595E-03
	0.8785	7.927E-03	8.385E-04	1.536E-03
	0.8875	6.335E-03	6.107E-04	1.565E-03
	0.8965	2.641E-03	2.955E-04	8.080E-05
2.725	0.4105	2.372E-01	5.750E-03	2.365E-02
	0.4195	2.273E-01	6.160E-03	2.163E-02
	0.4285	2.260E-01	6.625E-03	2.253E-02
	0.4375	2.166E-01	3.587E-03	2.029E-02
	0.4465	2.042E-01	3.445E-03	1.821E-02
	0.4555	2.009E-01	3.614E-03	1.742E-02
	0.4645	2.007E-01	3.268E-03	1.877E-02
	0.4735	1.907E-01	2.708E-03	1.696E-02
	0.4825	1.859E-01	2.708E-03	1.517E-02
	0.4915	1.809E-01	2.706E-03	1.511E-02
	0.5005	1.696E-01	2.708E-03	1.295E-02
	0.5095	1.668E-01	2.741E-03	1.272E-02
	0.5185	1.596E-01	2.700E-03	1.144E-02
	0.5275	1.538E-01	2.632E-03	1.066E-02
	0.5365	1.462E-01	2.667E-03	9.942E-03
	0.5455	1.483E-01	2.722E-03	1.060E-02
	0.5545	1.555E-01	2.887E-03	1.222E-02
	0.5635	1.651E-01	3.021E-03	1.178E-02
	0.5725	1.591E-01	3.020E-03	1.001E-02
	0.5815	1.512E-01	2.975E-03	1.029E-02
	0.5905	1.348E-01	2.773E-03	9.478E-03

	0.5995	1.206E-01	2.631E-03	7.499E-03
	0.6085	1.049E-01	2.481E-03	6.294E-03
	0.6175	9.317E-02	2.364E-03	5.229E-03
	0.6265	9.793E-02	2.442E-03	6.273E-03
	0.6355	9.959E-02	2.537E-03	6.399E-03
	0.6445	1.074E-01	2.721E-03	7.970E-03
	0.6535	1.191E-01	2.983E-03	8.533E-03
	0.6625	1.206E-01	3.175E-03	6.633E-03
	0.6715	1.098E-01	2.933E-03	9.866E-03
	0.6805	8.175E-02	2.536E-03	6.624E-03
	0.6895	7.732E-02	2.525E-03	5.155E-03
	0.6985	6.659E-02	2.355E-03	3.813E-03
	0.7075	6.104E-02	2.258E-03	3.196E-03
	0.7165	5.872E-02	2.206E-03	2.943E-03
	0.7255	5.653E-02	2.200E-03	2.747E-03
	0.7345	5.039E-02	2.193E-03	2.444E-03
	0.7435	5.143E-02	2.162E-03	3.386E-03
	0.7525	5.230E-02	2.237E-03	2.469E-03
	0.7615	4.408E-02	1.938E-03	2.229E-03
	0.7705	5.130E-02	2.217E-03	2.832E-03
	0.7795	4.673E-02	2.202E-03	2.414E-03
	0.7885	4.609E-02	2.146E-03	2.606E-03
	0.7975	5.341E-02	2.456E-03	3.207E-03
	0.8065	5.087E-02	2.414E-03	3.084E-03
	0.8155	4.990E-02	2.545E-03	2.674E-03
	0.8245	4.548E-02	2.499E-03	3.959E-03
	0.8335	3.692E-02	2.053E-03	5.682E-03
	0.8425	2.970E-02	1.957E-03	5.212E-03
	0.8515	2.114E-02	1.473E-03	3.333E-03
	0.8605	1.476E-02	1.236E-03	2.184E-03
	0.8695	1.115E-02	9.745E-04	1.635E-03
	0.8785	7.918E-03	9.327E-04	1.458E-03
	0.8875	6.515E-03	6.508E-04	1.462E-03
	0.8965	4.488E-03	4.311E-04	2.182E-04
	0.9055	1.192E-03	1.593E-04	4.690E-05
2.775	0.4105	2.441E-01	9.453E-03	2.674E-02
	0.4195	2.206E-01	5.640E-03	2.213E-02
	0.4285	2.206E-01	6.243E-03	2.080E-02
	0.4375	2.430E-01	9.030E-03	2.540E-02
	0.4465	2.115E-01	3.703E-03	2.005E-02
	0.4555	1.967E-01	3.452E-03	1.782E-02
	0.4645	1.902E-01	3.618E-03	1.672E-02
	0.4735	1.894E-01	3.735E-03	1.767E-02
	0.4825	1.852E-01	2.793E-03	1.634E-02
	0.4915	1.777E-01	2.697E-03	1.480E-02
	0.5005	1.727E-01	2.712E-03	1.378E-02
	0.5095	1.675E-01	2.739E-03	1.290E-02
	0.5185	1.589E-01	2.737E-03	1.192E-02
	0.5275	1.496E-01	2.717E-03	1.084E-02
	0.5365	1.515E-01	2.708E-03	1.075E-02
	0.5455	1.468E-01	2.693E-03	1.027E-02
	0.5545	1.458E-01	2.790E-03	1.093E-02
	0.5635	1.601E-01	3.026E-03	1.227E-02
	0.5725	1.630E-01	3.115E-03	1.121E-02
	0.5815	1.532E-01	2.996E-03	1.007E-02
	0.5905	1.397E-01	2.868E-03	1.035E-02
	0.5995	1.216E-01	2.708E-03	8.174E-03
	0.6085	1.064E-01	2.540E-03	6.732E-03
	0.6175	9.681E-02	2.481E-03	5.632E-03
	0.6265	9.221E-02	2.379E-03	5.854E-03
	0.6355	9.910E-02	2.499E-03	6.324E-03
	0.6445	1.013E-01	2.601E-03	7.057E-03
	0.6535	1.104E-01	2.827E-03	8.707E-03
	0.6625	1.201E-01	3.128E-03	7.159E-03
	0.6715	1.128E-01	2.961E-03	9.068E-03
	0.6805	9.172E-02	2.596E-03	8.178E-03
	0.6895	7.625E-02	2.349E-03	5.523E-03
	0.6985	6.682E-02	2.289E-03	4.099E-03
	0.7075	6.258E-02	2.273E-03	3.701E-03
	0.7165	5.531E-02	2.184E-03	2.950E-03
	0.7255	5.646E-02	2.214E-03	2.797E-03
	0.7345	5.166E-02	2.216E-03	2.609E-03
	0.7435	5.326E-02	2.132E-03	3.098E-03
	0.7525	5.073E-02	2.261E-03	2.669E-03
	0.7615	4.592E-02	2.108E-03	2.235E-03
	0.7705	4.543E-02	2.044E-03	2.548E-03
	0.7795	4.602E-02	2.143E-03	2.488E-03

	0.7885	4.199E-02	2.112E-03	2.304E-03
	0.7975	4.529E-02	2.149E-03	2.694E-03
	0.8065	5.421E-02	2.536E-03	3.471E-03
	0.8155	5.305E-02	2.526E-03	3.027E-03
	0.8245	4.540E-02	2.406E-03	3.241E-03
	0.8335	4.311E-02	2.216E-03	5.741E-03
	0.8425	2.874E-02	1.738E-03	4.978E-03
	0.8515	1.904E-02	1.345E-03	2.997E-03
	0.8605	1.259E-02	1.134E-03	2.015E-03
	0.8695	1.043E-02	1.054E-03	1.526E-03
	0.8785	1.137E-02	9.305E-04	1.974E-03
	0.8875	6.215E-03	7.055E-04	1.325E-03
	0.8965	4.927E-03	6.456E-04	2.109E-04
	0.9055	1.168E-03	2.013E-04	4.011E-05
2.825	0.4195	2.361E-01	9.753E-03	2.582E-02
	0.4285	2.222E-01	5.800E-03	2.230E-02
	0.4375	2.177E-01	6.235E-03	2.068E-02
	0.4465	2.032E-01	1.219E-02	2.078E-02
	0.4555	2.004E-01	3.840E-03	1.916E-02
	0.4645	1.917E-01	3.493E-03	1.749E-02
	0.4735	1.899E-01	3.591E-03	1.687E-02
	0.4825	1.912E-01	5.496E-03	1.858E-02
	0.4915	1.816E-01	2.888E-03	1.603E-02
	0.5005	1.700E-01	2.724E-03	1.508E-02
	0.5095	1.639E-01	2.741E-03	1.329E-02
	0.5185	1.571E-01	2.744E-03	1.240E-02
	0.5275	1.497E-01	2.707E-03	1.136E-02
	0.5365	1.421E-01	2.620E-03	1.046E-02
	0.5455	1.416E-01	2.708E-03	1.014E-02
	0.5545	1.427E-01	2.763E-03	1.065E-02
	0.5635	1.496E-01	2.842E-03	1.227E-02
	0.5725	1.544E-01	3.001E-03	1.142E-02
	0.5815	1.595E-01	3.136E-03	1.061E-02
	0.5905	1.467E-01	3.022E-03	1.065E-02
	0.5995	1.258E-01	2.769E-03	9.342E-03
	0.6085	1.115E-01	2.582E-03	7.243E-03
	0.6175	9.813E-02	2.462E-03	6.384E-03
	0.6265	9.342E-02	2.483E-03	5.553E-03
	0.6355	9.264E-02	2.440E-03	6.255E-03
	0.6445	9.515E-02	2.541E-03	6.422E-03
	0.6535	1.037E-01	2.756E-03	7.942E-03
	0.6625	1.161E-01	3.035E-03	8.360E-03
	0.6715	1.131E-01	3.033E-03	6.956E-03
	0.6805	1.000E-01	2.794E-03	9.257E-03
	0.6895	8.140E-02	2.453E-03	6.542E-03
	0.6985	6.913E-02	2.308E-03	4.658E-03
	0.7075	6.116E-02	2.150E-03	3.541E-03
	0.7165	5.693E-02	2.104E-03	3.017E-03
	0.7255	5.518E-02	2.196E-03	2.921E-03
	0.7345	5.041E-02	2.082E-03	2.593E-03
	0.7435	4.909E-02	2.155E-03	2.486E-03
	0.7525	4.748E-02	2.095E-03	3.060E-03
	0.7615	4.165E-02	2.017E-03	2.121E-03
	0.7705	4.479E-02	2.080E-03	2.390E-03
	0.7795	4.635E-02	2.204E-03	2.599E-03
	0.7885	4.706E-02	2.250E-03	2.558E-03
	0.7975	4.720E-02	2.216E-03	2.800E-03
	0.8065	5.236E-02	2.495E-03	3.351E-03
	0.8155	5.090E-02	2.579E-03	3.136E-03
	0.8245	4.791E-02	2.322E-03	3.058E-03
	0.8335	4.342E-02	2.371E-03	5.057E-03
	0.8425	3.419E-02	1.938E-03	5.837E-03
	0.8515	2.198E-02	1.583E-03	3.605E-03
	0.8605	1.794E-02	1.357E-03	2.852E-03
	0.8695	1.268E-02	1.135E-03	1.823E-03
	0.8785	6.256E-03	7.192E-04	1.028E-03
	0.8875	5.096E-03	5.625E-04	1.020E-03
	0.8965	2.831E-03	3.134E-04	8.434E-04
	0.9055	8.806E-04	1.744E-04	2.318E-05
2.875	0.4285	2.288E-01	1.054E-02	2.510E-02
	0.4375	2.282E-01	6.032E-03	2.292E-02
	0.4465	2.040E-01	6.289E-03	1.959E-02
	0.4555	2.037E-01	6.472E-03	1.870E-02
	0.4645	2.033E-01	4.266E-03	1.963E-02
	0.4735	1.855E-01	3.542E-03	1.703E-02
	0.4825	1.742E-01	3.501E-03	1.572E-02
	0.4915	1.708E-01	3.649E-03	1.463E-02

	0.5005	1.704E-01	3.046E-03	1.531E-02
	0.5095	1.677E-01	2.767E-03	1.392E-02
	0.5185	1.617E-01	2.744E-03	1.316E-02
	0.5275	1.548E-01	2.708E-03	1.217E-02
	0.5365	1.470E-01	2.718E-03	1.113E-02
	0.5455	1.422E-01	2.713E-03	1.072E-02
	0.5545	1.389E-01	2.756E-03	1.049E-02
	0.5635	1.383E-01	2.800E-03	1.100E-02
	0.5725	1.508E-01	2.978E-03	1.220E-02
	0.5815	1.618E-01	3.141E-03	1.146E-02
	0.5905	1.475E-01	3.025E-03	1.009E-02
	0.5995	1.387E-01	2.933E-03	1.094E-02
	0.6085	1.112E-01	2.625E-03	7.774E-03
	0.6175	1.008E-01	2.570E-03	6.750E-03
	0.6265	9.576E-02	2.472E-03	5.845E-03
	0.6355	9.076E-02	2.449E-03	6.473E-03
	0.6445	8.922E-02	2.447E-03	5.847E-03
	0.6535	9.802E-02	2.680E-03	7.156E-03
	0.6625	1.033E-01	2.815E-03	8.239E-03
	0.6715	1.157E-01	3.143E-03	6.956E-03
	0.6805	1.043E-01	2.921E-03	9.118E-03
	0.6895	8.650E-02	2.541E-03	7.708E-03
	0.6985	6.582E-02	2.231E-03	4.779E-03
	0.7075	6.521E-02	2.244E-03	4.074E-03
	0.7165	5.897E-02	2.185E-03	3.482E-03
	0.7255	5.484E-02	2.151E-03	3.004E-03
	0.7345	5.339E-02	2.066E-03	2.870E-03
	0.7435	4.778E-02	2.010E-03	2.449E-03
	0.7525	4.501E-02	1.939E-03	3.014E-03
	0.7615	4.556E-02	2.010E-03	2.306E-03
	0.7705	4.017E-02	1.918E-03	2.128E-03
	0.7795	3.827E-02	1.917E-03	2.185E-03
	0.7885	4.683E-02	2.208E-03	2.512E-03
	0.7975	4.365E-02	2.126E-03	2.579E-03
	0.8065	4.883E-02	2.374E-03	2.967E-03
	0.8155	4.876E-02	2.421E-03	3.222E-03
	0.8245	4.813E-02	2.535E-03	2.850E-03
	0.8335	4.542E-02	2.493E-03	4.503E-03
	0.8425	3.462E-02	2.143E-03	5.666E-03
	0.8515	2.410E-02	1.627E-03	4.214E-03
	0.8605	1.860E-02	1.439E-03	2.974E-03
	0.8695	1.129E-02	1.076E-03	1.610E-03
	0.8785	1.009E-02	9.859E-04	1.580E-03
	0.8875	6.150E-03	6.375E-04	1.190E-03
	0.8965	4.007E-03	4.608E-04	1.091E-03
	0.9055	1.684E-03	1.762E-04	5.003E-05
2.925	0.4375	2.227E-01	1.112E-02	2.403E-02
	0.4465	2.082E-01	5.966E-03	2.130E-02
	0.4555	2.082E-01	6.325E-03	2.009E-02
	0.4645	1.867E-01	6.467E-03	1.715E-02
	0.4735	1.912E-01	4.554E-03	1.861E-02
	0.4825	1.802E-01	3.629E-03	1.693E-02
	0.4915	1.708E-01	3.497E-03	1.555E-02
	0.5005	1.670E-01	3.694E-03	1.410E-02
	0.5095	1.782E-01	3.559E-03	1.718E-02
	0.5185	1.616E-01	2.824E-03	1.392E-02
	0.5275	1.482E-01	2.713E-03	1.252E-02
	0.5365	1.413E-01	2.668E-03	1.133E-02
	0.5455	1.384E-01	2.685E-03	1.068E-02
	0.5545	1.337E-01	2.725E-03	1.017E-02
	0.5635	1.315E-01	2.735E-03	1.053E-02
	0.5725	1.415E-01	2.930E-03	1.200E-02
	0.5815	1.520E-01	3.125E-03	1.169E-02
	0.5905	1.499E-01	3.134E-03	1.047E-02
	0.5995	1.306E-01	2.839E-03	1.000E-02
	0.6085	1.225E-01	2.805E-03	9.296E-03
	0.6175	1.007E-01	2.498E-03	6.860E-03
	0.6265	9.929E-02	2.552E-03	7.279E-03
	0.6355	9.008E-02	2.448E-03	5.734E-03
	0.6445	9.371E-02	2.557E-03	6.574E-03
	0.6535	9.031E-02	2.526E-03	6.338E-03
	0.6625	9.845E-02	2.766E-03	7.871E-03
	0.6715	1.103E-01	3.015E-03	7.925E-03
	0.6805	1.056E-01	3.064E-03	7.661E-03
	0.6895	9.261E-02	2.795E-03	8.765E-03
	0.6985	7.388E-02	2.393E-03	5.881E-03
	0.7075	6.545E-02	2.214E-03	4.382E-03
	0.7165	5.984E-02	2.281E-03	3.759E-03
	0.7255	4.987E-02	2.111E-03	2.831E-03
	0.7345	4.622E-02	1.984E-03	2.542E-03
	0.7435	4.727E-02	2.024E-03	2.512E-03
	0.7525	4.799E-02	2.109E-03	2.866E-03
	0.7615	4.796E-02	2.051E-03	2.810E-03
	0.7705	4.760E-02	2.126E-03	2.432E-03
	0.7795	4.304E-02	2.109E-03	2.429E-03
	0.7885	3.893E-02	1.940E-03	2.144E-03
	0.7975	4.068E-02	1.969E-03	2.376E-03
	0.8065	4.391E-02	2.261E-03	2.727E-03
	0.8155	4.609E-02	2.382E-03	3.130E-03
	0.8245	4.565E-02	2.485E-03	2.760E-03
	0.8335	4.851E-02	2.543E-03	4.017E-03
	0.8425	3.267E-02	2.010E-03	4.814E-03
	0.8515	2.378E-02	1.630E-03	4.159E-03
	0.8605	1.921E-02	1.440E-03	3.080E-03
	0.8695	1.395E-02	1.186E-03	2.025E-03
	0.8785	1.123E-02	1.017E-03	1.709E-03
	0.8875	6.774E-03	7.381E-04	1.269E-03
	0.8965	4.796E-03	5.186E-04	1.211E-03
	0.9055	1.697E-03	3.384E-04	7.095E-05
2.975	0.4465	2.039E-01	1.205E-02	2.227E-02
	0.4555	2.052E-01	6.081E-03	2.070E-02
	0.4645	1.999E-01	6.277E-03	1.925E-02
	0.4735	1.923E-01	6.588E-03	1.789E-02
	0.4825	1.894E-01	5.175E-03	1.903E-02
	0.4915	1.750E-01	3.787E-03	1.653E-02
	0.5005	1.686E-01	3.606E-03	1.500E-02
	0.5095	1.598E-01	3.612E-03	1.377E-02
	0.5185	1.721E-01	4.580E-03	1.603E-02
	0.5275	1.559E-01	2.879E-03	1.355E-02
	0.5365	1.473E-01	2.760E-03	1.229E-02
	0.5455	1.371E-01	2.653E-03	1.102E-02
	0.5545	1.354E-01	2.712E-03	1.081E-02
	0.5635	1.306E-01	2.709E-03	1.045E-02
	0.5725	1.324E-01	2.810E-03	1.079E-02
	0.5815	1.367E-01	2.952E-03	1.162E-02
	0.5905	1.447E-01	3.099E-03	1.078E-02
	0.5995	1.363E-01	2.957E-03	9.748E-03
	0.6085	1.230E-01	2.819E-03	1.015E-02
	0.6175	1.068E-01	2.613E-03	7.617E-03
	0.6265	9.390E-02	2.453E-03	6.965E-03
	0.6355	9.063E-02	2.445E-03	5.887E-03
	0.6445	8.624E-02	2.419E-03	6.570E-03
	0.6535	9.056E-02	2.573E-03	6.295E-03
	0.6625	8.953E-02	2.590E-03	6.974E-03
	0.6715	1.046E-01	2.932E-03	8.415E-03
	0.6805	1.105E-01	3.155E-03	6.814E-03
	0.6895	1.004E-01	2.913E-03	9.397E-03
	0.6985	7.987E-02	2.593E-03	6.964E-03
	0.7075	7.369E-02	2.481E-03	5.268E-03
	0.7165	5.677E-02	2.168E-03	3.558E-03
	0.7255	5.596E-02	2.170E-03	3.338E-03
	0.7345	5.237E-02	2.099E-03	3.001E-03
	0.7435	4.766E-02	2.098E-03	2.627E-03
	0.7525	4.703E-02	2.052E-03	2.635E-03
	0.7615	3.978E-02	1.860E-03	2.789E-03
	0.7705	4.313E-02	1.977E-03	2.250E-03
	0.7795	4.419E-02	2.005E-03	2.496E-03
	0.7885	3.882E-02	1.935E-03	2.245E-03
	0.7975	4.180E-02	1.990E-03	2.301E-03
	0.8065	4.089E-02	2.123E-03	2.482E-03
	0.8155	4.818E-02	2.294E-03	3.206E-03
	0.8245	5.254E-02	2.523E-03	3.414E-03
	0.8335	3.799E-02	2.162E-03	2.633E-03
	0.8425	4.100E-02	2.280E-03	5.400E-03
	0.8515	2.604E-02	1.668E-03	4.517E-03
	0.8605	2.195E-02	1.598E-03	3.542E-03
	0.8695	1.209E-02	1.098E-03	1.806E-03
	0.8785	1.116E-02	9.859E-04	1.650E-03
	0.8875	7.436E-03	7.833E-04	1.332E-03
	0.8965	4.667E-03	5.534E-04	1.087E-03
	0.9055	3.055E-03	4.925E-04	1.381E-04
3.025	0.4735	1.932E-01	6.243E-03	1.892E-02
	0.4825	1.799E-01	6.526E-03	1.676E-02
	0.4915	1.823E-01	6.265E-03	1.819E-02

	0.5005	1.688E-01	3.934E-03	1.625E-02
	0.5095	1.628E-01	3.665E-03	1.439E-02
	0.5185	1.589E-01	3.609E-03	1.450E-02
	0.5275	1.500E-01	3.706E-03	1.241E-02
	0.5365	1.458E-01	3.035E-03	1.329E-02
	0.5455	1.389E-01	2.733E-03	1.173E-02
	0.5545	1.355E-01	2.741E-03	1.105E-02
	0.5635	1.274E-01	2.703E-03	1.028E-02
	0.5725	1.293E-01	2.771E-03	1.101E-02
	0.5815	1.365E-01	2.902E-03	1.216E-02
	0.5905	1.435E-01	3.065E-03	1.159E-02
	0.5995	1.412E-01	3.089E-03	1.048E-02
	0.6085	1.272E-01	2.917E-03	1.041E-02
	0.6175	1.039E-01	2.645E-03	8.082E-03
	0.6265	9.398E-02	2.488E-03	6.810E-03
	0.6355	8.985E-02	2.508E-03	6.735E-03
	0.6445	8.471E-02	2.400E-03	5.556E-03
	0.6535	8.042E-02	2.399E-03	5.628E-03
	0.6625	9.445E-02	2.712E-03	7.090E-03
	0.6715	9.544E-02	2.872E-03	7.928E-03
	0.6805	1.143E-01	3.259E-03	8.295E-03
	0.6895	1.014E-01	3.025E-03	8.408E-03
	0.6985	8.578E-02	2.698E-03	8.134E-03
	0.7075	6.842E-02	2.362E-03	5.361E-03
	0.7165	6.395E-02	2.303E-03	4.345E-03
	0.7255	5.076E-02	2.069E-03	3.372E-03
	0.7345	4.867E-02	2.037E-03	2.867E-03
	0.7435	4.786E-02	2.147E-03	2.739E-03
	0.7525	4.507E-02	2.001E-03	2.462E-03
	0.7615	4.261E-02	1.945E-03	3.078E-03
	0.7705	3.972E-02	1.863E-03	2.163E-03
	0.7795	4.208E-02	1.958E-03	2.378E-03
	0.7885	3.980E-02	1.882E-03	2.343E-03
	0.7975	3.966E-02	1.953E-03	2.250E-03
	0.8065	4.224E-02	2.103E-03	2.686E-03
	0.8155	4.118E-02	2.159E-03	2.650E-03
	0.8245	4.108E-02	2.249E-03	2.757E-03
	0.8335	4.125E-02	2.284E-03	2.637E-03
	0.8425	3.494E-02	2.129E-03	4.024E-03
	0.8515	2.824E-02	1.767E-03	4.827E-03
	0.8605	1.912E-02	1.382E-03	3.221E-03
	0.8695	1.490E-02	1.129E-03	2.326E-03
	0.8785	1.020E-02	9.424E-04	1.489E-03
	0.8875	7.546E-03	7.565E-04	1.292E-03
	0.8965	4.828E-03	5.538E-04	1.059E-03
	0.9055	2.650E-03	4.662E-04	2.052E-04
	0.9145	5.674E-04	1.154E-04	2.461E-05
3.075	0.4645	2.102E-01	1.616E-02	2.418E-02
	0.4735	1.853E-01	6.412E-03	1.899E-02
	0.4825	1.807E-01	6.052E-03	1.749E-02
	0.4915	1.745E-01	6.556E-03	1.666E-02
	0.5005	1.863E-01	9.419E-03	1.978E-02
	0.5095	1.570E-01	4.021E-03	1.483E-02
	0.5185	1.602E-01	3.790E-03	1.486E-02
	0.5275	1.551E-01	3.662E-03	1.338E-02
	0.5365	1.486E-01	3.729E-03	1.234E-02
	0.5455	1.394E-01	3.330E-03	1.274E-02
	0.5545	1.324E-01	2.784E-03	1.150E-02
	0.5635	1.282E-01	2.707E-03	1.068E-02
	0.5725	1.256E-01	2.682E-03	1.079E-02
	0.5815	1.245E-01	2.734E-03	1.084E-02
	0.5905	1.404E-01	3.097E-03	1.218E-02
	0.5995	1.382E-01	3.108E-03	1.054E-02
	0.6085	1.320E-01	3.004E-03	1.002E-02
	0.6175	1.147E-01	2.791E-03	9.708E-03
	0.6265	1.005E-01	2.669E-03	7.496E-03
	0.6355	8.711E-02	2.449E-03	7.085E-03
	0.6445	8.016E-02	2.386E-03	5.465E-03
	0.6535	7.646E-02	2.364E-03	6.257E-03
	0.6625	7.618E-02	2.353E-03	5.430E-03
	0.6715	9.284E-02	2.692E-03	7.561E-03
	0.6805	1.041E-01	3.006E-03	8.417E-03
	0.6895	1.015E-01	3.055E-03	7.136E-03
	0.6985	8.275E-02	2.690E-03	8.002E-03
	0.7075	7.274E-02	2.483E-03	6.127E-03
	0.7165	5.959E-02	2.220E-03	4.305E-03
	0.7255	5.691E-02	2.206E-03	3.773E-03
	0.7345	5.343E-02	2.195E-03	3.232E-03
	0.7435	4.657E-02	2.088E-03	2.763E-03
	0.7525	4.583E-02	2.051E-03	2.676E-03
	0.7615	4.261E-02	2.021E-03	2.844E-03
	0.7705	4.122E-02	1.943E-03	2.627E-03
	0.7795	3.985E-02	1.980E-03	2.199E-03
	0.7885	3.614E-02	1.868E-03	2.114E-03
	0.7975	3.864E-02	2.007E-03	2.232E-03
	0.8065	3.722E-02	1.891E-03	2.398E-03
	0.8155	4.122E-02	2.132E-03	2.634E-03
	0.8245	4.177E-02	2.280E-03	3.034E-03
	0.8335	4.492E-02	3.170E-03	2.807E-03
	0.8425	3.672E-02	2.073E-03	3.663E-03
	0.8515	2.930E-02	1.867E-03	4.892E-03
	0.8605	2.020E-02	1.450E-03	3.532E-03
	0.8695	1.351E-02	1.122E-03	2.135E-03
	0.8785	1.022E-02	9.717E-04	1.475E-03
	0.8875	7.554E-03	7.754E-04	1.235E-03
	0.8965	6.043E-03	6.726E-04	1.249E-03
	0.9055	5.231E-03	6.796E-04	4.371E-04
	0.9145	9.600E-04	1.482E-04	4.010E-05
3.125	0.4735	2.076E-01	1.924E-02	2.332E-02
	0.4825	1.935E-01	6.863E-03	1.997E-02
	0.4915	1.682E-01	6.004E-03	1.630E-02
	0.5005	1.814E-01	6.648E-03	1.739E-02
	0.5095	1.687E-01	6.778E-03	1.565E-02
	0.5185	1.530E-01	4.252E-03	1.469E-02
	0.5275	1.580E-01	3.903E-03	1.504E-02
	0.5365	1.473E-01	3.719E-03	1.268E-02
	0.5455	1.379E-01	3.625E-03	1.173E-02
	0.5545	1.421E-01	4.571E-03	1.340E-02
	0.5635	1.264E-01	2.842E-03	1.127E-02
	0.5725	1.227E-01	2.755E-03	1.048E-02
	0.5815	1.276E-01	2.820E-03	1.138E-02
	0.5905	1.290E-01	2.908E-03	1.192E-02
	0.5995	1.358E-01	3.044E-03	1.121E-02
	0.6085	1.327E-01	3.105E-03	1.046E-02
	0.6175	1.130E-01	2.813E-03	9.982E-03
	0.6265	1.052E-01	2.716E-03	8.392E-03
	0.6355	8.873E-02	2.481E-03	7.585E-03
	0.6445	8.322E-02	2.405E-03	6.134E-03
	0.6535	8.164E-02	2.442E-03	6.221E-03
	0.6625	8.087E-02	2.458E-03	5.876E-03
	0.6715	9.168E-02	2.672E-03	7.260E-03
	0.6805	9.450E-02	2.856E-03	8.022E-03
	0.6895	1.043E-01	3.099E-03	7.464E-03
	0.6985	9.687E-02	3.009E-03	8.943E-03
	0.7075	7.284E-02	2.506E-03	6.772E-03
	0.7165	6.079E-02	2.309E-03	5.632E-03
	0.7255	5.402E-02	2.200E-03	3.686E-03
	0.7345	4.548E-02	2.048E-03	2.913E-03
	0.7435	4.776E-02	2.129E-03	2.872E-03
	0.7525	4.620E-02	2.033E-03	2.743E-03
	0.7615	4.332E-02	2.054E-03	2.551E-03
	0.7705	4.211E-02	2.062E-03	3.097E-03
	0.7795	3.962E-02	1.969E-03	2.268E-03
	0.7885	3.748E-02	1.854E-03	2.212E-03
	0.7975	4.113E-02	2.077E-03	2.511E-03
	0.8065	3.525E-02	1.925E-03	2.158E-03
	0.8155	4.271E-02	2.153E-03	2.777E-03
	0.8245	3.776E-02	2.085E-03	2.764E-03
	0.8335	3.767E-02	2.147E-03	2.535E-03
	0.8425	3.690E-02	2.155E-03	3.163E-03
	0.8515	2.738E-02	1.790E-03	4.170E-03
	0.8605	2.531E-02	1.559E-03	4.433E-03
	0.8695	1.468E-02	1.155E-03	2.378E-03
	0.8785	9.753E-03	1.036E-03	1.400E-03
	0.8875	1.054E-02	1.392E-03	1.690E-03
	0.8965	5.213E-03	6.079E-04	1.019E-03
	0.9055	2.019E-03	3.851E-04	6.077E-04
	0.9145	9.825E-04	1.776E-04	3.159E-05
3.175	0.4825	1.908E-01	2.257E-02	2.221E-02
	0.4915	1.815E-01	7.009E-03	1.896E-02
	0.5005	1.582E-01	5.947E-03	1.556E-02
	0.5095	1.556E-01	6.202E-03	1.516E-02
	0.5185	1.513E-01	6.511E-03	1.371E-02
	0.5275	1.425E-01	4.547E-03	1.506E-02

	0.5365	1.453E-01	3.853E-03	1.328E-02
	0.5455	1.371E-01	3.760E-03	1.198E-02
	0.5545	1.321E-01	3.582E-03	1.118E-02
	0.5635	1.244E-01	3.587E-03	1.046E-02
	0.5725	1.320E-01	3.072E-03	1.216E-02
	0.5815	1.212E-01	2.769E-03	1.119E-02
	0.5905	1.253E-01	2.947E-03	1.189E-02
	0.5995	1.358E-01	3.144E-03	1.206E-02
	0.6085	1.284E-01	3.002E-03	1.023E-02
	0.6175	1.238E-01	2.985E-03	1.008E-02
	0.6265	1.105E-01	2.822E-03	9.419E-03
	0.6355	9.319E-02	2.587E-03	7.100E-03
	0.6445	8.014E-02	2.492E-03	7.490E-03
	0.6535	7.801E-02	2.402E-03	5.515E-03
	0.6625	7.620E-02	2.438E-03	6.261E-03
	0.6715	8.133E-02	2.603E-03	6.270E-03
	0.6805	8.670E-02	2.677E-03	7.477E-03
	0.6895	8.970E-02	2.891E-03	7.154E-03
	0.6985	9.831E-02	3.025E-03	8.019E-03
	0.7075	7.658E-02	2.585E-03	7.444E-03
	0.7165	5.999E-02	2.264E-03	5.093E-03
	0.7255	5.162E-02	2.110E-03	3.734E-03
	0.7345	5.116E-02	2.112E-03	3.769E-03
	0.7435	4.947E-02	2.147E-03	3.128E-03
	0.7525	4.539E-02	2.109E-03	2.848E-03
	0.7615	3.980E-02	1.972E-03	2.403E-03
	0.7705	3.817E-02	1.938E-03	2.965E-03
	0.7795	4.096E-02	2.077E-03	2.453E-03
	0.7885	3.753E-02	1.996E-03	2.131E-03
	0.7975	3.586E-02	1.903E-03	2.152E-03
	0.8065	3.749E-02	2.029E-03	2.302E-03
	0.8155	3.901E-02	2.074E-03	2.603E-03
	0.8245	3.820E-02	2.153E-03	2.732E-03
	0.8335	4.223E-02	2.425E-03	3.093E-03
	0.8425	3.973E-02	2.243E-03	2.936E-03
	0.8515	3.030E-02	1.856E-03	4.134E-03
	0.8605	2.063E-02	1.577E-03	3.594E-03
	0.8695	1.587E-02	1.231E-03	2.635E-03
	0.8785	1.108E-02	9.497E-04	1.574E-03
	0.8875	8.691E-03	7.689E-04	1.329E-03
	0.8965	4.941E-03	7.493E-04	9.284E-04
	0.9055	2.786E-03	5.544E-04	7.786E-04
	0.9145	1.003E-03	1.666E-04	2.866E-05
3.225	0.5005	1.728E-01	7.365E-03	1.820E-02
	0.5095	1.615E-01	6.150E-03	1.646E-02
	0.5185	1.513E-01	6.073E-03	1.459E-02
	0.5275	1.500E-01	6.691E-03	1.361E-02
	0.5365	1.431E-01	5.597E-03	1.498E-02
	0.5455	1.419E-01	3.967E-03	1.313E-02
	0.5545	1.287E-01	3.726E-03	1.151E-02
	0.5635	1.246E-01	3.575E-03	1.065E-02
	0.5725	1.181E-01	3.453E-03	9.999E-03
	0.5815	1.167E-01	3.611E-03	9.898E-03
	0.5905	1.267E-01	2.931E-03	1.230E-02
	0.5995	1.224E-01	2.932E-03	1.188E-02
	0.6085	1.325E-01	3.154E-03	1.140E-02
	0.6175	1.227E-01	3.053E-03	1.009E-02
	0.6265	1.142E-01	2.897E-03	1.067E-02
	0.6355	9.220E-02	2.587E-03	7.313E-03
	0.6445	8.742E-02	2.591E-03	8.238E-03
	0.6535	7.998E-02	2.501E-03	5.900E-03
	0.6625	7.747E-02	2.458E-03	7.180E-03
	0.6715	8.019E-02	2.550E-03	6.170E-03
	0.6805	7.904E-02	2.583E-03	6.709E-03
	0.6895	9.196E-02	2.958E-03	7.946E-03
	0.6985	9.185E-02	2.977E-03	6.723E-03
	0.7075	8.235E-02	2.714E-03	8.123E-03
	0.7165	6.775E-02	2.464E-03	6.165E-03
	0.7255	5.861E-02	2.245E-03	4.945E-03
	0.7345	5.337E-02	2.106E-03	3.735E-03
	0.7435	4.447E-02	2.043E-03	2.957E-03
	0.7525	4.793E-02	2.179E-03	2.985E-03
	0.7615	4.363E-02	2.008E-03	2.765E-03
	0.7705	3.227E-02	1.824E-03	2.391E-03
	0.7795	3.808E-02	1.963E-03	2.548E-03
	0.7885	3.802E-02	2.025E-03	2.280E-03
	0.7975	3.424E-02	1.945E-03	2.188E-03

	0.8065	3.440E-02	2.052E-03	2.112E-03
	0.8155	3.092E-02	1.820E-03	2.172E-03
	0.8245	3.568E-02	2.011E-03	2.440E-03
	0.8335	4.096E-02	2.190E-03	3.193E-03
	0.8425	3.525E-02	2.221E-03	2.439E-03
	0.8515	2.689E-02	1.771E-03	3.273E-03
	0.8605	2.233E-02	1.573E-03	3.857E-03
	0.8695	1.710E-02	1.337E-03	2.830E-03
	0.8785	9.582E-03	9.576E-04	1.440E-03
	0.8875	1.004E-02	9.407E-04	1.502E-03
	0.8965	5.700E-03	6.663E-04	1.034E-03
	0.9055	4.118E-03	6.941E-04	1.078E-03
3.275	0.5095	1.619E-01	7.834E-03	1.740E-02
	0.5185	1.585E-01	6.081E-03	1.599E-02
	0.5275	1.516E-01	6.244E-03	1.432E-02
	0.5365	1.453E-01	6.533E-03	1.489E-02
	0.5455	1.388E-01	6.636E-03	1.222E-02
	0.5545	1.324E-01	3.993E-03	1.276E-02
	0.5635	1.214E-01	3.752E-03	1.075E-02
	0.5725	1.228E-01	3.755E-03	1.072E-02
	0.5815	1.159E-01	3.502E-03	9.677E-03
	0.5905	1.189E-01	3.698E-03	1.083E-02
	0.5995	1.168E-01	3.916E-03	1.076E-02
	0.6085	1.341E-01	3.237E-03	1.224E-02
	0.6175	1.227E-01	3.117E-03	1.035E-02
	0.6265	1.131E-01	2.966E-03	1.011E-02
	0.6355	1.005E-01	2.726E-03	8.761E-03
	0.6445	8.421E-02	2.506E-03	7.188E-03
	0.6535	7.271E-02	2.382E-03	6.834E-03
	0.6625	7.493E-02	2.442E-03	5.564E-03
	0.6715	7.666E-02	2.493E-03	5.862E-03
	0.6805	8.083E-02	2.665E-03	6.610E-03
	0.6895	8.680E-02	2.810E-03	7.768E-03
	0.6985	9.723E-02	3.220E-03	7.732E-03
	0.7075	9.472E-02	3.150E-03	8.598E-03
	0.7165	7.333E-02	2.582E-03	7.162E-03
	0.7255	5.823E-02	2.277E-03	5.481E-03
	0.7345	5.015E-02	2.105E-03	3.694E-03
	0.7435	4.379E-02	1.984E-03	2.993E-03
	0.7525	4.030E-02	2.020E-03	2.658E-03
	0.7615	3.999E-02	1.969E-03	2.783E-03
	0.7705	3.913E-02	1.992E-03	2.645E-03
	0.7795	3.430E-02	1.828E-03	2.617E-03
	0.7885	3.594E-02	1.901E-03	2.214E-03
	0.7975	3.617E-02	1.942E-03	2.268E-03
	0.8065	3.668E-02	1.967E-03	2.228E-03
	0.8155	3.778E-02	2.044E-03	2.867E-03
	0.8245	3.491E-02	1.999E-03	2.392E-03
	0.8335	3.442E-02	2.068E-03	2.745E-03
	0.8425	3.122E-02	2.037E-03	2.131E-03
	0.8515	3.103E-02	1.987E-03	3.327E-03
	0.8605	2.216E-02	1.627E-03	3.775E-03
	0.8695	1.756E-02	1.333E-03	3.057E-03
	0.8785	1.321E-02	1.160E-03	2.010E-03
	0.8875	8.111E-03	8.613E-04	1.206E-03
	0.8965	6.226E-03	7.339E-04	1.090E-03
	0.9055	3.998E-03	7.253E-04	9.993E-04
3.325	0.5185	1.678E-01	9.223E-03	1.913E-02
	0.5275	1.483E-01	6.103E-03	1.495E-02
	0.5365	1.602E-01	6.431E-03	1.512E-02
	0.5455	1.432E-01	6.335E-03	1.319E-02
	0.5545	1.309E-01	6.574E-03	1.178E-02
	0.5635	1.358E-01	4.380E-03	1.347E-02
	0.5725	1.156E-01	3.657E-03	1.054E-02
	0.5815	1.102E-01	3.710E-03	9.672E-03
	0.5905	1.153E-01	3.672E-03	1.037E-02
	0.5995	1.067E-01	3.561E-03	9.812E-03
	0.6085	1.157E-01	3.883E-03	1.100E-02
	0.6175	1.269E-01	3.215E-03	1.160E-02
	0.6265	1.176E-01	3.122E-03	1.032E-02
	0.6355	1.038E-01	2.855E-03	9.858E-03
	0.6445	8.714E-02	2.581E-03	7.212E-03
	0.6535	7.581E-02	2.463E-03	7.824E-03
	0.6625	6.839E-02	2.335E-03	5.480E-03
	0.6715	7.111E-02	2.433E-03	6.793E-03
	0.6805	7.538E-02	2.523E-03	6.121E-03
	0.6895	7.606E-02	2.665E-03	6.858E-03

	0.6985	8.710E-02	2.990E-03	7.381E-03
	0.7075	8.570E-02	2.911E-03	7.020E-03
	0.7165	7.064E-02	2.630E-03	7.065E-03
	0.7255	6.078E-02	2.399E-03	5.367E-03
	0.7345	4.937E-02	2.116E-03	3.721E-03
	0.7435	4.709E-02	2.079E-03	3.640E-03
	0.7525	4.475E-02	2.010E-03	3.092E-03
	0.7615	3.974E-02	1.976E-03	2.916E-03
	0.7705	4.396E-02	2.123E-03	3.261E-03
	0.7795	4.065E-02	2.015E-03	3.395E-03
	0.7885	3.288E-02	1.857E-03	2.158E-03
	0.7975	3.492E-02	1.969E-03	2.249E-03
	0.8065	3.263E-02	1.878E-03	2.088E-03
	0.8155	3.428E-02	1.922E-03	2.361E-03
	0.8245	3.377E-02	2.061E-03	2.305E-03
	0.8335	3.733E-02	2.126E-03	3.031E-03
	0.8425	3.290E-02	2.007E-03	2.412E-03
	0.8515	2.876E-02	2.117E-03	2.710E-03
	0.8605	2.393E-02	1.666E-03	3.928E-03
	0.8695	1.467E-02	1.346E-03	2.576E-03
	0.8785	1.261E-02	1.086E-03	1.955E-03
	0.8875	8.891E-03	8.672E-04	1.299E-03
	0.8965	4.524E-03	6.212E-04	7.696E-04
	0.9055	4.133E-03	7.272E-04	9.825E-04
3.375	0.5365	1.417E-01	6.149E-03	1.436E-02
	0.5455	1.314E-01	6.116E-03	1.408E-02
	0.5545	1.172E-01	5.824E-03	1.087E-02
	0.5635	1.197E-01	6.239E-03	1.083E-02
	0.5725	1.218E-01	4.787E-03	1.234E-02
	0.5815	1.129E-01	3.744E-03	1.055E-02
	0.5905	1.149E-01	3.885E-03	1.046E-02
	0.5995	1.154E-01	3.860E-03	1.100E-02
	0.6085	1.192E-01	3.923E-03	1.164E-02
	0.6175	1.231E-01	4.111E-03	1.073E-02
	0.6265	1.300E-01	4.352E-03	1.065E-02
	0.6355	1.087E-01	2.971E-03	1.114E-02
	0.6445	9.282E-02	2.794E-03	8.024E-03
	0.6535	8.260E-02	2.588E-03	8.333E-03
	0.6625	7.392E-02	2.459E-03	6.154E-03
	0.6715	7.373E-02	2.469E-03	7.187E-03
	0.6805	7.149E-02	2.437E-03	5.727E-03
	0.6895	7.487E-02	2.602E-03	6.592E-03
	0.6985	8.267E-02	2.894E-03	7.636E-03
	0.7075	9.156E-02	3.168E-03	7.118E-03
	0.7165	8.039E-02	2.883E-03	8.047E-03
	0.7255	6.430E-02	2.480E-03	6.441E-03
	0.7345	5.347E-02	2.195E-03	5.268E-03
	0.7435	4.508E-02	2.105E-03	3.480E-03
	0.7525	4.764E-02	2.176E-03	3.370E-03
	0.7615	3.693E-02	1.960E-03	2.638E-03
	0.7705	3.871E-02	1.966E-03	2.611E-03
	0.7795	3.768E-02	2.001E-03	2.941E-03
	0.7885	3.120E-02	1.809E-03	2.631E-03
	0.7975	3.106E-02	1.901E-03	2.008E-03
	0.8065	3.452E-02	1.961E-03	2.258E-03
	0.8155	3.040E-02	1.820E-03	1.965E-03
	0.8245	3.513E-02	2.032E-03	2.654E-03
	0.8335	3.253E-02	2.067E-03	2.609E-03
	0.8425	3.345E-02	2.099E-03	2.547E-03
	0.8515	2.802E-02	1.993E-03	2.327E-03
	0.8605	2.573E-02	1.900E-03	3.863E-03
	0.8695	1.942E-02	1.535E-03	3.410E-03
	0.8785	1.170E-02	1.058E-03	1.870E-03
	0.8875	7.912E-03	8.458E-04	1.146E-03
	0.8965	5.691E-03	6.874E-04	9.172E-04
	0.9055	6.474E-03	9.408E-04	1.473E-03
3.425	0.5365	1.675E-01	1.373E-02	1.955E-02
	0.5455	1.616E-01	6.934E-03	1.724E-02
	0.5545	1.409E-01	6.370E-03	1.400E-02
	0.5635	1.303E-01	6.150E-03	1.216E-02
	0.5725	1.096E-01	5.943E-03	9.723E-03
	0.5815	1.112E-01	6.579E-03	1.012E-02
	0.5905	1.141E-01	3.852E-03	1.107E-02
	0.5995	1.114E-01	3.853E-03	1.096E-02
	0.6085	1.163E-01	4.084E-03	1.114E-02
	0.6175	1.145E-01	4.069E-03	1.071E-02
	0.6265	1.177E-01	4.073E-03	9.829E-03

	0.6355	1.044E-01	3.866E-03	9.091E-03
	0.6445	9.380E-02	2.821E-03	9.234E-03
	0.6535	8.263E-02	2.603E-03	7.423E-03
	0.6625	7.227E-02	2.456E-03	8.022E-03
	0.6715	6.902E-02	2.419E-03	5.614E-03
	0.6805	7.093E-02	2.457E-03	6.090E-03
	0.6895	7.370E-02	2.564E-03	6.393E-03
	0.6985	7.820E-02	2.764E-03	7.386E-03
	0.7075	8.955E-02	3.170E-03	7.734E-03
	0.7165	8.024E-02	2.902E-03	7.492E-03
	0.7255	6.417E-02	2.518E-03	6.769E-03
	0.7345	5.767E-02	2.402E-03	6.348E-03
	0.7435	4.920E-02	2.221E-03	4.325E-03
	0.7525	4.085E-02	2.042E-03	2.972E-03
	0.7615	4.360E-02	2.174E-03	3.295E-03
	0.7705	3.825E-02	1.960E-03	3.196E-03
	0.7795	3.746E-02	2.018E-03	3.438E-03
	0.7885	3.462E-02	1.948E-03	2.526E-03
	0.7975	3.162E-02	1.872E-03	2.563E-03
	0.8065	3.360E-02	1.907E-03	2.201E-03
	0.8155	3.329E-02	1.957E-03	2.167E-03
	0.8245	2.741E-02	1.777E-03	2.232E-03
	0.8335	3.391E-02	2.054E-03	2.577E-03
	0.8425	3.441E-02	2.164E-03	2.875E-03
	0.8515	3.510E-02	2.277E-03	2.666E-03
	0.8605	2.732E-02	1.907E-03	3.771E-03
	0.8695	2.000E-02	1.542E-03	3.497E-03
	0.8785	1.361E-02	1.186E-03	2.238E-03
	0.8875	1.085E-02	9.570E-04	1.540E-03
	0.8965	6.277E-03	6.802E-04	9.953E-04
	0.9055	3.675E-03	4.575E-04	7.615E-04
3.475	0.5545	1.465E-01	7.125E-03	1.619E-02
	0.5635	1.262E-01	6.082E-03	1.240E-02
	0.5725	1.183E-01	5.949E-03	1.097E-02
	0.5815	1.044E-01	5.762E-03	9.526E-03
	0.5905	1.156E-01	6.591E-03	1.053E-02
	0.5995	9.557E-02	6.165E-03	8.815E-03
	0.6085	1.080E-01	3.882E-03	1.086E-02
	0.6175	1.103E-01	4.067E-03	1.156E-02
	0.6265	1.091E-01	4.239E-03	9.936E-03
	0.6355	1.057E-01	3.921E-03	9.214E-03
	0.6445	8.699E-02	3.446E-03	8.503E-03
	0.6535	8.301E-02	3.443E-03	7.010E-03
	0.6625	7.491E-02	2.444E-03	8.468E-03
	0.6715	6.769E-02	2.402E-03	5.615E-03
	0.6805	6.695E-02	2.415E-03	7.136E-03
	0.6895	7.010E-02	2.533E-03	5.993E-03
	0.6985	6.755E-02	2.586E-03	6.421E-03
	0.7075	7.575E-02	2.852E-03	6.652E-03
	0.7165	7.437E-02	2.846E-03	6.184E-03
	0.7255	6.907E-02	2.651E-03	7.213E-03
	0.7345	5.812E-02	2.402E-03	5.350E-03
	0.7435	4.200E-02	2.015E-03	3.373E-03
	0.7525	4.468E-02	2.076E-03	3.562E-03
	0.7615	3.950E-02	2.031E-03	3.252E-03
	0.7705	3.528E-02	1.940E-03	3.079E-03
	0.7795	3.560E-02	2.039E-03	3.124E-03
	0.7885	3.376E-02	1.922E-03	2.861E-03
	0.7975	3.200E-02	1.782E-03	2.746E-03
	0.8065	3.320E-02	1.922E-03	2.217E-03
	0.8155	2.670E-02	1.766E-03	2.255E-03
	0.8245	2.842E-02	1.811E-03	2.334E-03
	0.8335	3.188E-02	2.096E-03	2.401E-03
	0.8425	3.114E-02	2.072E-03	2.779E-03
	0.8515	3.368E-02	2.136E-03	2.461E-03
	0.8605	2.666E-02	1.921E-03	3.351E-03
	0.8695	1.870E-02	1.478E-03	3.256E-03
	0.8785	1.363E-02	1.274E-03	2.337E-03
	0.8875	8.650E-03	9.607E-04	1.241E-03
	0.8965	8.123E-03	1.199E-03	1.278E-03
	0.9055	3.669E-03	6.780E-04	7.187E-04
3.525	0.5635	1.363E-01	7.372E-03	1.463E-02
	0.5725	1.328E-01	6.261E-03	1.286E-02
	0.5815	1.123E-01	5.943E-03	1.057E-02
	0.5905	1.063E-01	5.878E-03	9.970E-03
	0.5995	1.076E-01	6.250E-03	9.439E-03
	0.6085	1.028E-01	6.654E-03	9.871E-03

	0.6175	1.198E-01	4.193E-03	1.267E-02
	0.6265	1.079E-01	4.175E-03	1.026E-02
	0.6355	1.089E-01	4.209E-03	9.656E-03
	0.6445	9.821E-02	3.855E-03	9.807E-03
	0.6535	8.266E-02	3.474E-03	7.167E-03
	0.6625	7.042E-02	3.208E-03	7.233E-03
	0.6715	6.453E-02	3.179E-03	5.732E-03
	0.6805	6.194E-02	2.417E-03	6.024E-03
	0.6895	6.299E-02	2.474E-03	5.337E-03
	0.6985	7.412E-02	2.744E-03	6.965E-03
	0.7075	7.877E-02	2.908E-03	7.562E-03
	0.7165	7.639E-02	2.967E-03	6.405E-03
	0.7255	7.353E-02	2.788E-03	7.460E-03
	0.7345	5.679E-02	2.434E-03	5.839E-03
	0.7435	4.749E-02	2.148E-03	4.644E-03
	0.7525	4.454E-02	2.169E-03	3.561E-03
	0.7615	3.616E-02	2.005E-03	3.114E-03
	0.7705	3.839E-02	2.011E-03	3.759E-03
	0.7795	3.783E-02	2.092E-03	3.012E-03
	0.7885	3.193E-02	1.833E-03	3.076E-03
	0.7975	2.994E-02	1.770E-03	2.601E-03
	0.8065	2.977E-02	1.862E-03	2.025E-03
	0.8155	2.838E-02	1.852E-03	1.997E-03
	0.8245	3.071E-02	1.947E-03	2.548E-03
	0.8335	2.558E-02	1.757E-03	1.801E-03
	0.8425	3.650E-02	2.208E-03	3.227E-03
	0.8515	2.495E-02	1.881E-03	1.852E-03
	0.8605	2.840E-02	1.931E-03	3.105E-03
	0.8695	1.772E-02	1.487E-03	3.038E-03
	0.8785	1.078E-02	1.135E-03	1.870E-03
	0.8875	9.445E-03	9.528E-04	1.369E-03
	0.8965	7.650E-03	1.278E-03	1.159E-03
	0.9055	6.742E-03	1.120E-03	1.255E-03
3.575	0.5815	1.257E-01	6.366E-03	1.252E-02
	0.5905	1.145E-01	6.106E-03	1.123E-02
	0.5995	1.064E-01	5.953E-03	9.740E-03
	0.6085	1.099E-01	6.340E-03	1.100E-02
	0.6175	1.076E-01	6.654E-03	1.031E-02
	0.6265	1.081E-01	7.275E-03	1.088E-02
	0.6355	1.028E-01	4.136E-03	9.500E-03
	0.6445	9.610E-02	3.924E-03	8.549E-03
	0.6535	9.011E-02	3.850E-03	8.658E-03
	0.6625	7.900E-02	3.620E-03	7.096E-03
	0.6715	6.133E-02	2.951E-03	7.148E-03
	0.6805	6.930E-02	3.334E-03	5.729E-03
	0.6895	6.383E-02	2.461E-03	5.995E-03
	0.6985	7.036E-02	2.684E-03	6.510E-03
	0.7075	7.317E-02	2.791E-03	7.189E-03
	0.7165	7.798E-02	3.026E-03	7.207E-03
	0.7255	7.668E-02	3.026E-03	7.513E-03
	0.7345	5.728E-02	2.491E-03	6.518E-03
	0.7435	4.845E-02	2.199E-03	6.400E-03
	0.7525	4.448E-02	2.162E-03	4.026E-03
	0.7615	3.298E-02	1.807E-03	2.626E-03
	0.7705	3.974E-02	2.096E-03	3.480E-03
	0.7795	3.227E-02	1.925E-03	3.070E-03
	0.7885	3.536E-02	2.015E-03	3.124E-03
	0.7975	3.536E-02	2.175E-03	2.859E-03
	0.8065	2.994E-02	1.876E-03	2.037E-03
	0.8155	3.082E-02	1.916E-03	2.592E-03
	0.8245	3.243E-02	1.952E-03	2.990E-03
	0.8335	2.618E-02	1.911E-03	2.015E-03
	0.8425	3.149E-02	2.098E-03	2.803E-03
	0.8515	2.933E-02	2.154E-03	2.374E-03
	0.8605	2.467E-02	1.913E-03	2.415E-03
	0.8695	1.825E-02	1.522E-03	3.084E-03
	0.8785	1.486E-02	1.332E-03	2.609E-03
	0.8875	9.425E-03	9.847E-04	1.405E-03
	0.8965	7.050E-03	1.240E-03	1.066E-03
	0.9055	6.102E-03	9.418E-04	1.071E-03
3.625	0.5905	1.163E-01	6.441E-03	1.188E-02
	0.5995	1.114E-01	6.106E-03	1.086E-02
	0.6085	1.005E-01	6.012E-03	9.910E-03
	0.6175	9.374E-02	5.920E-03	9.399E-03
	0.6265	9.671E-02	6.427E-03	9.979E-03
	0.6355	1.053E-01	7.412E-03	9.814E-03
	0.6445	1.113E-01	4.374E-03	1.073E-02
	0.6535	8.602E-02	3.699E-03	9.036E-03
	0.6625	8.460E-02	3.870E-03	7.552E-03
	0.6715	6.629E-02	3.295E-03	7.853E-03
	0.6805	6.244E-02	3.154E-03	5.064E-03
	0.6895	6.293E-02	3.179E-03	6.885E-03
	0.6985	7.226E-02	3.421E-03	6.280E-03
	0.7075	6.797E-02	2.624E-03	6.874E-03
	0.7165	7.779E-02	3.019E-03	7.556E-03
	0.7255	7.580E-02	3.031E-03	6.857E-03
	0.7345	6.284E-02	2.780E-03	6.967E-03
	0.7435	5.253E-02	2.387E-03	5.326E-03
	0.7525	4.516E-02	2.235E-03	4.919E-03
	0.7615	4.276E-02	2.187E-03	3.543E-03
	0.7705	3.320E-02	1.942E-03	3.081E-03
	0.7795	3.490E-02	2.017E-03	3.750E-03
	0.7885	3.481E-02	2.012E-03	3.515E-03
	0.7975	2.906E-02	1.819E-03	2.256E-03
	0.8065	2.998E-02	1.942E-03	2.803E-03
	0.8155	2.696E-02	1.856E-03	2.362E-03
	0.8245	2.738E-02	1.868E-03	2.005E-03
	0.8335	2.541E-02	1.931E-03	2.514E-03
	0.8425	2.808E-02	2.058E-03	2.379E-03
	0.8515	2.862E-02	2.132E-03	2.343E-03
	0.8605	2.752E-02	1.998E-03	2.825E-03
	0.8695	2.100E-02	1.704E-03	3.352E-03
	0.8785	1.637E-02	1.463E-03	2.893E-03
	0.8875	1.118E-02	1.206E-03	1.747E-03
	0.8965	5.213E-03	7.271E-04	7.716E-04
	0.9055	5.088E-03	8.602E-04	8.669E-04
3.675	0.5995	1.082E-01	6.570E-03	1.210E-02
	0.6085	1.008E-01	5.860E-03	9.702E-03
	0.6175	9.159E-02	5.888E-03	9.743E-03
	0.6265	1.062E-01	6.473E-03	1.114E-02
	0.6355	1.006E-01	6.713E-03	9.406E-03
	0.6445	1.164E-01	7.619E-03	1.038E-02
	0.6535	8.756E-02	6.665E-03	8.462E-03
	0.6625	7.675E-02	3.575E-03	7.197E-03
	0.6715	6.527E-02	3.355E-03	7.179E-03
	0.6805	6.811E-02	3.436E-03	6.586E-03
	0.6895	6.255E-02	3.381E-03	6.108E-03
	0.6985	5.487E-02	3.050E-03	4.646E-03
	0.7075	6.444E-02	3.401E-03	6.024E-03
	0.7165	7.200E-02	3.720E-03	6.741E-03
	0.7255	7.833E-02	3.025E-03	7.017E-03
	0.7345	6.027E-02	2.662E-03	6.395E-03
	0.7435	5.058E-02	2.288E-03	5.245E-03
	0.7525	4.449E-02	2.238E-03	4.253E-03
	0.7615	4.011E-02	2.118E-03	3.355E-03
	0.7705	3.729E-02	2.035E-03	3.704E-03
	0.7795	3.191E-02	1.992E-03	3.483E-03
	0.7885	3.560E-02	2.122E-03	3.566E-03
	0.7975	2.976E-02	1.856E-03	3.137E-03
	0.8065	2.764E-02	1.799E-03	2.800E-03
	0.8155	2.625E-02	1.801E-03	2.341E-03
	0.8245	2.904E-02	1.898E-03	2.282E-03
	0.8335	2.792E-02	1.848E-03	2.860E-03
	0.8425	2.842E-02	1.944E-03	2.755E-03
	0.8515	2.296E-02	1.852E-03	2.360E-03
	0.8605	2.644E-02	2.030E-03	2.254E-03
	0.8695	1.991E-02	1.658E-03	2.865E-03
	0.8785	1.589E-02	1.314E-03	2.772E-03
	0.8875	1.028E-02	1.049E-03	1.643E-03
	0.8965	8.168E-03	1.205E-03	1.196E-03
	0.9055	5.394E-03	8.630E-04	8.866E-04
3.725	0.6175	9.860E-02	6.020E-03	1.065E-02
	0.6265	9.723E-02	6.221E-03	1.041E-02
	0.6355	9.790E-02	6.413E-03	1.073E-02
	0.6445	9.410E-02	6.503E-03	8.719E-03
	0.6535	9.925E-02	7.014E-03	9.057E-03
	0.6625	8.096E-02	6.420E-03	8.255E-03
	0.6715	7.540E-02	3.554E-03	7.445E-03
	0.6805	6.241E-02	3.267E-03	7.897E-03
	0.6895	6.065E-02	3.264E-03	5.267E-03
	0.6985	5.443E-02	3.174E-03	4.873E-03
	0.7075	5.604E-02	3.276E-03	5.202E-03
	0.7165	6.553E-02	3.608E-03	6.514E-03
	0.7255	7.602E-02	4.110E-03	6.867E-03

	0.7345	7.390E-02	2.941E-03	8.078E-03
	0.7435	4.843E-02	2.312E-03	6.032E-03
	0.7525	4.054E-02	2.096E-03	5.353E-03
	0.7615	4.135E-02	2.118E-03	3.755E-03
	0.7705	3.767E-02	2.128E-03	3.648E-03
	0.7795	3.505E-02	2.036E-03	3.928E-03
	0.7885	2.921E-02	1.865E-03	2.342E-03
	0.7975	2.685E-02	1.791E-03	2.891E-03
	0.8065	2.852E-02	1.858E-03	2.970E-03
	0.8155	2.791E-02	1.824E-03	2.210E-03
	0.8245	2.521E-02	1.918E-03	2.095E-03
	0.8335	2.381E-02	1.757E-03	2.222E-03
	0.8425	2.620E-02	1.943E-03	2.575E-03
	0.8515	2.645E-02	2.050E-03	2.740E-03
	0.8605	2.291E-02	1.994E-03	2.286E-03
	0.8695	2.411E-02	2.412E-03	3.597E-03
	0.8785	1.433E-02	1.358E-03	2.495E-03
	0.8875	1.064E-02	1.068E-03	1.810E-03
	0.8965	7.715E-03	1.226E-03	1.138E-03
3.775	0.6265	8.615E-02	5.886E-03	9.643E-03
	0.6355	1.005E-01	6.437E-03	1.106E-02
	0.6445	9.433E-02	6.543E-03	9.345E-03
	0.6535	8.712E-02	6.098E-03	8.108E-03
	0.6625	7.102E-02	5.827E-03	7.757E-03
	0.6715	8.324E-02	6.307E-03	7.476E-03
	0.6805	6.544E-02	5.798E-03	8.121E-03
	0.6895	6.227E-02	3.372E-03	5.829E-03
	0.6985	6.187E-02	3.434E-03	6.983E-03
	0.7075	4.964E-02	3.122E-03	4.526E-03
	0.7165	7.145E-02	3.869E-03	7.038E-03
	0.7255	7.343E-02	3.879E-03	6.870E-03
	0.7345	6.696E-02	3.780E-03	6.307E-03
	0.7435	5.452E-02	3.182E-03	6.309E-03
	0.7525	4.648E-02	2.265E-03	6.358E-03
	0.7615	3.993E-02	2.108E-03	4.439E-03
	0.7705	3.460E-02	1.996E-03	2.883E-03
	0.7795	3.308E-02	2.038E-03	3.435E-03
	0.7885	2.992E-02	1.958E-03	3.366E-03
	0.7975	2.804E-02	1.851E-03	2.374E-03
	0.8065	2.446E-02	1.735E-03	2.341E-03
	0.8155	2.698E-02	1.885E-03	2.097E-03
	0.8245	2.771E-02	1.898E-03	2.305E-03
	0.8335	2.242E-02	1.767E-03	2.033E-03
	0.8425	2.522E-02	1.895E-03	2.362E-03
	0.8515	2.193E-02	1.786E-03	2.314E-03
	0.8605	1.972E-02	1.813E-03	1.937E-03
	0.8695	1.873E-02	1.788E-03	2.426E-03
	0.8785	1.446E-02	1.330E-03	2.493E-03
	0.8875	1.042E-02	1.044E-03	1.814E-03
3.825	0.6355	1.001E-01	6.773E-03	1.185E-02
	0.6445	1.044E-01	6.809E-03	1.083E-02
	0.6535	8.823E-02	6.495E-03	8.514E-03
	0.6625	9.157E-02	6.279E-03	9.494E-03
	0.6715	8.600E-02	6.177E-03	8.167E-03
	0.6805	6.772E-02	5.567E-03	7.914E-03
	0.6895	5.267E-02	5.469E-03	5.074E-03
	0.6985	5.495E-02	3.152E-03	6.408E-03
	0.7075	6.236E-02	3.466E-03	5.735E-03
	0.7165	6.298E-02	3.659E-03	6.174E-03
	0.7255	7.007E-02	4.022E-03	7.064E-03
	0.7345	6.925E-02	3.981E-03	6.131E-03
	0.7435	5.795E-02	3.663E-03	6.504E-03
	0.7525	5.048E-02	3.228E-03	4.841E-03
	0.7615	4.291E-02	2.763E-03	3.925E-03
	0.7705	3.808E-02	2.058E-03	3.449E-03
	0.7795	3.518E-02	2.060E-03	3.847E-03
	0.7885	2.988E-02	1.975E-03	3.871E-03
	0.7975	2.706E-02	1.906E-03	3.332E-03
	0.8065	2.555E-02	1.842E-03	2.211E-03
	0.8155	2.594E-02	1.885E-03	2.370E-03
	0.8245	2.984E-02	1.969E-03	3.209E-03
	0.8335	2.411E-02	1.813E-03	2.128E-03
	0.8425	2.524E-02	2.419E-03	2.699E-03
	0.8515	2.515E-02	1.889E-03	2.759E-03
	0.8605	2.573E-02	1.993E-03	2.669E-03
	0.8695	1.730E-02	1.627E-03	2.155E-03
	0.8785	1.589E-02	1.559E-03	2.752E-03
	0.8875	1.289E-02	1.319E-03	2.290E-03
	0.8965	6.837E-03	1.055E-03	9.817E-04
3.875	0.6535	9.834E-02	6.708E-03	9.877E-03
	0.6625	7.693E-02	5.812E-03	7.305E-03
	0.6715	7.541E-02	5.755E-03	7.823E-03
	0.6805	6.677E-02	5.402E-03	6.577E-03
	0.6895	4.943E-02	4.944E-03	6.542E-03
	0.6985	6.198E-02	5.712E-03	5.425E-03
	0.7075	5.717E-02	5.548E-03	4.886E-03
	0.7165	6.043E-02	3.505E-03	6.151E-03
	0.7255	6.403E-02	3.858E-03	6.554E-03
	0.7345	6.540E-02	3.953E-03	6.067E-03
	0.7435	6.280E-02	3.938E-03	6.768E-03
	0.7525	4.170E-02	3.084E-03	5.088E-03
	0.7615	4.563E-02	3.025E-03	4.972E-03
	0.7705	3.155E-02	2.541E-03	2.635E-03
	0.7795	3.233E-02	2.595E-03	3.276E-03
	0.7885	3.046E-02	1.974E-03	3.977E-03
	0.7975	3.065E-02	2.055E-03	3.968E-03
	0.8065	2.827E-02	1.998E-03	3.154E-03
	0.8155	2.484E-02	1.764E-03	3.098E-03
	0.8245	2.461E-02	1.879E-03	2.761E-03
	0.8335	2.633E-02	1.942E-03	2.462E-03
	0.8425	2.421E-02	1.810E-03	2.775E-03
	0.8515	2.337E-02	2.005E-03	2.964E-03
	0.8605	2.407E-02	1.915E-03	2.432E-03
	0.8695	2.181E-02	1.929E-03	2.536E-03
	0.8785	1.526E-02	1.497E-03	2.627E-03
	0.8875	1.337E-02	1.337E-03	2.346E-03
3.925	0.6625	9.137E-02	6.818E-03	9.370E-03
	0.6715	7.481E-02	5.896E-03	8.897E-03
	0.6805	7.664E-02	5.780E-03	7.239E-03
	0.6895	5.885E-02	5.323E-03	8.012E-03
	0.6985	4.861E-02	4.838E-03	4.856E-03
	0.7075	6.185E-02	5.635E-03	6.612E-03
	0.7165	5.519E-02	5.662E-03	5.173E-03
	0.7255	6.213E-02	6.393E-03	6.157E-03
	0.7345	5.986E-02	3.763E-03	5.831E-03
	0.7435	6.769E-02	4.062E-03	6.836E-03
	0.7525	4.458E-02	3.031E-03	5.978E-03
	0.7615	3.834E-02	2.911E-03	5.178E-03
	0.7705	4.391E-02	3.234E-03	4.395E-03
	0.7795	3.554E-02	2.754E-03	3.736E-03
	0.7885	3.203E-02	2.638E-03	3.986E-03
	0.7975	3.221E-02	1.985E-03	2.997E-03
	0.8065	2.798E-02	1.854E-03	3.555E-03
	0.8155	2.499E-02	1.851E-03	3.255E-03
	0.8245	2.544E-02	1.820E-03	2.638E-03
	0.8335	2.303E-02	1.851E-03	2.197E-03
	0.8425	2.485E-02	1.868E-03	2.864E-03
	0.8515	2.508E-02	2.054E-03	3.417E-03
	0.8605	2.393E-02	2.009E-03	2.773E-03
	0.8695	2.087E-02	1.916E-03	2.877E-03
	0.8785	1.483E-02	1.517E-03	2.362E-03
	0.8875	8.425E-03	1.474E-03	1.474E-03
3.975	0.6715	9.531E-02	7.290E-03	1.204E-02
	0.6805	6.599E-02	5.512E-03	6.582E-03
	0.6895	6.162E-02	5.309E-03	7.911E-03
	0.6985	5.199E-02	4.917E-03	4.610E-03
	0.7075	5.597E-02	5.280E-03	6.870E-03
	0.7165	5.221E-02	5.138E-03	4.912E-03
	0.7255	5.727E-02	6.034E-03	5.860E-03
	0.7345	5.862E-02	6.755E-03	5.681E-03
	0.7435	6.659E-02	4.034E-03	6.663E-03
	0.7525	5.723E-02	3.724E-03	7.174E-03
	0.7615	3.958E-02	3.114E-03	5.009E-03
	0.7705	3.932E-02	2.999E-03	4.738E-03
	0.7795	3.599E-02	2.914E-03	3.131E-03
	0.7885	3.056E-02	2.791E-03	3.541E-03
	0.7975	2.379E-02	2.554E-03	2.998E-03
	0.8065	2.536E-02	2.346E-03	2.118E-03
	0.8155	2.654E-02	1.842E-03	3.574E-03
	0.8245	2.415E-02	1.794E-03	2.167E-03
	0.8335	2.246E-02	1.791E-03	2.138E-03
	0.8425	2.221E-02	1.802E-03	2.259E-03
	0.8515	2.006E-02	1.808E-03	2.286E-03
	0.8605	2.572E-02	2.132E-03	3.125E-03

	0.8695	1.847E-02	1.791E-03	2.291E-03
	0.8785	1.545E-02	1.587E-03	2.533E-03
	0.8875	1.574E-02	2.078E-03	2.795E-03
4.025	0.6895	6.596E-02	5.718E-03	7.660E-03
	0.6985	5.384E-02	5.171E-03	6.955E-03
	0.7075	5.652E-02	5.231E-03	5.198E-03
	0.7165	6.146E-02	5.653E-03	5.990E-03
	0.7255	5.545E-02	5.278E-03	5.330E-03
	0.7345	6.079E-02	6.204E-03	6.149E-03
	0.7435	6.782E-02	6.895E-03	6.202E-03
	0.7525	4.627E-02	5.759E-03	5.299E-03
	0.7615	4.119E-02	3.049E-03	4.271E-03
	0.7705	3.931E-02	3.178E-03	3.829E-03
	0.7795	3.590E-02	3.000E-03	3.211E-03
	0.7885	3.405E-02	2.844E-03	4.123E-03
	0.7975	2.549E-02	2.412E-03	3.250E-03
	0.8065	2.432E-02	2.501E-03	2.580E-03
	0.8155	2.508E-02	2.470E-03	2.281E-03
	0.8245	1.952E-02	2.119E-03	1.811E-03
	0.8335	2.021E-02	2.123E-03	1.783E-03
	0.8425	2.165E-02	1.766E-03	2.207E-03
	0.8515	2.301E-02	1.833E-03	2.744E-03
	0.8605	2.218E-02	1.983E-03	2.704E-03
	0.8695	2.364E-02	2.098E-03	2.740E-03
	0.8785	1.459E-02	1.583E-03	2.305E-03
	0.8875	1.132E-02	1.699E-03	2.001E-03
4.075	0.6985	6.741E-02	5.779E-03	9.560E-03
	0.7075	5.090E-02	5.057E-03	5.280E-03
	0.7165	4.162E-02	4.595E-03	4.265E-03
	0.7255	5.725E-02	5.462E-03	5.717E-03
	0.7345	5.274E-02	5.626E-03	5.540E-03
	0.7435	6.172E-02	6.573E-03	6.008E-03
	0.7525	5.574E-02	5.973E-03	6.233E-03
	0.7615	4.944E-02	5.779E-03	6.559E-03
	0.7705	3.619E-02	2.866E-03	4.432E-03
	0.7795	3.691E-02	2.961E-03	3.253E-03
	0.7885	3.298E-02	2.958E-03	4.071E-03
	0.7975	2.734E-02	2.431E-03	3.506E-03
	0.8065	2.235E-02	2.284E-03	2.910E-03
	0.8155	2.056E-02	2.293E-03	2.076E-03
	0.8245	1.970E-02	2.359E-03	2.543E-03
	0.8335	2.193E-02	2.500E-03	2.851E-03
	0.8425	2.116E-02	2.307E-03	2.305E-03
	0.8515	1.921E-02	1.715E-03	2.261E-03
	0.8605	2.070E-02	1.829E-03	2.604E-03
	0.8695	1.478E-02	1.683E-03	1.734E-03
	0.8785	1.721E-02	1.726E-03	2.539E-03
	0.8875	9.490E-03	1.550E-03	1.679E-03
4.125	0.7075	6.091E-02	6.030E-03	6.856E-03
	0.7165	5.092E-02	5.120E-03	6.317E-03
	0.7255	4.569E-02	5.069E-03	4.626E-03
	0.7345	6.631E-02	6.153E-03	6.955E-03
	0.7435	6.244E-02	6.413E-03	6.413E-03
	0.7525	5.556E-02	6.161E-03	5.906E-03
	0.7615	4.756E-02	5.217E-03	6.503E-03
	0.7705	3.517E-02	4.558E-03	4.806E-03
	0.7795	3.472E-02	4.774E-03	3.368E-03
	0.7885	2.532E-02	2.520E-03	3.055E-03
	0.7975	2.666E-02	2.469E-03	3.480E-03
	0.8065	2.536E-02	2.509E-03	2.730E-03
	0.8155	2.695E-02	2.713E-03	3.554E-03
	0.8245	2.222E-02	2.414E-03	2.883E-03
	0.8335	2.271E-02	2.522E-03	2.917E-03
	0.8425	2.516E-02	2.703E-03	3.162E-03
	0.8515	2.767E-02	2.785E-03	3.470E-03
	0.8605	1.974E-02	2.598E-03	1.982E-03
	0.8695	2.298E-02	2.099E-03	2.707E-03
	0.8785	1.409E-02	1.566E-03	2.094E-03
	0.8875	1.052E-02	1.599E-03	1.847E-03
4.175	0.7255	4.776E-02	5.161E-03	5.028E-03
	0.7345	6.389E-02	6.177E-03	6.946E-03
	0.7435	5.066E-02	5.779E-03	5.362E-03
	0.7525	5.960E-02	6.470E-03	5.868E-03
	0.7615	4.302E-02	5.150E-03	5.687E-03
	0.7705	3.665E-02	4.648E-03	5.134E-03
	0.7795	3.243E-02	4.336E-03	4.072E-03
	0.7885	2.862E-02	4.163E-03	2.711E-03
	0.7975	2.934E-02	4.683E-03	3.796E-03
	0.8065	1.893E-02	2.177E-03	1.858E-03
	0.8155	2.659E-02	2.584E-03	3.427E-03
	0.8245	2.092E-02	2.419E-03	2.689E-03
	0.8335	2.101E-02	2.425E-03	2.307E-03
	0.8425	1.338E-02	2.044E-03	1.737E-03
	0.8515	1.588E-02	2.159E-03	1.918E-03
	0.8605	1.974E-02	2.516E-03	2.398E-03
	0.8695	1.622E-02	2.227E-03	2.088E-03
	0.8785	2.045E-02	2.529E-03	2.924E-03
	0.8875	1.116E-02	1.692E-03	1.939E-03
	0.8965	7.476E-03	1.294E-03	1.359E-03
4.225	0.7435	6.601E-02	6.594E-03	7.511E-03
	0.7525	5.738E-02	6.172E-03	5.444E-03
	0.7615	5.440E-02	5.837E-03	6.711E-03
	0.7705	3.676E-02	4.743E-03	3.878E-03
	0.7795	3.373E-02	4.297E-03	3.865E-03
	0.7885	3.140E-02	4.451E-03	2.752E-03
	0.7975	2.507E-02	3.957E-03	3.085E-03
	0.8065	2.100E-02	3.810E-03	2.753E-03
	0.8155	2.403E-02	2.514E-03	2.197E-03
	0.8245	2.431E-02	2.552E-03	3.235E-03
	0.8335	1.794E-02	2.395E-03	1.571E-03
	0.8425	2.008E-02	2.490E-03	1.928E-03
	0.8515	2.149E-02	2.602E-03	2.245E-03
	0.8605	1.692E-02	2.096E-03	2.235E-03
	0.8695	2.185E-02	2.913E-03	2.849E-03
	0.8785	1.777E-02	2.529E-03	2.576E-03
	0.8875	9.790E-03	1.732E-03	1.677E-03
4.275	0.7525	6.064E-02	6.689E-03	6.604E-03
	0.7615	4.596E-02	5.304E-03	5.488E-03
	0.7705	4.231E-02	5.264E-03	5.695E-03
	0.7795	2.964E-02	4.303E-03	3.251E-03
	0.7885	2.933E-02	4.164E-03	2.660E-03
	0.7975	2.767E-02	4.119E-03	3.631E-03
	0.8065	2.580E-02	4.073E-03	3.331E-03
	0.8155	2.637E-02	4.098E-03	3.350E-03
	0.8245	2.618E-02	4.528E-03	2.580E-03
	0.8335	2.131E-02	2.494E-03	2.184E-03
	0.8425	1.601E-02	2.217E-03	1.439E-03
	0.8515	1.749E-02	2.410E-03	1.645E-03
	0.8605	2.316E-02	2.861E-03	3.148E-03
	0.8695	1.845E-02	2.489E-03	2.416E-03
	0.8785	1.593E-02	2.427E-03	2.199E-03
	0.8875	1.270E-02	1.871E-03	2.177E-03
4.325	0.7705	4.458E-02	5.282E-03	6.763E-03
	0.7795	3.424E-02	4.317E-03	4.805E-03
	0.7885	2.342E-02	3.857E-03	2.312E-03
	0.7975	2.889E-02	4.272E-03	3.619E-03
	0.8065	2.580E-02	4.131E-03	3.503E-03
	0.8155	2.207E-02	4.195E-03	2.941E-03
	0.8245	2.866E-02	4.507E-03	2.799E-03
	0.8335	2.163E-02	3.907E-03	2.798E-03
	0.8425	9.435E-03	3.075E-03	1.096E-03
	0.8515	1.919E-02	2.434E-03	1.860E-03
	0.8605	1.805E-02	2.343E-03	2.445E-03
	0.8695	1.947E-02	2.570E-03	2.511E-03
	0.8785	1.884E-02	2.724E-03	2.643E-03
	0.8875	1.052E-02	1.894E-03	1.768E-03
4.375	0.7795	4.520E-02	5.547E-03	6.907E-03
	0.7885	2.360E-02	3.707E-03	2.745E-03
	0.7975	3.268E-02	4.849E-03	4.002E-03
	0.8065	2.120E-02	3.996E-03	2.893E-03
	0.8155	2.512E-02	4.019E-03	2.915E-03
	0.8245	1.999E-02	3.752E-03	2.621E-03
	0.8335	2.465E-02	4.258E-03	3.403E-03
	0.8425	1.996E-02	3.869E-03	2.634E-03
	0.8515	2.679E-02	4.366E-03	3.193E-03
	0.8605	2.069E-02	3.997E-03	2.691E-03
	0.8695	1.419E-02	2.132E-03	1.897E-03
	0.8785	1.657E-02	2.512E-03	2.253E-03
	0.8875	1.561E-02	2.098E-03	2.544E-03
4.425	0.7885	2.949E-02	4.535E-03	4.419E-03
	0.7975	2.577E-02	4.097E-03	2.486E-03
	0.8065	1.743E-02	3.903E-03	2.340E-03
	0.8155	2.396E-02	4.227E-03	2.328E-03
	0.8245	2.347E-02	4.340E-03	3.298E-03

	0.8335	2.529E-02	4.263E-03	3.296E-03
	0.8425	1.828E-02	3.608E-03	2.456E-03
	0.8515	1.673E-02	3.434E-03	2.196E-03
	0.8605	1.333E-02	3.156E-03	1.831E-03
	0.8695	1.659E-02	4.021E-03	1.938E-03
	0.8785	2.096E-02	2.540E-03	2.912E-03
	0.8875	1.277E-02	1.917E-03	2.073E-03
4.475	0.8065	2.224E-02	4.134E-03	3.021E-03
	0.8155	2.255E-02	4.178E-03	3.149E-03
	0.8245	1.493E-02	3.373E-03	1.516E-03
	0.8335	2.418E-02	3.910E-03	3.158E-03
	0.8425	1.868E-02	3.559E-03	1.844E-03
	0.8515	1.429E-02	3.315E-03	1.890E-03
	0.8605	1.610E-02	3.453E-03	2.021E-03
	0.8695	1.976E-02	3.820E-03	2.351E-03
	0.8785	1.996E-02	4.287E-03	2.602E-03
4.525	0.8245	2.494E-02	4.478E-03	3.131E-03
	0.8335	1.179E-02	3.158E-03	1.608E-03
	0.8425	1.518E-02	3.438E-03	1.331E-03
	0.8515	1.631E-02	3.672E-03	1.963E-03
	0.8605	1.770E-02	3.888E-03	1.854E-03
	0.8695	1.551E-02	3.885E-03	2.164E-03
	0.8785	1.512E-02	4.330E-03	2.056E-03
	0.8875	8.620E-03	3.046E-03	1.355E-03
4.575	0.8335	2.089E-02	4.512E-03	2.335E-03
	0.8425	1.507E-02	3.505E-03	1.960E-03
	0.8515	1.166E-02	3.358E-03	1.092E-03
	0.8605	1.606E-02	3.308E-03	1.601E-03
	0.8695	1.354E-02	3.309E-03	1.857E-03
	0.8785	2.177E-02	4.568E-03	3.086E-03
	0.8875	1.083E-02	3.144E-03	1.584E-03
4.625	0.8515	2.110E-02	4.451E-03	2.405E-03
	0.8605	1.564E-02	3.369E-03	1.426E-03
	0.8695	1.281E-02	3.237E-03	1.666E-03
	0.8785	1.766E-02	4.178E-03	2.430E-03
	0.8875	1.551E-02	3.906E-03	2.388E-03
4.675	0.8695	1.450E-02	3.670E-03	2.030E-03
	0.8785	1.539E-02	3.663E-03	2.060E-03
	0.8875	1.906E-02	4.308E-03	2.866E-03
4.725	0.8785	2.348E-02	4.653E-03	3.318E-03